İSTANBUL TEKNİK ÜNİVERSİTESİ ★ FEN BİLİMLERİ ENSTİTÜSÜ

BİR BUZDOLABI BUHARLAŞTIRICISININ KARLANMIŞ ŞARTLAR ALTINDAKİ PERFORMANSI VE BUZDOLABINDA ISI KÜTLE TRANSFER MEKANİZMALARININ MODELLENMESİ

DOKTORA TEZİ

Y. Müh. Cemil İNAN

503.95.0016.012

Tezin Enstitüye Verildiği Tarih: 14 Şubat 2000

Tezin Savunulduğu Tarih: 7 Haziran 2000

Tez Danışmanı:	**Prof. Dr. A. Nilüfer EĞRİCAN**
Diğer Jüri Üyeleri:	**Prof. Dr. Yalçın GÖĞÜŞ (ODTÜ)**
	Prof Dr. Taner DERBENTLİ (ITU)
	Prof. Dr. Taner ÖZKAYNAK (ITU)
	Doç. Dr. Ty A. NEWELL (UIUC)

HAZİRAN 2000

İSTANBUL TECHNICAL UNIVERSITY ★ INSTITUTE OF SCIENCE AND TECHNOLOGY

EVAPORATOR PERFORMANCE UNDER FROSTED CONDITIONS AND EVALUATION OF HEAT & MASS TRANSFER IN A DOMESTIC REFRIGERATOR

Ph.D. Thesis by

Cemil İNAN, M.Sc.

503.95.0016.012

Date of Submission: 14 February 2000

Date of defence examination: 7 June 2000

Supervisor (Chairman):	**Prof. Dr. A. Nilüfer EĞRİCAN**
Members of the Examining Committee:	**Prof. Dr. Yalçın GÖĞÜŞ (METU)**
	Prof Dr. Taner DERBENTLİ (ITU)
	Prof. Dr. Taner ÖZKAYNAK (ITU)
	Assoc. Prof. Dr. Ty A. NEWELL (UIUC)

JUNE 2000

PREFACE

DEDICATION

To Dad and Mom: Thank you for your continuos dedication to education. I know the sacrifices you made helped me end up where I am today.

ACKNOWLEDGMENTS

I would like to thank the following people for their assistance and support,

To my wife, and my daughter: Thank you for all the love, encouragement, patience, and support when I wanted to quit.

Former Head of R&TD department of Arcelik A.S, Refik Ureyen, who made this study possible by guiding me to the correct direction, and removing all the bureaucratic problems standing in front of me.

My Advisor, Professor A. Nilufer Egrican (ITU, Istanbul), for her patience, guidance, support and helpful insight, which greatly contributed to my work.

Professor Ty Newell (University of Illinois, Urbana-Champaign), for his guidance on physical modeling, support, creating the outline of the study, and the time he spent in answering my questions.

Dr. M. Yalcin Tanes, Manager of R&TD Center-Mechanical Technologies, and Dr. A. Kemal Tugcu, Director of Human Resources, of Arcelik A.S, for their continuous support and encouragement for the project.

Reseach Engineers Hakan Karatas and Cezmi Aydın of Arcelik A.S, and Mech. Eng. M.Sc. Deniz Seker for their technical support, and their time spent supplying material, and building the experimental and theoretical background of this study which greatly contributed to my work.

Professor Clark Bullard, Director of Air Conditioning and Refrigeration Center (ACRC), University of Illinois at Urbana-Champaign, for giving me the opportunity to make my study in the center, and the time he spent in discussing the refrigerator and evaporator modeling questions.

November 1999 Cemil İNAN

TABLE OF CONTENTS

LIST OF TABLES

LIST OF FIGURES

NOMENCLATURE

A:	Area [m^2]
A_F:	Frontal area of cabinet, or fin area of evaporator (Chapter-5) [m^2]
A_{free}:	Free flow area of evaporator [m^2]
$A_{min,fr}$:	Minimum flow area for frosted evaporator [m^2]
A_{min}:	Minimum flow area of evaporator for dry case [m^2]
A_n:	Total projection area of the objects in the cabinet [m^2]
$A_{o,fr}$:	Outer surface area of frosted tube [m^2]
A_o:	Tube outer surface area (Chapter-5) [m^2] or surface area of the objects on the shelves (Chapter-2) [m^2]
A_s:	Total inner surface area of refrigerator cabinet including shelves [m^2]
$A_{T,fr}$:	Total area of frosted surface [m^2] (A_o+A_F)
Bo:	Boiling number
C:	Water concentration in the air [kg water/kg air]
C_D:	Drag coefficient for flow over objects in the cavity [-]
C_D:	Drag coefficient of pressure loss element [-]
C_{Di}:	Drag coefficient for inertia and cabinet geometry [-]
$C_{p,air}$:	Specific heat of air [J/kgK]
C_p:	Specific heat [kJ/kgK]
D, D_a:	Diffusion coefficient for air/water systems [m^2/s]
D:	Depth of cabinet [m] (Chapter 2-3) Pipe diameter [m] (Chapter 4) Total evaporator depth [m] (Chapter-5)
d_0:	Tube outer diameter [m]
D_e:	Equivalent diameter [m]
D_h:	Hydraulic diameter [m]
d_i:	Tube inner diameter [m]
f:	Friction factor [-]
F:	Diffusion coefficient in the frost layer
F_{c-a}:	View factor (between cabinet and ambient) [-]
g:	Gravitational acceleration [m/s^2]
h, or h_C:	Convective heat transfer coefficient [W/m^2K]
h:	Enthalpy [J/kg] (Chapter-5)
H:	length of one side of duct [m] (Chapter-4)
h_a:	Air side heat transfer coefficient [W/m^2K] (Chapter-5)
h_{ai}:	Enthalpy of humid air at inlet condition [J/kg_air]
h_{ao}:	Enthalpy of humid air at outlet condition [J/kg_air]
h_D:	Mass transfer coefficient [m/s]
h_{eff}:	Effective heat transfer coefficient [W/m^2K]
h_{evap_pan}:	Mass transfer coefficient over pan surface [kg/s.m2.kPa]
h_{fg}:	Phase change (condensation or evaporation) enthalpy [kJ/kg]
h_{gasket}:	Mass transfer coefficient for infiltration [kg/s.kPa]
h_l:	Convective heat transfer coefficient for liquid flow [W/m^2K]

h_{lat}: Latent heat transfer coefficient [W/m^2K]
h_o: Equivalent heat transfer coefficient of frost layer [W/m^2K]
h_{sg}: Sublimation enthalpy of water [J/kg]
h_w: Mass transfer coefficient, pressure basis [kg_w/m^2 s kPa]
j: Mass flux [kg/m^2s]
k: Thermal conductivity [W/mK]
k_l: Thermal conductivity of liquid phase refrigerant [W/mK]
L : Height of cabinet [m], or length of duct segment [m] (Chapter-4)
Le: Equivalent length of duct necessary to generate an equivalent frictional loss to the separation loss due to the fittings, expansions, contraction etc.[m],
Lewis number (Chapter-3)

m: Mass flow rate [kg/s]
m_{cond_cab}: Mass transfer rate on cabinet surfaces [kg/s]
m_{cond_door}: Mass transfer rate on door surface [kg/s]
m_{door}: Water transport rate due to door openings [kg/s]
m_{evap_pan}: Water evaporation rate from free water surface in the pan [kg/s]
$m_{F,fr}$: Frosted fin parameter
m_F: Dry fin parameter
m_{fan}: Total mass flow rate at fan exit [kg/s]
m_{FF}: Mass flowrate of air coming from freshfood cabinet [kg/s]
m_{fr}: Frosting rate on evaporator surfaces [kg/s]
m_{Frz}: Mass flowrate of air coming from freezer cabinet [kg/s]
m_{inf}: Water transfer rate due to infiltration [kg/s]
m_{inf}: Water transport due to infiltration [kg/s]
m_δ: Mass rate that goes to increase the frost thickness [kg/s]
m_ρ: Mass rate that goes to increase the density [kg/s]
n: Number of shelves
NF: Number of fins
NP: Number of tubes on air flow direction
NT: Number of tubes perpendicular to air flow direction
P: Perimeter of cross section [m] (Chapter-4)
Static pressure [Pa] (Chapter-4)
Power [W] (Chapter-3)

PE, KE: Potential and Kinetic energies [J/kg]
Pr_l: Prandtl number for liquid refrigerant [-]
P_T: Total pressure of moist air, generally 101.3 kPa.
P_w: Water partial pressure water in air [kPa]
q: Heat transfer rate from calorimeter plate [W/m^2]
Q: Total heat transfer [W] (Chapter-2,5), or energy consumption [Wh] (Chapter-3)
q”: Heat flux ($=h_r\Delta T$)
$Q_{defrost}$: Heat gain from defrosting [W]
Q_{door_latent}: Latent heat transfer due to door openings [W]
$Q_{door\_sensible}$: Sensible heat transfer due to door openings [W]
$Q_{dooropening}$: Total heat transfer due to door openings [W]
Q_{evap}: Evaporator total heat transfer rate [W]
Q_{fan}: Heat gain from fan motor [W]
Q_{HG}: Heat gain from cabinet walls [W]

Q_{inf_latent}: Latent portion of infiltration heat transfer [W]
$Q_{inf\_sensible}$: Sensible portion of infiltration heat transfer [W]
$Q_{infiltration}$: Heat gain due to infiltration through door gasket and other cabinet penetrations [W]
Re_c: Critical Reynolds number for laminar sublayer region [-]
Re_l: Reynold number for liquid refrigerant flow [-]
T: Temperature [°C]
$t_{DEFROST}$: Duration of defrost period [Minutes]
u*: Friction velocity, expressed as; $u^*=(\tau_w/\rho)^{1/2}$
U: Free stream average velocity (bulk velocity)
u: Internal energy of cabinet air [J/kg]
UA: Overall heat transfer coefficient [W/°C]
V: Flow velocity [m/s], or volume [m^3]
w: Humidity ratio [kg_w/kg_a]
W: Total evaporator width [m], or width of cabinet [m]
Work into the system [W] (Chapter-5)
W_F: Finned width of evaporator [m]
z: Elevation from reference level [m]
Δm_{FF}: Change of water mass in the cabinet air [kg/s]
ΔP_f: Frictional pressure drop [Pa]
ΔP_{se}: Static pressure difference due to the stack effect [Pa]
Δt: Time difference [s]
ΔT_{FF}: Change of cabinet air temperature [°C]
ΔT_m: Logarithmic mean temperature difference [K]

GREEK LETTERS

γ : Gas phase in frost layer that consists of air and water vapor
χ : Densification rate [-]
υ: Specific volume [m^3/kg]
ν: Kinematic viscosity (momentum diffusivity) [m^2/s]
η_s: Overall surface effectiveness [-]
α: Thermal diffusivity [m^2/s]
$\alpha_{0,eff}$: Effective thermal diffusivity ($=k_{eff}/\rho_f C_p$) [m2/s]
β : Ice phase (Chapter-5), or thermal expansion coefficient [1/K]
δ : Laminar sublayer thickness [m]
δ_C : Concentration boundary layer thickness [m]
δ_F: Fin thickness [m]
δ_{fr}: Frost thickness [m]
$\delta_{fr\_previous}$: The frost thickness calculated one time step ago [m]
δ_T : Thermal boundary layer thickness [m]
δ_v : Hydraulic boundary layer thickness [m]
δ_0: The frost thickness when the frost surface temperature reaches the triple point temperature and the growth rate equals zero
ε: Volume fraction or finning factor (Chapter-5)
Surface emissivity (Chapter-3) [-]
ν: Kinematic viscosity [kg/m^2.s]

ρ:	Density [kg/m^3]
$\rho_{fr,previous}$:	Frost density calculated one time step ago [kg/m^3]
ρ_{fr}:	Frost density [kg/m^3]
σ:	Stefan-Boltzman coefficient, 5.67e-8 [W/m^{2}K^4]
τ_w :	Surface shear stress on the wall [N/m^2]

SUBSCRIPTS

a:	Ambient, or air
ai:	Air inlet
ao:	Air outlet
ave:	Average value
c:	Cold plate
CABINET:	Heat gain through cabinet walls
cabinet:	Refrigerator cabinet (FF or Frz)
cond:	Conduction heat transfer from calorimeter plate
conv:	Convective heat transfer from calorimeter plate
CONV:	Total convective heat transfer for open door
CONV_AC:	Heat transfer due to volumetric air change
CONV_CAB:	Convective heat transfer from cabinet
cv:	Control volume
d:	Door
DEFROST:	Defrost heater
FAN:	Heat gain from fan motor per day
FAN:	Evaporator fan
FF:	Freshfood cabinet
fr:	Frost or frosted conditions
Frz:	Freezer cabinet
HEATER:	Defrost heater
HG:	Heat gain
LAT_AC:	Latent heat transfer due to air change
LAT_CAB:	Latent heat transfer due to condensation on the surfaces
LATENT:	Total latent heat transfer
m:	Mean air temperature after mixing [°C]
mass:	Latent heat transfer from calorimeter plate
o:	Outlet
OD:	Total heat gain due to door opening per day
p:	Calorimeter plate (Chapter-3)
r, rad:	Radiation heat transfer from calorimeter plate
RAD:	Total radiation heat transfer for door opening
RAD_CAB:	Radiation heat transfer from cabinet
RAD_DOOR:	Radiation heat transfer form door surface
s:	Surface
sd:	Refrigerator inner wall surface
sf:	Single fin [m^2]
tp:	Triple point temperature of water
w:	Wall
∞:	Ambient, or free stream
0 :	Initial

DIMENSIONLESS NUMBERS

$Nu = \frac{h_C L}{k}$	Nusselt number
$Sh = \frac{h_D L}{D}$	Mass transfer Sherwood number
$\Pr = \frac{\nu}{\alpha}$	Prandtl number
$Sc = \frac{\nu}{D}$	Schmidt number
$\mathrm{Le} = \frac{\alpha}{\mathrm{D}}$	Lewis number
$\mathrm{Re} = \frac{\mathrm{uD}}{\nu}$	Reynold number
$\mathrm{Ra} = \frac{g\beta(T_s - T_\infty)L^3}{\nu\alpha}$	Rayleigh number
$\mathrm{Gr} = \frac{g\beta(T_s - T_\infty)L^3}{\nu^2}$	Grashoff number

EVAPORATOR PERFORMANCE UNDER FROSTED CONDITIONS AND EVALUATION OF HEAT AND MASS TRANSFER IN A DOMESTIC REFRIGERATOR

SUMMARY

In this study, understanding of how frost accumulates on evaporator surfaces and affects the heat transfer, airside pressure drop, and refrigerator performance are investigated. In order to make a realistic model of evaporator and simulate the refrigerator performance changes while more frost was deposited on the surfaces of evaporator, heat and mass transfer mechanisms of a refrigerator cabinet were also studied. The study was made in five individual chapters. After a short introduction in Chapter-1, in the Chapters 2 and 3 open door heat and mass transfer analysis and experimental study were made. In Chapter-4, the mathematical model of air distribution system was introduced. Finally in Chapter-5, the mathematical model of evaporator was given. Solvers for all models that were developed in the chapters from 2 to 5 were written in the EES® environment. Results of the studies are summarized in chapter basis below.

Chapter-2; a physical model for estimating the cabinet flow and heat transfer rates occuring when door is opened were introduced. Model was based on the momentum and energy equations for two-dimensional flow in Cartesian coordinates. The model includes effect of shelves, which changes from none to three, in all possible combinations. Verification was made by using the experimental measurements, and flow visualization techniques. Experimental study was made on a commercially available domestic refrigerator cabinet. Transient velocity and temperature profiles were measured along the height of the cavity opening. Results of open door studies were summarized by set of equations that shows the parameters contributing to the flow and heat transfer. Equations are,

Inlet air velocity (m/s):

$$U = \left[\frac{\beta \rho g (T_\infty - T_{ave}) LWD}{\rho_{ave} \left(\frac{A_s}{Re_c} + \frac{1}{2}(C_D A_n + 1.8 A_F) \right)} \right]^{1/2}$$

Heat transfer coefficient (W/m^{2}K):

$$h = 4.95 \frac{k}{\delta}$$

Mass flowrate (kg/s): $m = \frac{1}{2} C_2 A_F \rho_{ave} U$

$C_2(n) = 1.5 - 0.32n$ (n: number of the shelves)

$Re_c = 402.17 - (98.898)L$ (L: cavity height)

To solve these coupled equations, a solver was developed in EES® environment.

It was found that in an empty cabinet (without shelf) the inflow area was larger then the outflow area. This shows that the flow is accelerating along with the cabinet height. The maximum air velocity was measured at a point very close to bottom wall. Flow regimes in an open cavity were classified as three characteristic periods starting right after the door opening. Those were *initial transient period* (0 to 7-10 seconds), *transition period* (7-10 to 20 seconds), and *quasi-steady period*, (after 20 seconds). During the first period, one volumetric air exchange is established, and both inlet and outlet velocities are high. After one volumetric air exchange, the flow is mainly driven by wall temperatures. As wall temperature increases, velocity decreases. The convection heat transfer coefficient decreases when the number of shelves are increased. Experimental studies showed that, it was acceptable to take wall temperatures constant for the first 20 seconds of door opening. The model results and experimental results agreed within the error levels of ±10% for wall temperatures above 3°C, and ±30% for below 3°C.

Chapter-3; by help of heat and mass transfer analogy, the latent and sensible (convective + radiation) heat transfer, and mass transfer percentages in the total cabinet load were analyzed. According to this study, the daily heat gain of the cabinet for 20 times of door opening was increased by 15% to 32% for 30% RH to 100%RH respectively. In these analysis; ambient temperature was 25°C, wall temperature was 5 °C, duration of each door opening was 20 seconds, number of the shelves were three, and shelves were equally spaced. The percentages of heat gain coming from door openings will, of course, be increased in the refrigerators having better insulation. The latent and sensible loads caused by door opening were found to be equal for ambient conditions of 60% RH. The breakdown of modes of heat transfer that occur during door opening period is given below. The conduction heat transfer from cabinet walls during the 20 s of door opening is neglected.

Radiation heat transfer:	8.2%
Convection (sensible) heat transfer:	42%
Latent heat transfer:	49.8%

Chapter-4; a mathematical model for analyzing the air distribution system of a nofrost refrigerator was developed. Model was based on conservation of momentum and the first law of the thermodynamics. A solver was developed in EES® environment. A commercial refrigerator cabinet was used to compare the model results with the measurements and the CFD analysis. The estimated airflow rate, and static pressure were found compatible to measurements with less then 3% error. The difference between model and CFD analysis were maximum 15%. The results were found promising, and the solver could be used effectively in the areas of initial design of the air distribution system, selection of a fan, and balancing the airflow rates distributed between compartments of refrigerator.

Chapter-5; a refrigerator evaporator, tube on sheet type, was analyzed. Calculation procedure for obtaining the heat and mass transfer characteristics of the refrigerator evaporators that operate under dry and frosting conditions has been introduced. A mathematical model that was used to obtain heat transfer coefficients, and pressure drop characteristics was developed. The solver is capable of calculating the frost thickness, density, frost mass, overall heat transfer coefficient, exit temperature and humidity, and pressure drop values for each individual tube row for quasi-steady time steps.

As it is indicated in the literature, during the frost formation, both thickness and density increase with time. This phenomenon is due to the fact that some percentage of mass transfer goes to increase the thickness, and the remaining goes to increase density (this process can be called as densification of the frost). These percentages are found very important parameters on calculation of evaporator characteristics. Unlike the literature, where densification is calculated by using the analytical methods, these percentages were chosen as constant parameters. According to the study, when the densification ratio was increased from 0.2 to 0.5, the pressure drop decreased approximately three times, the accumulated frost mass increased 4%, and the heat transfer coefficient increased 5% (at the end of 12 hours operation time). By taking the densification ratio equal to 0.3, the effect of following parameters were investigated, the operation time is 12 hours.

> Effect of the evaporation temperature: Increasing the evaporator temperature from –35°C to –25°C results; 10% decrease on heat transfer coefficient, half of pressure drop, and 5 times lower frost mass.
>
> Effect of the airflow rate: When the flow rate is increased from 5 l/s to 25 l/s, the UA value increases 3 times, pressure drop increases more than 10 times, and frost mass increases 3.5 times.

Simulation of the real refrigerator case was studied. Airflow rate of each time step was calculated by using the updated pressure drop values of whole air distribution system and fan characteristic curves, as well. In order to do this, the solver developed in chapter-4 was integrated to solver of Chapter-5. Evaporator UA value and pressure drop values were obtained for three different inlet air relative humidity values. According to this study, UA showed first increasing trend until a peak value was reached, then relatively sharp decreasing trend that ended when the evaporator was completely blocked. On the other hand, pressure drop calculations showed exponentially increasing trend all the time. In addition, the pressure drop and frost thickness values were increased more rapidly for higher relative humidity values. Complete evaporator blockage is occurred after 45 hours and 110 hours of continuous operation time for inlet humidity values of 80%, and 50%, respectively.

In order to show how all individual models can be used in calculation of quasi-steady temperature and humidity values of cabinet air, a sample run in a freshfood cabinet was made.

Results of the evaporator model was compared to the experimental studies of Seker (1999). The estimated UA value was found 10% higher than the experimental value. However, the calculated pressure-drop value was 25% lower than the measured value. It should be noted that the experimental study was obtained for only 2 hours of operation time, therefore the model results will be reexamined after having more experimental results.

BİR BUZDOLABI BUHARLAŞTIRICISININ KARLANMIŞ ŞARTLAR ALTINDAKİ PEFORMANSI VE BUZDOLABINDA ISI KÜTLE TRANSFER MEKANİZMALARININ MODELLENMESİ

ÖZET

Bu çalışmada, ev tipi buzdolaplarında kullanılan kanatlı borulu tipten buharlaştırıcıların (evaporatörlerin) kuru ve karlanmış şartlar altındaki ısı transferi ve basınç düşümü modellerinin oluşturulması amaçlanmıştır. Bunu sağlıklı yapabilmek için buharlaştırıcının tek başına değil, içinde bulunduğu buzdolabı ünitesi ile birlikte etkileşiminin bir bütün olarak modellenmesinin gerekliliği görülerek çalışma buna göre şekillendirilmiştir. Bu kapsamda çalışma beş bölüm altında toplanmıştır. Kısa bir giriş ve çalışmanın amaçlarının özetlendiği Bölüm-1 'den sonra, Bölüm-2'de buzdolabında kapının açılması ile oluşan akış ve ısı transferinin fiziksel modeli tariflenmiştir. Bölüm-3 'te ısı/kütle transferi benzeşimi de kullanılmak suretiyle buzdolabı kapısının açılması ile meydana gelen ısı kazancının analizi yapılmıştır. Bölüm-4' te ise, buzdolabında bir fan vasıtasıyla dolaştırılan soğuk hava dağıtım şebekesinin matematik modeli ortaya konulmuş ve hesap sonuçları deneysel ölçümler ve CFD analizi neticeleriyle karşılaştırılmalı verilmiştir. Son olarak Bölüm-5'te ise bir buzdolabı buharlaştırıcısının kuru ve karlanmış şartlar altındaki performansı modellenmiştir. Bu son bölümdeki çalışmalar daha önceki bölümlerde elde edilen model sonuçları kullanılmak suretiyle bir buzdolabı ile entegre olarak yapılmıştır. Geliştirilen bütün modeller için çözüm algoritmaları ve bilgisayar programları EES® ortamında yazılmıştır. Aşağıda daha detaylı olarak bölüm bölüm olmak üzere yapılan çalışmalar ve sonuçları özetlenmiştir.

Bölüm-2; bir buzdolabı kapısının açıldığı andan itibaren oluşan akış ve ısı transferinin modellenmesi için kullanılabilecek fiziksel bir model geliştirilmiştir. Modelde kabinin boş ve içinde üç adede kadar raf bulunması kombinasyonları dikkate alınmıştır. Model sonuçları deneysel ölçüm neticeleri ile karşılaştırılmıştır. Deneysel çalışmalar pazarda mevcut bir nofrost (karlanmaz) buzdolabının taze gıda bölmesinde yapılmıştır. Kararsız modda, kabin ön düzlemindeki sıcaklık ve hız profillerinin zamana bağlı haritaları deneysel olarak çıkartılmıştır. Model sonuçları aşağıda verilen eşitliklerle ifade edilmiştir.

Giriş hava hızı (m/s):

$$U = \left[\frac{\beta \rho g (T_\infty - T_{ave}) LWD}{\rho_{ave}\left(\frac{As}{Rec} + \frac{1}{2}(C_D A_n + 1.8 A_F) \right)} \right]^{1/2}$$

Taşınım katsayısı (W/m^2K): $h = 4.95\frac{k}{\delta}$

Kütlesel debi (kg/s): $m = \frac{1}{2}C_2A_F\rho_{ave}U$

$$C_2(n) = 1.5 - 0.32n \qquad \text{(n: Raf sayısı)}$$

$$Re_c = 402.17 - (98.898)L \qquad \text{(L: Kabin yüksekliği)}$$

Bu birbirine bağlı eşitlikleri çözmek ve parametrik analizleri yapmak üzere bir bilgisayar programı EES® ortamında yazılmıştır.

Çalışmalar neticesinde, buzdolabı kabinine giren havanın işgal ettiği alanın çıkan havanınkinden daha fazla olduğu görülmüştür. Bu durum havanın kabin içine girdikten sonra akış yönünde hızlandığını göstermektedir. Ölçülen en yüksek hız değeri kabin dibinden 5-6 mm mesafededir. Buzdolabı kapısı açıldıktan sonra oluşan akış rejimi üç bölgeye ayrılmaktadır. Bunlar *başlangıç rejimi* (0 ile 7-10 saniye arası), *geçiş rejimi* (7-10 ile 20 saniye arası) ve *sanki-kararlı rejim* (20 saniyeden sonra). Başlangıç rejimi kabin içerisindeki soğuk havanın bir kez ortam havası ile yer değiştirmesi ile son bulmaktadır, ve bu rejim boyunca hem giriş hem de çıkış havası değerleri yüksektir. Bu hava değişimi son bulduktan sonraki akış kabin duvar sıcaklığına bağlı olarak gerçekleşmektedir. Duvar sıcaklıkları yükseldikçe hava hızı düşmektedir. Deneysel çalışmalar ilk 20 saniye boyunca duvar iç yüzey sıcaklıklarının sabit olarak alınabileceğini göstermiştir. Bu durum modelleme çalışmalarını oldukça kolaylaştırmıştır. Model sonuçları ile deneysel çalışmalar birbiri ile 3°C 'den yüksek duvar sıcaklıkları için ±10% hata ile uyumluyken, 3°C 'nin altında maksimum ±30% hata ile uyumlu bulunmuştur.

Bölüm-3; Isı/kütle transferi benzeşimi de kullanılarak bir buzdolabının kapısı açıldığında meydana gelen taşınım, ışınım ve gizli ısı transferi ile oluşan ısı kazancının kabinin toplam ısı kazancı içersindeki payı karşılaştırılmalı olarak incelenmiştir. Buna göre kabinin günlük ısı kazancı değeri, 20 kez kapı açılıp kapanması ile %30 ve %100 bağıl nem halleri için sırasıyla %15 ila %32 arasında artmaktadır. Bu değerler ortam sıcaklığının 25°C, kabin sıcaklığının 5°C, kabinde 3 adet raf bulunduğu ve her bir defasında kapının 20 s açıldığı kabulu ile yapılmıştır. Kabinin ısı kazancı ileri yalıtım teknikleri kullanılarak azaltıldığında kapı açma kapamadan gelen ısı kazancının payı da doğal olarak artacaktır. Çalışmanın bir diğer sonucu da %60 bağıl nem durumu için kapı açmadan gelen ısı kazancında duyulur ve gizli ısı kazançlarının birbirine eşit değerlerde olduğudur. Bu çalışmada elde edilen sonuçların rakamsal değeri aşağıda verilmiştir.

Işınımla ısı transferi:	%8.2
Taşınımla ısı transferi:	%42
Gizli ısı transferi:	%49.8

Bölüm-4; bir nofrost (karlanmaz) buzdolabında hava dağıtım sisteminin matematiksel modeli termodinamiğin 1. yasası temel alınarak oluşturulmuştur. Modelin çözümü için bir bilgisayar programı yazılmıştır. Bir ticari buzdolabı kabini üzerinde oluşturulan model uygulanarak elde edilen değerler deneysel çalışmalar ve CFD (Computational Fluid Dynamics - Hesaplamalı Akışkanlar Dinamiği) analizi sonuçlarıyla karşılaştırılmıştır. Buna göre, hesaplanan static basınç düşümü ve toplam hava debisi değerleri, deneysel ölçümlerle ±3% hata ile uyumlu bulunmuştur. CFD analizi sonuçları ile yapılan karşılaştırmada ise hata en çok %15 'tir. Bu nedenle, ortaya konulan matematiksel modelin, buzdolabı hava dağıtım sisteminin ön boyutlandırmasında, fan seçimi çalışmalarında ve bölmeler arası hava debisi dengelemeleri çalışmalarında kullanılabileceği sonucuna varılmıştır.

Bölüm-5; bu son bölümde, buzdolaplarında kullanılan kanatlı borulu türden buharlaştırıcıların kuru ve karlanmış şartlar altındaki ısı transferi ve basınç düşümleri analiz edilmiştir. Bu maksatla bir matematiksel model geliştirilerek çözüm algoritması ve parametrik çalışmalar için bir bilgisayar programı yazılmıştır. Program, kar kalınlığı, kar yoğuluğu ve kütlesi, ısı transfer katsayısı, çıkış sıcaklık ve bağıl nemi, ve hava tarafı basınç düşümü değerlerini her bir boru sırası için ayrı ayrı olmak üzere, zamana bağlı hesaplayabilmektedir.

Literatürde de belirtildiği gibi zamanla karın hem kalınlığı hem de yoğunluğu artmaktadır. Bunu nedeni, yoğuşan su buharının bir bölümünün üst kısımlarda donarak kar kalınlığını artırması, geriye kalanın ise kar tabakası arasına inerek yoğunluğu artırmasıdır. Önceki çalışmalardan farklı olarak, bu çalışmada karın yoğunluk artışı analitik çözümler yerine sabit bir parametre (yoğunlaşma oranı) olarak tanımlanmıştr. Yoğunlaşma oranının 0.2 den 0.5'e artırılması durumunda basınç düşümünün üç kat, toplanan kar ağırlığının %4 ve toplam ısı transfer katsayısının %5 arttığı görülmüştür (bu rakamlar 12 saattlik sürenin sonunda elde edilen değerlerdir). Yoğunlaşma oranını 0.3 alarak yapılan çalışmada ise şu sonuçlar elde edilmiştir.

> <u>Buharlaştırıcı sıcaklığının etkisi</u>: Buharlaştırıcı boruları içerisinden akan soğutkanın sıcaklığı –35°C'den –25°C'ye artırıldığında, ısı transfer katsayısı %10, basınç düşümü 10 kez ve toplanan kar kütlesi 5 kez azalmaktadır.
>
> <u>Hava debisinin etkisi</u>: Hava debisi 5 l/s 'den 25 l/s 'ye artırıldığında ısı transfer katsayısı 3 kez, basınç düşümü 10 defadan fazla ve toplanan kar kütlesi 3.5 kez artmaktadır.

Evaporatör performansının bir buzdolabı kabini ile birlikte nasıl etkilendiğini göstermek için bir bilgisayar benzeşim modeli oluşturulmuştur. Bunun için hava dağıtım sistemi modeli, açık kapı ısı kütle transferi modeli, ve evaporatör modeli birbirine bağlanmış ve verilen üç değişik giriş bağıl nemi şartlarında çalıştırlmıştır. Bu durumda eveporatör performansının değişimi uzun süreli olarak elde edilmiştir. Buna göre, evaporatör ısı transfer katsayısı (UA) ilk önce yavaşça artan bir eğilim göstermekte, bir tepe değeri yaptıktan sonra nispeten daha hızlı olarak düşmektedir. Buna karşın hava tarafı basınç düşümü parabolik olarak artan bir değişim göstermektedir. Bu şartlarda sürekli çalışan bir evaporatörün tamamen kar ile tıkanması için geçecek süre; %80 ve %50 giriş bağıl nem koşulları için sırasıyla, 45 ve 110 saat olarak saptanmıştır.

Bir diğer analiz ise yukarıdaki çözüm ağının bir buzdolabı kabininde sıcaklık ve bağıl nem değerlerinin değişiminin zamana bağlı görülebilmesi için yapılmıştır. Çalıma sonuçları bir örnek durum için grafiksel olarak gösterilmiştir.

Ortaya konulan buharlaştırıcı modelinin karşılaştırılması ve doğruluğunun irdelenmesi için, Şeker (1999) tarafından aynı tip buharlaştırıcılarda yapılan deneysel çalışma verileri kullanılmıştır. Buna göre, ısı transfer katsayısı deneysel ölçümlere göre %10 daha fazla hesaplanırken, basınç düşümü %25 daha az olarak hesaplanmıştır. Burada deneysel ölçümlerin 2 saatlik bir çalışmaya karşılık gelen karlanmış şartlarda yapıldığı öngörüldüğünden daha fazla ve uzun süreli deney sonuçları elde edildiğinde model tekrar sorgulanacaktır.

CHAPTER–1

INTRODUCTION

1.1 Motivations and Scope of the Study

As many other authors have noted, the main motivation of refrigerator related studies is mostly to decrease the energy consumption. In the beginning of 90's, attention was focused on ozone friendly refrigerants. As the conversion to new refrigerants is nearly complete, energy efficiency has increased in priority again, and it seems that it will stay a priority for the next decade.

Energy consumption and energy efficiency values of domestic refrigerators are currently measured according to standards. Current standards require only closed door tests for rating. However, it is believed that as Japanese standards (JIS) already require, open door refrigerator energy tests will soon be a requirement for other standards such as ISO, DIN, and DOE. Authors indicate that the basic simulation of daily door openings for a family usage will give 20% to 32% energy consumption increase over the rated value. Because competition forces companies to design more efficient refrigerators, the real measure of a good refrigerator will be the energy consumption value of on site usage instead in laboratory conditions.

The main energy consumption of a refrigerator is caused by heat gain from polyurethane insulation, gaskets, compressor(s), fan(s), defrost heaters, the sensible and latent heat gain through door openings, and the food placed into the refrigerator. Now, the heat gain through polyurethane insulation material can easily be determined and there are a lot of studies examining better insulation materials such as vacuum panels, new polyurethane foams, etc. There are also continuing studies to increase the efficiency of components such as compressors, fans and defrost systems. In parallel to developments in the electronics industry, variable speed compressors, new defrost algorithms such as neuro-fuzzy and adaptive defrosting, new cooling system circuits such as dual evaporator cycles, and tandem systems are being investigated. When the open door refrigerator tests becomes an obligation, efficient refrigerator design will require knowledge of open door heat and mass transfer processes. Therefore, the heat and mass transfer through door opening should be investigated in order to understand the main heat transfer modes.

In this study, the physics of airflow patterns for open and close door conditions will be investigated. Physical models of the heat and mass transfer characteristics will be developed. The physical models will be subject to experimental validation. Evaporator performance under frosting conditions will be investigated both experimentally and theoretically. Although it is not in the scope of this study, the final goal will be development of a model for dynamic thermal simulation of domestic refrigerators. This study will supply useful data to these simulation activities.

In order to classify the above mentioned topics, this study can be divided into the following sub-branches (chapters),

Open-door heat and mass transfer modeling and experimentation

- *Without shelf*
- *With shelves*

Air distribution system modeling and analysis

- *Close-door air distribution system analysis (on and off cycles) and experiments*
- *CFD analysis of air distribution system*

Evaporator performance under frosted conditions

- *Heat transfer analysis*
- *Pressure drop and flow analysis*
- *Cabinet temperature and relative humidity analysis*

According to this classification, the main goals of this study can be summarized as; understanding of how heat and mass transfer occurs during open and closed door conditions, how the frost accumulates on the evaporator and affects its performance, and finally how this frost can be managed.

CHAPTER-2

HEAT & MASS TRANSFER IN THE REFRIGERATOR AND FLOW MODELING STUDIES THROUGH DOOR OPENING

2.1 Background and Literature Survey

Buoyancy driven flow and heat transfer analyses in cavities are widely studied in the literature. While most of the studies are for enclosures, few of them are for one face open vertical cavities. The number of studies in this area increased recently, especially in 80's. This may be because of the increasing safety questions about nuclear reactor cooling when cooling system failure occurs, and the necessity of improving the cooling capacities of electronic circuits. Although the number of the studies started to decrease during 90's, natural convection in cavities are still strongly motivated by electronic industry.

For one-face open vertical cavities, experimental and theoretical analyses are made for both cold and hot wall temperature systems. In all studies, the wall temperatures are kept isothermal. Analysis is made mostly for 2-D and 3-D steady-state cases. Laleman et al. (1992) and Knackstedt et al. (1995) studied real refrigerator cabinet geometry, and all five walls of the cavity (including side-walls) are taken into account. Skok et al. (1991) and Quere et al. (1981) investigated flow and heat transfer analysis in the cavities of which bottom, back, and top walls are kept isothermal. They did not take into account the side-walls by choosing very large cavity. Chan & Tien (1985, 1986a, and 1986b), and Hess & Henze (1984) studied cavities where only back wall is heated while the other walls remained adiabatic.

A sketch of typical one face-open cavity geometry and demonstration of the flow are given in Figure 2.1. Such flows occur in household refrigerators and ovens under open door conditions, and also in the cavities of solar central receivers (Clausing, 1983).

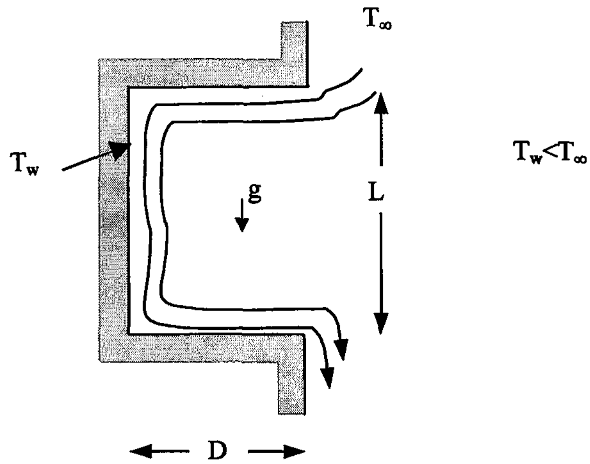

Figure 2.1 Typical geometry of one face open, vertical cavity

In previous studies, the characteristic length for Ra and Nu numbers is chosen as cabinet height, L, and the characteristic temperature difference is defined as (T_w-T_∞). All thermophysical properties of fluid are obtained at film temperature which is (T_w+T_∞)/2. Detailed discussions of cavity investigations follow.

Laleman et al. (1992) investigated the modes of energy losses incurred when the door of a refrigerator is opened. Analysis is done for FF cabinet of 20 cu.ft. domestic refrigerator. Although the study generally considered no shelf condition, the effect of shelf addition to the cabinet is also investigated. In order to measure average heat transfer coefficients on the inside surfaces of a refrigerator, aluminum calorimeters are used. These calorimeters are made of pure aluminum plates of 15" x 15" x1/4" with five thermocouples on it. The calorimeters are located on the inner walls of refrigerator. By repeating the lumped capacity analysis for each plate (the transient calorimeter method) the average heat transfer coefficients are calculated. The low emisivity of the polished plate reduces effect of radiation heat transfer. Open door tests are run under 40-85% RH and 295 K ambient conditions. According to the study, the following results are obtained.

- The latent load is a significant contribution in a humid environment. At about 60 % RH, the latent load equals the convective load.

- For typical plastic refrigerator linings, the radiative heat transfer coefficient is in the range of 2-3 $W/m^2\,K$; thus the radiative load represents about 50 % of the convective load.

- The buoyancy term of the Rayleigh number is primarily affected by temperature difference than by mass concentration differences.

- Shelf addition causes a reduction in the values of average convective heat transfer coefficients by about 20 %, however the overall energy loss is greater, due to the increased surface area.

- For typical door opening schedule, the load for conditions of 91% RH and 20K temperature difference accounted for a 22% increase on annual energy requirements.

Nu number and Ra number were based on characteristic length L, the compartment height, which is 0.61 m. A typical function, which correlates the Nu and Ra number, is given as;

$$Nu_L = CRa_L^{1/3}$$

Where,	C=0.158	for left wall
	C=0.159	for right wall,
	C=0.156	for rear wall,
	C=0.102	for floor.

Knackstedt et al. (1995) conducted a follow up study to Laleman et al. (1992). Heat transfer characteristics for open door conditions and flow regimes are investigated. The study investigated no shelf and multiple shelf conditions.

The experimental studies are conducted in a refrigerator whose inner cabinet dimensions are 0.73 m height, 0.7 m width, 0.5 m depth. For heat transfer coefficient measurements, the same experimental apparatus described by Laleman et al. (1992) is used. Flow visualization studies showed the air flow patterns for multiple shelf configurations. Below, simple breakdowns of the types of heat gain are provided. These values are valid only for the test refrigerator, which is equipped with calorimeter plates. Therefore, the percentage of radiation effect is lower than the normal case.

Table 2.1 Simple breakdown of the types of heat gain in a domestic refrigerator (Knacksted et al., 1995)

Bulk air (sensible and latent) added during door opening	54.1 %
Surface convective heat transfer during door opening	31.5 %
Mass transfer during door opening	11.6 %
Conduction	2.2 %
Radiation	0.6 %

As a results of their experimental studies followings are obtained.

- The average heat transfer coefficients in the refrigerator range from 0.55 to 5.21 W/m^2 K. The ceiling heat transfer coefficients were found to range from 4.7 to 5.4 W/m^2 K. The highest heat transfer coefficients are at the upper-front plates in the refrigerator where warm ambient air is pulled into the cabinet.

- As the number of shelves increases, the average heat transfer coefficients decreases.

- After door is opened, the flow is stagnant during the first 2 seconds, and begins to form a definitive flow pattern around 7 to 8 seconds.

- The air entering the uppermost compartment always reaches the rear, regardless of the height of the compartment. Besides, more warm air enters at the center of the shelf than the edge of the shelf.

Chan and Tien (1985) have performed a numerical study for natural convection in a two-dimensional open cavity under laminar steady-state conditions. The square cavity has one heated vertical wall facing a vertical opening and two insulated horizontal walls. Results are obtained for Ra numbers ranging from 10^3 to 10^9 at unit Pr number with constant properties and Boussinesq approximation. The SIMPLER algorithm was used for solving the governing equations.

The results of Chan and Tien's study are given below.

Table 2.2 Variations of Nu with Ra for the Square Open Cavity (Pr=1), Chan and Tien (1985).

	Ra						
	10^3	*10^4*	*10^5*	*10^6*	*10^7*	*10^8*	*10^9*
Nu	1.07	3.41	7.69	15	28.6	56.8	105

At the low Ra number of 10^3, the heat transfer mechanism is conduction dominated. The value of Nu is 1.07, very close to pure conduction (Nu=1). As Ra increases, a boundary layer begins to form for Ra=10^5.

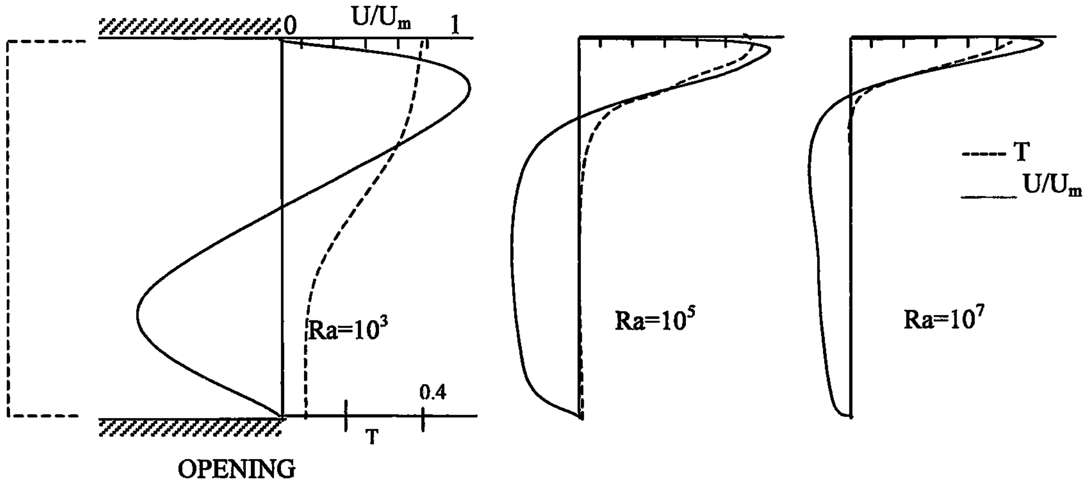

Figure 2.2 A sketch of horizontal velocity and temperature profiles at opening for different Ra values, (Chan and Tien, 1985).

Figure 2.2 shows horizontal velocity and temperature profiles at the opening for various Ra values. For Ra less then 10^3, the viscous effect makes inflow/outflow velocity profile symmetric. Maximum for the inflow velocity occurs near the bottom as fluid is sucked toward the heated wall. The outgoing flow accelerates toward the top of the opening, so that U_m (maximum exit velocity) is located near the top. The incoming flow is not at ambient temperature because of the conduction effect. At the moderate Ra of 10^5, the incoming velocity profile flattens. The maximum for outflow moves up further because of the stronger buoyancy effect. At the high Ra numbers of 10^7 the outflow occupies even a smaller portion of the opening, about 17%. The profile for inflow is flat and the maximum occurs near the exit flow. For high Ra values of 10^7, the local heat transfer coefficients and the velocity profile along the heated wall of a square cavity are in good agreement with the results of vertical flat plate calculations. The high Ra number profile indicates an accelerating flow in the cabinet.

Chan & Tien (1986a), laminar steady-state natural convection in a 2D rectangular shallow open cavity is investigated numerically. For numerical studies, SIMPLER algorithm is used. Study is made for aspect ratio (L/D) of 0.143. Ra values are taken up to 10^6 using constant properties and Boussinesq approximation. Findings of the numerical study compare favorably with experimental results of $Ra=10^6$. Chan and Tien used Laser Doppler Velocimetry in order to investigate the flows in the two-dimensional open cavity. Streamlines and isotherms are plotted for various Ra values.

They also compared the experimental results of shallow cavity, square open cavity, and isothermal vertical plate. At low Ra values, the Nu value for the square cavity is about 1.0 and that for the shallow cavity is about 0.143, both equal to the aspect ratios.

As Ra increases, both Nu for the square and the shallow cavities go through a transition where convection heat transfer increases. They approach asymptotic values as heat transfer becomes predominantly determined by the boundary-layer flows up the heated wall. It can be observed that these asymptotic results are close to that for a flat plate, Nu varying with Ra to the 0.284 power, independent of aspect ratio (a value of 0.25 is usually obtained for flat plate results). Both the experimental and numerical results show that the flow in the shallow cavity remains 'unicellular' throughout. There is no recirculation or secondary cell.

Skok et al. (1991) conducted a combined experimental and numerical study of buoyancy-driven flow in a side facing open cavity. The walls of the cavity are at uniform temperature T_w, and opening of the cavity faces a large quiescent body of fluid at temperature T_∞. If T_∞ exceeds T_w, cold fluid from within the cavity flows out near the bottom while warm ambient fluid flows in near the top.

The dimensions of FF compartment of a typical domestic refrigerator are H=0.9 m, D=0.6 m, W=0.75 m. The associated Ra number for the buoyancy driven flow is approximately 10^9. The present experimental studies were undertaken in a model cavity with an aspect ratio, L/D=1.5. In experimental studies the glycerol-water mixtures of different compositions are used, a wide range of Ra numbers were achieved while keeping the temperature difference between the hot and cold surfaces essentially constant.

Ra values of $3.5x10^6$ and $1.2x10^9$ were studied experimentally. A numerical solution procedure based on the control volume finite-difference scheme described by Patankar (1980) was used to investigate the flow numerically. The SIMPLER algorithm was used to solve for the velocity components, pressure field, and temperature. The following comments of the study are given,

The numerically predicted variation of the horizontal component of velocity at the plane of the cavity opening is plotted for several Ra numbers in Figure 2.3. The ordinate variable u/u_{max} is the local velocity normalized by the maximum outflow velocity in the cavity opening. Positive values are associated with outflow and negative values with inflow. With increasing Ra, the negative portion of the curve is observed to flatten, and the location of peak outflow velocity moves upward. The location at which the velocity profile changes sign mowed upward from a point only slightly above H/2 at $Ra_H=10^3$ to approximately 0.76H at $Ra_H=10^7$.

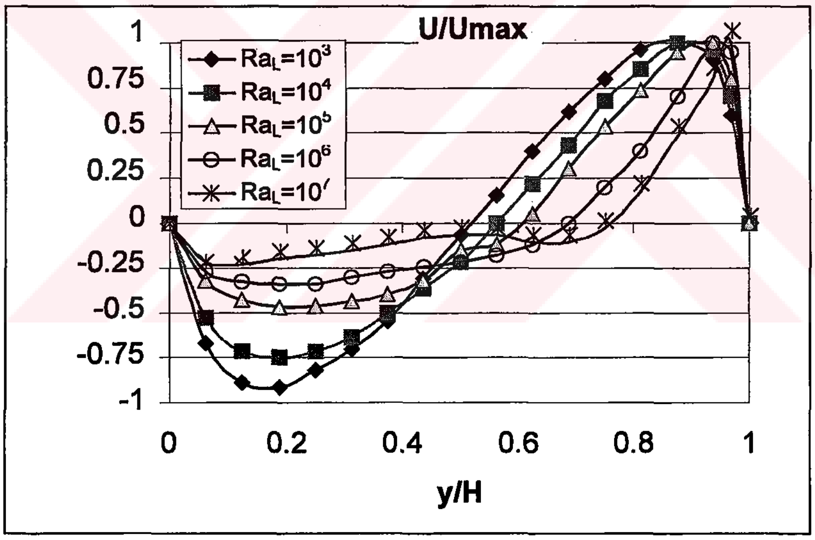

Figure 2.3 Schematic of Skok's (1991) velocity profiles in the plane of the cavity opening. y is vertical location measured from top of cavity.

At $Ra_H=10^3$ the maximum velocity entering the cavity is approximately 90 percent of the maximum outflow velocity, whereas for $Ra_H=10^7$ the maximum inflow velocity is only 23 percent of the max outflow velocity. For Ra numbers between 10^4 and 10^7 the maximum outflow velocity is predicted within two percent by:

$$Re_{L,max}=0.045(Ra_L)^{0.53} \qquad \text{where } Re_{L,max}=u_{max}L/\nu$$

Numerically predicted convective heat transfer coefficients are plotted for bottom, back, and top walls. And the results of the correlation are summarized in the Table 2.3.

Table 2.3 Least squares fits to the numerically predicted and experimentally measured plate-average Nu numbers (Skok et al. 1991).

Numerically predicted Nu numbers $10^4 \leq Ra_L \leq 10^7$		
Wall	**Correlation**	**Average deviation from data**
Back	$0.1x(Ra_L)^{1/3}$	±5%
Bottom	$0.39x(Ra_L)^{1/4}$	±5%
Top	$0.06x(Ra_L)^{1/3}$	±11%
Experimentally measured Nu numbers $3.5x10^6 \leq Ra_L \leq 1.2x10^9$		
Back	$0.086x(Ra_L)^{1/3}$	±8%
Bottom	$0.14x(Ra_L)^{1/3}$	±5%
Top	$0.033x(Ra_L)^{1/3}$	±12%

The cavity average Nu number correlation for Ra numbers between 10^4 and $1.2x10^9$ is;

$$\overline{Nu}_{L.cav} = 0.087Ra_L^{1/3}$$

Penot (1982) presented the numerical computations of free convection flow inside an isothermal open square cavity. The effects of Gr number and inclination of cavity are examined. The governing equations are solved under the Boussinesq approximation, both for steady-state and transient conditions. As a numerical method, finite difference (implicit ADI scheme) is used. The results of this study are given below.

For $Gr=10^5$, 10^6,and 10^7 the velocity field becomes of the boundary-layer type, with a central core in the cavity where the velocity is essentially uniform. The instabilities are apparent in the profiles. At $Gr=10^7$, location of the peak velocity is very close to the wall (typically a few percent of the cavity aperture size).

The transient Nu numbers are obtained for different Gr numbers, and the approximate steady state values are given in Table 2.4.

Table 2.4 The effect of Gr number on the cavity-average Nu values, (Penot, 1982).

	Gr						
	0	10^2	10^3	10^4	10^5	10^6	10^7
Nu_{cavity}	1	2	5	11	17	22	24

Hess and Henze (1984), their study presents the experimental results for natural convection in a cavity. The cavity model consisted of a cubical cavity with one heated wall, an aperture at the opposite wall, and the remaining walls are insulated. Water is used as the fluid in the experiments. A cubical cavity of 1 m on the side is centrally located inside the water tank whose dimensions are 2.9x3.05x1.07 m^3. Detailed velocity profiles are obtained using a Laser Doppler Velocimetry for Ra numbers between $3x10^{10}$ and $2x10^{11}$, corresponding to constant wall-temperature boundary condition. Characteristics of two and three-dimensional flows in the cavity are obtained with dye flow visualization technique.

Temperature differences between the plate (wall temperature) and the initially cold fluid, between 2°C and 13°C are established. (Ra=$3x10^{10}$ to $2x10^{11}$). As a result of the studies, the general characteristic of the flow areas are as follow (aspect ratio is unity).

- When the temperature of the vertical plate is raised to T_w, the fluid rises and is turned outward by the pressure gradient imposed by top.
- For the Ra number employed in these experiments, a boundary-layer type flow is established near the plate and the flow ascends for about 90% of the length of the heated plate before it is turned by the top wall.
- Considerable mixing is observed in the top corner region where the flow turns outward. The hot flow then follows the top wall and escapes to the tank (atmosphere).
- Surprisingly, it was observed that a large portion of incoming flow entered right below the escaping flow, forming a shear layer near the top of the aperture. This shear layer more pronounced for high Ra numbers.
- Dye patterns of the incoming flow show that the streamlines are almost parallel and horizontal. In addition, this flow is entrained all the way into the plate and fed to the boundary layer.
- An important difference between the high and low Ra number cases is the profile of the incoming flow. The low Ra number case shows slower and more uniform profile

throughout the aperture, while the high Ra number case has a stronger negative velocity region.

Dye experiments for several wall temperatures are performed at the boundary layer. The first indications of disturbance are observed at a local $Ra_l=2x10^{10}$ to $3x10^{10}$. Vortex streets are observed at $Ra=4x10^{10}$ and complete turbulence are observed at $Ra_l=7x10^{10}$ to $9x10^{10}$.

Chan and Tien (1986b), An experimental investigation on natural convection in a two-dimensional open cavity is performed using Laser-Doppler Velocimetry. The cavity is rectangular with one vertical heated wall facing a vertical opening, and with the two horizontal walls insulated. Studies for an open shallow cavity with an aspect ratio of 0.143 and Ra numbers ranging from 10^6 to 10^7 under the steady laminar conditions are carried out using water as the working fluid. The cavity is 4.45 cm high, 31.1 cm long, and 61.0 cm wide. The two-dimensional shallow cavity therefore has height-to-length aspect ratios of 0.143. They found that the error in the temperatures measurements greatly affects the overall Ra numbers such as, 22 percent for low Ra numbers and 2 percent for high Ra numbers. The percent error for Nu_L ranges from 28 to 18 for low to high Ra values.

Clausing (1983), in the study, a simple analytical model presented, which indicated that the ability to heat the air inside the cavity often controls the convective losses from cavity of solar receivers. A brief description of the refined model is presented. Emphasis is placed on using available experimental evidence to substantiate the hypothesized mechanisms and assumptions. As a result of the studies a correlation is derived for calculation of average Nu number;

$$Nu = 0.082Ra^{1/3}\left[-0.9+2.4\left(\frac{Tw}{T\infty}\right)-0.5\left(\frac{Tw}{T\infty}\right)^2\right] \qquad Ra>1.6x10^9;\ 1<T_w/T_\infty<2.6$$

The absolute deviation between this correlation and the 119 data points, which were examined, is 1.0 percent. It is noted that the influence of T_w/T_∞ becomes very weak for $T_w/T_\infty>2$. Due to this nature a value of 2 is suggested for $T_w/T_\infty>2.6$ until data in this region become available.

Chen et al. (1983), the purpose of their study was to report significant findings concerning the pulsating nature of the flow in cavities. The flow test section is an open rectangular cavity with variable aspect ratio (L/D) and orientation angle (α). An overall cavity wall temperature, T_W, is defined by averaging the mean temperatures at three (top, back, and bottom) inside copper walls. Smoke and shadowgraph techniques are used for flow visualization. Mean temperature distribution measurements in the cavity, have been performed for the free convection regime in still room air at T_∞=293 K. The effect of inclination angle on the pulsating behavior is photographed.

Photographs showed the appearance of a thermal boundary layer on the bottom wall of the cavity (L/D=1) for three different orientation angles. At α=0°, vertical cavity, the boundary layer separated strongly at the bottom wall entrance corner and reattached about halfway along this wall. The reattachment point oscillated erratically about this location. The entrance corner and the mean reattachment point delimited a region of strong clockwise-recirculation flow of oscillating size from which variously size eddies are irregularly ejected into the cavity. As a consequence, the bulk of the flow within the cavity appeared well mixed and turbulent in nature. With increasing α the bottom wall recirculation zone becomes smaller as reattachment position is replaced towards the entrance corner.

Quere et al. (1981), numerical results are reported for thermally driven laminar flow in a two-dimensional rectangular geometry with one plane, the aperture plane, removed. All three internal walls in the cavity are kept at the same temperature, T_w. The governing equations were solved by using the finite difference technique. Parameters varied in the calculations are cavity aspect ratio and inclination angle with respect to gravity, inside wall temperature, and Gr number. The value of Pr number is fixed to 0.73.

The numerical results for air in an open cavity are given below. The variables of interest are Gr, $\Delta T=T_w-T_\infty$, cavity aspect ratio, and angle of inclination (α) The steady state results for Gr=10^5 and ΔT=50 K shows cold fluid entering the cavity through the bottom two-thirds of the aperture plane. Hot fluid leaving the cavity emerges through the top one-third of the aperture plan. Intense shearing of the flow arises at the horizontal plane in the cavity where the entering and emerging flow fields meet. By contrast with the entering flow, which is drawn almost radially from the surroundings, the flow emerging from the cavity is quickly deflected vertically upward by buoyant forces. The air heated in the cavity, particularly at the vertical back wall, drives the flow and is the cause of a substantial amount of entrainment from the surrounding fluid medium, especially along horizontal plates above cavity. For values of $Gr>10^7$ the flow field becomes noticeably unsteady.

The velocity profiles showed a decreasing boundary-layer thickness and a displacement of maximum velocity toward their respective walls as Gr increases. The uniform entrance profile occupies about two-thirds of the cavity aperture plane for $Gr=10^4$, increasing to a value of about ¾L for $Gr=10^6$ and 10^7. It would appear that the local acceleration of the flow on both walls is due to the contribution of buoyant forces to the momentum balance in the cavity. From a relative comparison of the temperature profiles, it is readily seen that the depth of penetration of cold flow into the cavity increases with Gr number.

The results show that, in general, Nu number increases with increasing Gr number and decreasing aspect ratio.

Table 2.5 Average Nu number on each cavity wall
(T_W- T_∞=50 K, L/D=1, α=0°), Quere et al. (1981).

	Top wall	**Back wall**	**Bottom wall**
$Gr=10^4$	1.16	0.725	3.02
$Gr=10^5$	2.79	2.74	5.22
$Gr=10^6$	5.09	6.29	8.39
$Gr=10^7$	9.05	17.66	21.53
$Gr=3x10^7$	12.23	24.12	28.92

2.2 Basic Theory of Open-Door Cabinet Flow and Heat Transfer Modeling

The airflow through a refrigerator cabinet when the door is opened is important for calculation of heat and mass transfer to a refrigerator. As it is frequently indicated in the literature, the flow in such rectangular open cavities is transient and three-dimensional in nature. The presence of shelves and food in the refrigerator compartment make the heat and mass transfer calculations and flow analysis even more complex. The orientation of shelves, shelf size, type and location of the foods are varied. Therefore, it is a highly complex situation to analyze and it is difficult to find a common solution that can be applied to different refrigerators.

A reasonable basis to start is modeling of an empty cabinet (no shelf and no food). This model will then be improved by adding shelves in different configurations.

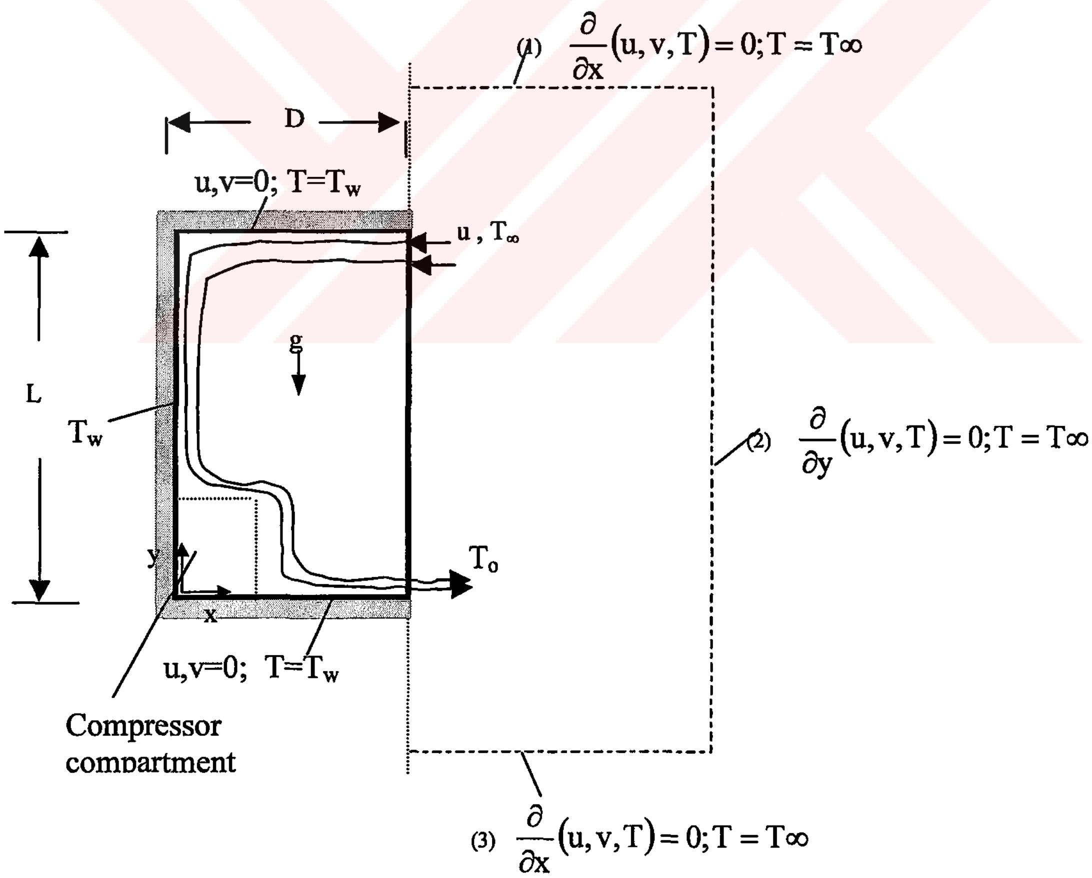

Figure 2.4 Geometry and boundary conditions of problem
(Effect of the compressor compartment is neglected in the studies)

Refrigerator cabinet schematic is shown in Figure 2.4. In this figure, boundary conditions of the problem are indicated and they are also summarized below.

$T=T_w$		*at all inner surfaces of cavity*
$u=0,\ v=0$		*at all surfaces*
$\dfrac{\partial}{\partial x}(u,v,T)=0$	$\dfrac{\partial}{\partial y}(u,v,T)=0$	*at imaginary planes, which is chosen far enough from cavity opening*
$T=T_\infty$		*at imaginary planes*

Governing Equations:

For the flow over a vertical surface, it has often been assumed that transition to turbulence occurs when the local Rayleigh number is equal to 10^8 (Oosthuizen and Naylor, 1999). For the one face open type cavities, the turbulent regime is observed at $Ra_L=7.10^{10}$ to 9.10^{10} by Hess and Henze (1984). On the other hand, Quere et al (1981) and Chen et al (1983) observed instabilities in the square open cavity flow when Ra equals to 10^7. From their experimental studies, they agreed that the bulk of the flow in the cavity appeared well mixed and turbulent in nature. Therefore in the present study, since Ra number mostly greater then 10^8 the flow assumed turbulent.

The governing equations for natural convection turbulent flow in a Cartesian Coordinates are given below. In these equations, the flow is assumed as 2-D in the x and y directions. The continuity, momentum and energy equations governing two-dimensional flow of a newtonian fluid, for the steady-state case can be written as,

Continuity:

$$\frac{\partial \bar{u}}{\partial x}+\frac{\partial \bar{v}}{\partial y}=0 \qquad (2.1)$$

Momentum (x):

$$\bar{u}\frac{\partial \bar{u}}{\partial x}+\bar{v}\frac{\partial \bar{u}}{\partial y}=-\frac{1}{\rho}\frac{\partial \bar{p}}{\partial x}+\frac{\partial}{\partial y}\left((\nu+\varepsilon)\frac{\partial \bar{u}}{\partial y}\right) \qquad (2.2)$$

Momentum (y):

$$\bar{u}\frac{\partial \bar{v}}{\partial x}+\bar{v}\frac{\partial \bar{v}}{\partial y}=-\frac{1}{\rho}\frac{\partial \bar{P}}{\partial y}+\frac{\partial}{\partial y}\left[(\nu+\varepsilon)\left(\frac{\partial \bar{v}}{\partial y}\right)\right]-g\beta(\bar{T}-T_\infty) \qquad (2.3)$$

Energy:

$$\bar{u}\frac{\partial \bar{T}}{\partial x}+\bar{v}\frac{\partial \bar{T}}{\partial y}=\frac{\partial}{\partial y}\left[(\alpha+\varepsilon_H)\frac{\partial \bar{T}}{\partial y}\right] \tag{2.4}$$

Where, the time-averaged mean values are indicated by over bar. In this equations ε is known as the eddy viscosity and ε_H is known as the eddy diffusivity.

In the equations, the Boussinesq approximation is used, in other words, ρ is assumed constant everywhere except in the body force term of the y momentum equation where it is replaced by $g\beta(T-T_\infty)$. The boundary conditions of geometry are given in Figure 2.4. In order to solve the above mentioned equations numerical methods are mostly preferred in the literature.

In the present study, instead of solving the governing equations, a steady state flow and heat transfer model is introduced. Extensive experimental data of Knackstedt et al. (1995) will be used to derive expressions for empirical modeling terms. Velocity and temperature profiles on door opening plane will be obtained experimentally for number of shelf configurations. Results for model will be compared to both experimental heat transfer coefficients of Knackstedt et al. (1995) and measured velocity and temperature data of present study. Finally, an estimate of mass transfer effects from door openings will be presented.

2.2.1 Steady state open-cabinet flow modeling

The airflow through a one face open rectangular cavity is caused by air density differences along the height of the cavity. Air density difference is caused by the temperature differences between the cavity surfaces and the surroundings. However, other forces balance against the flow such as friction on the surfaces, drag and dissipation caused by objects in the cavity, flow turning and edge effects, and the inertial effect of accelerating room air as it flows into the cavity.

In order to get physical understanding of cabinet flow and its driving mechanisms, a model is introduced. The model is based on a steady force balance for the whole cabinet volume,

$$F_{buoyancy} = F_{drags} = F_{friction} + F_{inertia} \qquad (2.5)$$

In this equation the buoyancy force, acting to the volume, can be defined as following;

$$F_{buoyancy} = \rho_\infty g \beta (T_\infty - T_{ave}) L.W.D \qquad (2.6)$$

Here,

ρ_∞: Density at ambient temperature [kg/m^3]
β : Thermal expansion coefficient [1/K]
L: Height of cabinet [m]
W: Width of cabinet [m]
D: Depth of cabinet [m]
T_∞: Ambient (inlet) temperature [K]
T_{ave}: Average fluid temperature [K] , $T_{ave} = (T\infty + To)/2$
T_o: Outlet temperature
T_w: Wall temperature [K]

In the eqn. 2.6, the average air temperature is used in the buoyancy term instead of the wall temperature. This definition helps to relate the fluid flow and heat transfer equations.

The friction force,

$$F_{friction} = A_s \tau_w \qquad (2.7)$$

A_s: Total inner surface area [m^2]

τ_w: Surface shear stress on the wall [N/m^2]

Surface shear stress is expressed as;

$$\tau_w = -\mu \frac{dU}{dy} \tag{2.8}$$

The flow is assumed turbulent and a laminar sublayer has been formed within the boundary layer. The "law of wall" rule can be applied, Bejan (1995), von Karman (1939). Law of wall equations are given in text books (e.g. Bejan , 1995).

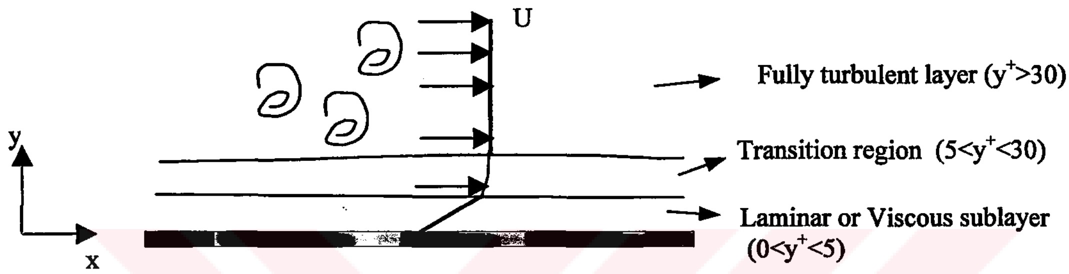

Figure 2.5 Schematic view of velocity profile and "law of wall" description

Where,

$u^+=U/u^*$, $y^+= yu^*/\nu$
u^* is friction velocity and expressed as; $u^*=(\tau_w/\rho)^{1/2}$
U: free stream average velocity (bulk velocity)
τ_w : wall shear stress

If it is assumed that the velocity distribution in the sublayer region (this region is called either the viscous sublayer or laminar sublayer) is linear then the velocity gradient can be rearranged as;

$$\frac{du}{dy} \cong \frac{U}{\delta} \tag{2.9}$$

Here,

U: Average velocity of mainstream [m/s]
δ : Sublayer thickness [m]

For the laminar sublayer region, a critical Reynolds number, Stern (1988), can be defined that describes the balance of momentum dissipation between the wall and the fluid. The sublayer thickness, δ, is also the primary layer constituting heat transfer between the cavity walls and the airflow through the cavity.

$$Re_c = \frac{U\delta}{\nu}, \quad \text{or} \quad \delta = \frac{Re_c\, \nu}{U} \tag{2.10}$$

Here,

Re_c: Critical Reynolds number for laminar sublayer region [-]
ν: Kinematic viscosity [kg/m^2.s]

Finally, the total drag force can be expressed as;

$$F_{drag} = \frac{1}{2}\rho_{ave}(C_D A_n + C_{Di} A_F)U^2 \tag{2.11}$$

A_F: Frontal area of cabinet $A_F = LW$ [m^2]
A_n: Total projection area of the objects in the cabinet [m^2]
C_D: Drag coefficient for flow over objects in the cavity [-]
C_{Di}: Drag coefficient for inertia and cabinet geometry [-]
ρ_∞: Air density at ambient temperature [kg/m^3]

The first term in Equation (2.11) represents drag forces caused by flow over objects in the refrigerator cabinet. The second term represents other inertial drag forces such as potential to kinetic energy conversion (acceleration of air), and geometric effects such as flow turning around corners, edges, etc. Substituting all relations into eqn. (2.5) we obtain the steady state average velocity of the main flow into a cabinet.

$$U = \left(\frac{\beta\rho_\infty g(T_\infty - T_{ave})LWD}{\rho_{ave}\left(\frac{A_s}{Re_c} + \frac{1}{2}(C_D A_n + C_{Di} A_F)\right)} \right)^{1/2} \tag{2.12}$$

Here, $$T_{ave} = \frac{T_\infty + T_o}{2} \tag{2.13}$$

2.2.2 Steady state open-cabinet convective heat transfer modeling

Total heat transfer between a cabinet and its surroundings is determined from equations (2.14) through (2.18). In these equations, the inflow and outflow areas are assumed equal. The objects on the shelves are taken in to account as participating to heat transfer. The surface temperatures of the objects are assumed equal to the cabinet wall temperature. In order to get a common convention, the temperature difference between wall and the ambient is used to define the convective heat transfer to the cavity. Analyzing the change of energy of the airflow through a cabinet yields,

$$Q = mC_p(T_\infty - T_o) \tag{2.14}$$

or

$$Q = -h(A_s + A_o)\left[\frac{T_\infty - T_o}{\ln(\theta)}\right] \tag{2.15}$$

$$\theta = \exp\left[\frac{-h(A_s + A_o)}{mC_p 1000}\right] \tag{2.16a}$$

$$T_o = T_w - \theta(T_w - T_\infty) \tag{2.16b}$$

Where

$$m=(1/2)A_F\,\rho U \tag{2.17}$$

$$h = \frac{k}{\delta_T} \cong \frac{k}{\delta} \tag{2.18}$$

T_o: Air outlet temperature [°C]

A_o: Surface area of the objects, if any, in contact with the airflow [m^2]

h: Convective heat transfer coefficient [W/m^2K]

δ_T: Thermal boundary layer thickness. For air (Pr=0.723), thermal boundary layer is approximately equal to hydrodynamic boundary layer. ($\delta \cong \delta_T$)

k: Thermal conductivity of air [W/mK]

Solution alghoritm of above defined equations numbered from (2.12) to (2.18):

The heat transfer and fluid mechanic relations, defined above, are coupled. An equation solver, such as EES® (Engineering Equation Solver®), can solve these coupled equations. This program uses well-known "Newton-Raphson" iterative method. For a given geometry and specified physical parameters, values of the average velocity of the flow, total heat transfer, average heat transfer coefficient, and outlet temperature can be determined.

The solver program list is given in Appendix A.

2.3 Verification of the Model

2.3.1 Data reduction from Knacksted et al.'s (1995) study

The summary of Knackstedt et al (1995)'s study had been given in section 2.1. Here, in order to give evaluation procedure of the convection coefficients, the "transient calorimeter" method will be introduced briefly. The transient technique used in Knackstedt's experiments was extensively employed by Clausing et al. (1987). The technique uses polished aluminum plates as calorimeters to determine the rate of heating on a given surface. All plates are made from polished 6061-T6 Al and are 6.35 mm thick. Each plate is backed by 19 mm of styrofoam, bringing the total thickness of the apparatus to the 25.4 mm. Plates are equipped with 5 T/C's, average of them represents plate temperature. Due to the high conductivity of the plate, the lumped capacitance method can be used (Laleman et al., 1992). Equation (2.19) shows the initial energy balance for the calorimeter.

$$m_p Cp_p \frac{dT_p}{dt} = q_{conv} + q_{mass} + q_{rad} + q_{cond} \tag{2.19}$$

The left hand side of the equation represents the time rate change of internal energy in the aluminum calorimeter. The right hand side of the equation represents the energy gain and losses due to convective heat transfer (q_{conv}), mass transfer (q_{mass}), radiation (q_{rad}), and conduction (q_{cond}) respectively. Subscript "p" represents plate.

$$m_p Cp_p \frac{dT_p}{dt} = h_c A\left(T_\infty - T_p\right) + h_{mass} h_{fg} A(C_\infty - C_p) + h_r A(T_\infty - T_p) + \frac{k_{wall}}{\delta_{wall}} A(T_s - T_p) \tag{2.20}$$

Where h_c, h_r, and h_{mass} are convection, radiation and mass transfer coefficients, respectively. C is water concentration in the air [kg water/kg air]. Using heat and mass transfer analogies (details of these analogies will be discussed later in Chapter 3), the solution of above equation for h_c yields,

$$h_{mass} = \frac{hcD_a^{2/3}\alpha^{1/3}}{k_a} \tag{2.21}$$

$$h_c = \left[\left(\frac{h_{fg}D_a^{2/3}\alpha^{1/3}}{k_{air}}\right)(C_\infty - C_p) + (T_\infty - T_p)\right]^{-1}\left[\left(\frac{m_p Cp_p}{A}\frac{dT_p}{dt}\right) + h_r(T_\infty - T_p) + \frac{k_{wall}}{\delta_{wall}}(T_s - T_p)\right] \tag{2.22}$$

All variables in eqn. (2.22) are known except the time derivative of plate temperature, dT/dt, which will be obtained from experimental data. First, the average temperatures of each calorimeter plate are plotted with time during 180 seconds just after door opening. Then curve fit values are obtained, slope of this curve is the missing part, dT/dt, of eqn. (2.22). The curves are found linear, and the slopes of the curves therefore remain constant after first 5 s (Knackstedt et al., 1995), when the transient effects are dominant. By using this procedure, the convective heat transfer coefficients are obtained for each plate. Experiments are repeated for three different wall temperatures, changing in between from 0 to 10 °C, and variety of shelf configurations. No shelf, one shelf, two shelves, and three shelves cases and their all-possible configurations are examined. Ambient temperature is 22 °C and it is kept constant during all experiments. The average heat transfer coefficients of every individual compartment are obtained by using Knackstedt et al. (1995)'s raw data, given for plate by plate. Results are summarized in Appendix B.

The cabinet geometry and input data, which is taken from Knackstedt's experimental studies, are given in Table 2.6. Also shown in Table 2.6 is the refrigerator geometry of a cabinet used in the present experimental study.

Table 2.6 Geometry of the Freshfood cabinets used in experimental studies

	Knackstedt's study	Present Study
Height, L (m)	0.7239	0.94
Width, W (m)	0.6985	0.67
Depth, D (m)	0.4953	0.63
Area of shelf (one side only) (m^2)	0.346	0.422
Area of rear wall (m^2)	0.506	0.63
Area of side wall (m^2)	0.359	0.592
Area of floor (m^2)	0.346	0.422
Volume of cabinet (m^3)	0.25	0.4
Characteristic length (L_{chr})	0.7239	0.94
k_{air} (W/mK)	0.02516	0.02516
ρ_{air} (kg/m^3)	1.23	1.23
$C_{p,air}$ (kJ/kgK)	1.006	1.006
Ambient temperature (K)	295	294-298
ΔT	18.5 K	18-20 K
Heat transfer area, As (m^2)	1.915	2.658

2.3.2 Tuning and verification of the model for no-shelf case

Knackstedt's results are used to tune the parameters in the model formulated in the previous section. The model has been run for a variety of conditions. Appendix B contains data used for model validation.

In the equations from (2.12) to (2.15), Re_c, C_D and C_{Di} are tuning parameters that will be adjusted by comparing to Knackstedt's (1995) data. As far as appropriate values, we would expect $Re_c<1000$ (where various outside influences relative to flow over a flat plate or in a channel, e.g. flow turnings etc.) would cause early destabilization to turbulence. For C_D and C_{Di}, values of unity indicate a pressure drop of a "velocity head", i.e. flow running in to an object loses its velocity in mean flow direction. C_D and C_{Di} values greater then unity indicate that velocity head is lost more than once, e.g. if each "turn" in the cabinet (~3) must be restarted, then C_D will be approximately 3. If flow turning or flow around object is more efficient (that is only partial separation around object), then drag coefficient will be less then unity. In refrigerators, the goal should be to get large C_D's in order to obtain slower cavity flow, similar to a parachute. This is a different goal than airplane, car, and other similar systems.

The results of Knackstedt's experimental studies are given in details in Appendix B. After obtaining these data, EES® has been run for following parameter range;

Re_c: from 100 to 1000
C_{Di}: from 1 to 10

All of the other values including geometry and air properties are given in Table 2.6. Comparison of the results from EES® simulations and data of the no shelf studies, given in Table 2.9, allows values for the drag and turbulence terms to be determined. Both velocity and temperature profiles on the door-opening plane showed that the inflow and outflow areas are not symmetrical, (all researchers agree on this observation). This phenomenon can be explained as follow. The Rayleigh number range that refrigerator cabinets operate in tends to be one where the flow continues to accelerate within the cabinet. The higher velocity outlet air requires less area then the slower moving inlet air. In addition, the relation between boundary layer thickness and heat transfer coefficient needs to be improved. In order to take into account these observations, eqns. (2.12), (2.17), and (2.18) have been rearranged as shown in Eqns. (2.23), (2.24), and (2.25).

$$U = \left(\frac{\beta \rho_\infty g (T_\infty - T_{ave}) LWD}{\rho_{ave} \left(\frac{A_s}{Re_c} + \frac{1}{2} (C_D A_n + C_{Di} A_F) \right)} \right)^{1/2} \qquad (2.23)$$

$$h = \frac{k}{\delta_T} \cong C_1 \frac{k}{\delta} \qquad (2.24)$$

$$m = (1/2)\, C_2\, A_F\, \rho_{ave} U \qquad (2.25)$$

Here,

C_1 : Correction for convective heat transfer coefficient versus linearized boundary layer thickness relation.

C_2 : Correction for frontal area percentage which is used for inflow. C2=1 indicates inflow and outflow occupy equal portion of opening (%50-%50 case).

Each of these parameters is evaluated and the results obtained are listed in Appendix C. Each coefficient is checked to determine how it affects the flow and heat transfer characteristics. The results are compared to Knackstedt et al. (1995)'s data. Correction coefficient values that give the reasonable predictions for velocity and heat transfer values are determined. The final coefficients are given in the Table 2.7. As it is seen from the table, C_2 is obtained as 1.5, which indicates that the inflow air occupies 75% of the door-opening area (A_F). Since there is no experimental data, the C_D value, which is the drag coefficient for the flow over objects, is not given in the table. However, it is recommended that C_D can be taken as unity for initial calculations.

Table 2.7 Final correction coefficients
(no shelf case only)

Rec=330
C_D= not defined (*)
C_1=4.95
C_2=1.5
C_{Di}=1.8

(*) Although C_D is not defined yet, it is recommended to take as unity for initial studies.

Then, eqns. (2.22), (2.23), and (2.24) are rearranged as follows for no shelf case,

$$\boxed{U = \left(\frac{\beta \rho_\infty g (T_\infty - T_{ave}) LWD}{\rho_{ave} \left(\frac{A_s}{\mathrm{Re}_c} + \frac{1}{2}(C_D A_n + 1.8 A_F) \right)} \right)^{1/2}} \qquad (2.26)$$

$$\boxed{h = 4.95 \frac{k}{\delta}} \qquad (2.27)$$

$$\boxed{m = (0.75) A_F \rho_{ave}} \quad (2.28)$$

After obtaining eqns. (2.26-2.28), further studies have been done in order to understand the effect of wall and ambient temperature on flow characteristics. The results have been shown in following figures and tables.

Table 2.8 The effect of wall temperatures on the flow characteristics for no shelf case (*).

T_w [°C]	h[W/m²K]	h_{plate}(**)	Qh [W]	Nu	Nu_{plate}(**)	u [m/s]
2	3.58	4.07	128.8	103.8	117.9	0.138
3	3.48	4.00	119.1	100.9	115.9	0.135
4	3.39	3.93	109.7	98.0	113.8	0.131
5	3.29	3.87	100.5	95.0	111.6	0.127
6	3.19	3.79	91.63	91.9	109.3	0.123
7	3.08	3.72	83.03	88.8	107	0.119
8	2.98	3.64	74.73	85.5	104.6	0.115
9	2.86	3.56	66.73	82.2	102.1	0.111
10	2.75	3.47	59.05	78.8	99.42	0.106
11	2.63	3.38	51.69	75.2	96.63	0.102

(*) Ambient temperature, T_∞=21.85 °C.
(**) Average values for vertical flat plate, which has same height with cabinet, obtained from the correlation of Churchill and Chu (1975).

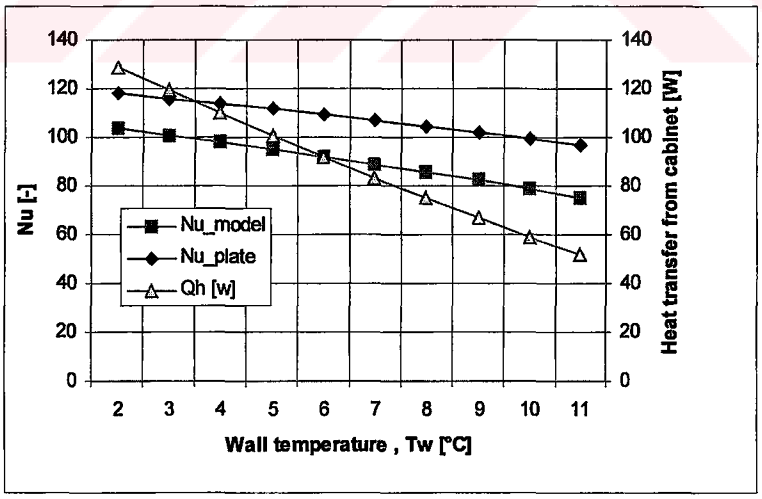

Figure 2.6 The effect of wall temperature on the heat transfer coefficients, for no shelf case (T_∞=21.85 °C).

From the Figure 2.6, it can be seen that the cavity average Nu number is almost parallel to the vertical plate values. (This trend of the model will later be reexamined by formulating the Re_c in terms of cavity height, L (see Chapter 2.5).

2.3.3 Tuning and verification of the model for multi-shelf case

The model for a cavity with no shelf is extended to allow a cabinet with shelves. The primary effects of shelves are in the cavity drag and heat transfer surface area. It should be noted that the shelf supports are equally spaced for all experiments as it is seen from the Figure 2.7.

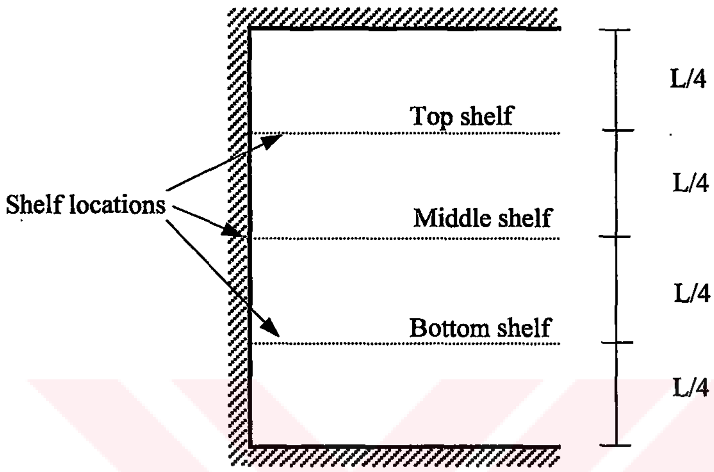

Figure 2.7 Schematic representation of shelf locations in the cabinet. Maximum numbers of the shelves are three. L is cavity height.

In order to obtain the general form of equations it is sought to find a relation between tuning coefficients and number of shelves. The cavity average heat transfer coefficients are obtained for each shelf configuration. Experimental velocity profiles at the door opening plane showed that the number of the shelves primarily effects the percentage of the inflow area (velocity profiles are given in Chapter 2.4). In addition, the drag coefficient is affected by the flow direction changes. Therefore, the tuning coefficient C_2 that represents the inflow area percentage is modified. The correlation between tuning coefficient C_2 and the number of the shelves is obtained as;

$$C_2(n) = 1.5 - 0.32n \tag{2.29}$$

The following equation shows the relation between the number of the shelves and the drag coefficient.

$$C_{Di}(n) = 1.8047e^{(0.6328n)} \tag{2.30}$$

By using these relations (Eqn. 2.29 and 2.30), multi-shelf cabinet flow and heat transfer can be modeled. One can obtain the flow characteristics by using the general form of the equations. In Table 2.9, the experimental results are compared to predicted values.

Table 2.9 Cavity average Nusselt number comparisons.

	Experimental		Model	
	Tw_cavity	Nu_cavity	Nu_cavity	Error %
No shelf				
	0.8	99.2	103.7	4.6
	3.5	91.2	96.6	5.9
	5.4	95.7	91.3	-4.6
	9.8	95.6	77.9	-18.5
One shelf				
	0.2	80.3	94.7	17.9
	1.5	88.6	91.7	3.5
	9.6	73.7	70.8	-4.0
Two shelves				
	-0.2	76.8	92.4	20.2
	3.0	91.2	85.2	-6.6
	7.8	70.2	73.4	4.6
Three shelves				
	-0.9	64.1	87.4	36.5
	3.1	81.8	79.2	-3.1
	7.8	65.6	68.4	4.3

A comparison of all experimental data and model results for number of the shelves are shown in the Figure 2.8. The details of experimental data are also given in Appendix D.

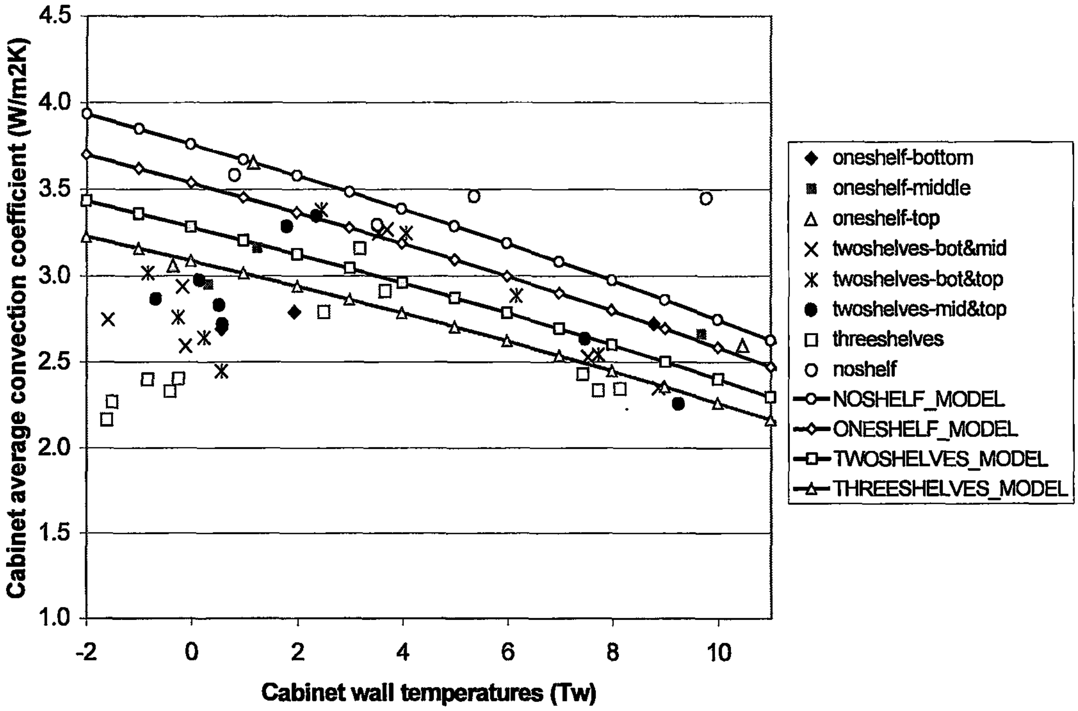

Figure 2.8 Cabinet average heat transfer coefficients. Experimental data and model results are shown together. Details of experimental results are given in Appendix D.

As it can be seen from Table 2.9, a maximum error (36%) appears for wall temperatures below or around freezing temperature. Knackstedt et al. (1995) did not indicate any frosting on the calorimeter plates during their experiments for low plate temperatures. In addition, Tao et al. (1993) observed no frost formation on the flat plate for the temperature as low as -5 °C at ambient temperature of 20 °C. Since the frost formation is less likely to be occurred, the reason for the high error levels can be explained as; either the presence of subcooled condensate on the plates, or the heat and mass transfer analogy is not applicable for this region. Since the Eqn. (2.22) does not take into account this phenomenon, the experimental data might be erratic on this region. The error for other wall temperatures is generally around ±5%.

2.3.4 The effect of cavity height

In order to understand the effect of the cavity height, the experimental data from no shelf to three shelves is reviewed. For each case, the top shelf region remains unaffected from the other shelves. Lower shelf regions are affected by the flow of the higher shelf cavities. Therefore, the top shelf compartment of each shelf configuration can be treated as if it is an individual cavity. By sorting Knackstedt's (1995) experimental data, Figure 2.9 is obtained. Further details are also given in Appendix E.

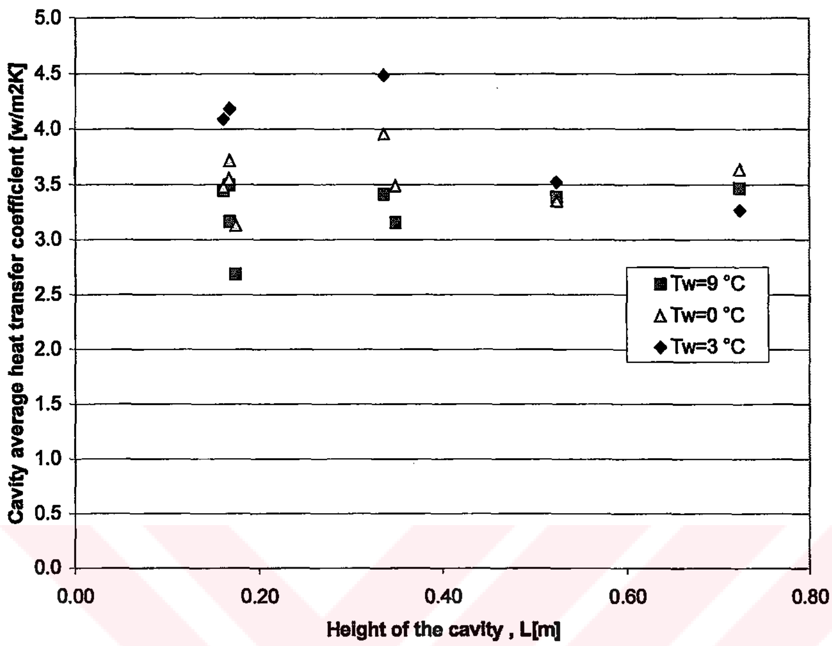

Figure 2.9 Experimental heat transfer coefficient vs. cavity height for three different wall temperatures

The data in the Figure 2.9 looks scattered, and there is no definitive pattern observed. However, it would be approximately true to assume the heat transfer coefficient remains constant with changing cavity height for the same wall temperature. This observation is compatible results from Skok et al. (1991). In addition, air velocity measurements show a similar trend with the inflow air velocity almost constant over different cavity heights (see Chapter 2.4).

This may be because the buoyancy force remains unchanged with changing cavity height. It should be noted that this is true only when other dimensions of cavity remains same. Because the heat transfer and fluid mechanics problems are coupled, the overall effect of height cannot be directly seen from either equation. However, it can still be said that the multiplication of temperature difference and cavity height in the equation (2.26) remains constant with changing cavity height. On the other hand, the surface area of the cavity also increased and therefore the friction force, acting against flow, increases as well. However, since the friction force is not dominant comparing to the others this effect is ignored.

The results of equations from (2.26) to (2.28) are compared to experimental data. The error between model predictions and the experimental results are found to be increasing monotonically with the cavity height. Apparently, the model does not have the capability to model cavity height changes. The critical Reynolds number (Re_c) parameter is chosen as a correction term. The critical Reynolds number parameter adjusts the turbulence level of the flow. That is, boundary layer is affected by changes of critical Reynolds number. The goal is to express Re_c as a function of the cavity height. After numerous runs on the EES®, Re_c is found to be as given in the following equation.

$$Re_c = 402.17 - (98.898)L \qquad (2.31)$$

In this equation, the unit for L is [m]. Using this relation, the model has been run for different wall temperatures. The results are shown in Figure 2.10.

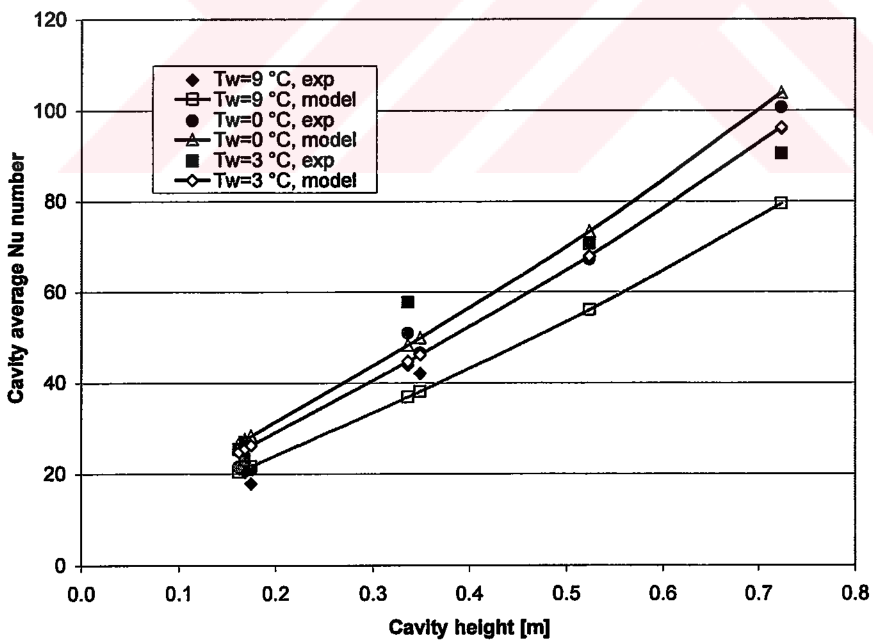

Figure 2.10 Comparison of experimental and predicted cavity average Nu number values for different cavity heights.

The comparisons of the results are also shown in tabular form in Appendix E. According to these results, the error remains under 20%, except one case, which is

40%. This exceptional data is at a wall temperature of (–1.7)°C. Therefore, as previously indicated, this difference is most likely because of either presence of frost or subcooled condensate on the calorimeter plates.

2.4 Experimental Studies

2.4.1 Experimental setup and procedure

In order to understand flow and heat transfer characteristics of a typical refrigerator cabinet (Freshfood cabinet), velocity and temperature values at the door-opening plane are measured. All experiments are carried out in room temperature, which is roughly between 22-25 °C. Velocity measurements are made with a hand held anemometer and temperature measurements are made using type "T" thermocouples (T/C). The experimental studies examined the following configurations:

- No shelf
- One shelf at 11.5 inches (292 mm) from top
- One shelf at 26.5 inches (673 mm) from top
- Two shelves at both 11.5 inches (292 mm) and 26.5 inches (673 mm) from top

The total height of cabinet is 37 inches (940 mm). In the beginning of a door opening, the Freshfood cabinet air temperature was kept approximately 2.7-3.5 °C in the center location while average wall temperature is 3.5-5.2 °C. The experimental set-up is shown in Figure 2.11.

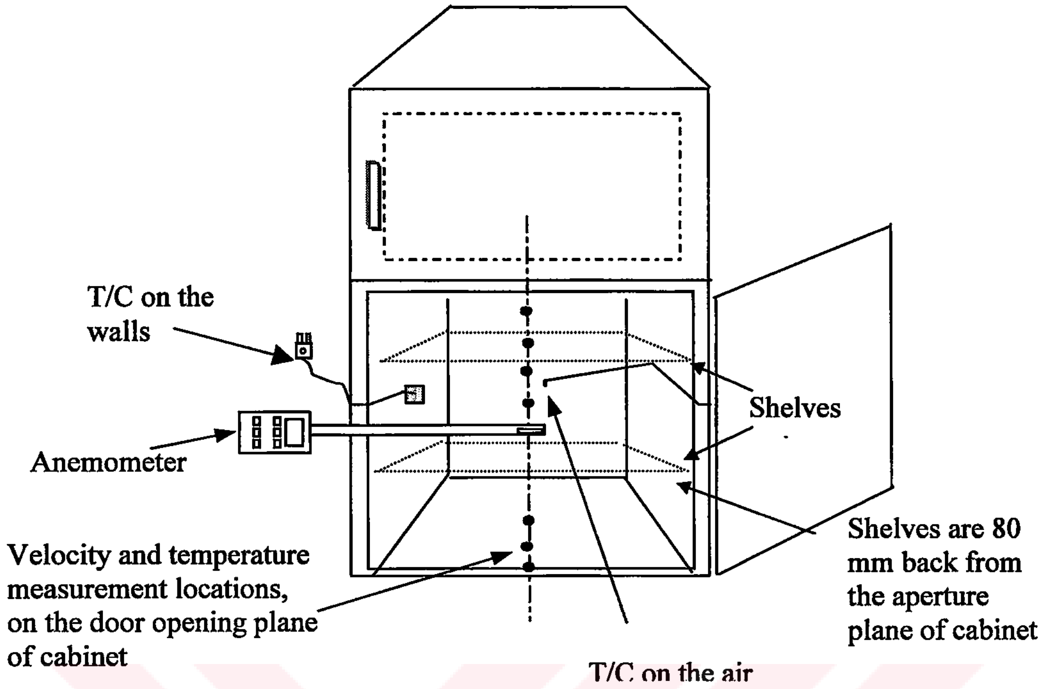

Figure 2.11 Experimental set-up

The experimental procedure:

Air velocity and temperature measurements are made separately according to following procedure.

Step.1) Refrigerator is set to lowest FF thermostat level and left running until the wall temperature decreases below 1 °C.

Step 2) The door is opened and a foam cover placed over the FF damper outlet to prevent back flows from Freezer section. Then, the door is closed and the refrigerator is unplugged.

Step 3) When the temperature at the center of FF reaches 2.7 °C (at this time the wall temperature would be around 3.6 °C) the door is opened and the velocity sensor is placed immediately at the measurement location. The tip of anemometer sensor is covered with a piece of aluminum foil to prevent the air movements during placement of the sensor in its location. The foil is removed slowly just before the first data is taken.

Step 4) While keeping the sensor tip at the same location, velocity data is taken for 80 seconds. Data is collected every 2.5 s.

Step 5) After finishing all velocity measurements, temperature measurements are made repeating the steps 1 to 3. In this case, all temperature data from 28 T/C's are recorded simultaneously after the door is open.

2.4.2 Experimental results

2.4.2.1 Results of velocity measurements

All data obtained from measurements are summarized in Figures from 2.12 to 2.16. In Figure 2.12, transient experimental data is shown for the no shelf case only. From this figure, all transients can be seen.

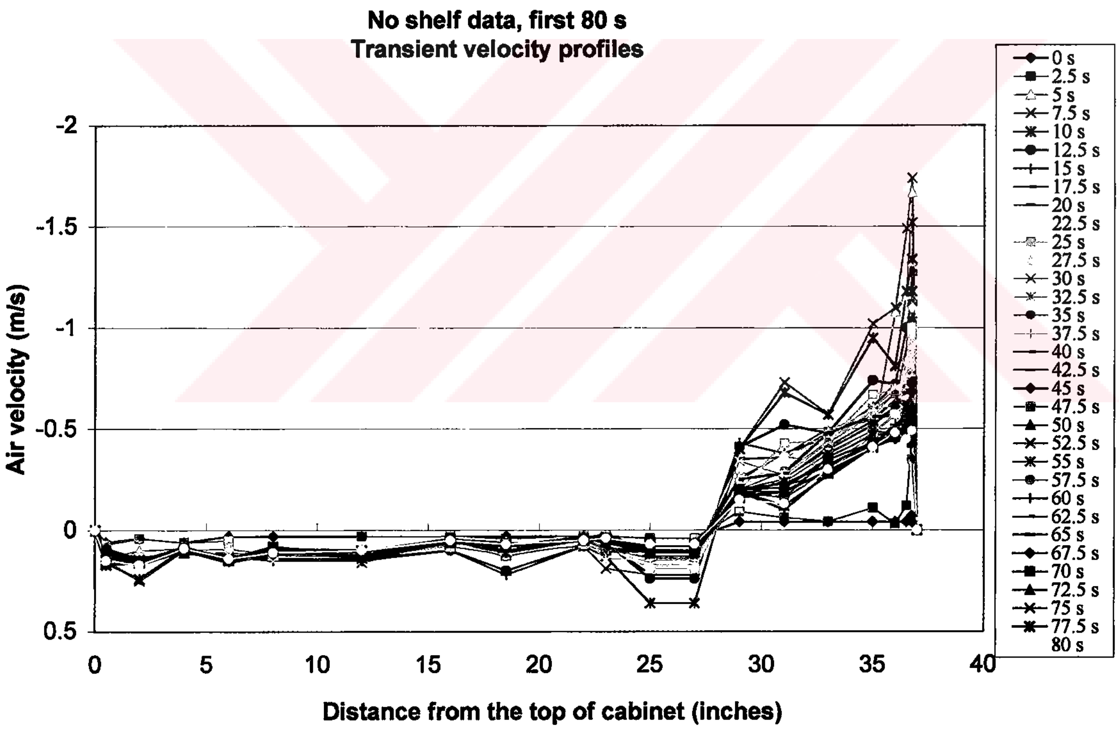

Figure 2.12 The transient velocity profiles at door opening plane (No shelf case). Minus sign represents outflow.

The maximum outlet velocity reaches its peak value of 1.7 m/s between 5 and 7.5 seconds. After this time, it can be assumed that the cold air in the cabinet is completely replaced by ambient air (one volumetric air change). Location of peak velocity is very close (approximately 5-6 mm) to the bottom wall of the cavity.

It is observed that after 10 seconds of door opening the intensity of the transients become weak. Figures 2.13 –2.16 support this observation. There is negligible difference between first 20 seconds average profile and last 40 seconds average profile. Details of the development of transient velocity profiles are included in Appendix G (no shelf case) and Appendix H (one shelf on top case). In order to avoid effects from transients and other fluctuations, the time average profiles are obtained in the Figures 2.13 to 2.16. Time averaging is made for the first 20 s, last 40 s, and all 80 s, respectively. Figures from 2.13 to 2.16 show the average velocity profiles.

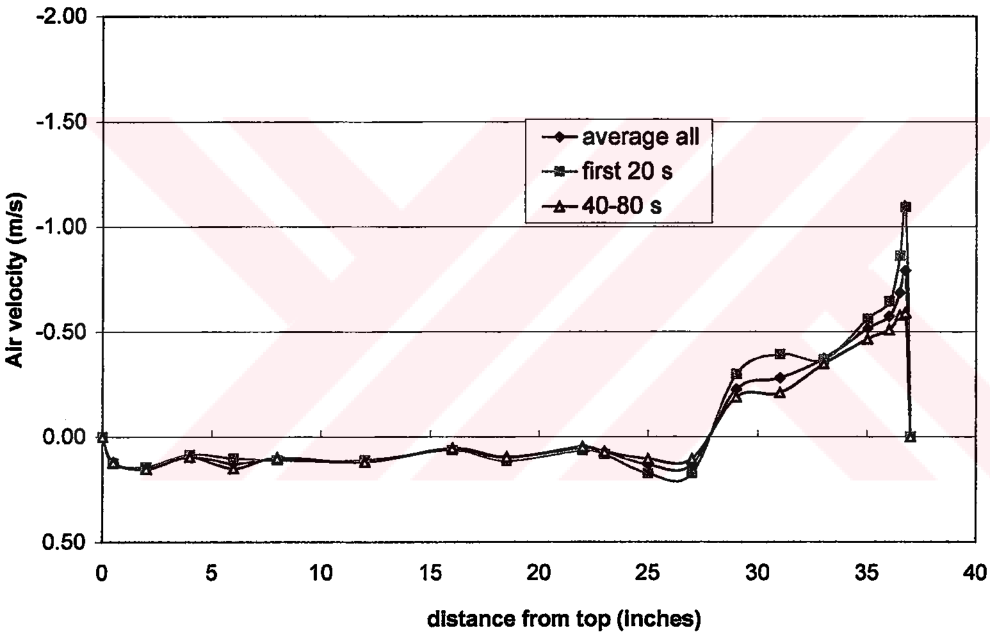

Figure 2.13. Cabinet no-shelf data, average velocity profiles. Minus sign represents outflow.

The air inflow (positive velocities) is very steady and uniform for all shelf configurations while outflow velocity variations are significant especially at locations close to the wall. This result is very important for flow modeling studies. The modeling of inflow, which is almost steady, is becomes relatively easy job. Outflow velocities are complex (especially with shelves) because part of some flow spilling out of a shelf may be drawn into lower shelf regions.

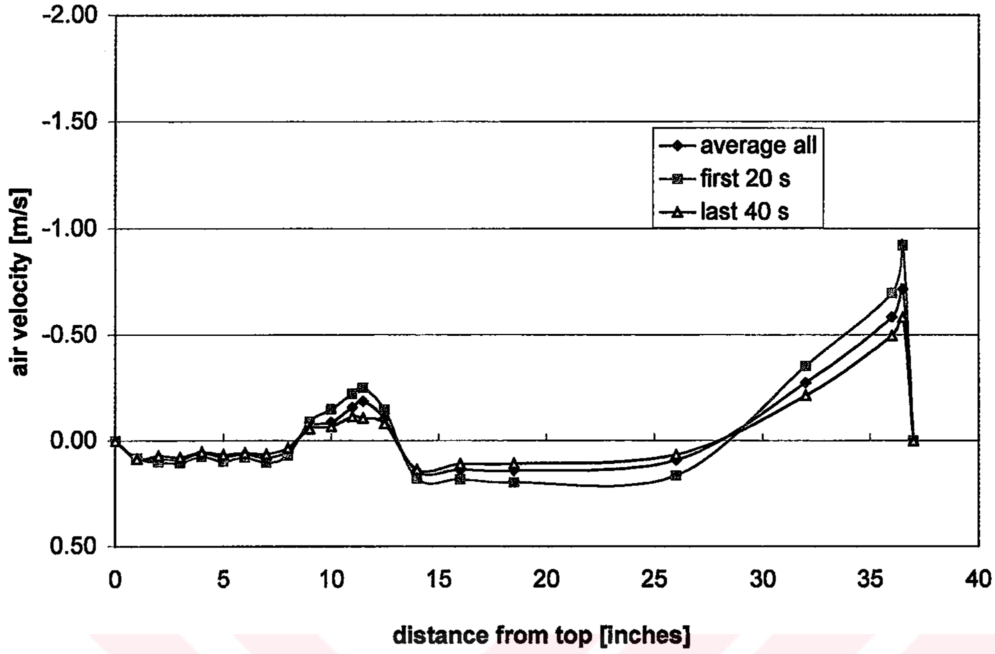

Figure 2.14 Cabinet one shelf on top data, average velocity profiles. Minus sign represents outflow.

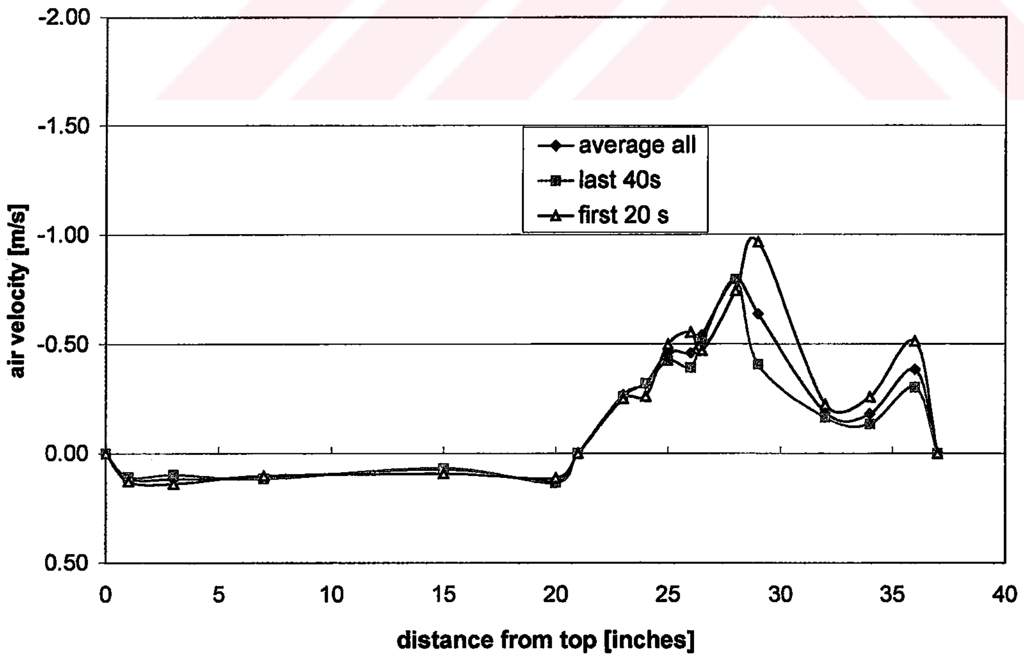

Figure 2.15 Cabinet one shelf on bottom data, average velocity profiles. Minus sign represents outflow.

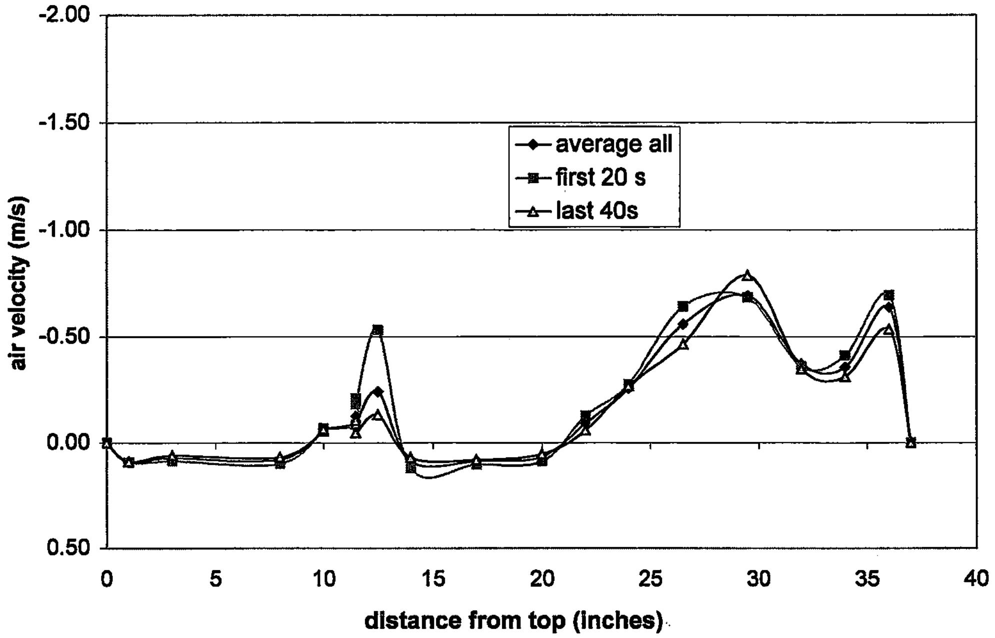

Figure 2.16 Cabinet two shelves data, average velocity profiles. Minus sign represents outflow.

Estimation of the location between inflow and outflow is important. During the velocity measurements, lightweight threads hanging on the top of cabinet are used to visually identify the flow switching point. It is also observed that measured outflow velocities are higher then the theoretical maximum values, which can be obtained from following definition.

<u>Definition of Maximum flow velocity</u>: The maximum velocity for a cavity whose height L is can be derived by using energy equation (White, 1991). Briefly,

Kinetic energy = Maximum potential energy

$$\frac{1}{2}\rho_{ave}U^2 = \frac{1}{2}\rho_\infty g\beta(T_w - T_\infty)L \qquad \Rightarrow \qquad U_{max} = \left(\frac{\rho_\infty g\beta(T_w - T_\infty)L}{\rho_{ave}}\right)^{1/2} \qquad (2.32)$$

For instance, for no shelf case the maximum measured velocity is 1.8 m/s and it is calculated as 0.7 m/s by using the Eqn. (2.32). This difference may be explained by the transient limitations of the anemometer. However, this result is valid mostly during the first 10 seconds after door opened when the outlet temperature changes rapidly. After 20 seconds, the temperature fluctuations that disturb the velocity measurements become relatively negligible. The steady state weighted average outflow velocities drop to approximately 0.3 m/s. This value is reasonable when we compared the inflow mass flow rate and corresponding outflow mass flow rate.

2.4.2.2 Results of temperature measurements

Similar to velocity measurements, temperature data have been collected. The temperature profiles on the door-opening plane is obtained for different shelf configurations. These profiles will help understanding the location of air inflow and outflow for different shelf configurations. For this purpose, thermocouples are located as listed in Appendix I. The results are given in Figures from 2.17 to 2.20.

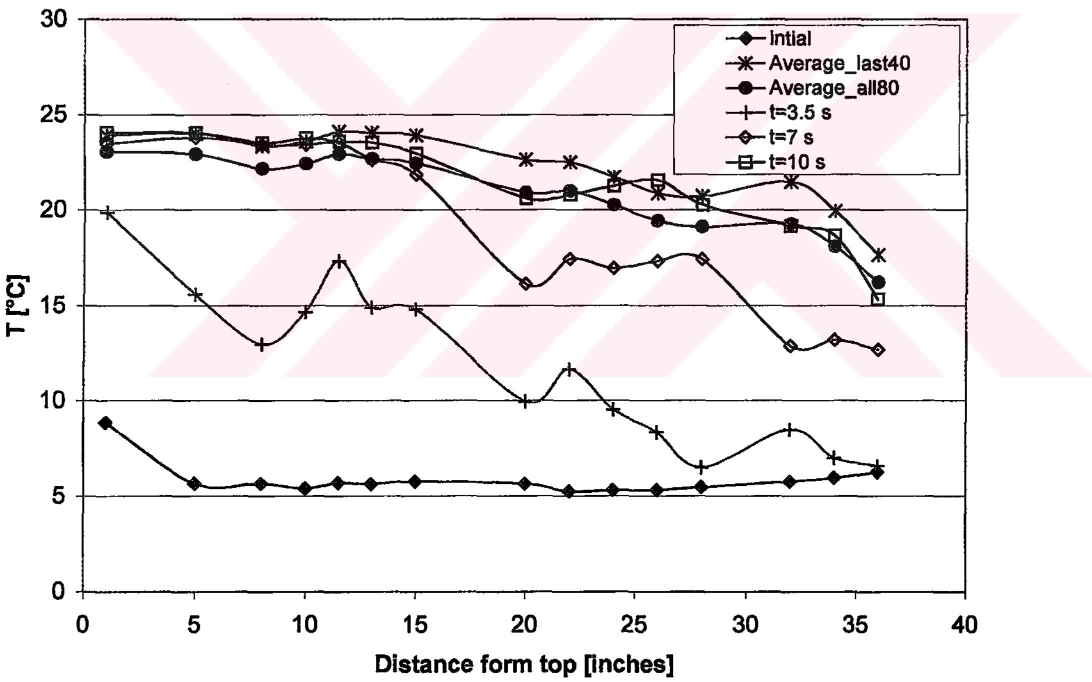

Figure 2.17 Temperature profiles for cabinet no shelf data, on the door-opening plane for different time intervals

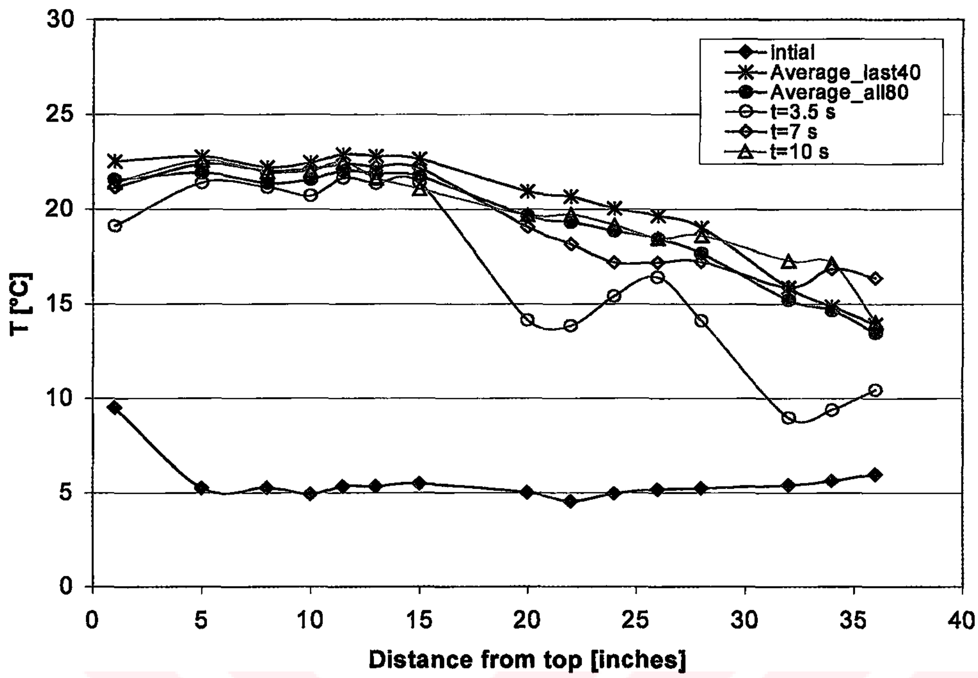

Figure 2.18 Temperature profiles for cabinet one shelf on bottom data, on the door-opening plane for different time intervals.

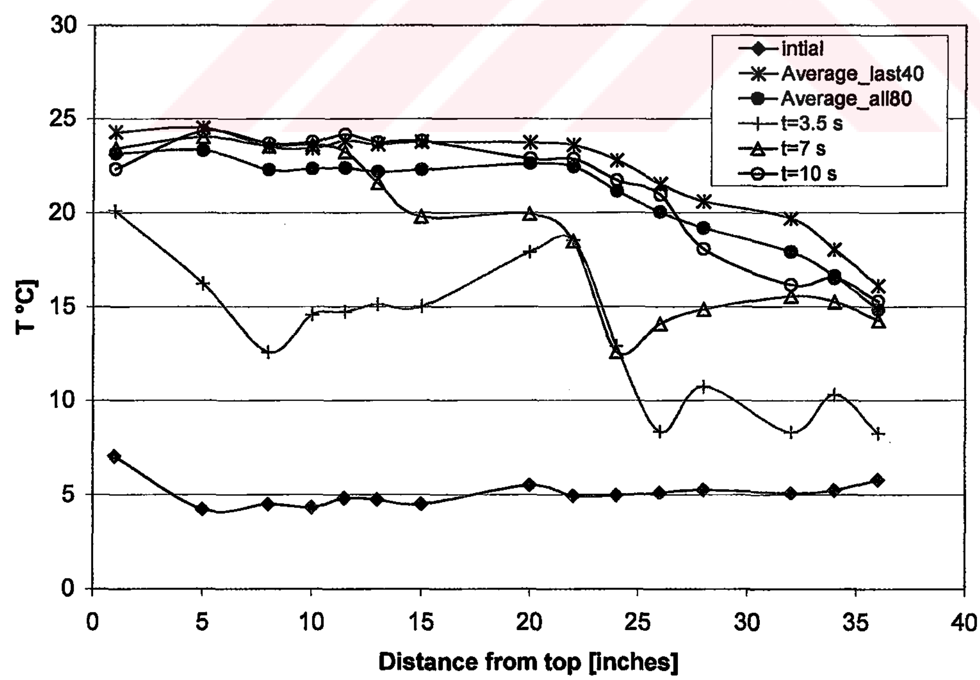

Figure 2.19 Temperature profiles for cabinet one shelf on top data, on the door-opening plane for different time intervals.

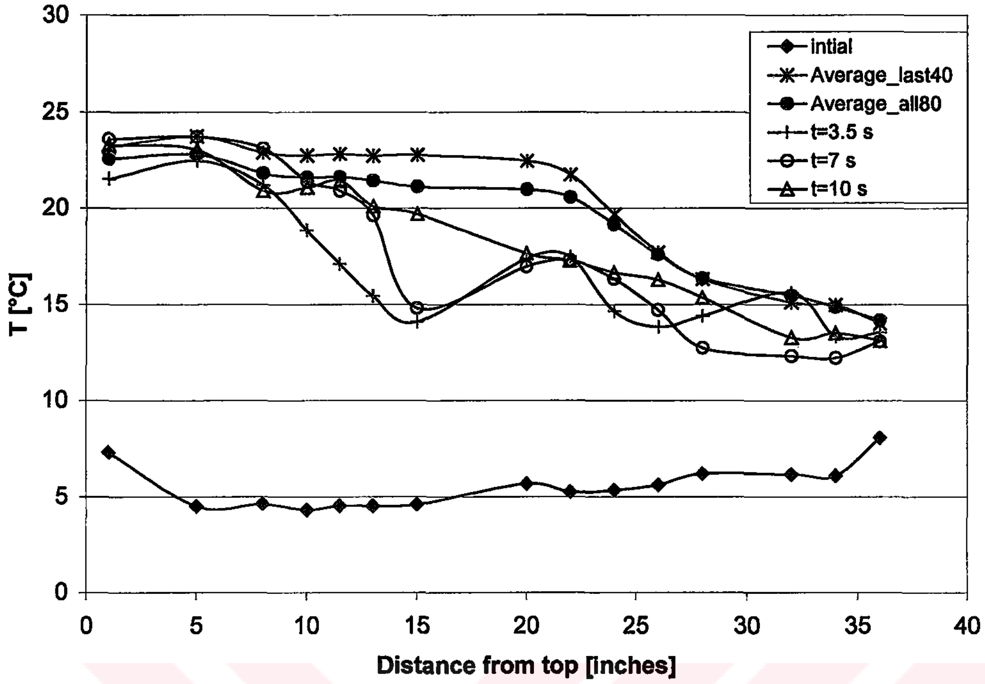

Figure 2.20 Cabinet two shelves data, temperature profiles on the door-opening plane for different time intervals.

Figure 2.21 shows the transient behavior of temperature over the door opening time period. Figure 2.21 is given only for no-shelf case. By using these transient profiles, it is possible to classify flow regimes as follow;

Flow regimes: Open-door refrigerator cavity flow can be classified by three respective flow regimes. Both velocity and temperature profiles are used to support these classifications (see Figure 2.12 and 2.21). Although transient values are given only for the no-shelf case, these comments are also valid for the one and two shelf cases. These regimes are:

I- Initial Transient Period: This period starts with door opening and finishes after 7-10 seconds. During this time while cold air drains from the bottom portion of the cabinet, at same time fresh air enters the top portion of cavity. This period is assumed to end after one volumetric air change. During this period both inlet and outlet air velocities are high. Furthermore, both temperature and velocity values have high transients (see figures 2.12 and 2.21). Change of temperature and velocity values are not linear with respect to time.

II- Transition Period: This period occurs from 7-10 seconds to 20 seconds after the door is opened. During that time, temperature and velocity linearly approach their quasi-steady values. While the wall temperature changes, the steady values also change (see Figure 2.12 and 2.21).

III- Quasi-Steady Period: After 20 seconds, the flow can be assumed steady state if average wall temperatures remain constant. As long as wall temperatures are relatively constant, both velocity and temperature values are steady (see Figures from 2.13 to 2.21). For modeling purposes, it would be satisfactory to define quasi-steady values for every 20 seconds with regards to average wall temperatures over this duration. Modeling studies are made only for this period.

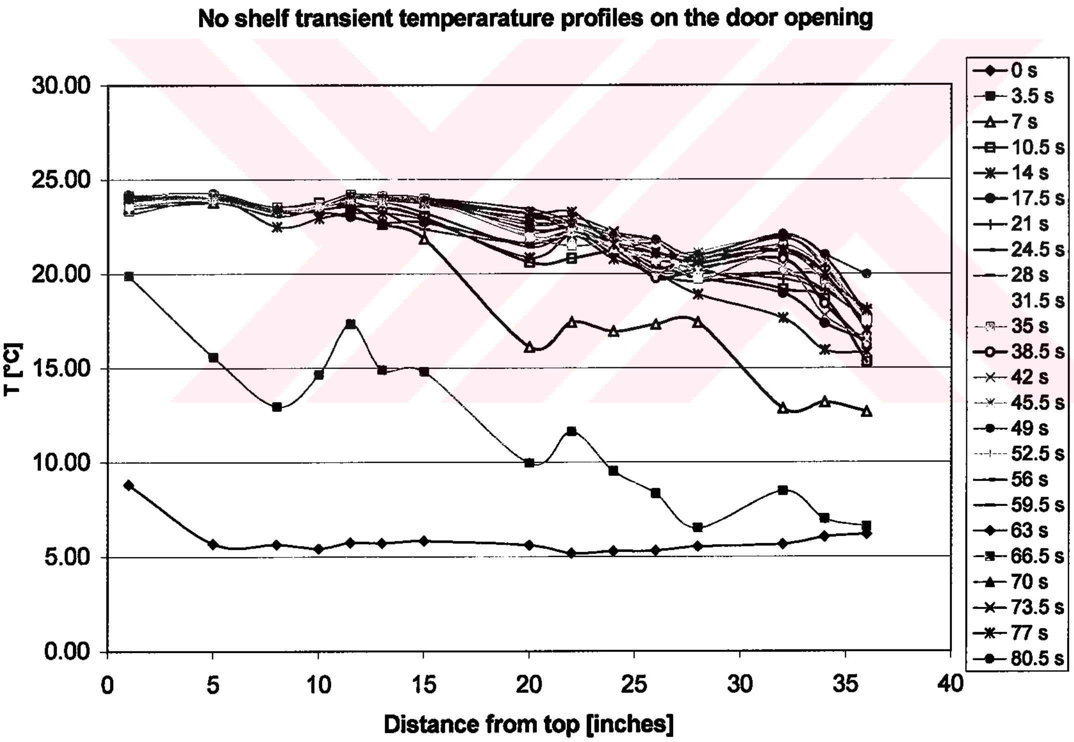

Figure 2.21 Transient temperature profiles on the door opening for no shelf case

<u>Comparison of present model and experimental studies:</u> Comparisons are made for the no shelf data in Table 2.10.

Table 2.10 Comparison of results of the model and experimental studies

	Model (Eqns. 2.26 to 2.28)	**Experiments**	**Error %**
Inlet air velocity ,U [m/s] (T_a=20°C, T_w=5°C)	0.15	0.12	+25
Outlet temperature, T_o [°C] (T_a=24°C, T_w=8.3 °C)	22.1	20.66	+7%
Mass flowrate, m [kg/s] (T_a=20 °C, T_w=5°C)	0.082	0.068	+24%

In Table 2.10, air velocity comparisons are made only for inflow, because the inflow temperature and velocity are steady. Although velocities are estimated at relatively high error levels, it is believed that most of the errors come from the uncertainty of the probe for very low velocities. The outlet average air temperature is estimated as less then 7% error.

2.5 Conclusions of Open Door Flow and Heat Transfer Studies

1) A physical model for estimating cavity flow and heat transfer characteristics is introduced. The model results are summarized in the equations numbered from 2.26 to 2.28. Presented model's validation is based upon Knackstedt et al.'s (1995) experimental results. The model is formulated for the no shelf to three-shelf cavity conditions. Therefore, it is recommended to use the model for cavities of which aspect ratio similar to domestic refrigerator's cabinet aspect ratio. Although there is no general convention, the inside depth of refrigerator cabinets (from back wall to door) basically changes from 0.4 to 0.65 m. And the inside width is from 0.5 to 0.7 m. Furthermore, the model is verified for cavity height from 0.16 m to 0.72 m. Aspect ratios for these ranges are as follow,

   L/D: 0.25 - 1.8
   L/W: 0.23 - 1.4

2) The model predictions have been compared to the no shelf case and multi shelf cases. No shelf, one shelf, two shelves and three shelves with their all-possible configurations are examined. From velocity and temperature measurements, the addition of a shelf decreases the inflow area percentage. The drag coefficient (C_{Di}) increases. This can be explained that the exiting air from upper shelves blocks the inlet air to lower shelves. This effect is taken in to account by adjusting the inflow area and cavity drag coefficients. Model verification results are summarized in Table 2.9. According to this table, the model agrees with experimental data with less then 10% error for the wall temperatures of 3 °C and 9 °C. However, the error increases to almost 30% for the wall temperatures less then 0 °C. In this temperature range, ice formation on the calorimeter plates may cause this error.

3) Skok et al.'s (1991) cavity average Nu number correlation ($Nu=0.087Ra^{1/3}$) indicates that the convective heat transfer coefficient remains constant with changing cavity height. Knackstedt et al.'s (1995) experimental studies also show same trend. However, presented model showed that estimated heat transfer coefficient is decreasing monotonically with increasing cavity height. In order to

correct this behavior, the critical Re number (Re_c) is used as correctional term. Re_c parameter expressed as a function of cavity height. This equation is given in Eqn. (2.31). The model agrees with experimental data with less then 20% error (See Figure 2.10, and Appendix E).

4) Knackstedt et al. (1995) used a "transient calorimeter method", and obtained the local heat transfer coefficients in a refrigerator cabinet. The average local heat transfer coefficients of individual data are sorted and reduced in to new formats. The results are summarized in Appendix B.

5) Model results are compared with literature values for similar conditions. Only empty cavity flow studies exist in the literature. Comparisons have been made only for the no shelf case. Vertical velocity and temperature profiles for the no shelf case agree with Skok et al. (1991), and Chan and Tien (1986a, 1986b). Both velocity and temperature measurements show that inflow and outflow areas are not equal for normal operation conditions of refrigerator. Approximately 25% of opening is occupied by outflow and the remaining 75% is occupied by inflow. For high Ra values of 10^7-10^8, outflow area percentage as low as 18 % have been indicated by some authors Skok et al. (1991), Chan and Tien (1986a), and Penot (1982). The difference in inflow/outflow area indicates the level of airflow acceleration within the cabinet.

6) The maximum velocity occurs at a point very close to bottom wall (approximately 5-6 mm from the wall). This observation is also supported by Penot (1982), Skok et al. (1991), and Chan and Tien (1985).

7) The effect of ambient temperature on flow characteristics is summarized in the Figure 2.22. Ambient temperature is changed from 16°C to 42 °C, and corresponding Ra number values obtained for x axis of the figure. Geometry of the cavity is given in first column of Table 2.6.

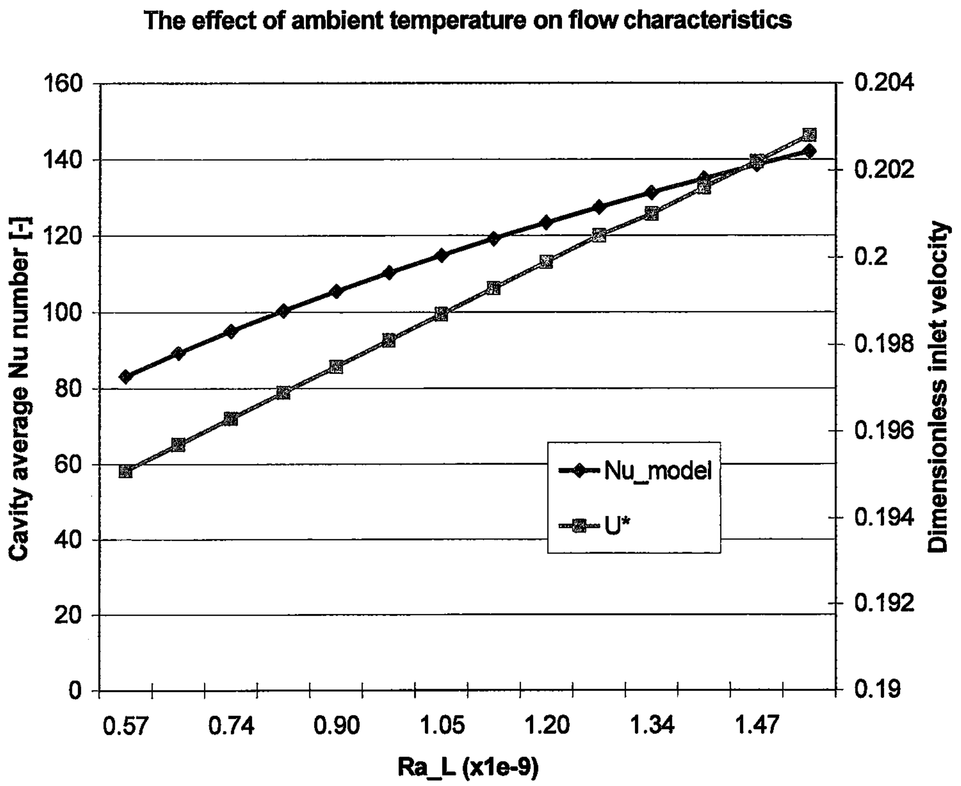

Figure 2.22 The ambient temperature effect on flow characteristics. U* is dimensionless velocity which is U/U_c, and $U_c=(g\beta(T_w-T_a)L)^{1/2}$.

8) The flow regime for an open cavity is classified as three characteristic periods. Those are *initial transient period* (0 to 7-10 seconds), *transition period* (7-10 to 20 seconds), and *quasi-steady period* (after 20 seconds). During the initial transient period, cold air in the cabinet flows out, drawing fresh air into the cabinet (like spilling a bucket). This period finishes after one volumetric air change established. During that period both inlet and outlet velocities are high. After one volumetric air exchange, the flow is mainly driven by wall temperatures. As wall temperatures increase, velocity decreases (see figures 2.12 to 2.16).

9) A comparison with literature data has been made for the no-shelf case. The results are given in Figure 2.23, compare the model to Skok et al. (1991), and Churchill and Chu (1975). In this figure the model is presented for three different wall temperatures while the cavity height changes from 0.17 to 0.92 m.

As it is seen from the figure, the difference between model and Skok's results increases with increasing Ra number. Skok's correlation is valid for Ra numbers between 10^4 and $1.2x10^9$. In the present study, the Ra number mostly close to upper limit of their correlation. The error 20% for Ra=$9x10^8$, 7% for $4x10^8$.

Generally, model predictions are greater then Skok et al.'s (1991) data. This may be because their experiment does not include side walls which have relatively high Nu numbers in general. In their study the effect of side walls are eliminated by using very wide cavity.

However, the model and vertical flat plate has almost parallel curves. The results of model become closer to vertical flat-plate values with increasing Ra numbers. This observation is compatible to Chan and Tien (1986a)'s results.

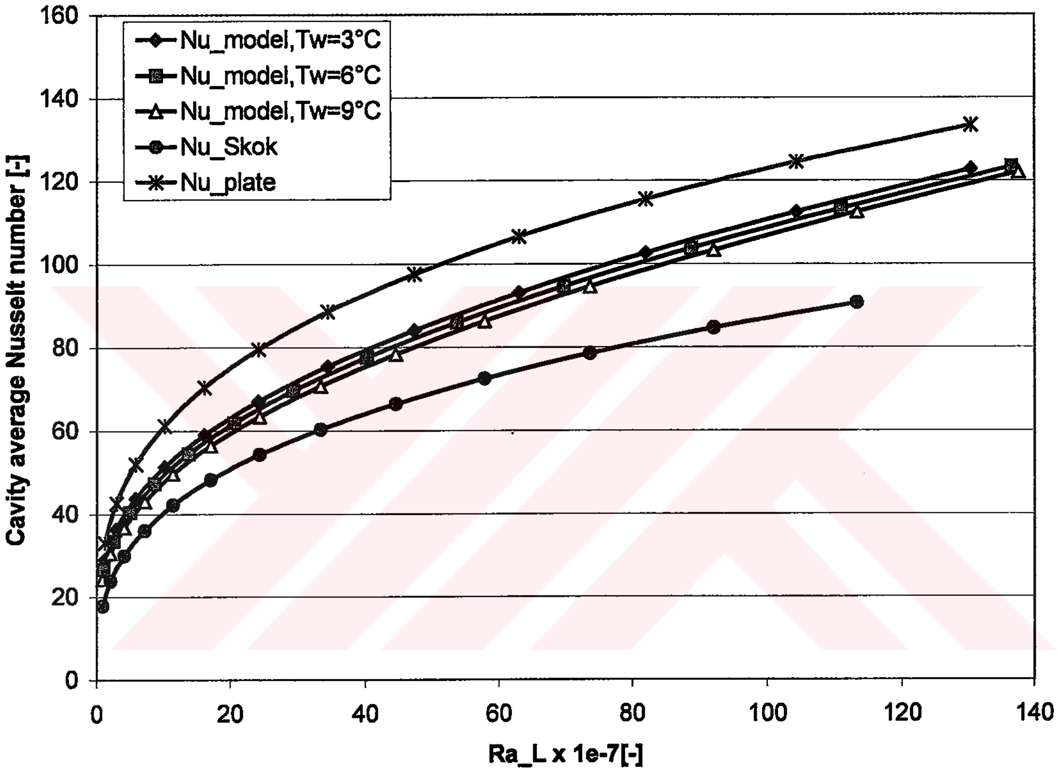

Figure 2.23 Comparison of the model estimations with Skok et al. (1991) and vertical flat plate results. Plate average Nu number is obtained from Churchill and Chu (1975). Ambient temperature is 25 °C.

10) The effects of the shelves on the cabinet air and wall temperatures are summarized in Figure 2.24. The presence of shelves keeps the cabinet and walls colder then the no-shelf case. Another interesting result is when one shelf is located on top of the cabinet, the air and wall temperatures are warmer than when it is located bottom. This phenomenon can be explained as follow, relatively colder exiting air temperature from one shelf portion makes an air curtain effect for the shelves below it and keeps underneath compartments colder.

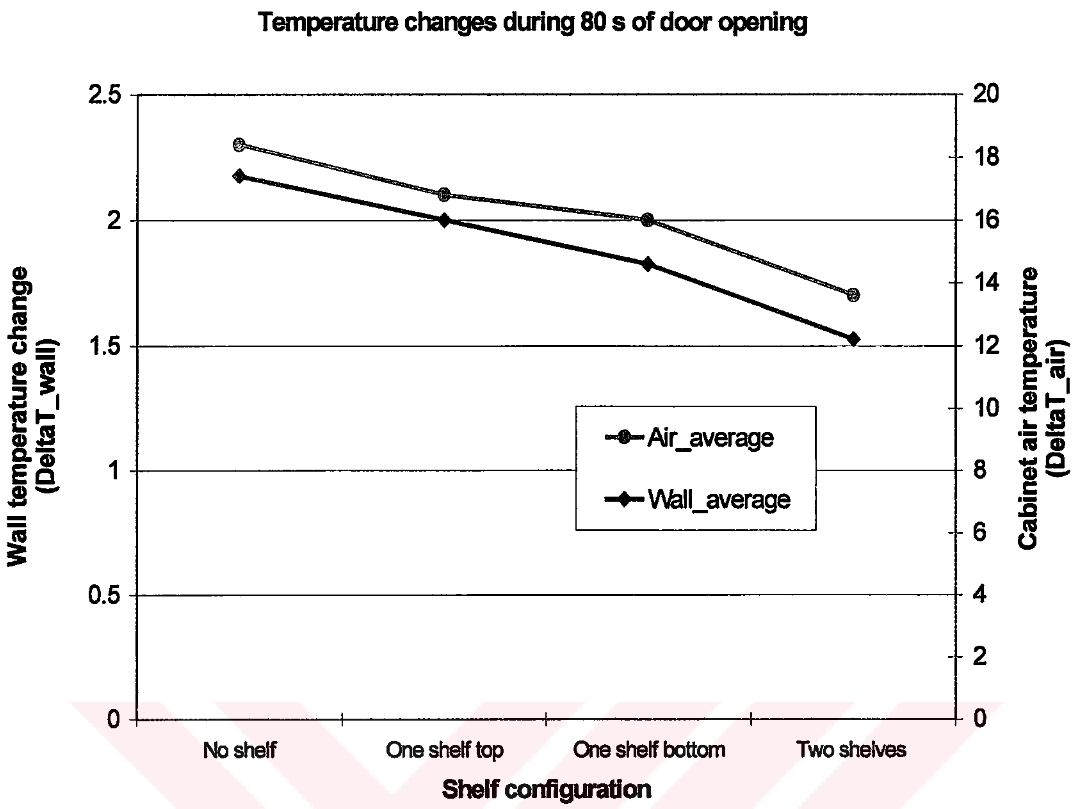

Figure 2.24 The change on cabinet air and wall temperatures during 80 s of door opening. DeltaT is the difference between average temperature of last 40 s and the initial temperature ($DeltaT=T_{last40s}-T_{initial}$).

From Figure 2.24, the maximum temperature increase on wall temperatures is 2.27 °C during 80 seconds of door opening time (this value is measured as low as 1.74 °C). In addition, this difference is maximum 0.4 °C during 20 seconds of door opening time. These results show that, it is acceptable to take wall temperatures constant for the first 20 seconds. Of course, this assumption will make modeling studies easier.

11) At the bottom of each shelf, temperature and velocity fluctuations are observed (see figures from 2.12 to 2.16). It is obvious that in this region the flow is three-dimensional. Therefore, a simple anemometer is not sufficient for measurements. Knackstedt et al.'s (1995) flow visualization of refrigerator cabinets show this transient characteristics.

Some additional comments are listed below.

1) Hot film anemometers, as used in this study, are only accurate for isothermal studies. Therefore, on the applications that have high temperature fluctuations such as open door velocity measurements will have significant errors. Other temperature insensitive flow measurements, such as Laser Doppler Anemometry, should be used.

2) From the studies, it is observed that the depth of each shelf is important. In the present studies, depth of the shelves is 80 mm shorter then the cabinet depth. This allows 80 mm clearance between door inner surface and shelf front edge. The increase on this value creates more air-curtain effect for underneath shelves.

3) In the buoyancy force definition, which is given in equation 2.6, L ,cavity height, is characteristic length and W.D is bottom area of the cavity. The result of multiplication of these lengths is volume of the cavity. This will emphasize that either of the cavity lengths will affect the buoyancy force equally. In order to see the difference, the study can be repeated by replacing "W.D" term of Eqn. 6 by "W.L" which is opening area of the cavity.

CHAPTER-3

MASS TRANSFER IN THE REFRIGERATOR AND ANALYZES OF HEAT TRANSFER MODES THROUGH DOOR OPENING

3.1 Background and Literature Survey

Condensation and evaporation of water on surfaces are common problems of HVAC industries. The basic process of mass transfer is simple, unfortunately, no general convention seems to be established, so we are left with a variety of solution techniques. All should be compatible or shown to be equivalent.

In domestic refrigerators, the water condensation on the inner surfaces occurs when the surface temperature goes below wet bulb temperature of cabinet air. This situation typically occurs when the refrigerator door is opened. The condensed water will tends to evaporate after door is closed as the relative humidity level of cabinet air decrease below saturation, and the wall temperature becomes higher then air temperature. Open pan on the shelves that contains water (or juice) is a typical problem that evaporation process takes place. Unwrapped foods, fruits, and the vegetables add water in to the cabinet, as well. The journey of water vapor loaded into the cabinet air, through above defined evaporation processes, ends up on the evaporator surfaces, because it is the coldest surface in the system. Another typical evaporation problem is defrost water collected on the drain tray. Sizing of the tray is done to evaporate the defrost water without causing any overflow even in worst case, when the maximum possible water load is created. Some of these processes are investigated in the literature. The following are the results of those studies found in the open literature.

Sparrow et al. (1983) performed experiments to measure the mass transfer coefficients for natural convection evaporation from a horizontal water layer. Owing to the latent heat requirements of the evaporation process, the temperature of the water layer is depressed relative to the ambient temperature. This gives rise to a buoyancy which overpowers the oppositely directed buoyancy associated with the concentration gradient of the water vapor. The experiments encompassed two orders of magnitude in the Rayleigh number and, in addition, the effects of two geometrical parameters were investigated. One of these is the size of the horizontal annual frame that surrounds the water containment pan. The other effect is the step caused by the difference between the water level and the height of the pan side wall. Both the presence of the frame and of the step decrease the mass transfer coefficient. Narrow frames give rise to a sharp decrease, but further enlargements of frame size have little additional effect. The step-height effect was found to be independent of both the Rayleigh number and the frame size, enabling a universal correlation. Furthermore, for all of the investigated steps and frames, $Sh \sim Ra^{0.205}$.

Prata and Sparrow (1986) investigated the evaporation of water from a partially filled, open-topped cylindrical container situated in the lower wall of a flat, rectangular duct. During the course of the experiments, parametric variations are made of the air flow in the duct and of the distance "H" between the evaporating surface and the top of the container. Supplementary experiments were conducted with Toluene as the evaporating liquid. It is found that the evaporation rate does not decrease monotonically with increasing H. Rather, a local maximum in the evaporation rate occurred at $H/D \sim 0.5$ (D is container diameter) for all the Reynolds numbers investigated.

Chuck and Sparrow (1987) performed an experimental study to determine the mass transfer characteristics for evaporation from partially filled pans of distilled water recessed in the floor of a flat rectangular duct through which turbulent air flow was passed. The parametric variations were made of the Reynolds number of the air flow, the streamwise length of the pan, and the distance between the top of the pan and the water surface (named as step height). The step height is used as a characteristic dimension for Reynolds and Sherwood numbers. Measured Sherwood numbers are well correlated with the Reynolds number. By making use of the analogy between heat and mass transfer, they described how Nusselt numbers can be obtained from the Sherwood number correlation.

This study can be used for estimating the evaporation rates and mass transfer coefficients over the partially filled pans in the refrigerator. However, these results may not be relevant to the airflow patterns in a refrigerator because the flow is not necessarily parallel to the water surface. Model's sensitivity to the step height also makes it difficult to apply to the general problems of evaporation from pans located on refrigerator shelves.

Goldstein and Cho (1995) reviewed the studies about "mass transfer measurements using naphthalene sublimation method". They concluded that this method is particularly useful in complex flows and geometries and for flows with large gradients in wall transport rate. They reviewed a large number of studies related to the naphthalene sublimation method, naphthalene thermal properties, naphthalene coating techniques, and thickness measurement techniques.

Nirdosh and Sedahmed (1995) experimentally investigated the free convection mass transfer inside a cubical cavity. In order to do this, they measured the limiting currents for the cathodic deposition of copper from acidified copper sulphate solutions. The data were found to fit the equation, $Sh=0.259(Sc.Gr)^{0.3}$. Because the geometry was an upward facing open cavity, the results of this study can not be directly applied to refrigerator geometries.

Bansal and Xie (1999) investigated evaporation rates of defrosted water from water trays in domestic refrigerators. A dynamic simulation model was developed. The model was used to investigate the effect of ambient temperature, relative humidity, air velocity and tray temperature by comparing the eight different arrangements of tray position in the compressor compartment. Their results show that, the rate of water evaporation decreased sharply with the increase in either the ambient air temperature or its relative humidity. The rate of water evaporation increases by about 300% and 30% respectively as the air velocity increases from 0.0 to 0.2 m/s, and 0.2 to 2 m/s during the compressor "on" cycle. The evaporation rates decrease by about 20% as the relative humidity increases from 45% to 90%.

Bansal and Xie 's (1999) study is good example for obtaining the evaporation mass transfer coefficient over horizontal surfaces. However, the application of the model is limited to certain types of refrigerators, and requires detailed knowledge of the refrigeration system, such as a compressor surface-temperature correlation for different ambient conditions.

After analyzing the available methods in the literature, it is decided to use the analogy between the mass and heat transfer equations. By means of this analogy the mass transfer coefficients will be obtained by making use of open door heat transfer coefficients, obtained previously as given in Eqns. (2.26)-(2.28). The details of analogy are given in Chapter 3.2.

3.2 Cabinet Mass Transfer Coefficient Determination by means of Heat and Mass Transfer Analogy

Mass transfer equations are often expressed in terms of concentration or water vapor partial pressure forms (vapor density is another). The partial pressure form is the most basic form because this is the driving potential for the process. $P_{w\infty}$ is the vapor partial pressure in the system and P_{ws} is saturation pressure of vapor at surface temperature.

If	$P_{ws}>P_{w\infty}$	Evaporation (if surface is wet)
	$P_{ws}<P_{w\infty}$	Condensation

The most familiar mass transfer process is the drying of a wet surface that is exposed to wind. The air current that comes in contact with the surface of the water layer becomes saturated with water vapor. The mass concentration of water in the near-surface air is different than its concentration in the free stream. This concentration difference has the ability to drive more water vapor out of the surface water layer. This evaporation process will be enhanced in proportion with the air speed, and the temperature. This example system is shown in the Figure 3.1.

From boundary layer analyses, we find the basis for an analogy that allows the convective and concentration transfer coefficients to be related. This allows a heat transfer experiment to be used to find a mass transfer coefficient and vice versa

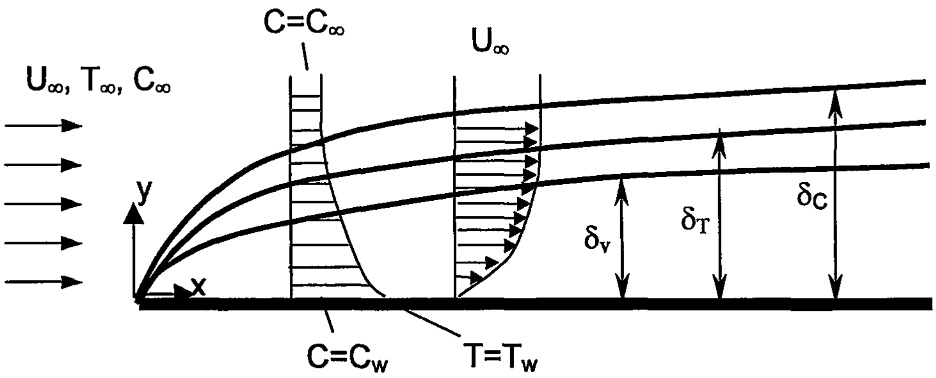

Figure 3.1 Thermal (δ_T), hydraulic (δ_V), and concentration (δ_C) boundary layers for air flow on a wet plate. Schematic velocity and concentration profiles are also shown.

For moist air, the thermophysical properties are of similar magnitude (ν~16x10^{-6} m^2/s, α~22x10^{-6} m^2/s, and D~26x10^{-6} m^2/s). Therefore, boundary layers are also similar. The boundary layer equations for an incompressible steady flow over a flat plate (Figure 3.1) can be written as;

x momentum
$$u\frac{\partial u}{\partial x}+v\frac{\partial u}{\partial y}=-\frac{1}{\rho}\frac{\partial P}{\partial x}+\nu\frac{\partial^2 u}{\partial y^2} \quad (3.1)$$

Energy
$$u\frac{\partial T}{\partial x}+v\frac{\partial T}{\partial y}=\alpha\frac{\partial^2 T}{\partial y^2} \quad (3.2)$$

Concentration
$$u\frac{\partial C}{\partial x}+v\frac{\partial C}{\partial y}=D\frac{\partial^2 C}{\partial y^2} \quad (3.3)$$

If the pressure term, in the x-momentum equation, is ignored all three equation have similar expressions. When the boundary conditions are the same, the solutions will be same, with the main difference being functional relations in terms of ν (momentum diffusivity), α (thermal diffusivity), and D (concentration diffusivity). Thus, if the bulk (mixture) flow configuration is the same in both problems, and if the wall boundary condition is the same, the mass transfer result is obtained directly from the heat transfer result through the following transformation.

Nu→Sh Pr→Sc Re→Re

Experimental heat transfer results are often correlated in an empirical equation, in textbooks (e.g. Incropera and Dewitt, 1990).

$$Nu = c\,\mathrm{Re}^m\,\mathrm{Pr}^n \tag{3.4}$$

According to the heat and mass transfer analogy, mass transfer results can be correlated in the same form.

$$Sh = c\,\mathrm{Re}^m\,Sc^n \tag{3.5}$$

The ratio of these two equations results in an expression linking the heat and mass transfer coefficients.

$$\frac{Nu}{Sh} = \left(\frac{\mathrm{Pr}}{Sc}\right)^n \tag{3.6}$$

For flat plate in laminar flow, n=1/3 for Sc>0.5, (Bejan, 1995).

In these equations,

$Nu = \dfrac{h_C L}{k}$ Nusselt number [-]

$Sh = \dfrac{h_D L}{D}$ Mass transfer Sherwood number [-]

$\mathrm{Pr} = \dfrac{\nu}{\alpha}$ Prandtl number [-]

$Sc = \dfrac{\nu}{D}$ Schmidt number [-]

α: Thermal diffusivity [m^2/s]
D: Mass diffusivity [m^2/s]
ν: Kinematic viscosity (momentum diffusivity) [m^2/s]

Finally, the following equations are obtained that give the mass transfer coefficient and mass flux relations respectively.

$$h_D = h_C \frac{D}{k}\left(\frac{\alpha}{D}\right)^{1/3} \tag{3.7}$$

$$j = h_D\left(C_w - C_\infty\right) \tag{3.8}$$

where,

h_D:	Mass transfer coefficient [m/s]
h_C:	Thermal convection coefficient [W/m^{2}K]
j:	Mass flux [kg/m^{2}s]
C_W:	Concentration at the surface [kg/m^3]
C_∞:	Concentration in the free stream [kg/m^3]

Mass transport equations –partial pressure basis:

While concentration is often used in more general mass transfer applications, often for HVAC humidifying/dehumidifying applications, it is found that partial pressure is more convenient. Fundamentally, the partial pressure of a species is the driving potential for mass transfer (similar to total pressure driving mass flow overall and temperatures as the driving potential for heat transfer). On this basis, the mass flux equation can be written as;

$$j = h_w\left(P_{ws} - P_{W\infty}\right) \tag{3.9}$$

where,

h_W:	Mass transfer coefficient, pressure basis [kg_W/m^2 s kPa]
P_{WS}:	Saturation pressure of water at wall temperature [kPa],
$P_{W\infty}$:	Partial pressure of water in free stream [kPa]

In the Eqn. (3.8), the water concentration had been used as a source term. In order to find its equivalent for partial pressures the following concentration and specific humidity ratio relations are used.

$$C = \frac{m_w}{V}, \quad \Rightarrow \quad w = \frac{m_w}{m_a}, \quad \Rightarrow \quad C=\rho_a w$$

From basic thermodynamic textbooks, following relation is also known.

$$w = 0.622\frac{P_w}{P_T - P_w} \tag{3.10}$$

and similarly,

$$C = 0.622\frac{P_w}{P_T - P_w}\rho_a \tag{3.11}$$

Or, with less then 2% error, Eqn. (3.11) can be simplified as (P_T=101.3 kPa) ;

$$C = 0.00626 P_w \rho_a \tag{3.12}$$

P_w: Water partial pressure in the mixture [kPa]
P_T: Total pressure of moist air, generally 101.3 kPa.
w: Humidity ratio [kg_w/kg_a]
m_a: Mass of dry air [kg]
m_w: Mass of water [kg]
V: Volume [m^3]
ρ_a: Air density [kg/m^3]

The mass flux equation can now be expressed in terms of water partial pressures. Rewriting of Eqn. (3.9) yields;

$$j = h_D 0.00626 \rho_a (P_{ws} - P_{W\infty}) \tag{3.13}$$

here the mass transfer coefficient, h_w, arises as;

$$h_w = 0.00626 h_D \rho_a \tag{3.14}$$

Using Eqn. (3.7) the h_w value can be defined as function of convective heat transfer coefficient and the transport properties.

$$h_w = 0.00626 \rho_a h_C \frac{D}{k}\left(\frac{\alpha}{D}\right)^{1/3} \tag{3.15}$$

3.3 Estimation of Door Opening Effect on Total (Sensible plus Latent) Heat Gain of a Cabinet

This section estimates the effect of mass transfer due to door openings on a cabinet. The results are compared to the overall loading of the cabinet. The cavity heat transfer coefficients had been obtained previously in Chapter-2. The mass transfer coefficients, using the heat and mass transfer analogy developed in the previous section, can be used to determine the mass transfer cabinet loading. Assumptions and boundary conditions of the problem are given below. Calculations are made for a typical top-mount refrigerator cabinet.

- Geometry [m]: L=1.054, W=0.635, D=0.584

- Cabinet wall temperature (T_w) is taken 5°C that is assumed equal to cabinet air temperature (T_{FF}). Ambient temperature (T_∞) is 25°C. These temperatures are standard values that are required for refrigerator energy consumption tests (ISO standards).

- Total duration of each door opening (DO) is taken 20 seconds. This is a typical value for domestic refrigerator tests. One volumetric air change of cabinet air is completed during first 7 s of door opening. Steady buoyancy-driven flow condition is assumed after this time. The wall temperature assumed remains constant during first 20 s of door opening.

- Number of door openings (NDO) is assumed 20 times per day.

- Inner surface of the door is taken in to account for both heat and mass transfer calculations by assuming it as a vertical flat plate. Heat transfer coefficient for the door is calculated by using Churchill and Chu 's (1975) correlation for vertical surfaces.

- Cabinet UA value is assumed to be 1.45 W/°C. This is similar to values obtained for this types of cabinet from reverse heat leak tests.

- Radiation heat transfer is also taken into account. The emissivity (ε) of refrigerator plastic liner is taken as 0.96.

- The average value of relative humidity in the cabinet is taken as 25% for steady operation conditions. This value is measured as low as 20% in typical nofrost refrigerators, when there is no humidity load in the refrigerator, (Karatas, 1999, Stein, 1999).

- Heat gain caused by fan motor is included. Fan power for typical cabinets is 8 W. The fan operates approximately 50% of the total time. Therefore, total continuous energy input to the system is 4 W.

- The heat gain due to defrost process is also included. Defrost heater power is 100 W. The duration of each defrost is assumed 20 minutes. Defrost occurs every 8 hours of compressor run time. Since the compressor cycle ratio is assumed 50%, the defrost is made every 16 hours for a duration of 20 minutes.

The following equations define the cabinet load relations.

$$Q_{HG} = Q_{CABINET} + Q_{DEFROST} + Q_{FAN} + Q_{OD} \tag{3.16}$$

$$Q_{CABINET} = (UA)_{cabinet}(T_{\infty} - T_{FF})(24h) \tag{3.17}$$

$$Q_{DEFROST} = P_{HEATER}\frac{t_{defrost}}{60}\left(\frac{24}{16}h\right) \tag{3.18}$$

$$Q_{FAN} = P_{FAN}\frac{1}{2}(24h) \tag{3.19}$$

where,

Q_{HG}:	Cabinet total heat gain per day [Wh]
$Q_{CABINET}$:	Heat gain through cabinet walls [Wh]
Q_{FAN}:	Heat gain from fan motor per day [Wh]
$Q_{DEFROST}$:	Heat gain from defrost heater per day [Wh]
Q_{OD}:	Total heat gain due to door opening per day [Wh]
$t_{DEFROST}$:	Duration of defrost period [Minutes]
$(UA)_{cabinet}$:	Total conductance of cabinet [W/C]

P_{HEATER}: Defrost heater power [W]
P_{FAN}: Fan motor power [W]

$$Q_{OD} = Q_{CONV} + Q_{RAD} + Q_{LATENT} \tag{3.20}$$

$$Q_{RAD} = \left[Q_{RAD\_CABIN} + Q_{RAD\_DOOR}\right]\left(\frac{DO}{3600}\right)NDO \tag{3.21}$$

$$\Rightarrow Q_{RAD} = \left[\sigma\varepsilon A_s F_{c-a}(T_\infty^4 - T_w^4) + \sigma\varepsilon A_{sd}(T_\infty^4 - T_w^4)\right]\left(\frac{DO}{3600}\right)NDO \tag{3.22}$$

$$F_{c-a} = \left(2(n+1)\frac{D}{L} + 2\frac{D}{W} + 1\right)^{-1} \tag{3.23}$$

here,

Q_{RAD}:	Total radiation heat transfer for door opening [Wh]
Q_{RAD_CAB}:	Radiation heat transfer from cabinet [Wh]
Q_{RAD_DOOR}:	Radiation heat transfer form door surface [Wh]
σ:	Stefan-Boltzmann coefficient, 5.67e-8 [W/m^{2}K^4]
ε:	Surface emissivity [-]
A_s,A_{sd}:	Cabinet and door surface areas respectively [m^2]
F_{c-a}:	View factor (cabinet-ambient) [-]
n:	Number of shelves

$$Q_{CONV} = Q_{CONV\_CAB} + Q_{CONV\_AC} \tag{3.24}$$

$$Q_{CONV\_CAB} = \left[hA_s(T_\infty - T_w)\left(\frac{DO-7}{3600}\right) + h_d A_{sd}(T_\infty - T_w)\left(\frac{DO}{3600}\right)\right]NDO \tag{3.25}$$

$$Q_{CONV\_AC} = \rho(LWD)C_p(T_\infty - T_{FF})\frac{1000}{3600}NDO \tag{3.26}$$

$$Q_{LATENT} = (Q_{LAT\_CAB} + Q_{LAT\_AC}) \tag{3.27}$$

$$Q_{LAT\_CAB} = \left(m_{cond\_cab}(DO-7) + m_{cond\_door}(DO)\right)h_{fg}\frac{1000}{3600} \quad (3.28)$$

$$Q_{LAT\_AC} = (w_{\infty} - w_{FF})\rho LWDh_{fg}\frac{1000}{3600} \quad (3.29)$$

where,

Q_{CONV}:	Total convective heat transfer for open door [Wh]
Q_{CONV_CAB}:	Convective heat transfer from cabinet [Wh]
Q_{CONV_AC}:	Heat transfer due to volumetric air change [Wh]
Q_{LATENT}:	Total latent heat transfer [Wh]
Q_{LAT_CAB}:	Latent heat transfer due to condensation on the surfaces [Wh]
Q_{LAT_AC}:	Latent heat transfer due to air change [Wh]
h_{fg}:	Condensation enthalpy [kJ/kg]
C_p:	Specific heat [kJ/kgK]
m_{cond_cab}:	Mass transfer rate on cabinet surfaces [kg/s]
m_{cond_door}:	Mass transfer rate on door surface [kg/s]
w_{∞}:	Humidity ratio at ambient conditions [kg_w/kg_a]
w_{FF}:	Humidity ratio at steady cabinet conditions (RH=25%) [kg_w/kg_a]
h, h_d:	Convective heat transfer coefficient for cabinet and door, respectively [W/mK]

Total sensible heat transfer for open door condition is sum of radiative and convective heat transfers.

$$Q_{SENSIBLE} = Q_{RAD} + Q_{CONV} \quad (3.30)$$

Then the sensible and latent heat transfer ratio is defined as,

$$Ratio_{SENS\_LAT} = \frac{Q_{SENSIBLE}}{Q_{LATENT}} \quad (3.31)$$

The results of calculations are given below.

From Figure 3.2, it is seen that the latent heat transfer equals to sensible (convective) heat transfer in the cavity for ambient relative humidity of 60%. Latent heat transfer becomes almost double of sensible heat transfer for RH=90%.

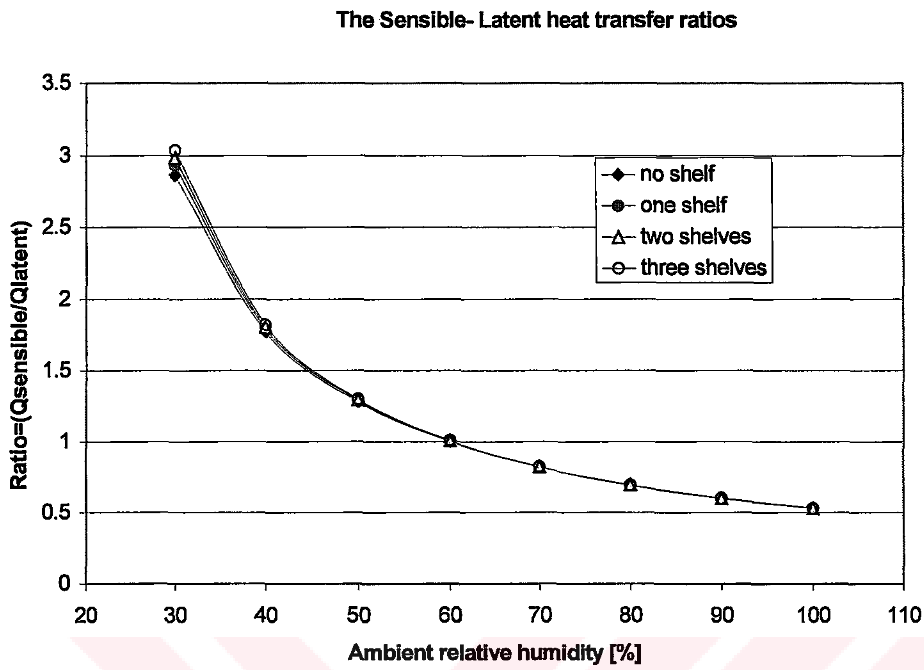

Figure 3.2 The change of sensible/latent heat transfer ratio with respect to ambient air relative humidity and number of the shelves.

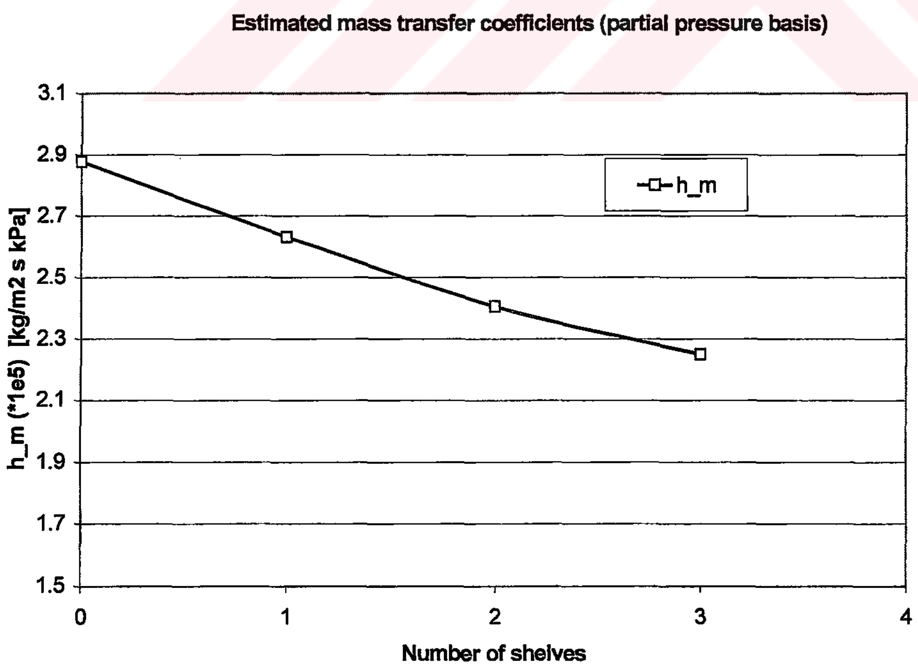

Figure 3.3 Mass transfer coefficient versus shelf numbers.

The slight changes on mass transfer coefficient due to air thermophysical property change with respect to relative humidity are neglected.

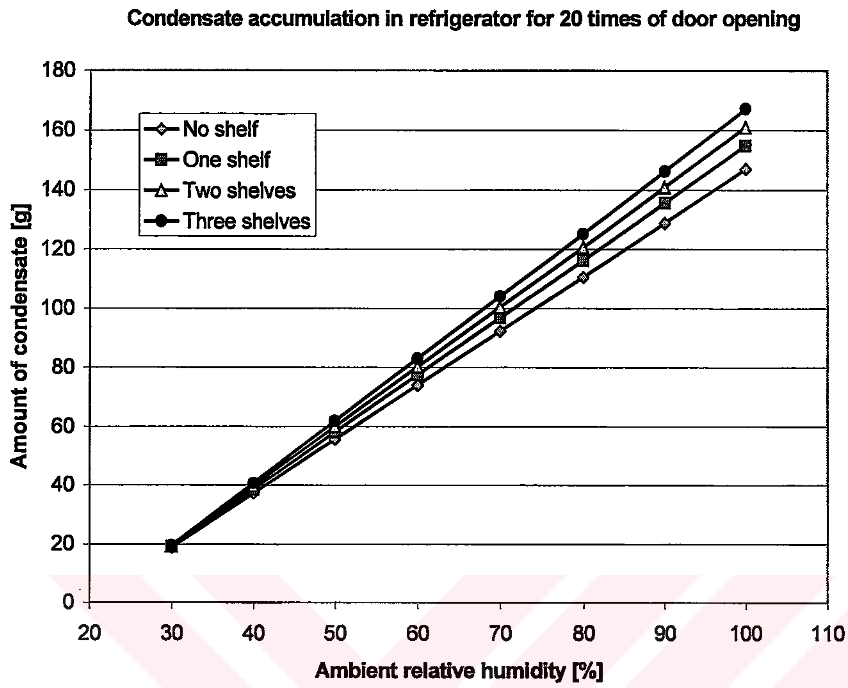

Figure 3.4 Total condensate (water) accumulation on the surfaces for different ambient humidity and shelf configurations.

Total water accumulation in the refrigerator show that it is changing from 18 g to 170 g for 20 times of door opening. This water will eventually be deposited on cold evaporator surfaces in the form of frost. The effect of this frost on heat transfer and flow characteristics will be investigated in Chapter 5.

In order to see the additional heat gain caused by door opening, the following formulation is used.

$$RATIO_{OD}(\%) = \frac{Q_{OD}}{Q_{CABINET} + Q_{FAN} + Q_{DEFROST}} 100 \qquad (3.32)$$

The results are shown in Figure 3.5. According to this figure, the increase because of door opening on the daily heat gain of cabinet is changing from 15% to 32% for 20 times of door opening. For instance, three shelves case at 60% RH, door opening causes 22% increase on cabinet heat gain base value.

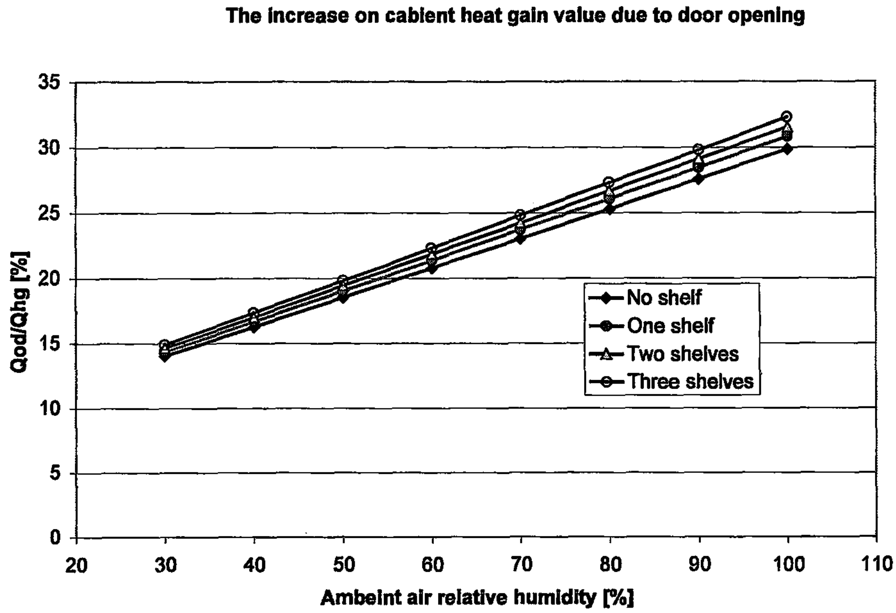

Figure 3.5 The effect of door opening on daily heat gain of cabinet (Eqn 3.32).

The breakdown of modes of heat transfer that participate to cabinet heat transfer during door opening is given in Table 3.1.

Table 3.1 Breakdown of loads at door opening (*)

Radiation heat transfer	8.2%
Convection heat transfer	42%
Latent heat transfer	49.8%

(*) Three shelves case, %60 RH

According to this table, the radiation heat transfer is only 8% of total heat gain that occurrs during door opening period. The largest portion of heat gain belongs to latent heat transfer which is 49.8%. The conduction heat transfer from cabinet walls during the 20 s of door opening is ignored in these calculations.

CHAPTER-4

CLOSED DOOR FLOW MODELING IN A NOFROST REFRIGERATOR

4.1 Introduction

In the previous chapter, open door flow and heat transfer characteristics were investigated both theoretically and experimentally. Now, a similar type of study will be repeated for closed-door refrigerator cabinet conditions. The study concentrates on the freshfood cabinet. Refrigeration of this cabinet is done by the cold air circulated over evaporator by means of a fan (see Figure 4.2). The air gets colder passing over cold evaporator surfaces. The evaporator surfaces are below freezing temperature, thus moisture in the air is deposited on the evaporator surfaces as frost. Therefore, the refrigerator performance is strongly dependent on air distribution system.

Heat and mass transfer analyses depend on flowrate and type of air distribution system in a refrigerator. Two types of air distribution system are commonly used in domestic refrigerators. These are named "singleflow" and "multiflow" systems. In the singleflow type, air is blown into freshfood compartment from a single duct outlet, which is located close to the top of the compartment. Because of this, singleflow refrigerators are designed with wire type shelves only, which allows air circulation between compartments. However, in the multiflow system, the air is delivered to each shelf compartment separately. Because of this feature, it is possible to design special compartments whose temperature is different than the others. In multiflow refrigerators, the shelves are made of either plastic or glass, so that air cannot pass between compartments.

Because of the importance of the air distribution system, a model that allows us to estimate both the air-flowrate to each compartment, and the total amount of air circulated by fan for different static pressure heads became a necessity. Therefore, a model is developed and details of it will be described below. The model predictions are compared to both experimental and computational fluid dynamic (CFD) analysis results.

4.2 Mathematical Model of Air Distribution System

Let us consider a duct connected between points a to b. The duct may have size changes, fittings in it, elevation changes, and have a fan on it. A basic representation of the system is shown in Figure 4.1.

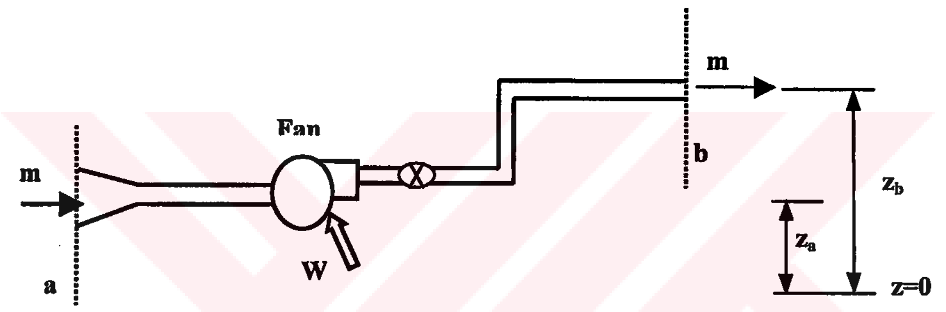

Figure 4.1 Duct-Fan system representation

The first law of thermodynamics (for steady-state steady-flow, SSSF system) can be written for the system as following,

$$0 = \dot{m}_a(h_a + PE_a + KE_a) - \dot{m}_b(h_b + PE_b + KE_b) + \dot{Q} - \dot{W} \tag{4.1}$$

where,		
	h:	Enthalpy [J/kg]
	m:	Mass flow rate [kg/s]
	PE, KE:	Potential and Kinetic energies [J/kg]
	Q:	Heat transfer rate [W]
	W:	Work into the system [W]

The goal is to try and convert this equation to a form in terms of pressure drops and mass flowrates. Rewriting the 1st law for an adiabatic system yields;

$$0=\dot{m}\left[(u_a-u_b)+(P_a\upsilon_a-P_b\upsilon_b)+(gz_a-gz_b)+\left(\frac{V_a^{\ 2}}{2}+\frac{V_b^{\ 2}}{2}\right)\right]-\dot{W} \qquad (4.2)$$

where,	h:	Enthalpy, h=u+Pυ
	u:	Internal energy [J/kg]
	υ:	Specific volume [m^3/kg]
	V:	Flow velocity [m/s]
	z:	Elevation from reference level [m]
	P:	Static pressure [Pa]
	g:	Gravitational acceleration [m/s^2]

Note that if potential energy (PE), kinetic energy (KE), and work (W) terms are neglected (basic flow through a valve or straight pipe), we have:

$$h_a=h_b \rightarrow u_a+P_a\upsilon_a=u_b+P_b\upsilon_b \qquad \text{or,} \qquad (4.3a)$$

$$P_a\upsilon_a-P_b\upsilon_b=u_b-u_a \qquad (4.3b)$$

But, from dissipation it is known that $P_b < P_a$ and if flow is incompressible, $\upsilon_a \cong \upsilon_b = \upsilon$, then Eqn. 4.3b can be expressed as following.

$$\upsilon(P_a-P_b)\cong u_b-u_a \qquad (4.4)$$

In this equation, the left hand side shows the drop in flow work, and the right hand side show the change in internal energy, which can be treated as frictional pressure loss. The static pressure drop across the duct can be expressed as follows.

$$P_a-P_b=\rho(u_b-u_a)+\rho g(z_b-z_a)+\rho\left(\frac{V_b^{\ 2}}{2}-\frac{V_a^{\ 2}}{2}\right)+\rho\frac{W}{\dot{m}} \qquad (4.5)$$

here, ρ: Density [kg/m^3]

The first term on the right hand side of the Eqn (4.5), $\rho(u_b-u_a)$, represents frictional pressure drop (see eqn. 4.4), ΔP_f, which is known it is a function of the Reynolds number.

$$\Delta P_f = f\left(\frac{L}{D}\right)\left(\frac{V^2}{2}\right)\rho \quad \text{And} \qquad f \approx C\,Re^{-0.2} \tag{4.6}$$

For smooth ducts, C= 0.19 for 5000<Re<2,000,000.

Rearranging the Eqn. (4.6) for mass flowrate yields;

$$\Delta P_f = 0.147\left(\rho^{-0.8}\nu^{0.2}\right)\left(LD^{-4.8}\right)\dot{m}^{1.8} \tag{4.7a}$$

If the duct segment has more then one-size duct in it, then the frictional pressure drop would be;

$$\Delta P_f = 0.147\left(\rho^{-0.8}\nu^{0.2}\right)\dot{m}^{1.8}\left(L_1 D_1^{-4.8} + L_2 D_2^{-4.8} + \ldots\right) \tag{4.7b}$$

Let $$\alpha_{a-b} = 0.147\left(\rho^{-0.8}\nu^{0.2}\right)\left(L_1 D_1^{-4.8} + L_2 D_2^{-4.8} + \ldots\right) \tag{4.7c}$$

Where,

- L: Length of duct segment [m]
- D: Equivalent or hydraulic diameter of duct [m]
- ν: Kinematic viscosity [m^2/s]
- ΔP_f: Frictional pressure drop [Pa]

Finally the pressure drop between points a and b can be expressed in the following form.

$$P_a - P_b = \alpha_{a-b}\dot{m}^{1.8} + \rho g(z_b - z_a) + \left(\frac{8}{\pi^2}\right)\rho^{-1}\dot{m}^2(D_b^{-2} - D_a^{-2}) + \rho\frac{W}{\dot{m}} \tag{4.8}$$

In this equation, the potential energy term is given by assuming that the density of the working fluid is constant and it is much greater than the ambient fluid (for instance water flows in the pipes). On the other hand, this term is mostly ignored in air distribution systems as it is significantly small compare to the fan static pressure increase. However, when the fan turns off the thermal gravity effect (stack effect) type flow become dominant. Therefore, it is valuable to organize the equation so that the thermal gravity effect can be shown explicitly.

The static pressure difference due to the thermal gravity effect, which is potential head, is described below,

$$\Delta P_{se} = g(\rho_a z_a - \rho_b z_b) \tag{4.9}$$

By using the expression given in the ASHRAE Fundamentals (1997), one can get following expression for thermal gravity effect in duct flow,

$$\Delta P_{se} = g(\rho_a - \rho_{ave})(z_a - z_b) \tag{4.10}$$

Where,

ΔP_{se}: Static pressure difference due to the stack effect [Pa]
ρ_a: Air density at cabinet temperature [kg/m3]
ρ_{ave}: Air density at average temperature of air in the duct segment [kg/m3]

Note that when this definition is used, the static pressures should be treated as gauge pressures at given elevations. When this expression of stack-effect is placed in the Eqn. (4.8), the following expression is obtained.

$$P_a - P_b = \alpha_{a-b}\dot{m}^{1.8} + g(\rho_a - \rho)(z_b - z_a) + \left(\frac{8}{\pi^2}\right)\rho^{-1}\dot{m}^2(D_b^{-2} - D_a^{-2}) + \rho\frac{W}{\dot{m}} \tag{4.11}$$

where $\rho = \rho_{ave}$.

If a fan with known characteristics is specified, this equation can be solved directly for the system operation point. A polynomial curve-fit expression for fan power will be substituted into Eqn. (4.11). Assuming a second order relation between static pressure and volumetric flowrate.

$$\Delta P = a - b\dot{V}^2\ , \tag{4.12a}$$

The fan power, therefore can be written as;

$$W = -(a\dot{V} - b\dot{V}^3) \qquad (4.12b)$$

or, in terms of mass flowrate,

$$W = -(a\rho\dot{m} - b\rho^3\dot{m}^3) \qquad (4.12c)$$

Then Eqn. 4.8 becomes,

$$P_a - P_b = \alpha_{a-b}\dot{m}^{1.8} + g(\rho_a - \rho)(z_b - z_a) + \left(\frac{8}{\pi^2}\right)\rho^{-1}\dot{m}^2(D_b^{-2} - D_a^{-2}) + \left(-a\rho^2 + b\rho^4\dot{m}^2\right) \qquad (4.13a)$$

Alternatively, if the fan characteristic curve is not known, the static pressure increase through the fan can be used. Eqn. 4.8 can be rearranged as follows.

$$P_a - P_b = \alpha_{a-b}\dot{m}^{1.8} + g(\rho_a - \rho)(z_b - z_a) + \left(\frac{8}{\pi^2}\right)\rho^{-1}\dot{m}^2(D_b^{-2} - D_a^{-2}) - \Delta P \qquad (4.13b)$$

Note that in both equations (4.13a) and (4.13b) the last terms on the right-hand side are source terms (but these terms also acts as "sinks" – actually, they are reversible conversion terms (Bernoulli type terms) for conversion of energy between flow work, kinetic energy and potential energy). If these source terms are zero, and there is still temperature differences between segments, the potential energy term will be the source term. This will allow us to estimate the rate of back flows with temperature differences between compartments, and no fan operations.

Now a general expression for the pressure change of a duct segment as a function of mass flowrate is obtained. For a given duct network, pressure drop across each pipe segment and conservation of mass relations (that is sum of inflows and outflows in every node should be equal to zero) for each node connecting pipe segments can be written. Then the number of unknowns (Static pressures at each node and mass flowrates) are equal to the number of equations. By using the equation solvers, such as EES® or Microsoft Excel®'s "Solver" option, the solutions can be obtained.

The trick to successfully implementing this method is to set up the equations in a manner that does not violate the 2nd law, that is, the direction of flow and direction of pressure drop due to friction must be consistent.

In the following pages, an application of above described method is given.

4.3 Application of the Model on a Nofrost Refrigerator

4.3.1 Description of air distribution system of the model refrigerator

Schematic of a freshfood compartment of a refrigerator is shown in the Figures 4.2 and 4.3. Experimental data has been obtained from a cabinet air duct similar to Figure 4.2 , and 4.3. Also CFD analysis results are available for a portion of the duct system as outlined in Figure 4.3.

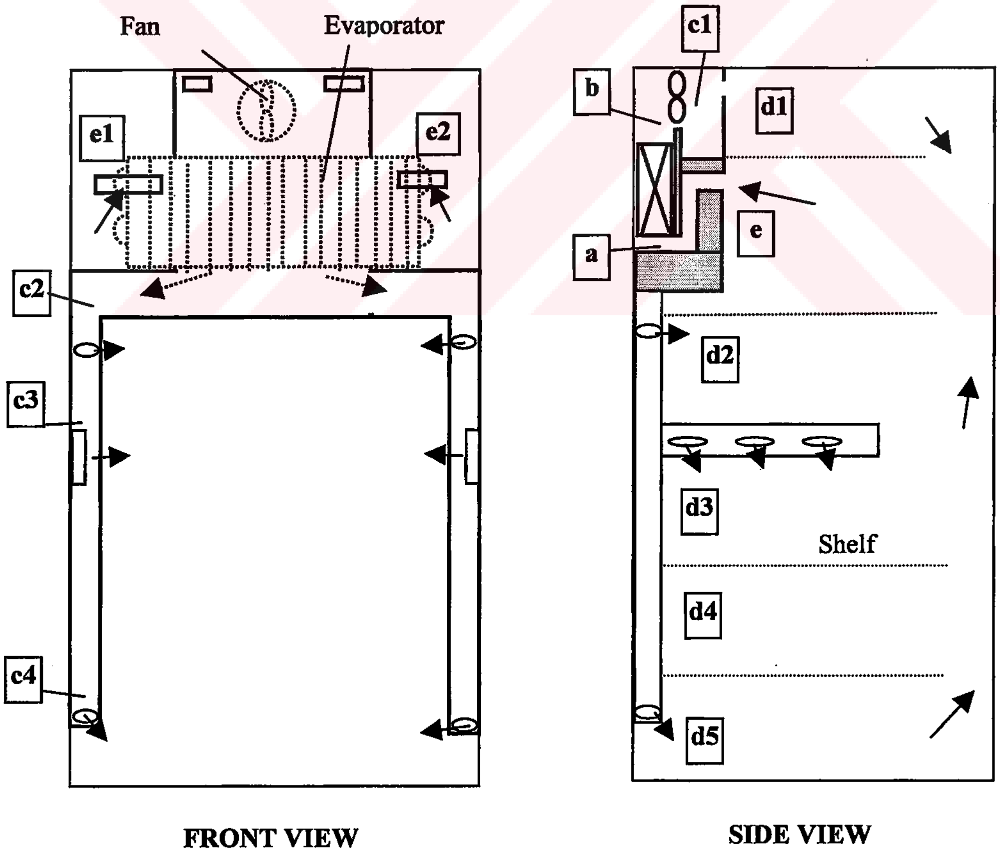

Figure 4.2 Schematic view of air distribution system in the model refrigerator

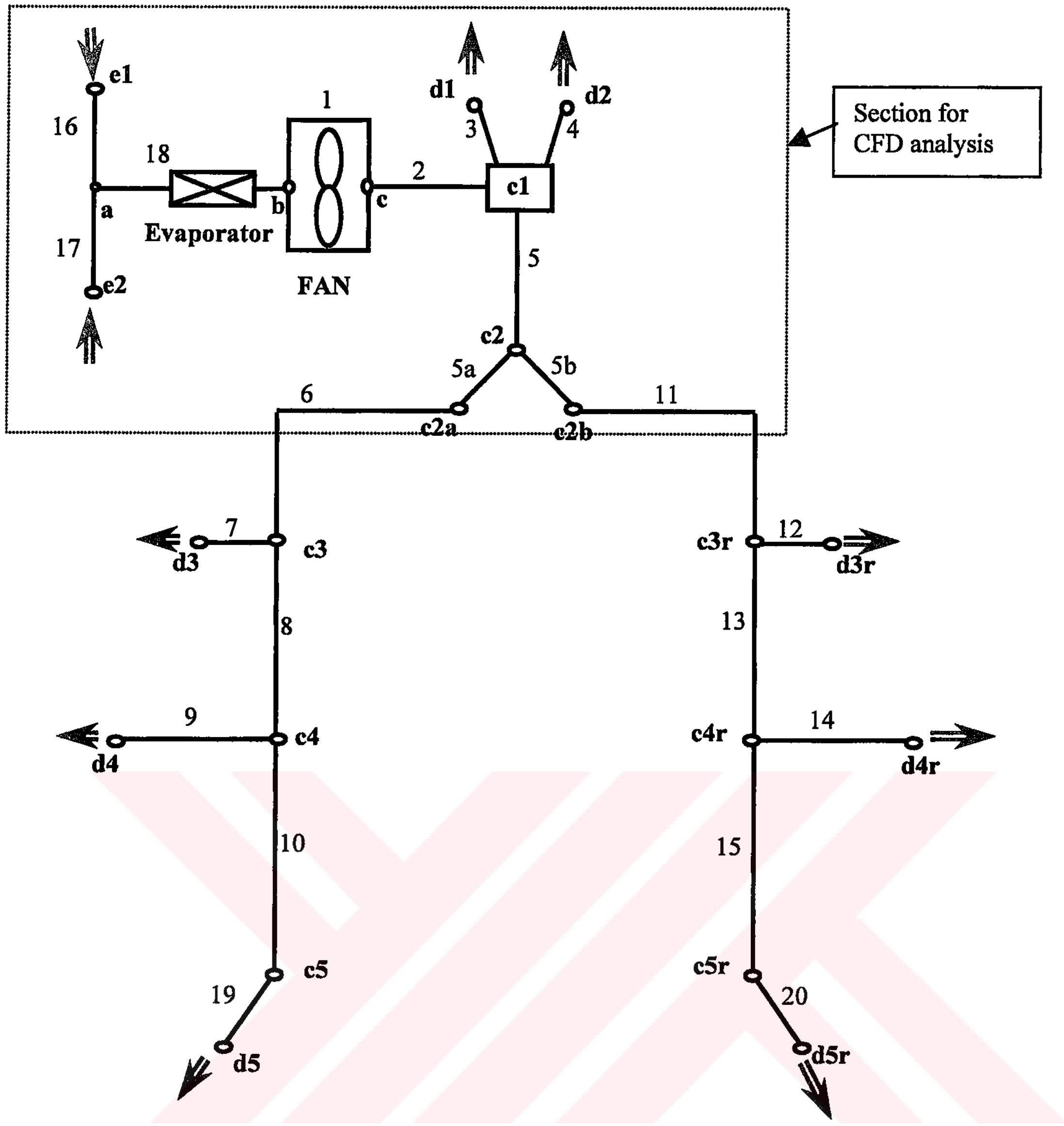

Figure 4.3 Schematic of FF cabinet air-distribution network. In this figure, the numbers represent duct segments. The letters; "a" and "b" represent evaporator inlet and outlet nodes respectively, "c" the nodes in the network, "d" duct exit diffusers, and "e" return duct.

4.3.2 Application of flow model to the cabinet

Equation (4.13b) is written for each duct segment of the air distribution network shown in Figure 4.3. Because the flow network consists of fittings whose shapes are not found in general duct fitting databases, approximate values for fitting coefficients are estimated. Drag coefficients are obtained from ASHRAE Fundamentals Handbook (SI), 1997. The following assumptions are made,

- The pressure losses due to the fittings are expressed in terms of equivalent duct length Le. The definition of Le is,

$$Le = 5.52 C_D \frac{\dot{m}^{0.2} D^{0.8}}{(\rho \nu)^{0.2}}$$

here, Le: Equivalent length of duct necessary to generate an equivalent frictional loss to the separation loss due to the fittings, expansions, contraction etc.[m]

C_D: Drag coefficient of pressure loss element [-]

D: Pipe diameter [m]

- Since the duct cross-sections are non-circular, the following equations are used to calculate their equivalent diameters. (ASHRAE Fundamentals Handbook, 1997) such as,

Noncircular Ducts, $D_h = \frac{4A}{P}$

Rectangular Ducts, $D_e = \frac{1.3(HW)^{0.625}}{(H+W)^{0.25}}$

D_h: Hydraulic diameter [m]

D_e: Equivalent diameter [m]

A: Duct area [m^2]

P: Perimeter of cross section [m]

H: Height (length of one side of duct) [m]

W: Width (length of adjacent side of duct) [m]

- The flow in air discharge openings (such as d1, d2, d3, d3r) of the ducts are assumed to be orifice type and the discharge coefficient is taken as unity. This means there is no "vena contracta" effect.

- As the flows are mainly turbulent, and the exits are open, the drag coefficients (C_D)at the exit of ducts (such as d4,d5, d4r,d5r) are assumed unity.

- Calculations are made at isothermal conditions at ambient temperature, therefore the thermal gravity effect is eliminated.

4.3.3 Results of calculations

Calculation Method: The Freshfood air distribution system (see Figure 4.3 and 4.4) is analyzed. First, the approximate fitting and loss coefficients at duct exits obtained from ASHRAE Fundamentals Handbook (1997). Then, corresponding equivalent duct lengths are obtained. Eqn. (4.13b) and nodal mass balances are applied over the network. The static pressure at the exit and inlet of each opening set to zero. Finally, by using EES® Equation Solver, the problem is solved for different static pressure increases through the fan section. Resulting static pressures and mass flow rates at each individual duct segment are obtained. The solver listing is given in Appendix K.

The results are given in a tabulated format.

Table 4.1 Calculations of EES® solver for FF cabinet air distribution system.

ΔP_{FAN}	Fan flowrate [l/s]	Exit diffuser flowrates [l/s]								Return ducts [l/s]	
[Pa]	Qfan	Qd1	Qd2	Qd3	Qd4	Qd5	Qd3r	Qd4r	Qd5r	Qe1	Qe2
50	11.15	1.45	1.45	0.79	0.93	2.46	0.77	0.91	2.39	6.14	5.01
45	10.57	1.38	1.38	0.75	0.88	2.33	0.73	0.86	2.27	5.83	4.75
40	9.97	1.30	1.30	0.71	0.83	2.19	0.69	0.81	2.13	5.49	4.48
35	9.32	1.21	1.21	0.67	0.78	2.05	0.65	0.76	1.99	5.13	4.18
30	8.62	1.12	1.12	0.62	0.72	1.89	0.60	0.70	1.84	4.75	3.87
25	7.86	1.03	1.03	0.56	0.65	1.72	0.55	0.64	1.68	4.33	3.53
20	7.02	0.92	0.92	0.51	0.58	1.54	0.49	0.57	1.50	3.87	3.16
15	6.07	0.80	0.80	0.44	0.50	1.33	0.43	0.49	1.29	3.35	2.73
10	4.95	0.65	0.65	0.36	0.41	1.08	0.35	0.40	1.05	2.73	2.22
0.1	0.48	0.07	0.07	0.04	0.04	0.10	0.03	0.03	0.12	0.27	0.22
0	0	0	0	0	0	0	0	0	0	0	0

4.3.4 Experimental study

Velocity measurements: In order to measure exit velocities at each opening, small rectangular ducts, whose dimensions are given in Table 4.2, are located at each outlet. A handheld anemometer (TSI, Velocicalc® model) is used to measure the duct exit velocities. As many as possible velocity readings are taken for each outlet, then the average velocity is calculated. The volumetric flowrates are calculated according to these average velocities.

Table 4.2 Results of experimental air flowrate measurements (*)

Duct exits	*Average Velocity [m/s] (**)*	*Exit duct Area [m²]*	*Flowrate [l/s]*	*Flow Ratio (exit/total) [%]*	*exit duct height H [mm]*	*exit duct width W [mm]*
e1	1.58	0.00346	5.46	56.4	36	96
e2	1.32	0.00320	4.22	43.6	34	94
d1	3.96	0.00024	0.96	9.5	9	27
d2	3.96	0.00024	0.96	9.5	9	27
d3	0.79	0.00158	1.24	12.3	25	63
d4	0.66	0.00112	0.74	7.3	20	56
d4+	0.43	0.00075	0.32	3.2	3.5	215
d5	2.06	0.00116	2.38	23.5	17	68
d3R	0.58	0.00158	0.91	9.0	25	63
d4R	0.6	0.00112	0.67	6.6	20	56
d4R+	0.38	0.00075	0.29	2.8	3.5	215
d5R	1.42	0.00116	1.64	16.2	17	68

(*) The lengths of measurement ducts located on each duct outlet are 5 cm.
(**) Velocity measurements are made with Velocicalc (TSI) anemometer
(+) d4 and d4r have two part exits therefore the second part is indicated as "+" sign.

Static pressure measurements: A micro manometer is used for measurements. Specifications of micro manometer are given in Appendix L. The manometer required pressures greater than 7 Pa. The measurements are made only the locations where the static pressure is above 7 Pa. These locations are, just before the evaporator (node **"a"**) and after fan outlet (node **"c1"**) (see Figure 4.3). The results of the measurements are given in Table 4.3.

Table 4.3 Results of air static pressure measurements

Location	**Reading** [inch water column]	**Pressure** [Pa]
Pc1-Pa	0.156	39.0
Pc1	0.09	23.5
Pa	0.07	-16.5

The measurements are made by using 1/8" PVC hose. Numerous small holes (1mm in diameter) are drilled along 20-30 mm length of hose from its end. The tip of the hose is closed. Then the PVC hose is fixed to the location such a way that the dynamic pressure is not measured.

Fan characteristics: The fan speed in the refrigerator cabinet is measured as 3380 rpm, at ambient temperature of 25°C. However, available fan characteristics data is measured at 2500 rpm (Melamed, 1997). By using the fan laws, the data are corrected for 3380 rpm. The results are given in Table 4.4.

$$\frac{Q_2}{Q_1} = \frac{rpm_2}{rpm_1} \qquad \frac{\Delta P_2}{\Delta P_1} = \left(\frac{rpm_2}{rpm_1}\right)^2 \qquad (4.14)$$

Table 4.4 Fan characteristics (*)

@2500 rpm		@ 3380 rpm	
ΔP (Pa)	Q (l/s)	ΔP (Pa)	Q (l/s)
26.90	0.03	49.17	0.04
22.10	6.52	40.39	8.82
18.90	8.96	34.54	12.12
16.20	11.15	29.61	15.07
9.60	15.10	17.55	20.41
4.00	19.05	7.31	25.75
0.90	21.38	1.65	28.91

(*) Fan: 90 mm Thorngren

4.3.5 CFD analyzes

In order to understand the flow characteristics around the fan and evaporator, a CFD analysis had been performed (Aydin et al., 1998). The details are given as follow,

Method: First, the FF evaporator and air distribution system's 3D Solid Model was created in the I-DEAS environment. Then, all the volumes that airflow passes through are subtracted so it's solid model and volumes obtained. The 3D solid model of the evaporator tubes & fins, fan, and fan housing are created separately and located into the previously obtained volume. Finally the geometry is ready for meshing now, (See Figure 4.4).

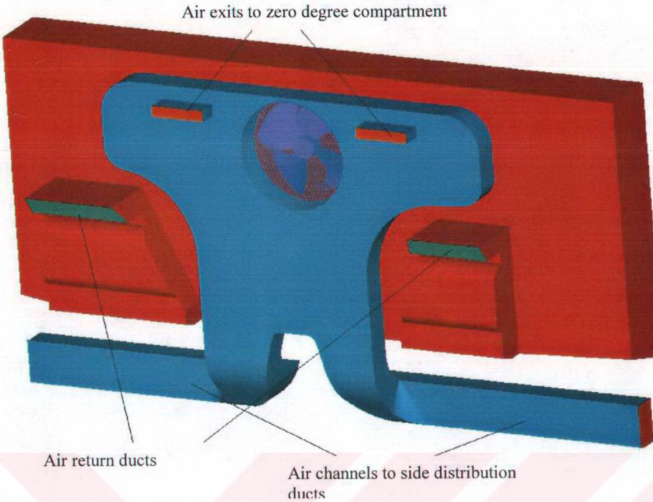

Figure 4.4 FF evaporator, fan and air distribution section 3-D solid model

The next job is to create appropriate solution meshes. In order to allow further geometry changes, evaporator, fan and related volumes are separately meshed. In that section, the tetrahedron and hexahedron meshing elements are widely used. The total numbers of meshing elements are 1,200,000. In order to increase the sensitivity, narrower meshes are used for the volumes in fan blades and in evaporator fins.

When the procedure is completed, the finite volume model is transferred to STAR HPC, which is running in an Origin 2000 Super Computer. All the separate mesh sections are conjugated by using "arbitrary mesh interface" in that program. The details of CFD analysis are given in the study of Aydin et al. (1998).

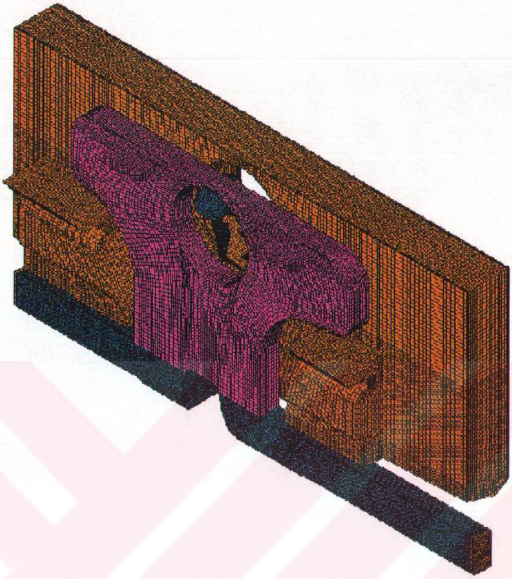

Figure 4.5 3-D view of meshed geometry

Boundary conditions:

Air thermophysical properties:

T= –20 °C
ρ =1.377 kg/m^3
μ=1.622x10^{-5} Pa s

The fan in the system is a 90 mm Thorngren fan, with a fan speed of 2500 RPM.

The pressures at the exits and return duct inlets are set to zero (atmospheric pressure). Since left and right air distribution ducts are not included, the pressure at point "c2" (see Figure 4.2, and 4.3) is set to 5 Pa in order to take into account the pressure drop through these ducts.

As a turbulence model, the k-ε RNG model is used. Finally, a solution with the SIMPLE algorithm is obtained after 3000 iterations.

Analysis results:

The velocity and pressure in the air distribution system are obtained. The results are given in the Figures 4.6-4.8.

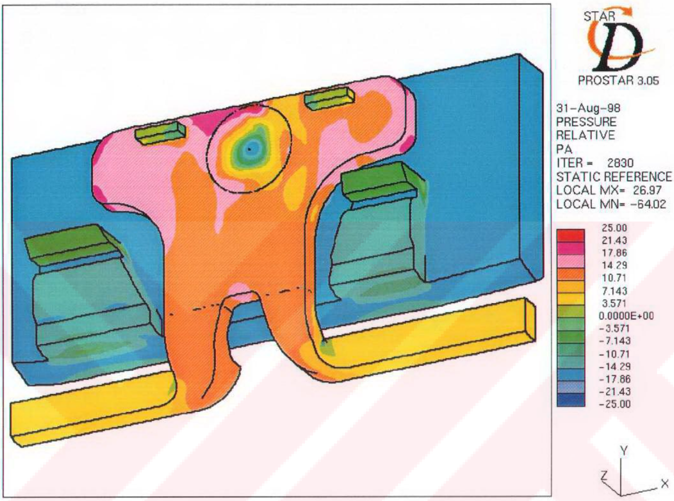

Figure 4.6 Static pressure distribution in the analysis section (3-D view)

In the Figure 4.6, the general static pressure distribution is shown. The lowest pressure is seen in the evaporator cabinet, before the fan. The air after the fan moves to the side as a swirling flow (see Figure 4.10). The highest-pressure areas occurred on the duct walls close to the fan exit. These locations are sources of flow induced noise. In the center region of the fan, low-pressure areas are also seen.

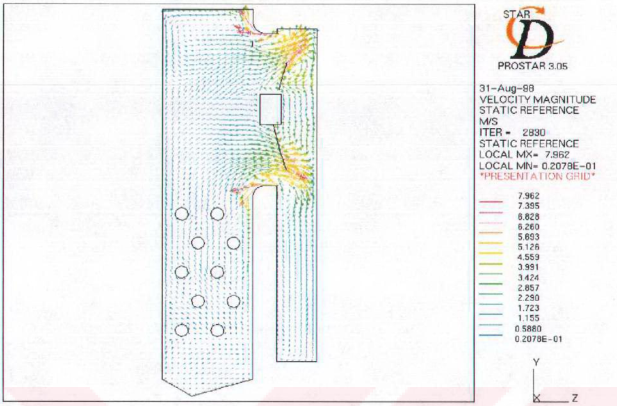

Figure 4.7 Air velocity distribution. Cross section plane is in the center of the fan. Evaporator pipes are seen in the figure.

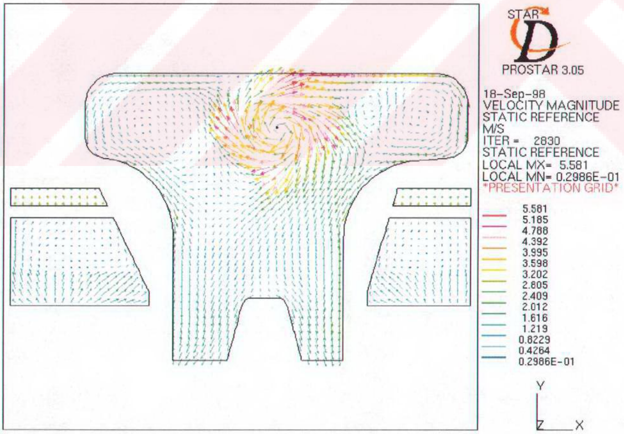

Figure 4.8 Air velocity distribution on fan exit and return holes.

The air velocity passing through evaporator is fairly uniform (Figure 4.7). Velocity changes and flow separations caused by evaporator tubes are also visible. There are some back flows from the clearance between fan tip and housing, This is because of both pressure difference between fan inlet and exit sections and the geometry. In Figure 4.8, exiting air from the fan is clearly seen. The air moves both forward and to the sides as a swirling flow. Since the duct walls are close, the swirling air will hit the walls. Then the dynamic pressure of swirling air will convert to static pressure. The duct design right after fan is therefore important, since the pressure drop and the most of air borne noise comes from this section.

It is estimated that the static pressure increase on the fan is 20 Pa. The air flowrates for each exit port are estimated and given in Table 4.5. More figures about the CFD analysis are given in Appendix J.

4.3.6 Comparison of the results

Airflow rates: The results of all calculations are given in Table 4.5. In this table both experimental versus calculated data and CFD versus calculated data are given. Since the CFD calculations are made only for 20 Pa, the EES runs are made for same conditions and compared on 4th and 5th columns.

Table 4.5 Comparison of results for air flowrates.

	ΔP_{fan} = 40 Pa Ta=25°C		ΔP_{fan} = 20 Pa Ta=-20°C	
Exit	**Experimental**	**Calculated**	**CFD**	**Calculated**
e1	5.46	5.49	4.39	3.57
e2	4.22	4.48	3.50	2.91
d1	0.96	1.30	1.44	0.84
d2	0.96	1.30	1.27	0.84
d3	1.24	0.71		0.46
d4	1.06	0.83	**2.71 (*)**	0.54
d5	2.38	2.19		1.42
d3R	0.91	0.69		0.45
d4R	0.96	0.81	**2.47 (**)**	0.53
d5R	1.64	2.13		1.39
Total	***10.13***	***9.96***	***7.89***	***6.48***

(*) Flowrate is sum of d3, d4, and d5
(**) Flowrate is sum of d3R, d4R, and d5R

Static pressures: As previously explained, the pressure measurements are made only for the nodes **"a"** and **"c1"**. Measurements are made both individually and as differences of these two points. The results are given in Table 4.6.

Table 4.6 Comparison of experimental versus calculated static pressures

Location	Static Pressure [Pa] (measured)	Static Pressure [Pa] (calculated)	Error [%]
Pc1-Pa	39.0	40	+2.5
Pc1	23.5	22.23	-5.4
Pa	-16.5	-17.40	+5.5

Operation point: By using the fan and system characteristics data, Figure 4.9 is obtained. The intersection of the fan and system curves gives the operation point. The operation point is estimated roughly 10 l/s at 40 Pa, which is in good agreement with both calculated and measured flowrates.

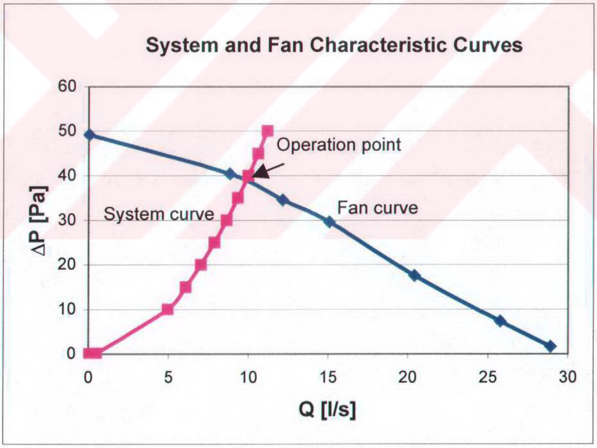

Figure 4.9 System & Fan characteristic curves

4.4 Conclusions

1) A model for estimating the flowrate and pressure drops in a flow network is introduced. Results of the model are compared to both experimental studies and CFD analysis. The model is found to be in good agreement with experimental and analytical results. Static pressure and total flowrate are within 10% error.

2) It is recommended to use this method in the design and rough sizing of air distribution ducts of Nofrost refrigerators. The fittings and duct shapes used in domestic refrigerators do not match with industrial ones. Because the model's success is strongly dependent on these coefficients, a study of obtaining the pressure drag coefficients of fittings is very important.

3) The use of this method will give some insights to design engineers, but CFD techniques should be used for more detailed analysis.

4) The results of this flow model will later be used in Chapter-5 to estimate the flow characteristics over an evaporator, and the effect of frosting on both heat transfer and pressure drop.

CHAPTER-5

EVAPORATOR PERFORMANCE UNDER FROSTING CONDITIONS

5.1 Background and Literature Survey

Heat and mass transfer analysis of a cabinet during open door conditions were introduced in Chapter 2 and 3. Air distribution system modeling that allows estimating the airflow rates depending on duct geometry and fan characteristics was investigated in Chapter 4. In this final chapter, the effect of frosting on evaporator heat transfer and flow characteristics are investigated.

The amount of condensate that is accumulated on the inner surfaces of the refrigerator while the door is open starts to evaporate after the door is closed. Other sources of water mass-transfer such as infiltration, evaporation from open water pans, and foods placed on the shelves also add more moisture to the cabinet air. During a closed-door period, a fan circulates this relatively moist cabinet air through cold evaporator surfaces. The typical evaporator surface temperature is far below the freezing temperature (< -20 °C); therefore, frost will be formed on the evaporator surfaces. Thickness and density of frost change with time (depending on air velocity, air and surface temperature, and the moisture content of incoming air). The frost layer establishes a thermal resistance that changes with time as thickness increases. Therefore, the overall heat transfer coefficient of the evaporator changes. Surface roughness is significantly higher for frosted surfaces. Furthermore, increasing frost thickness starts narrowing the air passages. Therefore, the pressure drop through evaporator increases, and correspondingly, the flow rate decreases. Because of these close relations, it is clear that an analysis of the frosted evaporator can be regarded as a coupled problem of flow, heat, and mass transfer modes occurring simultaneously.

As the frost thickness increases with time, it will start blocking the evaporator passages. In order to prevent blockage and assure performance, it is necessary to remove this frost from the evaporator. The process called defrosting melts the frost by means of an electric heater. The defrost system and when to implement defrosting are another important design parameters. Standards (e.g. ISO) put limitations on the temperature increase in food packages located in both freezer and freshfood compartments during the defrosting period. Usually, the complete removal of frost and having a minimum temperature increase in compartments are taken as the primary design goals. As the worst case scenarios are taken into account, the energy optimization is not a primarily attacked issue.

The decision of defrost in the refrigerator is made by using either a mechanical timer or more complicated electronic algorithms. In mechanical defrost timers, the total run-time of the compressor between defrosts is fixed in order to assure that frost formation does not block the evaporator and the total amount of frost can be safely defrosted. Because of the safety precautions, the run-time is obtained by checking the worst-case scenarios (it is generally kept around 8 hours), therefore it does not reflect the nominal conditions. However, in the electronically controlled refrigerators, the defrost decision is made by means of certain defrost algorithms. The most common algorithms are known as "Neuro-Fuzzy Defrosting" and "Adaptive Defrosting". In Neuro-Fuzzy systems, the ambient temperature, and the number and duration of door openings are used for the decision to start defrost. The control system learns and continuously updates the door opening patterns of the user and starts defrost when the door is less likely to be opened. Completion of the defrost is based upon not only the temperature of the evaporator, but also the duration of the defrost and the cabinet temperatures. Finally, the adaptive defrost system uses the duration of the previous defrost to judge the compressor run-time for the next defrost. For example, if a defrost lasts longer than the base time, then the compressor run-time for the next defrost will be set shorter, and the algorithm continuously refreshes itself after each defrost.

The treatment of evaporator surfaces is another issue. In order to increase the defrost efficiency and decrease the effect of frost on the evaporator, coatings on evaporator surfaces are widely used. There are numerous patented coatings available for this purpose (e.g. Sol-Gel's). Manufacturers can change the formulas to change the contact angle between the water droplet and the evaporator surface to meet specific requirements. The coatings are mainly two types, hydrophilic (keeps water droplets on the surface) and hydrophobic (easily draining and water free surfaces). Hydrophobic coatings are preferred in refrigerator evaporators. The main disadvantage of these coatings is that the effectiveness decreases with time. Roughly, after 500-1000 defrost cycles, the coating will lose its efficiency. The increasing number of research projects on surface coatings promise that in near future, this problem might be eliminated.

The above-mentioned explanations show the necessity of understanding the mechanisms of frost buildup on the evaporator surfaces, and its effect on the heat and mass transfer characteristics. Although there are a number of studies in the literature, they are mostly valid for certain geometry and flow conditions. Moreover, most studies are on heat pumps that have higher temperature and airflow rates than domestic refrigerator applications. The air distribution system and position of the evaporator are the other main differences between these two applications. In this study, the heat and mass transfer analysis will be made for domestic refrigerator evaporators. A model will be developed for analyzing the frosted evaporator performance. The model will be used to investigate the effect of airflow rate, air humidity, evaporation temperature, and inlet air temperature on frosting. Model results will be compared to experiments of Seker (1999). The model will be able to investigate more efficient defrost systems and algorithms. The final goal can be extended as obtaining the denser and more evenly distributed frost on the evaporator surfaces that will help to increase the time between defrosts, and therefore decrease energy consumption.

A detailed literature survey is given below. For convenient use of this survey, it is presented in two parts as "The frost formation on surfaces and its characteristics" and "Effect of frost on flow and heat transfer characteristics of evaporator".

5.1.1 The frost formation on surfaces and its characteristics

Hayashi et al. (1977) considered three consecutive periods that describe the evaluation of a frost layer. These classifications are also used by other researchers such as Tao et al. (1993), and Ismail and Salinas (1999).

I: The crystal growth period (one-dimensional),
II: The frost-column growth period (three-dimensional),
III: The frost layer full-growth period (quasi-steady growth period)

I) One-dimensional crystal growth period: This first and rather short period is characterized by the condensation and subsequent freezing of small water droplets. In this period, water condenses on nucleation sites of the plate coalescing to form bigger droplets of uniform size, which then start to freeze. Next, frost crystals are generated on these ice nuclei, and grow in a vertical direction at about the same rate. This period is not taken into account in most modeling studies (Tao et al. (1993)). This period will be used for the choice of the initial properties of the frost layer.

II) Three-dimensional frost column growth period: During this period, the frost layer is characterized by a more uniform aspect due to the branching and interconnecting of the ice crystals. The frost layer acts like a homogeneous porous material made of solid ice matrix and pores filled with moist air. The mass transfer towards the frost layer leads to the growth and densification of the porous deposit.

III) The frost layer full-growth period: This period arises when the surface temperature becomes equal to the water triple point temperature due to the increased frost thermal resistance. Water vapor condensing at the top of the frost layer forms a liquid film that soaks into the frost layer, and freezes in the colder areas towards the cold wall. Then, a cyclic process of melting, freezing and growth occurs until thermal equilibrium of the entire frost layer is reached.

A local volume averaging technique is widely preferred for estimating the thermophysical properties of a frost layer, which consists of ice crystals and moist air (Tao et. al, 1993, Ismail & Salinas , 1999, Gall et al. 1997). This technique is valid for the second and third periods of frost growth. It considers an elementary control volume (V), where both ice (V_β) and moist air (V_γ) coexist. Then the volumetric fractions are given by,

$$\varepsilon_\beta = V_\beta / V \qquad \text{and} \qquad \varepsilon_\gamma = V_\gamma / V \tag{5.1}$$

$$\varepsilon_\beta + \varepsilon_\gamma = 1 \qquad \text{and} \qquad \left(\frac{\partial \varepsilon_\beta}{\partial t}\right) = -\left(\frac{\partial \varepsilon_\gamma}{\partial t}\right) \tag{5.2}$$

The equivalent thermophysical properties of this medium are defined as follows

Frost density; $$\rho_f = \varepsilon_\beta \rho_\beta + \varepsilon_\gamma (\rho_v + \rho_a) \tag{5.3}$$

Frost specific heat; $$C_p = \frac{\varepsilon_\beta \rho_\beta C_\beta + \varepsilon_\gamma (C_v \rho_v + C_a \rho_a)}{\rho_f} \tag{5.4}$$

Effective thermal conductivity; $$k_{eff} = \varepsilon_\beta k_\beta + \varepsilon_\gamma \frac{k_v \rho_v + k_a \rho_a}{\rho_v + \rho_a} + (k_\beta - k_\gamma) G \tag{5.5}$$

Effective diffusivity; $$D_{v,eff} = \varepsilon_\gamma D (1 + F) \tag{5.6}$$

Where,

D:	Vapor-air binary molecular diffusivity [m^2/s]
G:	A function derived from thermal conductivity tensor
$\alpha_{0,eff}$:	Effective thermal diffusivity (=$k_{eff}/\rho_f C_p$) [m2/s]
F:	Diffusion coefficient
V:	Volume [m^3]
ρ:	Density [kg/m^3]
C:	Specific heat [kJ/kg]
k:	Thermal conductivity [W/mK]
t:	Time [s]
ε:	Volume fraction

<u>Subscripts:</u>

β :	Ice phase
γ :	Gas phase that consists of air and water vapor
f:	Frost
v:	Water vapor
a:	Air
0 :	Initial

In the Eqn. (5.6), the effective diffusivity term includes a constant, F, the diffusion factor. Its value depends upon geometry and the ambient and surface temperatures, and there is no common convention about the value of F. F is defined for the frost layer and for the frost surface separately. Tao et al. (1993) defined the F value as 0.11 for Tc=253 K and 3 for T_c=263 K (surface temperature of plate) for flow over flat plate. According to experiments of Gall et al. (1997), the F value was found to be between 0 to 1.5. Ismail and Salinas (1999) numerically obtained this coefficient for the frost surface region (F_s) as -0.33, which is constant throughout the flat plate (plate and ambient air temperatures are 263 K, and 293 K, respectively).

The correlation used to obtain the effective thermal conductivity of frost layer is given below.

Mao et al. (1992): $$k_{eff} = 0.02422 + 7.214x10^{-4}\rho_{fr} + 1.1797x10^{-6}\rho_{fr}^2 \quad (5.7)$$

Ostin and Andersson (1991):

$$k_{eff} = -8.71x10^{-3} + 4.39x10^{-4}\rho_{fr} + 1.05x10^{-6}\rho_{fr}^2 \quad (5.8)$$

Lee et al. (1997): $$k_{eff} = 0.132 + 3.13x10^{-4}\rho_{fr} + 1.6x10^{-7}\rho_{fr}^2 \quad (5.9)$$

Sanders (1974): $$k_{eff} = 1.202x10^{-3}\rho_{fr}^{0.963} \quad (5.10)$$

The dimensions for the frost density is [kg/m^3] and that for the thermal conductivity is [W/mK].

The following equations are used for the calculation of frost thickness and density as given by Mao et al. (1992).

Frost thickness: $$\delta_{fr} = 0.156\left(\frac{x}{d_H}\right)^{-0.098} w_\infty^{1.723}\Delta T^{1.1}\,Re_{dH}^{0.343}\,Fo_{dH}^{0.655} \quad (5.11)$$

Average frost density: $$\rho_{fr} = 5.559x10^{-6}\left(\frac{x}{d_H}\right)^{-0.137} w_\infty^{-0.413}\Delta T^{-0.997}\,Re_{dH}^{0.715}\,Fo_{dH}^{0.252} \quad (5.12)$$

where $\Delta T = T_{tp} - T_c$ is the difference between the triple point and plate temperatures, and d_H is the hydraulic diameter. The applicable range of the above relations is

$-15°C < T_c < -5°C$, $3x10^3 < Re_{dh} < 7x10^3$, $13 < Fo_{dh} < 104$, $0.004 < w_\infty < 0.01$

The important equation for predicting the asymptotic frost layer thickness is given below,

$$\delta_0 = \frac{D_{eff,0} \frac{d\rho_v}{dT} k'(T_{tp} - T_{c0})}{h_{m,0}(w_\infty - w_s)} \tag{5.13}$$

where, $k' = \frac{k_{eff}}{k_{frost-surface}}$

δ_0 is the frost thickness when the frost surface temperature reaches the triple point temperature and the growth rate equals zero.

During frost formation, both thickness and density are found to increase. There are different approaches to calculate the percentage of condensed water that increases the density of the frost layer. O'Neal and Tree (1985) offers an analytical equation for this purpose. Another observation is made by Ostin and Andersson (1991). Their experimental results indicate that half of the condensed water vapor increases the thickness and the other half increases the density of frost layer (Ostin and Andersson, 1991). Mao et al. (1991, 1992 and 1993) experimentally measured the density of frost for laminar air flow over horizontal plate, and they gave the correlation for density change of frost with time.

Some more details of the previous studies are given below,

Tao et al. (1993) simulated the frost deposition on a cold surface exposed to warm moist airflow using a one dimensional, transient formulation based on the local volume averaging technique. The spatial distribution of the temperature, ice-phase volume fraction (related to the average frost density), and rate of phase change within the frost layer are predicted. The results indicate that the local effective vapor mass diffusivity is up to seven times larger than the molecular diffusivity of water vapor in air expressed by Fick's law for frost temperatures between 264 K and 272 K. This result is comparable with data measured for water vapor diffusion in snow.

Frost growth on an initially clean cold surface is divided into two periods: an early, relatively short, crystal growth period, and a fully developed frost layer growth period. Due to structural differences, only in the fully developed growth period can the frost layer be modeled as a homogeneous (in a macroscopic sense), porous medium. During the early crystal growth stage, convective heat and mass transfer over ice columns, rather then diffusion within the frost, is the main mechanism for frost growth. It is indicated that the mass rate of phase change per unit volume, m (which is the rate of densification), has a maximum absolute value near the frost-air interface, the warm side of frost layer. This trend leads to frost in that region densifying faster than that at the region close to the cold plate. For Tc=263 K, during the early growth period, heat flux (Q) increases with time, indicating the strong fin-effects. As the frost grows further, Q decreases monotonically. It is concluded that under the same ambient conditions (T_∞, u_∞, w_∞) the phase change effect is weaker for the low cold plate temperature. On the other hand the reduction on heat transfer (sensible + latent heat) due to frost build up is more significant for the cold plate at a lower surface temperature.

Ostin and Andersson (1991) made an experimental study for the formation of frost in parallel horizontal plates facing a forced air stream at varying temperatures, relative humidities and air velocities. Both the surface temperature of the plates and the relative humidty of air stream are found to have important effects for the frost thickness. The actual area of testing is on two aluminum plates that are each 10 mm thick, 800 mm long and 300 mm wide. Inlet air temperature is kept constant around 20°C. The thickness of frost is measured by a micrometer. The mass of frost is recorded by a digital-weighing machine. The whole test section is weighed by means of shaft mechanism. Frost thermal conductivity (k) and specific heat capacity (ρC_p) are measured by means of the transient method. As a result of the study, two different frost growth periods are observed. One is monotonic growth the other is cyclic growth period.

The frost mass is found to increase linearly with time for different plate temperatures and air humidities. The rate of increase of frost mass with time is found to be almost independent of the cold plate temperatures, whereas the inlet air humidity had a more pronounced effect. The mass rate increased by a factor of 2.3 and 3.6 at 51% and

72% humidity, compared with 31% test run. Once frost has developed on the plate and the frost surface temperature has risen to a constant value, after the initial transient period, further frost deposition is mainly dependent on the air humidity.

Both the cold plate temperature and the air humidity were found to have a large effect on the frost thickness. Decrease of plate temperature from –7 to –20 °C almost doubled the frost thickness for inlet air humidity of 30%. When increasing the inlet air humidity from 31 to 72% at cold plate temperature of -10°C the frost thickness increased by 86%.

During the time of frost formation, both thickness and density is found to increase. Experimental results indicate that half of the condensed water vapor increases the thickness and the other half increases the density of frost layer. The effect of air velocity on the thickness was found to be negligible. However, the effect of velocity on the mass rate is considerable. The mass rate is increased by a factor of 2.4 for a test run with a velocity of 5.7 m/s compared to 2.6 m/s.

Lee et al. (1997) developed an analytical model for the formulation of a frost layer on a cold flat surface by considering the molecular diffusion of water, and heat generation due to the sublimation in the frost layer. The frost growth process is divided in to two periods: a crystal growth period and a fully developed frost growth period. The previous results are not accurate in predicting the surface temperature of the frost. The rate of water vapor transferred from air to frost surface per unit area, resulting from the differences between an absolute humidity of the air and saturated absolute humidity of the frost surface. A portion of the water vapor transferred into the frost surface from moist air increases the frost layer density and the rest of it increases the frost thickness.

A closed loop wind tunnel is used for experimentation. Air inlet temperature is kept constant as 25 °C and relative humidity (50% to 80%) and air velocity over the plate (0.5 to 2 m/s) are changed. In the study, the analogy between heat and mass transfer on the frost surface is used. As a result of the experimental study a Lewis (Le) number expression obtained. This equation can be used to obtain the mass transfer coefficient (h_m).

$$Le = 0.89\left(\frac{w_a}{w_{STD}}\right)^{0.66}\left(\frac{V_a}{V_{STD}}\right)^{0.097} \tag{5.14}$$

V is air velocity over the plate. STD represents baseline condition which is T_a=25°C, RH=70%, V=1.0 m/s, T_p=-15°C, Le=0.89.

The surface temperature of the frost rises with increasing air humidity. The increase of surface temperature of the frost is due to the increase of the thermal conductive resistance of the frost layer. The latter increase results from the rapid growth of the frost layer with a low density due to the large driving potential of the mass transfer with increasing humidity. The air velocity is changed from 0.5 to 2 m/s. The thick frost grows with increasing air velocity. The surface temperature of frost increases rapidly with increasing air velocity. The difference in frost thickness between the leading edge and downstream areas of the flat plate reduces with increasing air velocity.

Gall et al. (1997) derived a one-dimensional transient formulation to predict frost growth and densification on a cold wall exposed to moist airflow. The model is based in a local volume averaging technique. In the study, a 1D frost growth model is introduced. Focus is given to the estimation of diffusion, resistance factor (F). The results are compared with previous results in the literature. An experimental study for limited range is made and results are given. According to experiments, the F value is found to be between 0 to 1.5 (Nevertheless, it is generally difficult to get a single satisfying value of F for the whole test duration). Finally, it is observed that the effective vapor mass diffusivity throughout the frost reaches values several times larger than the molecular diffusivity, so that the presented model is in agreement with experimental data.

Ismail and Salinas (1999) numerically evaluated the parameters involved in modeling the process of frost formation on flat cold surfaces subject to the flow of humid air. The model employs one-dimensional transient formulation based upon the local volume averaging technique. The modeling process was validated by comparison with available experimental data. Numerical experiments were conducted to determine the best initial values of the diffusivity, initial radius and geometry of the ice crystals. This model was applied to the known case of flow of humid air over a single cold flat-plate to predict the frost temperature, density and thickness distribution, and void fraction along the flow direction. The results were compared with available results in the literature. The model was then extended to solve the case of flow of humid air between two parallel cold plates for which there are no available results. They indicated the importance of the initial values. It is concluded that a good initial value of the radius of the ice column could be $52x10^{-6}$ [m]. Diffusion factor on frost surface layer (F_s) can be taken as a constant at (–0.33).

5.1.2 Effect of frost on flow and heat transfer characteristics of evaporator

Effects of frost on evaporators are studied mostly for heat pump applications. There are also some studies on refrigerator evaporators. The effect of frost appears in the overall heat transfer coefficient and pressure drop terms. According to these studies, the pressure drop through an evaporator asymptotically increases as frost builds up. It is not clear whether there is a general pattern for overall heat transfer value (UA). While some studies showed the increasing-trend (e.g. Rite and Crawford (1991), Ali and Crawford (1992)), some show a decreasing-trend as indicated by Ogawa et al. (1993), and some show first increasing and then a decreasing trend (Stoecker (1957), Hosoda and Uzahashi (1967)). The overall heat transfer coefficient is not purely a function of the frost thickness but also a function of the geometry, the frost properties and the flow rate of the air flowing across the coils. As such, the complexity of the problem is apparent. Therefore, there is no common consensus on the UA change of evaporators. Apparently, it has different patterns for different evaporators and flow conditions.

One of the earliest investigators to report the variations of UA with frost was Stoecker (1957). He tested two different evaporator fin pitches (9 and 4 fins per inches). The airflow rate was maintained constant using flow dampers. He reported that:

- There is an initial increase in UA with the onset of frosting. This is attributed to an increase in heat transfer area as a result of increasing surface roughness when the frost first forms. The roughness also increases the flow velocity of the air and this results in an increase in UA.

- Eventually the value of UA decreases. This trend is a result of the insulating effect of the frost as the frost layer grows.

Rite and Crawford (1990) experimentally studied the frosting effect on contact resistance. They found that the decrease in the contact resistance due to the filling of the gaps between the evaporator tube and mechanically joined fins is negligible. Ali and Crawford (1992) insisted that the increase on UA value is because of having larger local velocities because of increasing frost thickness.

One of the latest studies on a commercial refrigerator showed that the general pattern of evaporator effectiveness value (UA/mC_p) can be evaluated as three consecutive periods (Stein ,1999). During these periods, effectiveness value first increases, then remains almost constant, and finally decrease sharply as frost starts blocking the evaporator passages. The duration of these periods (increasing, steady, and decreasing) change with the frosting rate.

Some more details of previous studies are given as follow.

Rite and Crawford (1991) evaluated the effect of frost on the UA-value and the airside pressure drop of a domestic refrigerator-freezer evaporator with interference fit fins. The parameters for the experiments were as follow; fin density: 5 mm/fin, the air-velocity: 0.4-1.3 m/s, surface temperature: -29°C to -23°C, relative humidity: 52% to 72%, air temperature: -2°C to –7°C. Over a ten-hour test period, during which the airflow was maintained at a constant rate, the UA-value was found to steadily increase as frost was deposited on the coil. This UA-value increase was accompanied by a substantial increase in the air-side pressure drop. In an effort to determine the reasons behind the increase in the UA-value, a section of the evaporator was instrumented with thermocouples. It was determined that the increase was due to an increased air-side heat transfer coefficient and an increase in the surface area of the evaporator due to the surface roughness of the frost. The decrease in the contact resistance due to the filling of the gaps between the evaporator tube and mechanically joined fins was determined to be negligible.

Frosting and defrosting effects on coil heat transfer were discussed by Niederer (1976). Niederer studied finned tube air coolers with four different fin patterns were examined. These patterns included a heat exchanger with 6 fpi (4.2 mm/fin), 4 fpi (6.4 mm/fin), and two with a variable number of fins. Ammonia was used as the refrigerant in the cooler and the evaporator was run in flooded condition so as to maintain a constant refrigerant temperature of 20 F (-6.7 °C) throughout the heat exchanger. The air inlet temperature was maintained at 32 F (0 °C) with a relative humidity of 85%. The air flow through the coil was allowed to vary as frost collected on the coil. The result that Niederer found was that the increase in the heat transfer coefficient on the air side of the coil due to the initial frost formation was more than offset by the reduced airflow through the coil. This led to a reduction in air cooler heat transfer capacity. Niederer also concluded that the reduction in airflow was more apparent for the closer fin spacing heat exchangers than the wider fin spacing exchangers. In addition, the variable fin-spacing coils were less affected than the constant fin-spacing coils for the same amount of accumulated frost.

Gatchillov and Ivanova (1979) studied the frosting of extended surface air coolers with copper tubes and aluminum fins. Three different fin spacing for the same counterflow heat exchanger configuration were looked at: 7.5 mm, 10 mm, and 15 mm. The environmental conditions studied included inlet air relative humidities of 74% and 88%, an inlet air temperature of 0°C and air velocities of between approximately 1.5 m/s to 7.6 m/s. The main temperature difference between the air and the brine filled coil was maintained at approximately 7°C. The main emphasis was on characterizing the effect of humidity and air velocity on frost thickness, roughness, and density. they found that over a ten-hour test period the frost thickness increased more rapidly with higher air relative humidities and higher air velocities. The surface roughness is important because it influences both the pressure drop across the coil (higher friction factor) and the heat transfer coefficients on the outer tube surfaces. The density of the frost was found to increase with time, velocity, and relative humidity.

Barrow (1985) undertook an analytical study of the frosting process on plane wall surfaces and surfaces with straight fins. The two geometries that were chosen were designed to be a useful representation of the heat transfer surfaces on heat pump evaporator coils. Through this analysis, Barrow arrived at several conclusions. Comparing the insulating effect of the frost in the plane surface case with its effect when there are fins on the surface, Barrow found that the insulating effect is much less apparent when there are fins. The reason for this is that the high conductivity of the fin core material is the controlling parameter for heat transfer through the fins with the frost having negligible influence. Therefore, the surface geometry of the fins as well as their thermal properties are important in the assessment of the effects of frosting. Another conclusion that he came to was that the insulating effect of frost does not completely explain the reduction in heat transfer capacity of frosted evaporators. This capacity reduction is mainly due to the reduction in airflow through the coil due to the blockage of the coil. One this premise is accepted, it can be seen that the thickness of the frost is much more important than its density or thermal conductivity as far as heat transfer is concerned. However, the thermal properties of the frost are important for predicting the growth rate of the frost.

Kondepudi and O'Neal (1987 and 1990) studied frosting in heat pump evaporators with a variety of fin configurations: flat, wavy, and louvered. The following testing conditions were considered: Air velocity: 0.7 m/s, 1 m/s ; Fin spacing: 2,54 mm/fin, 1.4 mm/fin; Relative humidity: 65%, 80%: Air inlet temperature: 0°C; Refrigerant temperature: -12°C. It was found that the louvered fins had slightly higher frosting rate than the others and significantly higher pressure drop. The louvered fin heat exchanger also proved to have a larger overall heat transfer than other two and retained this advantage even with an accumulation of frost. Unlike previous researchers' findings, Kondepudi and O'Neal did not find any detrimental effect on the heat transfer coefficient, enthalpy change, or effectiveness due to frost formation for the fifty-minute test duration. The tests were limited to fifty minutes because heat exchanger blockage at that point was so extensive that a constant airflow across the coil could not be maintained. Two additional findings that were made were that the frosting rate increased as relative humidity increased and as air velocity increased.

Three computer simulation models of the evaporator portion of a heat pump system under dry, wet, and frosted conditions were developed by *Oskarsson et al. (1990a and 1990b)*. The models consist of a detailed finite element model, a three-region model, and a parametric model. All of the models utilize a number of coefficients derived empirically by various researchers. The coefficients that were used involve heat transfer coefficients for the refrigerant and air sides of the exchanger as well as frost growth rate coefficients and pressure drop factors both the refrigerant side and the frosted side. One important point that must be mentioned is that no attempt was made to modify the air side heat transfer coefficient to account for the apparent augmentation provided by the initial frost formation as described by many researchers previously cited. The finite element model which divides the evaporator into fifty sections was determined to be the most accurate although it did require an extremely long time to run. It was used as a benchmark along with some experimental data to verify the accuracy of the other two models. The three-region model divides the evaporator into only three parts (two-phase region, transitional region, and superheated region), neglects the refrigerant side pressure drop, and assumes that no dehumidification of the air takes place in the superheated section of the evaporator. Although it was very fast computationally-compared with the finite element model, it was found to give results in very good agreement with the finite element model. The last model, the parametric model, was determined to be satisfactory but required that different coefficients be put into the model depending on whether the coil was dry, wet, or frosted. This model uses two parameters, the coil characteristic and the coil enthalpy effectiveness, to describe the coil performance. Data generated by the three-region model were used to develop the coefficients needed to define the coil characteristic and the effectiveness.

5.2 Frosted Evaporator Modeling

5.2.1 Geometry of evaporator

A variety of evaporators is used in domestic refrigerators. Although the main concern is always thermal performance, the manufacturability is another important feature that sometimes causes an evaporator to have lower performance. Tube passes, fin-tube contacts, and the shape of fins change from one company to another. Refrigerator evaporators differ from heat pump evaporators (heat exchangers). The main differences are the fin densities and the direction of air flow. In refrigerators, fin densities are generally less then that of the heat pump evaporators. While the fin spacing of refrigerator evaporators are around 10 mm, fin spacing is generally less then 5 mm in heat pump evaporators. Another typical difference is seen on the evaporator refrigerators' fin spacing, which is not same throughout the evaporator. Generally, in the bottom portion of refrigerator evaporators that humid air first contacts, the fin spacing is larger then the upper portions. This is to prevent the quick blockage of evaporator. The fin spacing in heat pump evaporators is kept constant along the evaporator.

Another difference between the evaporators is related to airflow type. Unlike heat pumps where air pass the evaporator as cross flow, the airflow in refrigerators are mostly counter flows where air flows through vertical direction in the evaporator. These differences are summarized in Figure 5.1.

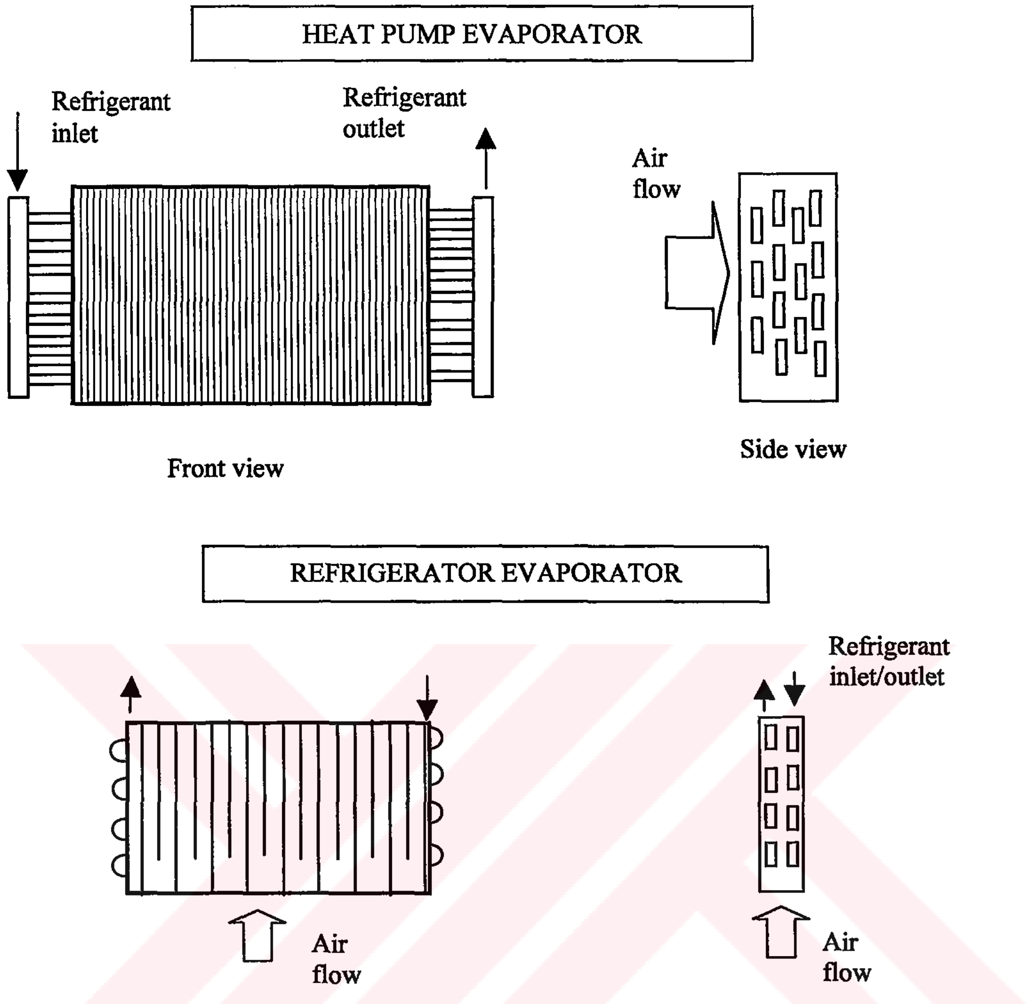

Figure 5.1 A schematic view of heat pump and refrigerator evaporators

As previously indicated, most of the studies about frosted evaporators are for heat pump applications. Results of these studies are not directly applicable to refrigerator evaporators because of above defined differences. Even for studies related to refrigerator evaporators, because of geometry variability, the results are difficult to generalize. Those explanations show why it is necessary to study on the specific evaporator geometry.

In this study, the evaporators manufactured by Brazeway Inc. are investigated. Some details of these evaporators are given in Figure 5.2. While the fin density, number of tubes and air flow rates are chosen as parameters of the study, other characteristics such as fin geometry, tube spacing and alignment, and tube-fin contact remained same throughout the studies. Basic dimensions of evaporator are shown in Figure 5.2.

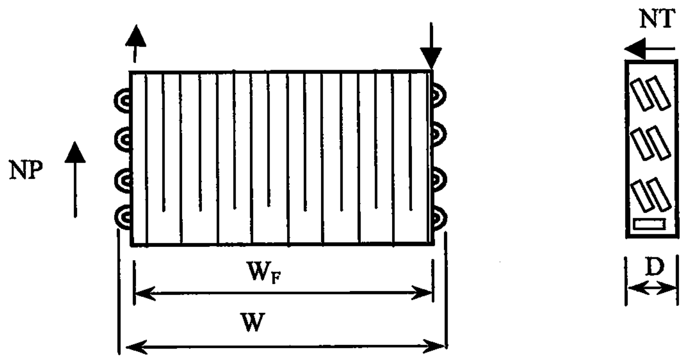

Figure 5.2. The overall dimensions of refrigerator evaporator (NP: number of tube on air flow direction, NT: Number of tubes perpendicular to flow direction)

Below, the details of evaporator geometry and fin are given.

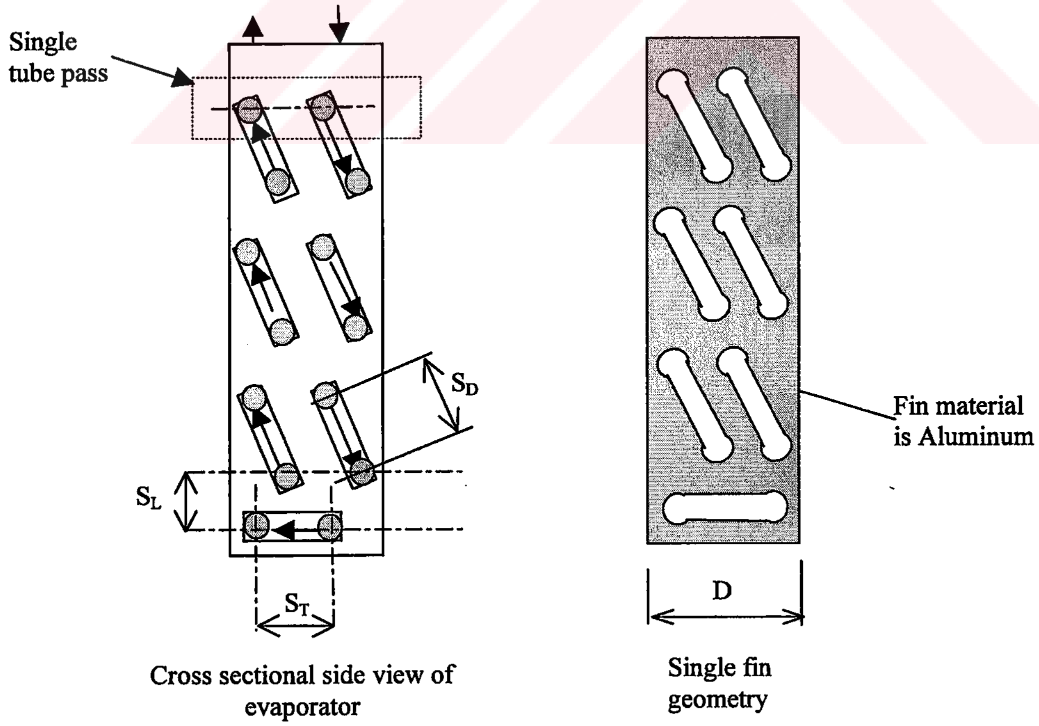

Figure 5.3 Cross-sectional view of evaporator and single fin geometry

The following geometrical calculations are made for a single tube pass. This allows expanding the calculation for evaporators that have different fin spacing and pass numbers. It should be noted that these equations are given for dry evaporator.

Total tube length including the return bends is given as follow,

$$L = NT\left(W - 2\left(R_b + \frac{d_0}{2}\right) + 2\left(\frac{2\pi R_b}{4}\right)\right) \tag{5.15}$$

$$R_b = \frac{S_D}{2} \tag{5.16}$$

The cross sectional free flow area of duct, where evaporator located, is

$$A_{free} = W.D \tag{5.17}$$

The minimum cross-sectional flow area,

$$A_{min} = (D - NT.d_0)(W - NF.\delta_F) \tag{5.18}$$

Tube inner surface area,

$$A_i = NT(\pi d_i L) \tag{5.19}$$

Tube outer surface area,

$$A_o = \pi d_0 (L - NF.\delta_F) NT \tag{5.20}$$

Total fin surface area,

$$A_F = NF.A_{sf} \tag{5.21}$$

Total heat transfer area,

$$A_T = A_o + A_F \tag{5.22}$$

Fin area ratio,

$$\varepsilon = \frac{A_T}{A_o} \tag{5.23}$$

where,

A_o:	Tube outer surface area (primary area) [m^2]
A_F:	Fin surface area (secondary area) [m^2]
$A_T = A_F + A_o$:	Total heat transfer area [m^2]
A_{min}:	Minimum flow area [m^2]
A_{free}:	Free flow area [m^2]
A_{sf}:	Surface area of single fin [m^2]
δ_F:	Fin thickness [m]
d_0:	Tube outer diameter [m]
d_i:	Tube inner diameter [m]
W:	Total evaporator width [m]
D:	Total evaporator depth [m]
W_F:	Finned width of evaporator [m]
NF:	Number of fins
NT:	Number of tubes perpendicular to air flow direction
NP:	Number of tubes on air flow direction
ε:	Fin area ratio [-]

5.2.2 Mathematical model

5.2.2.1 The overall heat transfer coefficient (UA)

The following assumptions are made to characterize a frosted evaporator.

- All heat transfer surfaces are below freezing temperatures
- Frost thickness and density are homogeneously distributed on each tube pass
- The whole frosting process is assumed as quasi-steady
- The thermal conductivity coefficient of frost layer depends on only the density of frost
- Whole frost layer is described by using the average thermal properties
- The thermal radiation heat transfer between evaporator and surrounding surfaces are assumed negligible
- All heat and mass transfer processes are regarded as one dimensional

- The air at the inlet of evaporator is perfectly mixed

The overall heat transfer coefficient for dry, finned evaporator can be defined as follows.

$$\frac{1}{UA}=\frac{1}{h_r A_i}+\frac{1}{h_a \eta_s A_T}+R_{tw}+R_c+R_f \tag{5.24}$$

The tube material is aluminum and tube walls are relatively thin, therefore the thermal resistance of tube wall (R_{tw}) can be neglected. The further simplification of equation (5.24) may be done by taking the contact resistance (R_c) between fin and tube surface (R_c) and the fouling resistance (R_f) on both refrigerant and air side as zero. The contact resistance for refrigerator evaporators have been found to be negligible by Rite and Crawford (1991). Final form assumed for the UA value is,

$$\frac{1}{UA}=\frac{1}{h_r A_i}+\frac{1}{h_a \eta_s A_T} \tag{5.25}$$

The refrigerant flow is assumed to be two-phase only, i.e there is not any superheat region. In actual conditions, the evaporator operates with some degree of superheat value. For instance, DOE requires that the refrigerator cooling system should be charged so that 2-3 °C superheat value is obtained at the exit of evaporator at ambient temperature of 32 °C. Admiraal and Bullard (1993) modeled an evaporator as three consecutive zones, which are two-phase, superheated, and desuperheated. Oskarsson et al. (1990a-b) modeled evaporators as consisting of two-phase, transition, and superheated regions. In the present study, in order to simplify the model, the evaporator is assumed to have a single zone, which is two-phase only. For this case, the convective heat transfer coefficient on refrigerant side is obtained from Chato-Wattelet (1993) correlation. Since this correlation is developed for low flow rates of refrigerant, it is found suitable for this study as well. The correlation is given as,

$$h_r=h_l\left(4.3+0.4\left(Bo.10^4\right)^{1/3}\right) \tag{5.26}$$

where,

$$Bo = \frac{q''}{G.h_{fg}} \tag{5.27}$$

and

$$h_l = 0.023\, Re_l^{0.8}\, Pr_l^{0.4}\, \frac{k_l}{d_i} \tag{5.28}$$

As the heat flux is required to get the heat transfer coefficient, h_r, the equations should be solved by using the total heat transfer rate that will be defined later.

A_o:	Tube outer surface area (primary area) [m^2]
A_F:	Fin surface area [m^2]
$A_T = A_F + A_o$:	Total heat transfer area [m^2]
h_a:	Air side heat transfer coefficient [W/m^2K]
U:	Overall heat transfer coefficient [W/m^2K]
η_s:	Overall surface effectiveness [-]
h_{fg}:	Phase change enthalpy [kJ/kg]
h_l:	Convective heat transfer coefficient for liquid flow [W/m^2K]
k_l:	Thermal conductivity of liquid phase refrigerant [W/mK]
Re_l:	Reynold number for liquid refrigerant flow [-]
Pr_l:	Prandtl number for liquid refrigerant [-]
d_i:	Tube inner diameter [m]
Bo:	Boiling number
q”:	Heat flux (=$h_r\Delta T$)

The use of surface effectiveness, η_s, combines the fin and tube surfaces as if they are only one surface at an average surface temperature. The definition of the surface effectiveness is given as (Incropera and DeWitt, 1996),

$$\eta_s = 1 - \frac{A_F}{A_T}(1 - \eta_F) \tag{5.29}$$

Here, η_F is dry fin efficiency of evaporator. Fin efficiency directly depends on geometry and fin material. As shown in Figure 5.3 for fins that are not continuous, it is quite difficult to find an analytical expression for fin efficiency. Karatas (1996) studied similar fins by using the finite element method. He found following curve-fit description of fin efficiency.

$$\eta_F = -3.429 m_F^4 + 6.457 m_F^3 - 4.308 m_F^2 + 0.736 m_F + 0.949 \qquad (5.30)$$

Where m_F is fin parameter given by Karatas (1996).

$$m_F = \sqrt{\frac{2h_a d_0^2}{k_F \delta_F}} \qquad (5.31)$$

here,

k_F: Thermal conductivity of fin material [W/mK]
δ_F: fin thickness [m]
d_0: Tube outer diameter [m]

Air-side heat transfer coefficient is studied experimentally by Karatas (1996). He found the Colburn j factors for the evaporator given in Figures 5.3 and 5.4. By using these correlations, the airside heat transfer coefficient is defined as follows.

$$h_a = 0.113\, Re_a^{0.755}\, Pr^{1/3}\, \varepsilon^{-0.420} \frac{k_a}{d_o} \qquad (5.32)$$

$300 < Re_a < 1000$, and $3.43 < \varepsilon < 5.92$

If ε factor becomes smaller than 3.43, the following relation should be used.

$$h_a = 0.113\, Re_a^{0.719}\, Pr^{1/3}\, \varepsilon^{-0.407} \frac{k_a}{d_o} \qquad (5.33)$$

$300 < Re_a < 1000$, $1.0 < \varepsilon < 5.92$

here, ε is finning factor. The Reynolds number is defined as;

$$Re_a = \frac{G_{max} d_o}{\mu} \qquad (5.34)$$

where,

$$G_{max} = \frac{\rho_a \dot{V}}{A_{min}} \tag{5.35}$$

$$A_{min} = [W - (NT)d_o][D - (NF)\delta_F] \tag{5.36}$$

Effect of frost: The equations given above can be arranged to include the frost effect. The basic idea is finding a heat transfer coefficient for the air-side, which consists of the heat and mass transfer coefficients. Oskarsson et al. (1990a-b) and Seker (1999) used following definition for an effective heat transfer coefficient, h_{eff}.

$$h_{eff} = h_a + h_{lat} \tag{5.37}$$

where h_{lat} is obtained by applying the instantaneous energy balance on frost surface,

$$Q = h_a \eta_s A_T (T_a - T_s) + h_w \eta_s A_T h_{sg} (P_{wa} - P_{ws}) \tag{5.38}$$

Introducing the so-called latent heat transfer coefficient, h_{lat}, allows us to organize the above equation in terms of temperature differences only.

$$Q = h_a \eta_s A_T (T_a - T_s) + h_{lat} \eta_s A_T (T_a - T_s) \tag{5.39}$$

where,

$$h_{lat} = \frac{h_w h_{sg} (P_{wa} - P_{ws})}{(T_a - T_s)} \tag{5.40}$$

T_a and P_{wa} is the average of air inlet and outlet conditions of each tube pass.

$$T_a = \frac{T_{ai} + T_{ao}}{2} \tag{5.41}$$

$$P_{wa} = \frac{P_{wi} + P_{wo}}{2} \tag{5.42}$$

here,

h_w:	Mass transfer coefficient [kg/m^{2}skPa]
h_{sg}:	Sublimation enthalpy of water vapor [J/kg]
h_{lat}:	Latent heat transfer coefficient [J/kg]
P_{wa}:	Water partial pressure in ambient conditions [kPa]
P_{ws}:	Saturation pressure of water at surface temperature [kPa]
T_{ai}:	Air inlet temperature [°C]
T_{ao}:	Air outlet temperature [°C]

With the presence of frost, some additional changes should be made on the definitions of surface and flow areas. The new definitions are given as follow,

$$A_{o,fr} = \pi(d_0 + 2\delta_{fr})[L - (NF)(\delta_F + 2\delta_{fr})] \tag{5.43}$$

$$A_{min,fr} = [D - (NT)(d_o + 2\delta_{fr})][W - (NF)(\delta_F + 2\delta fr)] \tag{5.44}$$

$$A_{T,fr} = A_{o,fr} + A_F \tag{5.45}$$

The fin surface area (A_F) is assumed to remain constant while frost builds up, as it is a flat surface. Dry evaporator fin efficiency definition will again be used. A change because of frost will be made in fin parameter, m_F, by replacing "h_a" with "h_o".

$$m_{F,fr} = \sqrt{\frac{2h_o d_0^2}{k_F \delta_F}} \tag{5.46}$$

Here, h_o is total heat transfer coefficient on the frosted surface that is defined by including the frost layer thermal resistance,

$$h_o = \left(\frac{1}{h_{eff}} + \frac{\delta_{fr}}{k_{fr}}\right)^{-1} \tag{5.47}$$

The final form of overall heat transfer coefficient with the presence of a frost layer (including the heat and mass transfer coefficients) can be written as;

$$\frac{1}{(UA)_{fr}} = \frac{1}{h_r A_i} + \frac{1}{h_{eff} \eta_s A_{T,fr}} + \frac{\delta_{fr}}{k_{fr} \eta_s A_{T,fr}} \tag{5.48}$$

This definition is also used by Oskarsson et al. (1990a-b). A simplified form of this equation can be obtained by using the definition of h_o,

$$\frac{1}{(UA)_{fr}} = \frac{1}{h_r A_i} + \frac{1}{h_o \eta_s A_{T,fr}} \tag{5.49}$$

In the present model, Eqn. (5.49) will be used to model the overall heat transfer coefficient.

where,

$(UA)_{fr}$: Overall heat transfer coefficient of frosted evaporator [W/K]
$A_{T,fr}$: Total heat transfer area of frosted evaporator [m^2]
$A_{min,fr}$: Minimum flow area [m^2]
Ao,fr: Outer surface area frosted tube [m^2]
h_{eff}: Effective heat transfer coefficient [W/m^2K]
h_{lat}: Latent heat transfer coefficient [W/m^2K]
h_o: Equivalent heat transfer coefficient of frost layer [W/m^2K]
k_F: Fin material thermal conductivity [W/mK]
δ_F: Fin thickness [m]
m_F: Dry fin parameter
$m_{F,fr}$: Frosted fin parameter

5.2.2.2 Frost thermal conductivity (k_{fr})

Frost thermal properties have been studied by numerous researchers. All of them gave thermal conductivity relations in terms of frost density. Among these relations, a selection criterion has been set including the frost density range, and inlet air temperature as well as the geometry. Detailed comparisons of previous studies were made by Seker (1999). Finally, the correlations of Ostin and Anderssen (1991), and Sanders (1978) were found as applicable to frosting on refrigerator evaporators. According to Seker's study, Sander's definition is chosen as it covers most of the range of refrigerator operation conditions. The same relation will also be used in this study, which is;

$$k_{fr} = 1.202.10^{-3} \rho_{fr}^{0.963} \tag{5.50}$$

k_{fr}: Frost thermal conductivity [W/mK]
ρ_{fr}: Frost density [kg/m^3]

5.2.2.3 Frosting rate (m_{fr})

In order to calculate the frosting rate (mass transfer rate), calculation of the mass transfer coefficient is required. The heat and mass transfer analogy will be assumed for this purpose. Details of the analogy were given in Chapter-3. According to this, equation (3.15) can be rewritten for the mass transfer coefficient (h_W) as;

$$h_w = 0.00626 \rho_a h_a \frac{D_a}{k_a} \left(\frac{\alpha}{D_a} \right)^{1/3} \tag{5.51}$$

In this case, the frosting rate can be calculated by using the following formula,

$$m_{fr} = h_w A_{T,fr} (P_{wa} - P_{ws}) \tag{5.52}$$

On the other hand, this value can also be calculated by using the inlet and outlet air humidity ratios.

$$m_{fr} = \dot{m}_a (w_i - w_o) \tag{5.53}$$

Humidity ratios can be expressed in terms of water partial pressures.

$$w = 0.622 \frac{P_w}{P - P_w} \tag{5.54}$$

here,

k_a: Thermal conductivity of air [W/mK]

D_a: Diffusion coefficient for air/water systems [m^2/s]
$A_{T,fr}$: Total area of frosted surface [m^2]
h_w: Mass transfer coefficient [$kg/s.m^2.kPa$]
P_{ws}: Water partial pressure at surface, assumes saturation [kPa]
P_{wa}: Water partial pressure at airside [kPa]
P: Total atmospheric pressure [kPa]

5.2.2.4 Frost thickness and density calculation

The rate of water vapor transferred from air to unit area of frost surface is resulting from the differences between partial pressure of vapor in air and the partial pressure of vapor on the surface. A portion of water vapor transferred into the frost surface from moist air increases the frost layer density and the rest of it increases the frost thickness (Tao et al. (1993), Ostin and Andersson (1991)). The important question arises as "what portion increases the thickness, and what portion increases density?" There is no common consensus about these percentages yet. The dependence to the time, flow characteristics and surface geometry makes it difficult to find common relations. Ostin and Andersson (1991) observed that roughly the half of mass goes to increase the thickness, and the other half goes to increase density. Another approach is defined by O'Neal and Tree (1985), which is a purely analytical definition. This approach was also used by Seker (1999). Preliminary checks showed that there was important differences between Ostin and Andersson's observations and O'Neal and Tree's approach. Therefore the "densification rate, χ" is chosen as a parameter for the numerical analysis. The details of these analyses will be given later in this chapter. Until accurate values of frost density for domestic refrigerator application is obtained, the densification rate will be used as a parameter. The frost thickness and density increase relations will be based on this parameter, that is;

$$m_\rho = \chi m_{fr} \tag{5.55}$$

$$m_\delta = (1-\chi) m_{fr} \tag{5.56}$$

The frost thickness and density increase for a given time step is given below.

$$\Delta\delta_{fr} = \frac{m_\delta \Delta t}{A_T \rho_{fr\_previous}} \tag{5.57}$$

$$\Delta\rho_{fr} = \frac{m_\rho \Delta t}{A_T \delta_{fr\_previous}} \tag{5.58}$$

Then by using these definitions, the frost thickness and density values reached after one time step can be calculated as follow.

$$\delta_{fr} = \delta_{fr\_previous} + \Delta\delta_{fr} \tag{5.59}$$

$$\rho_{fr} = \rho_{fr\_previous} + \Delta\rho_{fr} \tag{5.60}$$

where,

m_{fr}:	Frost deposition rate [kg/s]
m_ρ:	Mass rate that goes to increase the density [kg/s]
m_δ:	Mass rate that goes to increase the frost thickness [kg/s]
χ :	Densification rate [-]
δ_{fr}:	Frost thickness [m]
ρ_{fr}:	Frost density [m]
$\delta_{fr\_previous}$:	The frost thickness calculated in previous time step [m]
$\rho_{fr,previous}$:	Frost density calculated in previous time step [kg/m^3]

As it can be seen from Eqns. (5.57) and (5.58) that it is necessary to estimate an initial value in order to start calculations. Depending on the densification rate the solution may be strongly sensitive to these initial values. Seker (1999) studied the effect of initial values and came to a conclusion that the values of density and thickness at time zero can be used as 40 kg/m3 and 0.05 mm respectively. These values will also be used in this study, and the conclusions will be made according to these assumptions.

5.2.2.5 The total heat transfer rate

Total heat transfer rate of evaporator can be calculated by using air-side enthalpy change of humid air.

$$Q = \dot{m}_a \left(h_{ai} - h_{ao}\right) \tag{5.61}$$

Alternatively, if we neglect the sensible heat transfer which is used to cool the ice below 0°C, the total heat transfer rate can be obtained from following equations,

$$Q = Q_{sensible} + Q_{latent} \tag{5.62}$$

$$Q = (UA)\Delta T_m + m_{fr} h_{sg} \tag{5.63}$$

On the other hand, this value can also be calculated by using the frosted UA value (it includes the sensible and latent heat transfer coefficients).

$$Q = (UA)_{fr}\, \Delta T_m \tag{5.64}$$

where,

Q :	Total heat transfer from evaporator surfaces [W]
ΔT_m:	Logarithmic mean temperature difference [K]
h_{ai}:	Enthalpy of humid air at inlet condition [kJ/kg_air]
h_{ao}:	Enthalpy of humid air at outlet condition [kJ/kg_air]
h_{sg}:	Sublimation enthalpy, assumed constant [kJ/kg]
m_a:	Air mass flow rate [kg_air/s]
P:	Total air pressure [Pa]
w_i:	Inlet air humidity ratio [kg/kg_air]
w_o:	Outlet air humidity ratio [kg/kg_air]

The following relations are given in ASHRAE Fundamentals Handbook (1997) for the saturation pressure of water vapor.

$-100°C < T < 0\ °C$

$$\ln(P_{ws}) = \frac{C_1}{T} + C_2 + C_3 T + C_4 T^2 + C_5 T^3 + C_6 T^4 + C_7 \ln(T) \tag{5.65}$$

$0°C < T < 200\ °C$

$$\ln(P_{ws}) = \frac{C_8}{T} + C_9 + C_{10}T + C_{11}T^2 + C_{12}T^3 + C_{13}\ln(T) \tag{5.66}$$

where, P_{ws} [Pa], T [K]

Table 5.1 Coefficients given in Eqns. (5.43) and (5.44) (ASHRAE Fund. Handbook, 1997)

C1= -5674.359	C8=-5800.2206
C2=6.392524	C9=1.3914993
C3=-9677.843	C10=-4.8640239E-2
C4=6.22157E-7	C11=4.1764768E-5
C5=2.0747825E-9	C12=-1.4452093E-8
C6=-9.484024E-13	C13=6.5459673
C7=4.1635019	

Enthalpy of humid air can be calculated by following relation given in ASHRAE Fundamentals Handbook (1997).

$$h = 1.006T + w(2501 + 1.805T) \tag{5.67}$$

where,

T: Dry bulb temperature of air [°C]
w: humidity ratio of air [kg/kg_air]

5.2.2.6 Pressure-drop calculations and its effect on air flowrate

The airside pressure drop of a dry refrigerator evaporator is not considerable relative to the other pressure drops in the fan exit, air distribution channels, fittings etc. Therefore, this pressure-drop is mostly neglected in air-distribution system sizing. However, as frost starts to build up on evaporator surfaces, the pressure drop becomes significant because frosting increases surface roughness and narrows air passages. According to Rite and Crawford (1991), Ali and Crawford (1992), and Seker (1999) the pressure drop almost exponentially increases as frost thickness increases. The increase on pressure-drop results in a decrease on airflow rate. Therefore, all the frosting and heat transfer parameters are affected. Because of this phenomenon, the heat and mass transfer relations should be solved simultaneously.

In this study, after obtaining the pressure-drop for each time step, the fan air flowrate will be calculated for next step by using the solver developed in Chapter-4. The same refrigerator cabinet and air distribution system will again be used for air flowrate calculations.

Most airside pressure-drop models are assume the following equation, which is typical of the pressure drop across finned tubes (Ali and Crawford, 1992).

$$\Delta P = E + FV^2 \tag{5.68}$$

In this relation, "E" represents an arbitrary experimental constant. "F" is another constant that represents the geometry of evaporator, fluid properties, and friction factor as well. Ali and Crawford (1992) defined the constants experimentally for a typical nofrost refrigerator evaporator, which has 8 tube passes.

E= 0.011623 [in.H_2O]

F= 5.847e-7 [in.H_2Omin^2/ft^2]

The original equations were given in English units, and are used in similarly here. V is air velocity [ft/min], which is obtained from the minimum flow area cross-section.

$$V = \frac{\dot{V}}{A_{min,fr}} \tag{5.69}$$

Where $A_{min,fr}$ was given in equation (5.44). Since the above-defined equation is given for whole evaporator, by dividing it to number of tube passes, the average pressure-drop relation for a single tube pass can be obtained as an approximate value. This definition will help us analyze the evaporator as if it consists of separate tube rows.

Seker (1999) studied the Brazeway type of evaporators as the one used in presented study. He calculated the pressure-drop value by using the Kays and London (1992) definiton.

$$\Delta P = \frac{G_{max}^2}{2\rho_i}\left[\left(1+\sigma^2\right)\left(\frac{\rho_i}{\rho_e}-1\right)+f\,\frac{A_{T,fr}}{A_{min,fr}}\,\frac{\rho_i}{\rho_m}\right] \tag{5.70}$$

$$\sigma = \frac{A_{min,fr}}{W.D} \tag{5.71}$$

here,

ρ_i:	The density of air at the inlet [kg/m^3]
ρ_e:	The density of air at the outlet [kg/m^3]
ρ_m:	The density of air at average air temperature [kg/m^3]
f:	Friction factor [-]

An important parameter in this equation arises as friction factor "f". This value is experimentally defined for dry evaporators by Karatas (1996) as;

$$f = 0.152\,Re^{-0.164}\,\varepsilon^{-0.331} \tag{5.72}$$

Ali and Crawford's (1992) correlation is obtained for the frosted case, therefore it includes the surface roughness change. Their correlation is not directly applicable to Brazeway type evaporators because of the geometry differences. Karatas's (1996) study is made on the same type of evaporator (Brazeway type). However, the main disadvantage arises as it is only made for dry evaporator. On the other hand, as the airflow through evaporator is mostly laminar, the surface roughness change will not be important in the domestic refrigerator applications. Therefore, Seker and Karatas's definitions and procedure are assumed for use in this study.

5.2.2.7 Calculation of frost/air interface (surface) temperature

The most important calculation step is the evaluation of the average surface temperature for each time step. The surface temperature and corresponding water saturation pressure are the driving mechanisms for frost accumulation. Therefore, each new step for calculation of frost thickness and heat transfer values require the surface temperature. To calculate this value, the energy balance relation on the frost surface is written. In this equation, all the vapor is assumed to condense on the surface.

$$Q = Q_{sensible} + Q_{latent} = h_a \eta_s A_T (T_s - T_a) + m_{fr} h_{sg} \tag{5.73}$$

The air temperature is assumed as the average value of inlet and outlet temperatures for each pass.

$$T_a = \frac{T_{ai} + T_{ao}}{2} \tag{5.74}$$

From the air-side, we also know that the total heat transfer rate is,

$$Q = \dot{m}_a (h_i - h_o) \tag{5.75}$$

The unknowns in the above equations are T_{ao} and T_s. These values can be solved for each time step.

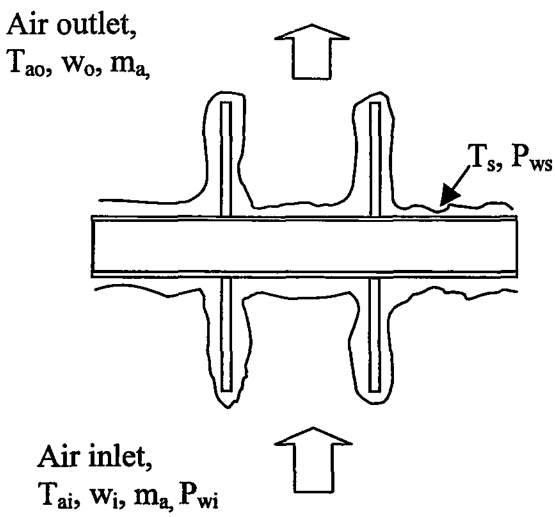

Figure 5.4 Flow around a portion of frosted evaporator

5.2.3 Inlet conditions of the evaporator

In domestic refrigerators, the return air temperature and humidity depends upon the air distribution system. In refrigerators with a single evaporator, the air returned from freezer and freshfood cabinets are mixed just before the evaporator. On the other hand, in the dual evaporator refrigerators, the air enters each evaporator separately, so they are not mixed. Figure 5.5 summarizes the single and dual evaporator refrigerator's inlet conditions.

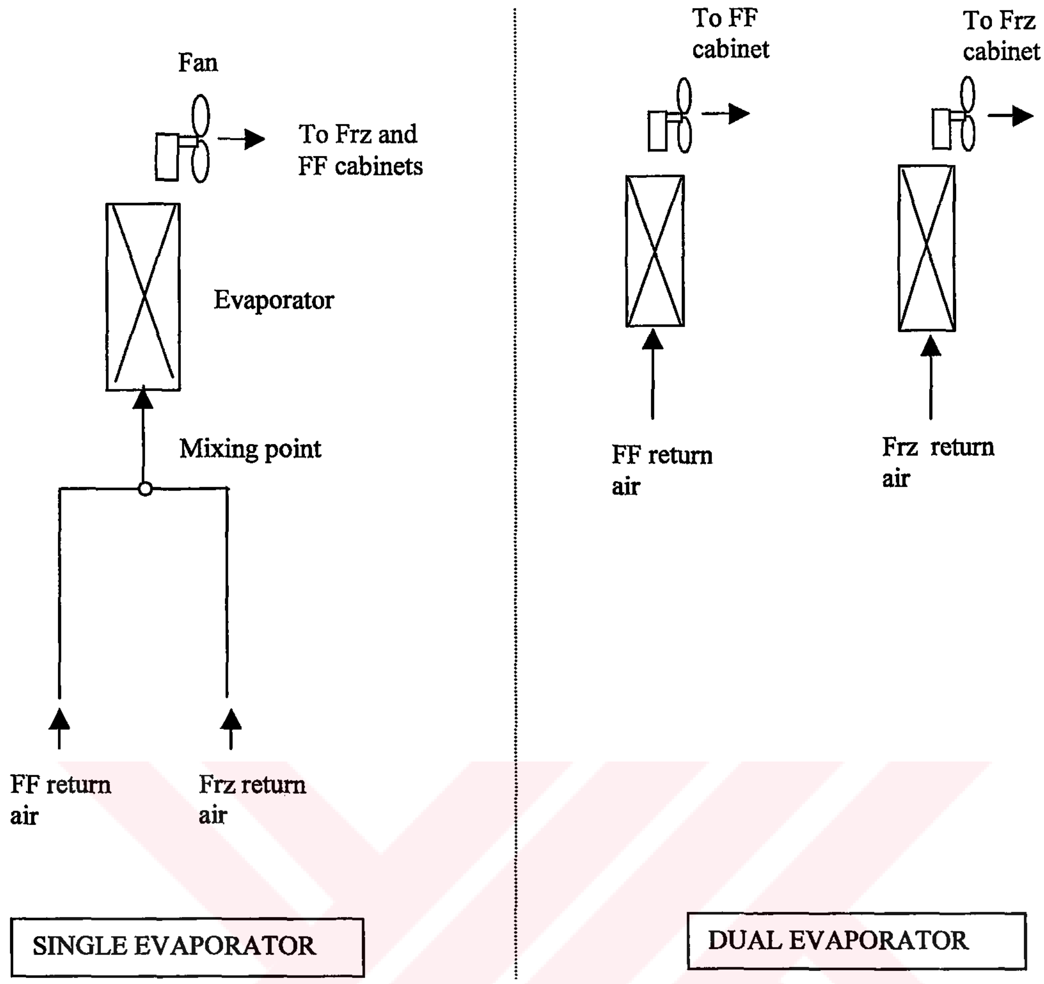

Figure 5.5 Schematic representation of return air for both single and dual evaporator cases.

For the single evaporator case, the evaporator inlet is results of two air stream's mixing. When the air return temperatures and humidity are known the mixture temperature and humidity ratio can be calculated according to equations (5.76) and (5.77). In these equations, the perfect mixing of two air streams are assumed. In reality, there is neither enough space nor time available, therefore mixing is not perfect. Moreover, the freshfood air mostly comes through the middle of evaporator and the freezer air comes from the sides. Observations on refrigerators (e.g. Stein, 1999) showed that, the frosting starts from the middle section where the humid and warm freshfood air first hits cold evaporator surfaces. This example shows that air is not perfectly mixing before evaporator. However, it is convenient to assume that the mixing is perfect for simplification.

$$T_m = \frac{m_{FF}.T_{FF} + m_{Frz}.T_{Frz}}{m_{fan}} \tag{5.76}$$

$$w_m = \frac{m_{FF} w_{FF} + m_{Frz} w_{Frz}}{m_{fan}} \tag{5.77}$$

where,

T_m: Mean air temperature after mixing [°C]
T_{FF}: Freshfood return temperature [°C]
T_{Frz}: Freezer return temperature [°C]
w_m: Mean humidity ratio of mixture [kg/kg_air]
w_{FF}: Humidity ratio of Freshfood return air [kg/kg_air]
w_{Frz}: Humidity ratio of Freezer return air [kg/kg_air]
m_{fan}: Total mass flow rate at fan exit [kg/s]
m_{FF}: Mass flowrate of air coming from freshfood cabinet [kg/s]
m_{Frz}: Mass flowrate of air coming from freezer cabinet [kg/s]

In the modeling studies, the inlet air temperature and humidity are used as parameters. Therefore, it is not important for the model whether the inlet conditions are the result of two air streams mixing or only one air stream. However, the model is capable of calculating the mixture conditions when it is required.

5.2.4 Calculation method

Evaporator performance under frosting conditions are calculated by using the following methodology. The basic idea is slicing the evaporator into tube passes in the airflow direction such that each portion has one horizontal row of tubes. This process is shown in Figure 5.6.

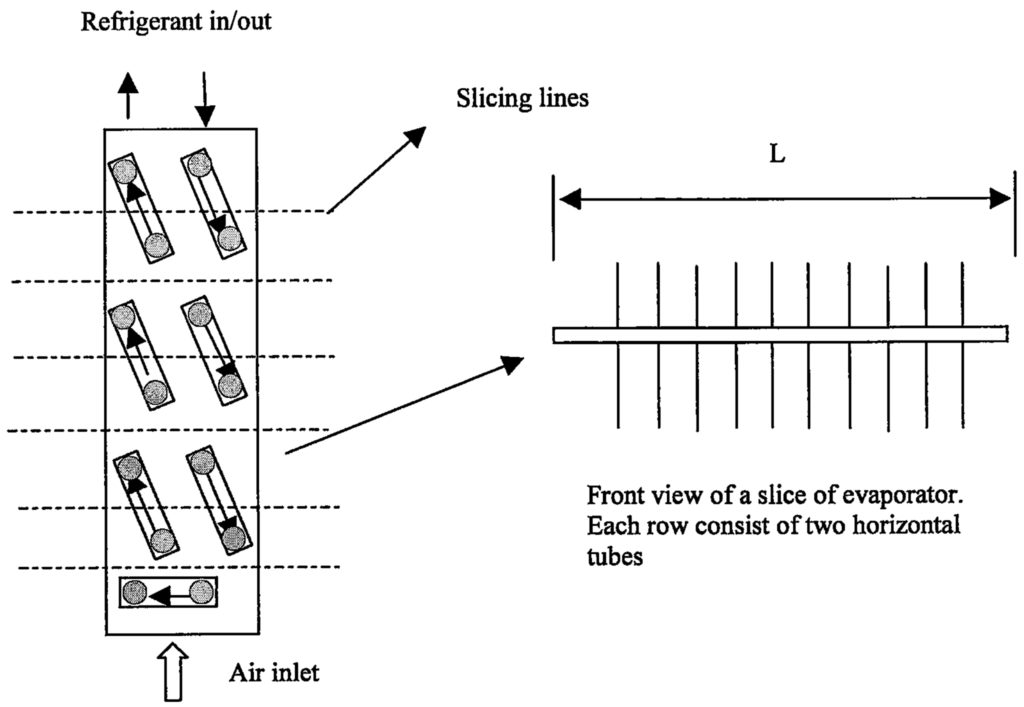

Figure 5.6 Slicing the evaporator into equal portions (the evaporator in the figure is named 7 pass evaporator)

The coupled problem of frosted evaporator performance calculations are made according to the following flow-chart. At the time t, equations are solved instantaneously for each evaporator slice starting from bottom. The exit values of each section are taken as inlet values of the next section. The solution progresses until all rows are solved. After that, the solution progress is started again. This time, the results of previous calculations are taken as initial values. The flow chart is summarized in Figure 5.7. In order to obtain an iterative solution of equations, Newton's method is applied. The solver program is written in EES format. Details of the program can be seen in Appendix-M. At time zero, the solution algorithm starts with initial values of frost thickness and density which are 0.05 mm and 40 kg/m^3, respectively.

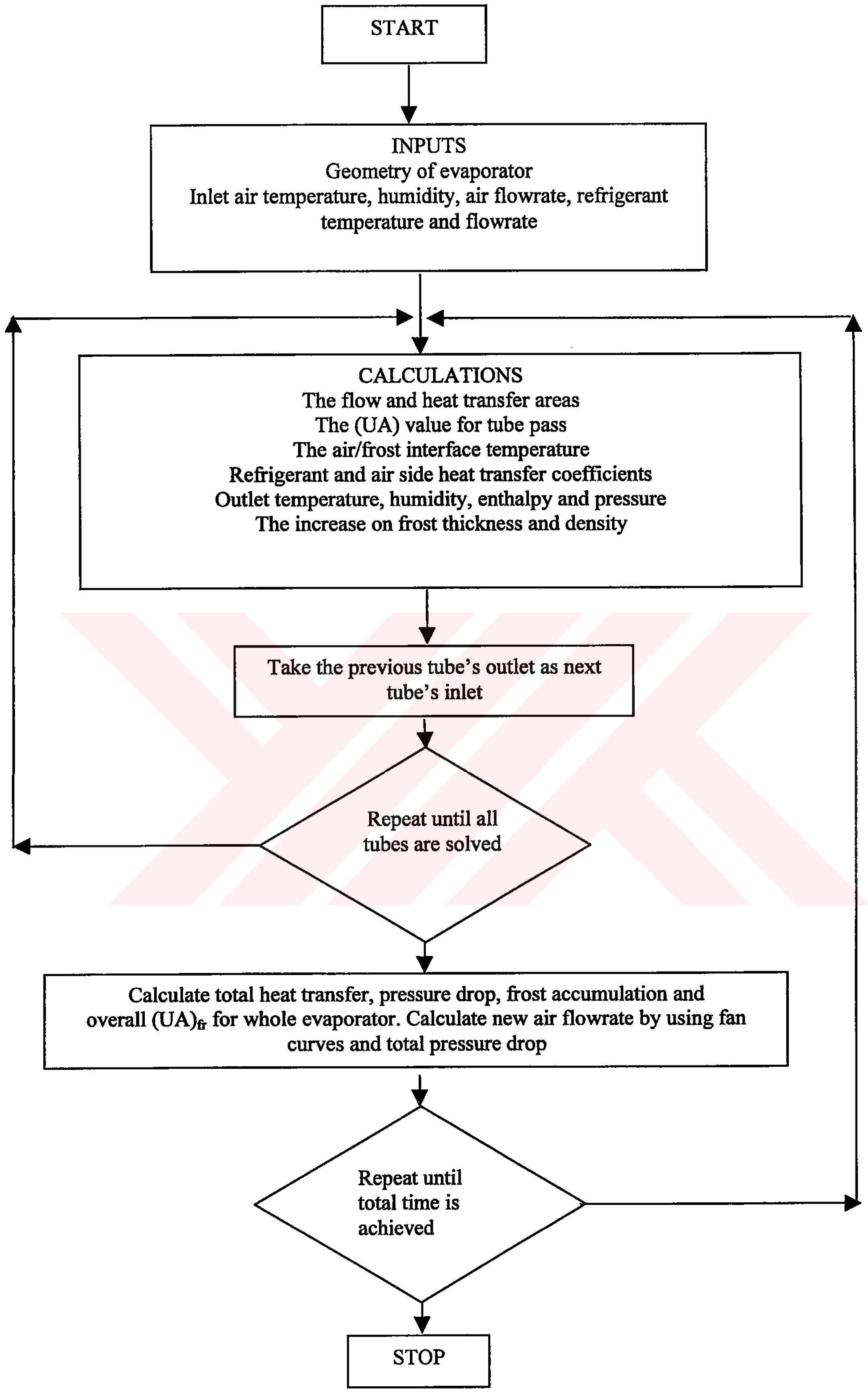

Figure 5.7 The flow chart for the solution algorithm of frosted evaporator

5.2.5 Results of calculations

The geometry of evaporator properties that were used in calculations are given in Table 5.2.

Table 5.2 Evaporator geometry

Width of evaporator (W):	535 mm
Depth of evaporator (D):	50 mm
Tube outer diameter:	8 mm
Tube inner diameter:	6.72 mm
Single fin surface area in a row (one face):	746.1 mm^2
Number of tube passes:	13
Numbers of fins on bottom three rows (fin spacing is 20 mm):	25
Numbers of fins in remaining rows of the evaporator (fin spacing is 10 mm):	49
S_D=22 mm, S_T=22 mm. S_L=19.053 mm	

The program has been run for different parameters while the geometry of evaporator remains same. The results are given below in details. In these runs, the airflow rate is kept constant during the frost accumulation process.

5.2.5.1 The effect of densification rate

There is research on frost density that has examined the effects of geometry and flow conditions (e.g. Mao et al., 1991,1992,1993). Unfortunately, results of these studies are not directly applicable to domestic refrigerator evaporators. Limitations mostly come from the inlet air temperatures, air velocity and geometry of the cold surface. Therefore, in order to see its importance, the percentage of condensed water that increases the density of frost (this will be called herein after as densification ratio or densification rate, χ) is chosen as a parameter. For fixed geometry and flow conditions, the evaporator heat transfer and pressure drop characteristics are calculated for different densification ratios. Results of these studies are given in Figures 5.8, 5.9, and 5.10.

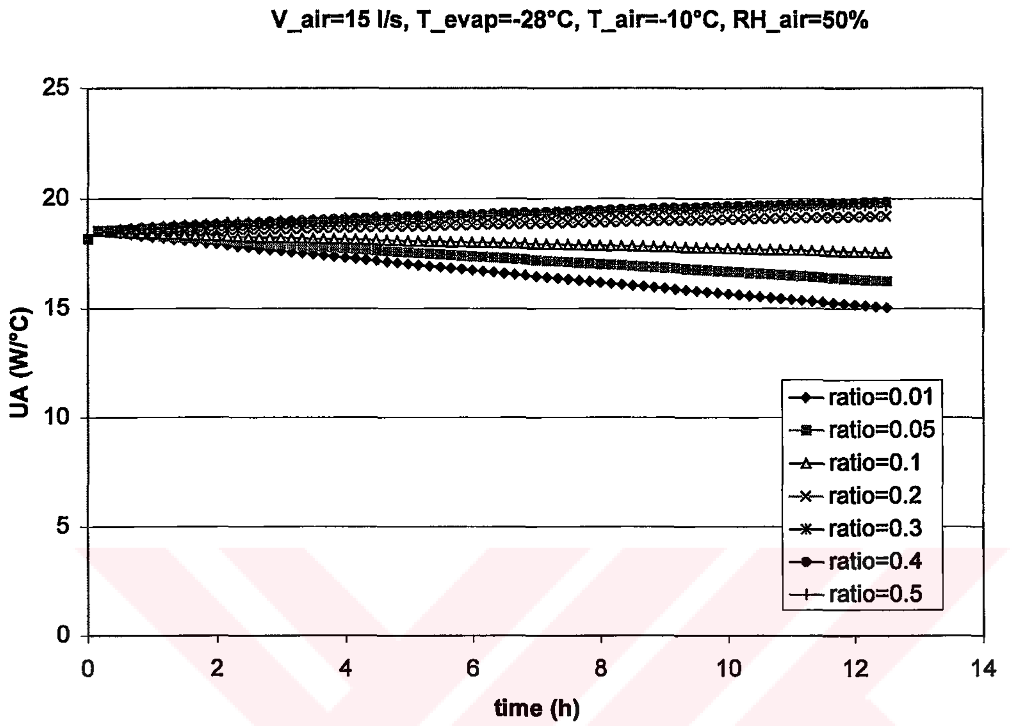

Figure 5.8 Heat transfer coefficient change with the densification ratio. Refrigerant is R134a and flow rate is 5 kg/h.

As shown in Figure 5.8, the densification ratio greatly affects the trend of the overall heat transfer coefficient. For ratios of less then 0.1 overall heat transfer coefficient decreases with time. For ratios greater then 0.1, it increases with time. This phenomenon can be explained by the competing effects of frost insulation effect versus the area and local heat transfer increase. Lower values of the ratios cause lower density frost build-up on the surfaces. The thickness of frost is higher for lower densification rates. Moreover, lower density frost has lower conductivity. Therefore, for the densification ratios lower then 0.1, the insulating effect of increasing frost layer is dominant. This causes a decrease of heat transfer coefficient. For frost densification ratios greater than 0.1, insulating effect of the frost layer becomes less than the increase of heat transfer area and the local heat transfer coefficient increase. Frost narrows the air passages, causing increased local air velocity, and therefore increasing local air-side heat transfer coefficient.

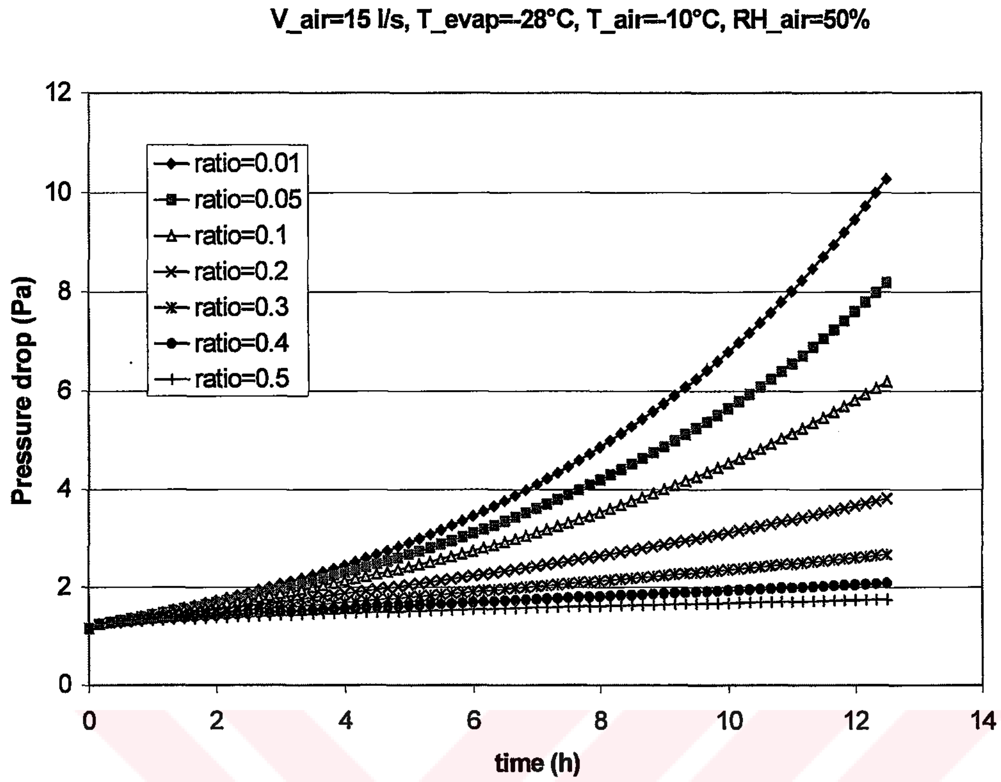

Figure 5.9 Pressure-drop change with the densification rate. (Refrigerant is R134a and flow rate is 5 kg/h)

The effect of densification rate is seen clearly on pressure drop characteristics. The lower ratios cause higher pressure-drops (see Figure 5.9). This is because higher frost thickness values are obtained at lower densities. Increasing thickness of frost increases velocity. Pressure-drop increases with the second power of velocity, therefore the difference between curves more rapidly increases with time. For example, the pressure-drop value for ratio=0.1 is six times higher than the value of ratio=0.5 at the end of 12 hours.

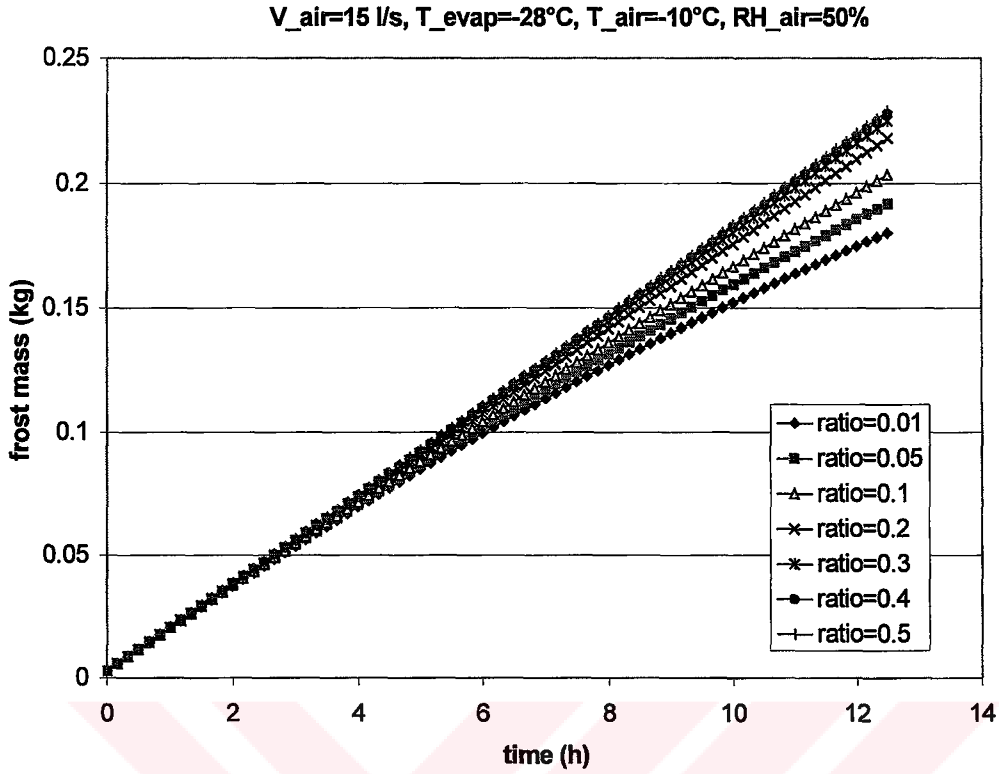

Figure 5.10 Frost accumulation rate change with the different densification rates. (Refrigerant is R134a and flow rate is 5 kg/h)

Frosting rate is also affected by density changes as shown in figure 5.10. The increasing densification ratio causes more frost accumulation on evaporator surfaces.

The results given above showed that the densification ratio and therefore the density of frost, is a key parameter for frosted evaporator calculations. Because accurate information is not available yet, it is decided to choose an approximate value for a parametric investigation of frost effects. After examining the density changes obtained by Mao et al. (1991, and 1993), a densification ratio of 0.3 will be used. The results of the calculations will be compared to results from an experimental study of Seker (1999).

5.2.5.2 Results of some parametric runs

After choosing a densification ratio, which is χ=0.3, the solver has been run for three different values of evaporation temperature and air flowrate. The results of calculations are summarized below.

The effect of evaporation temperature: Figure 5.11 shows the overall UA value change with respect to time. UA is increasing as the frost thickness increases. The reason for this trend was explained previously. The insulating effect of frost layer is less than the surface area increase and local heat transfer coefficient increase due to higher local velocities.

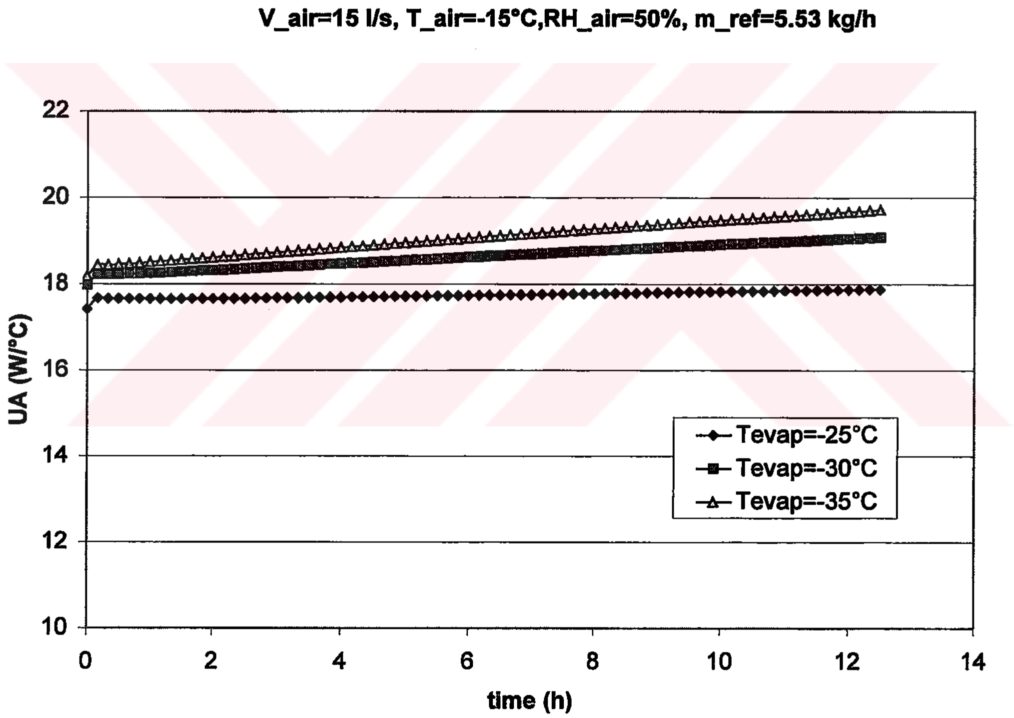

Figure 5.11 Overall heat transfer coefficient change with respect to evaporation temperature (χ=0.3).

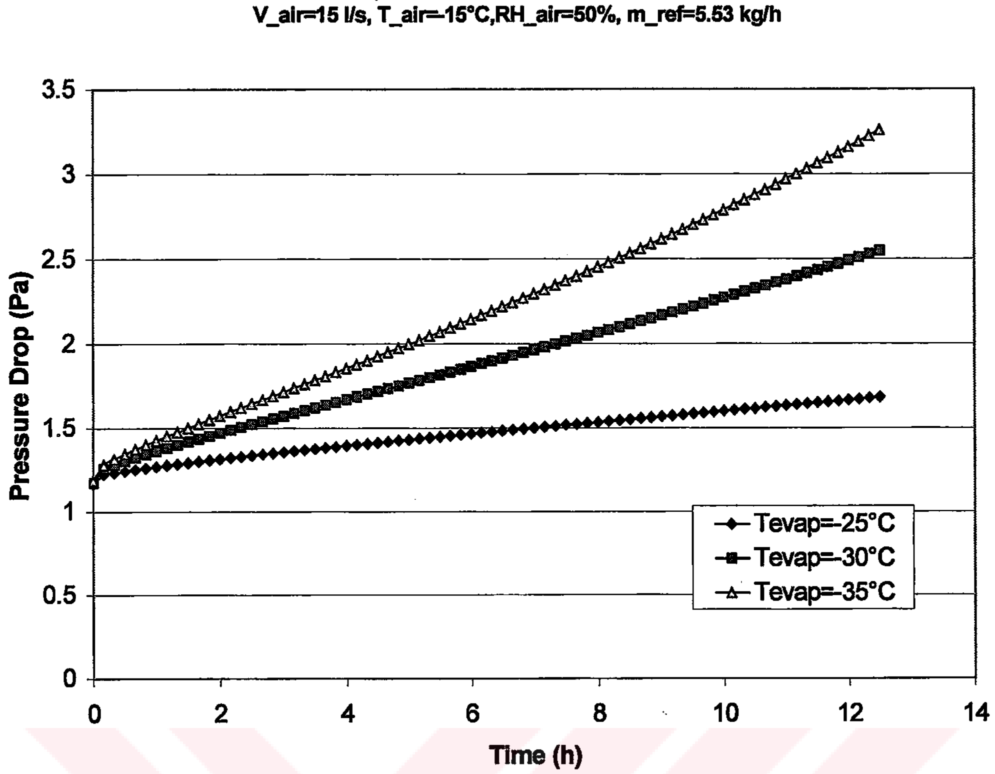

Figure 5.12 Pressure drop change with respect to evaporation temperatures (χ=0.3).

Although the UA value change is not significant for evaporation temperatures of –25°C to –35°C, the pressure drop is significantly affected. At the end of 12 hours, the pressure drop doubles for –35°C with respect to –25°C value (Figure 5.12). This is because the frost deposition rate and therefore, the frost thickness, increase at lower evaporator surface temperatures.

The frost accumulation rate is shown in Figure 5.13. Accumulated frost mass is almost five times more for –35°C than the value of –25°C. This difference shows the importance of surface temperature. The difference between the saturated vapor pressure corresponding to surface temperature and the partial pressure of water vapor at air temperature is the main driving force for mass transport. When the evaporation temperature decrease from –25 °C to –35°C, frost mass increases from 50 g to 250 g at the end of 12 hours.

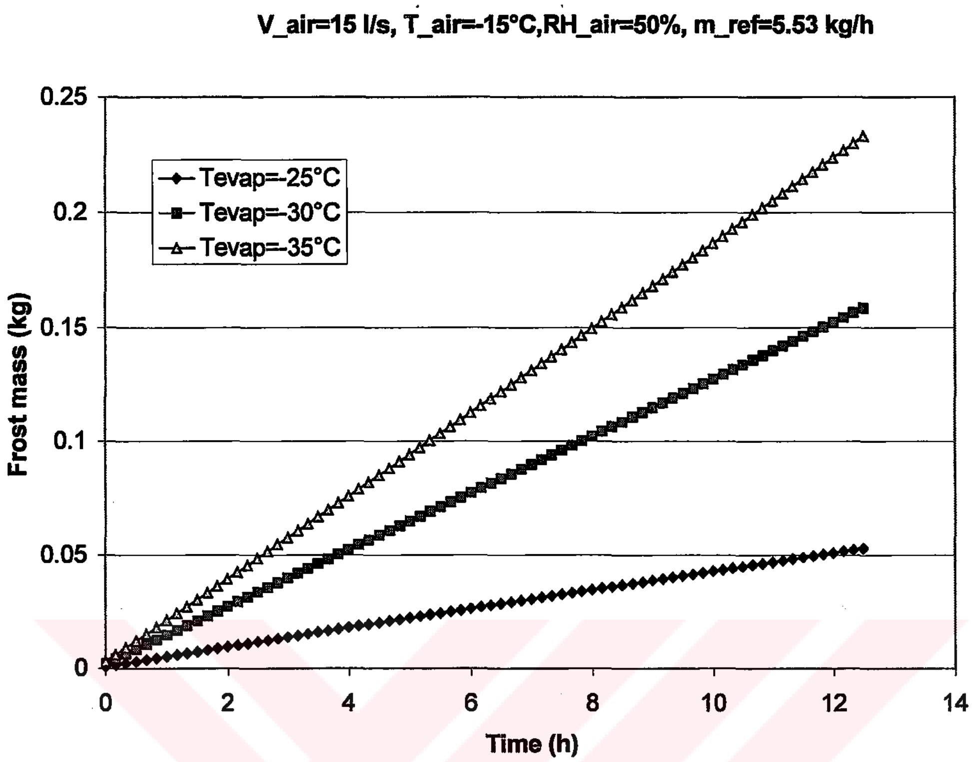

Figure 5.13 Frost accumulation rates for different evaporation temperatures (χ=0.3)

<u>The effect of air flowrate</u>: The effect of air velocity is examined by changing the air flowrate to 5 l/s, 15 l/s, and 25 l/s, respectively. Values of all the other parameters are shown at the top of each figure. The range of air flowrate is chosen such that they cover values typical of domestic refrigerator applications.

As seen from Figure 5.14, the UA values increase with increased air flowrate. This trend is expected because the air-side heat transfer coefficient strongly depends on Reynolds number and therefore the local air velocity. When the air flowrate is increased five times, the UA value increases 3 times.

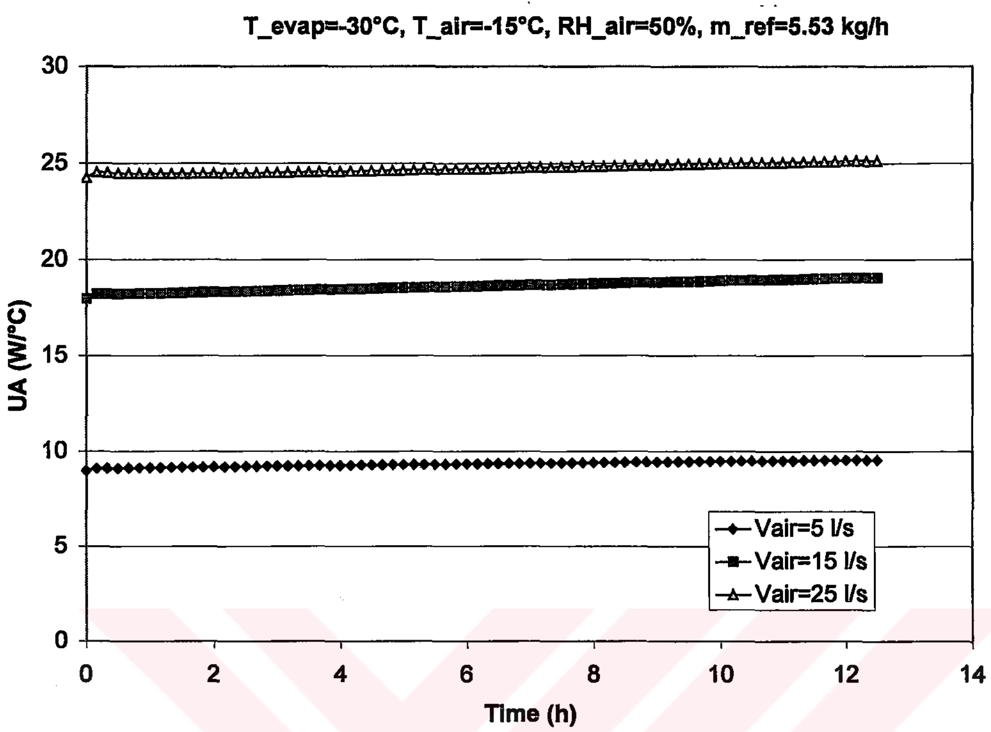

Figure 5.14 Overall heat transfer coefficient (UA) change with air flowrate (χ=0.3).

The pressure-drop characteristics show exponentially increasing trend for higher air flowrates (see Figure 5.15). For example, at the end of 12 hours, the pressure-drop increases almost three times for 25 l/s with respect to the starting value.

This change is almost negligible for low airflow rates of 5 l/s over the same time period. This phenomenon can be explained such that the frost thickness is higher for higher air flowrate. The mass transport coefficient is directly proportional to the local heat transfer coefficient assuming the heat and mass transfer analogy is valid.

On the other hand as the frost thickness increases, the air passages becomes narrower and therefore the local velocity increases. Since the pressure drop increases with respect to the square of velocity, the pressure drop curves show an exponentially increasing trend.

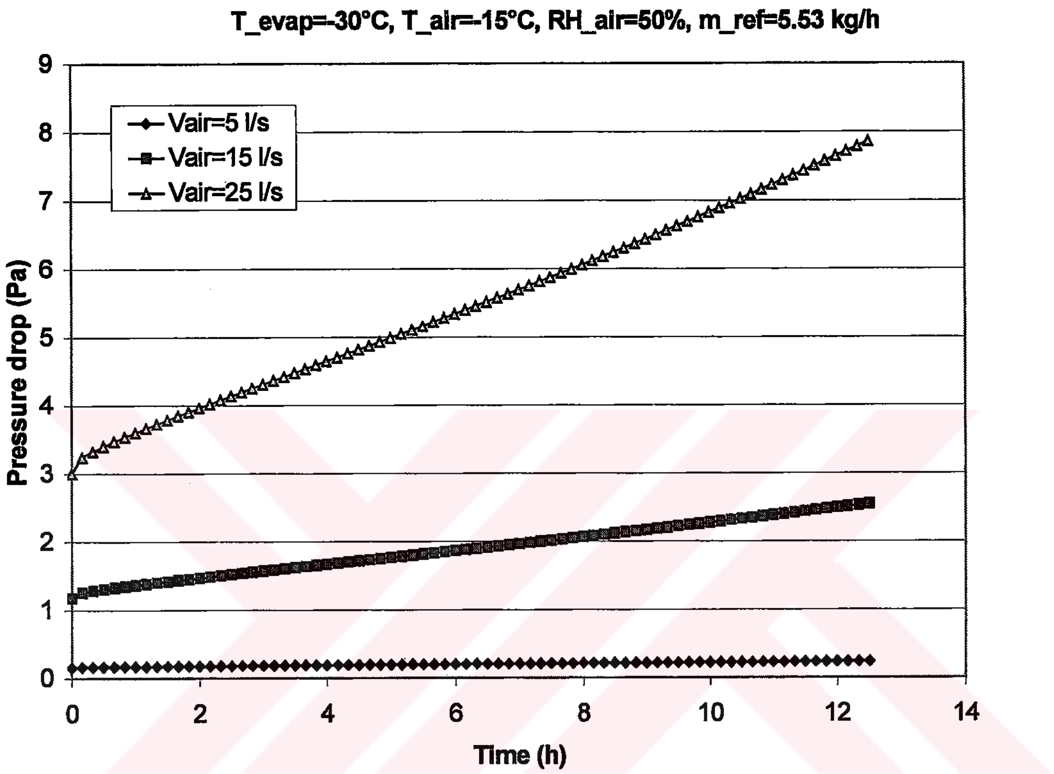

Figure 5.15 Pressure drop characteristics for different air flowrates (χ=0.3).

Figure 5.16 shows the frost accumulation rate on the evaporator surfaces. As expected, the frost mass increases with increasing air flowrate. The total frost mass at the end of 12 hours can vary from 50 g to 200 g due to air flowrate.

The order of magnitude of these ranges is compatible with the refrigerator experiments of Stein (1999). The information of the total frost mass with respect to given flow condition is also important for design of the defrost system.

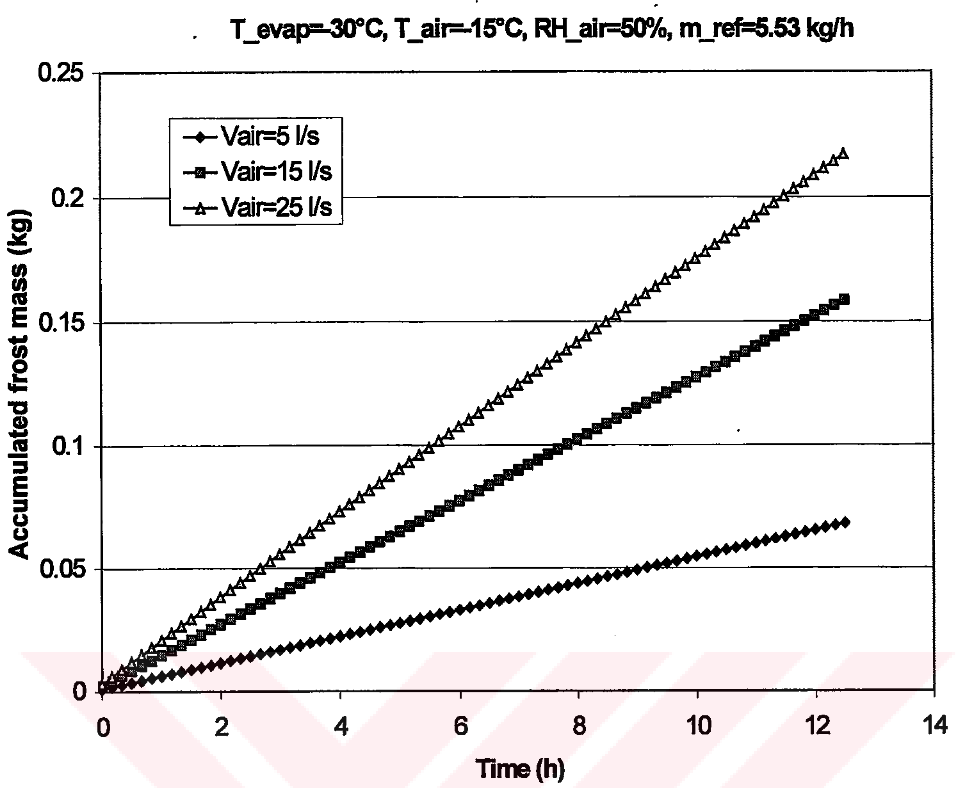

Figure 5.16 Frost mass accumulated on the evaporator surface with respect to the air flowrate (χ=0.3).

5.2.5.3 Frost thickness change for each evaporator row

The simulation program is designed to run each tube pass separately. Therefore, it is possible to obtain the heat and mass transfer characteristics for each individual tube pass. As an example, the program has been run for a set of conditions. The frost thickness values for each tube are plotted in Figure 5.17. The frost thickness is almost two times thicker for first row than the last row (13^{th} row). This is because of the driving force is higher for first row as the air humidity ratio and temperature is higher relative to the other rows. This result is compatible with experiments of Stein (1999) and Seker (1999). The frost curves for first three rows, where fin spacing is different, are different from the others. As previously indicated the fin spacing for first three rows is two times larger than the remaining rows.

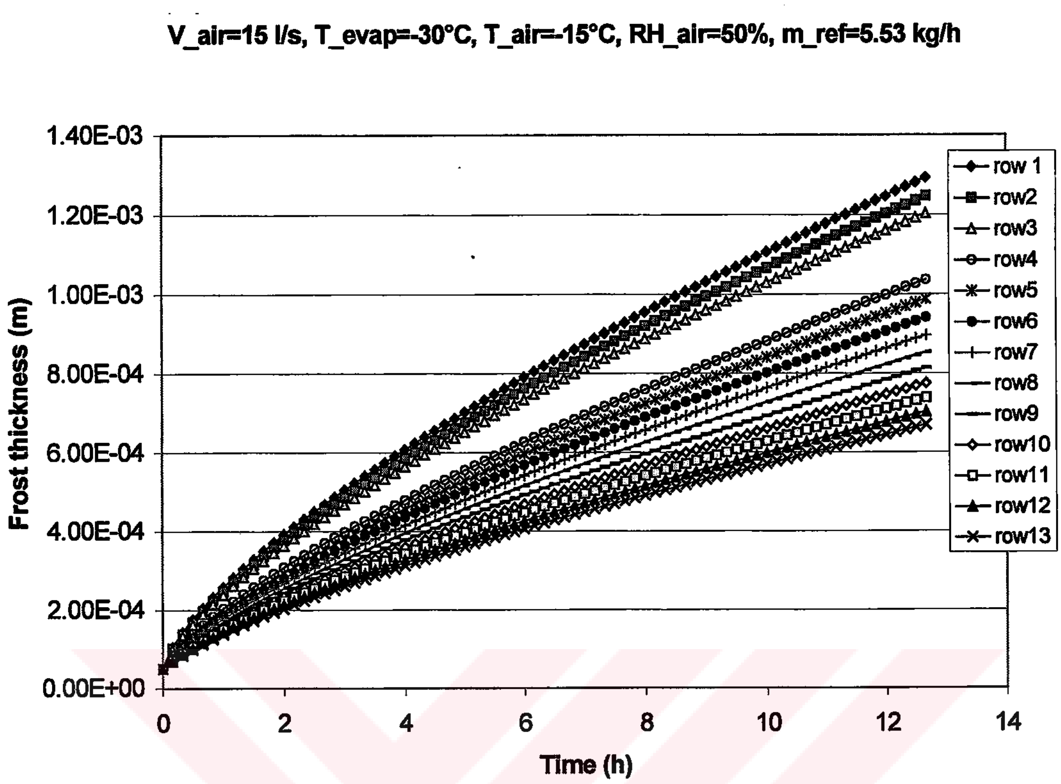

Figure 5.17 Frost thickness change with respect to time for each individual tube row. (χ=0.3).

5.2.5.4 The change of evaporator characteristics with variable air flow rate (simulating the actual case in a domestic refrigerator)

The air flowrate through an evaporator was assumed constant for all runs previously described. However, in an actual refrigerator, the flowrate decreases with increasing pressure drop caused by frost buildup. All the heat and mass transfer characteristics are affected as well. In order to show this effect, the simulation program was organized such that the fan and duct system characteristics are included in the solution procedure. The solver calculates the new air flowrate after each time step by using the previous pressure drop value on the evaporator. For this purpose, the solver, which was developed previously for air-distribution system analysis (given in Chapter-4), is integrated into the simulation algorithm given in Appendix-K. Therefore, the pressure drop characteristics of the air distribution system are also included.

Calculations are made for the same air distribution and cabinet system geometry given in Figures 4.2 and 4.3.

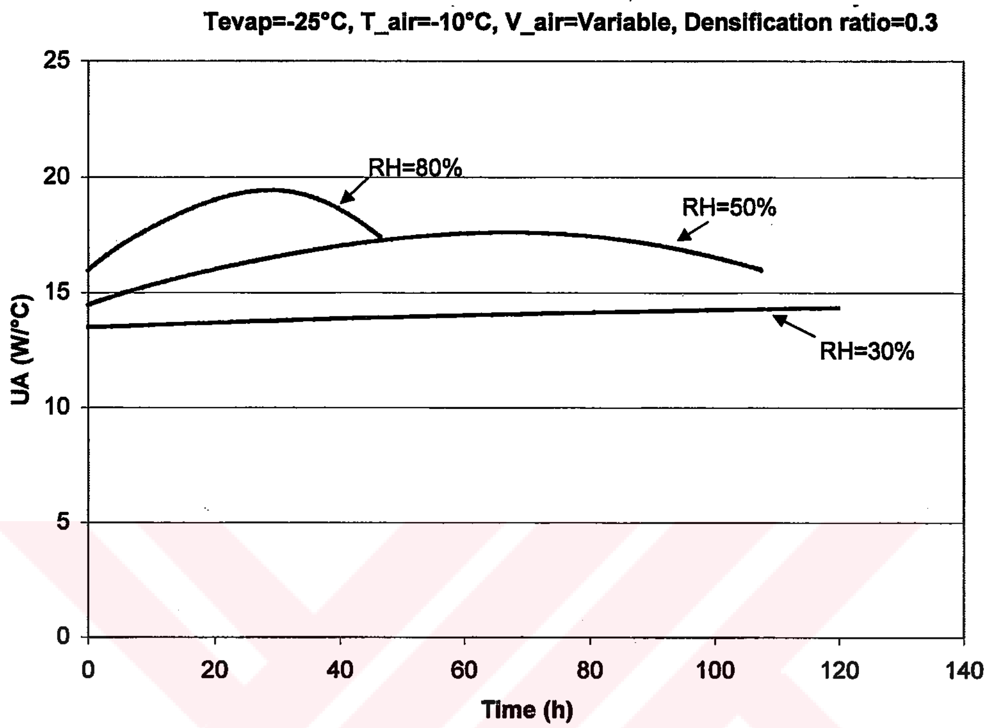

Figure 5.18 Overall heat transfer coefficient change for variable air flowrate case (χ=0.3).

The results of overall heat transfer coefficient (UA) calculations are summarized in Figure 5.18. From the figure, it can be seen that the starting points of curves are not same. This is because the UA value represents a combination of sensible and latent heat transfer coefficients. The lower UA value is therefore calculated for lower relative humidity case where the latent heat transfer rate is also lower.

The curves show discontinuities for higher relative humidity cases. This is caused by frost blockage of the air passages.

UA curves show an initially increasing trend until a peak value is reached. After the peak is achieved, it decreases rapidly. This phenomenon can be explained as initially the insulating effect of the frost layer is smaller relative to the area increase and local heat transfer increase effects. This trend continues until the peak value is reached. After this point, the pressure drop drastically increases and the air flowrate decreases. The heat transfer coefficient decreases due to the flowrate decrease. The curve shape strongly depends on the inlet-air relative humidity. While the peak value is reached at around 30 hours of operation for 80% relative humidity, it is 70 hours for 50% relative humidity. A similar trend was also observed on a domestic refrigerator tested by Stein (1999).

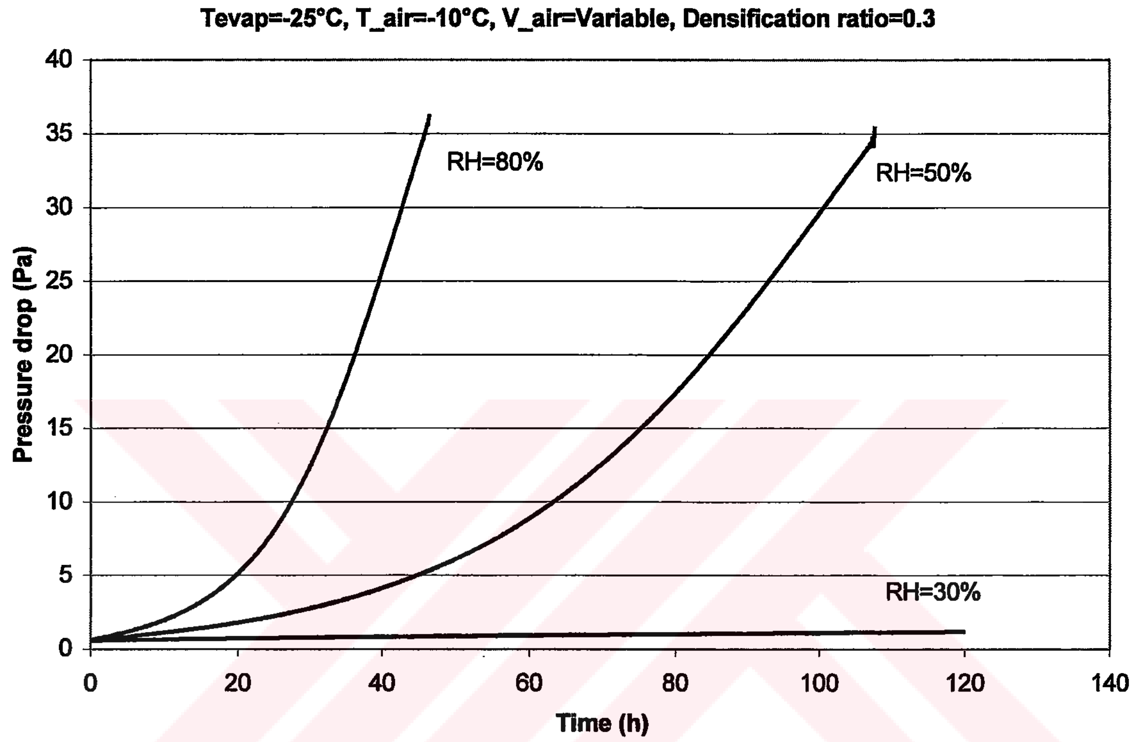

Figure 5.19 Pressure-drop characteristics for three different inlet relative humidity values. The air flowrate is variable (χ=0.3).

The pressure drop characteristics are shown in the Figure 5.19. Figure 5.19 shows the curves until the evaporator is blocked by frost. The strong dependency of pressure-drop to relative humidity is seen in the figures. The blocking of the evaporator occurs at around 45 hours for 80% RH, and 110 hours for 50% RH. The maximum pressure drop value is appears as 36 Pa. The fan can produce a 40 Pa pressure increase, with 36 Pa spent on the evaporator and the remaining on the duct system.

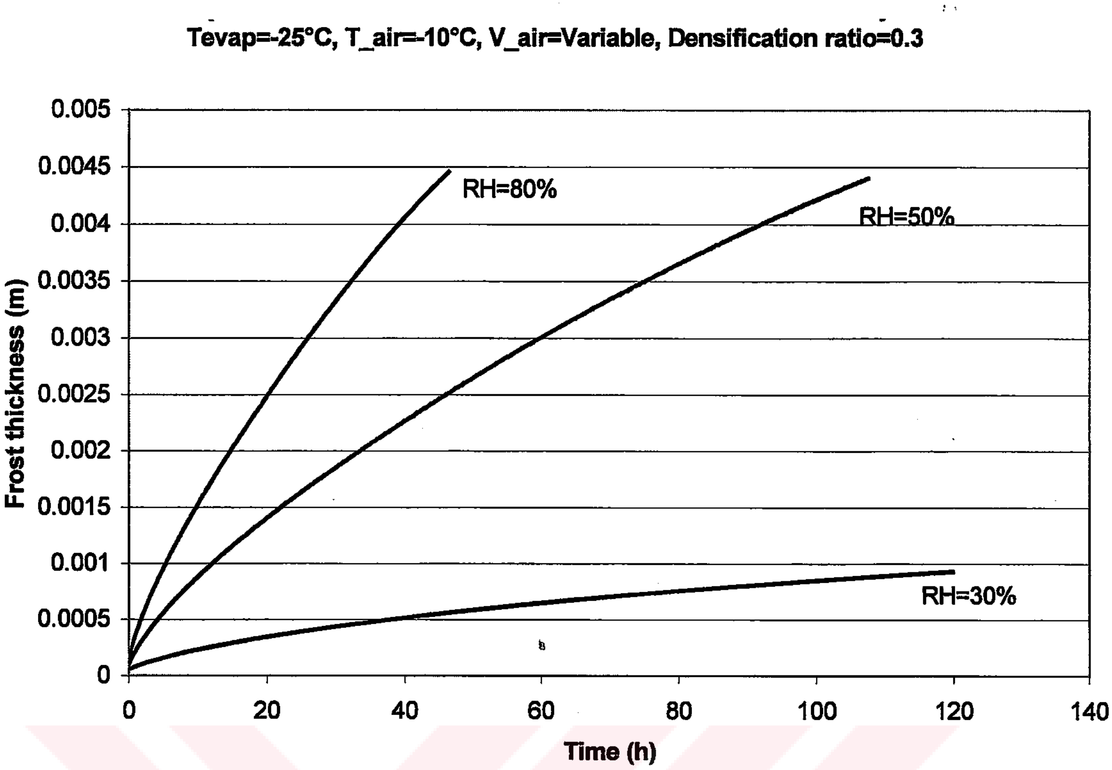

Figure 5.20 The change of average frost thickness value for three different inlet relative humidity values.

The frost thickness reaches as much as 4.5 mm where the fin spacing is 10 mm (Figure 5.20). After this point frost blocks the evaporator passages. The operation time required to reach the maximum thickness values are the same as given in Figure 5.19.

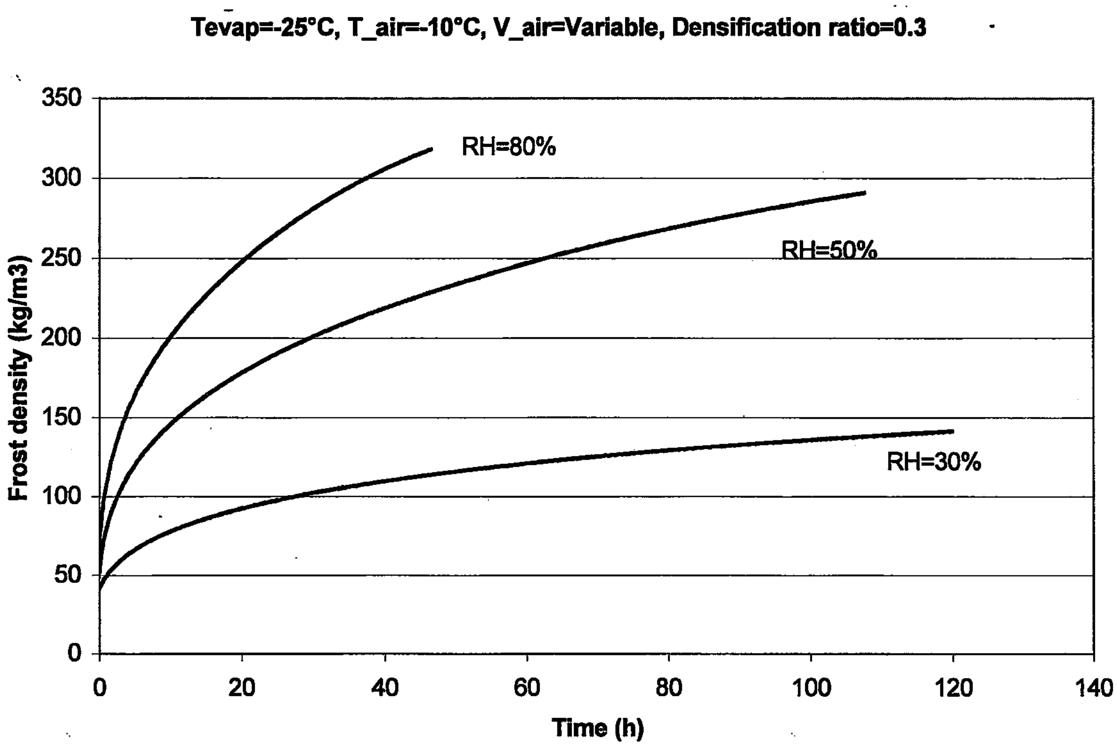

Figure 5.21 Frost density change for different relative humidity values.

Figure 5.21 shows the frost density change. The density increases faster for higher relative humidity values than lower ones. Although the air inlet temperature and geometry are not very similar to their studies, the density range given in the Figure 5.21 falls into the overall range measured by Mao et al. (1991,1992, and 1993). This result shows that the densification ratio assumed in this study is not too far from the actual one.

5.2.5.5 Calculation of quasi-steady cabinet temperature and relative humidity level

This section ties together the overall moisture loading effects on a refrigerator evaporator. The door opening model from Chapter 2 and 3 coupled with the air distribution model (Chapter 4) and evaporator frosting model of this chapter are coupled together.

The cabinet geometry and the assumptions, made in Chapter 3.3, are assumed along with the airflow distribution system modeled in Chapter 4.

Applying the first law of thermodynamics to the cabinet whose schematic is shown in Figure 5.22 yields;

$$m\left(\frac{du}{dt}\right) = Q_{HG} + Q_{dooropening} + Q_{\inf iltration} + Q_{fan} + Q_{defrost} - Q_{evap} + W_{cv} \qquad (5.78)$$

In other words,

$$\rho_{FF} V_{FF} C_p \left(\frac{\Delta T_{FF}}{\Delta t}\right) = Q_{HG} + Q_{dooropening} + Q_{\inf iltration} + Q_{fan} + Q_{defrost} - Q_{evap} \qquad (5.79)$$

where,

m :	Mass of air in the cabinet [kg]
u:	Internal energy of cabinet air [J/kg]
Q_{HG}:	Heat gain from cabinet walls [W]
$Q_{dooropening}$:	Heat gain due to door openings [W]
$Q_{infiltration}$:	Heat gain due to infiltration through door gasket and other cabinet penetrations [W]
Q_{fan}:	Heat gain from fan motor [W]
$Q_{defrost}$:	Heat gain from defrosting [W]
Q_{evap}:	Total heat transfer removed by evaporator [W]
W_{cv}:	The work done on the border of control volume [W]
ρ_{FF}:	Air density at average cabinet temperature [kg/m^3]
V_{FF}:	Cabinet volume [m^3]
ΔT_{FF}:	Change of cabinet air temperature [°C]
Δt:	Time difference [s]

And the conservation of water mass equation in the control volume can be written as;

$$\frac{dm_{FF}}{dt} = m_{\inf} + m_{door} + m_{evap\_pan} - m_{fr} \qquad (5.80)$$

or, for a certain time step;

$$\frac{\Delta m_{FF}}{\Delta t} = m_{inf} + m_{door} + m_{evap\_pan} - m_{fr} \quad (5.81)$$

where,

m_{inf}:	Water transport due to infiltration [kg/s]
m_{door}:	Water transport due to door openings [kg/s]
m_{evap_pan}:	Water evaporation rate from pan surface [kg/s]
m_{fr}:	Frosting rate on evaporator surfaces [kg/s]
Δm_{FF}:	Change of water mass in the cabinet air [kg/s]

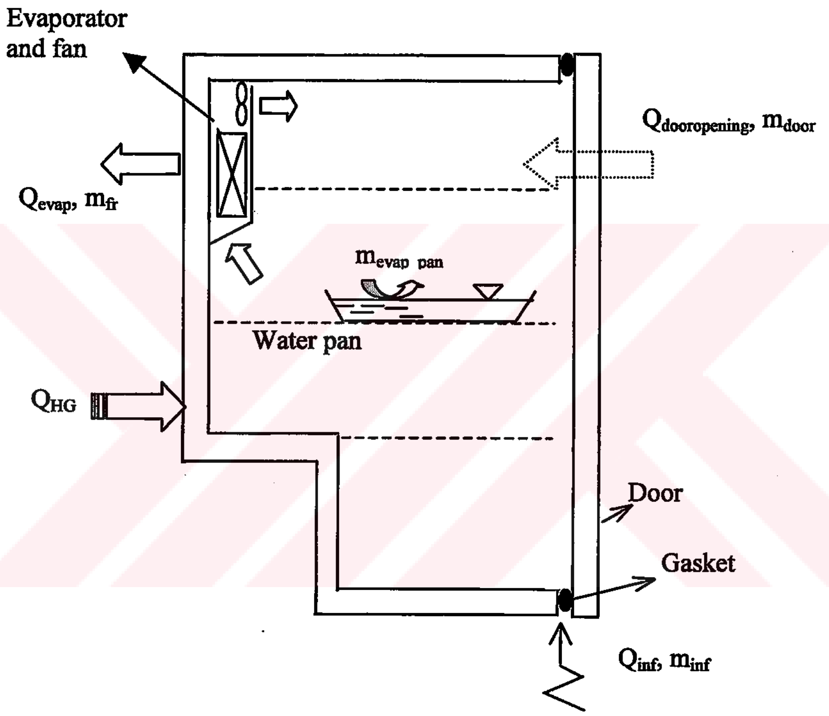

Figure 5.22 Schematic representation of heat and mass transfer mechanisms in freshfood cabinet

The explanations of the heat and mass transfer mechanisms given in Equations from 5.78 to 5.81 are given below.

Evaporator load, which is the total of latent and sensible loads, can be calculated by using the equation (5.64).

$$Q_{evap} = (UA)_{fr}\,\Delta T_m \quad (5.82)$$

where,

Q_{evap}: Evaporator total heat transfer rate [W]
$(UA)_{fr}$: Overall heat transfer coefficient of evaporator [W/°C]
ΔT_m: Logarithmic temperature difference [°C]

The heat gain through the cabinet walls is calculated by use of the cabinet heat transfer coefficient ($UA_{cabinet}$). Since the UA value is obtained experimentally, it also includes the sensible heat gain caused by air infiltration through the cabinet.

$$Q_{HG} = UA_{cabinet}(T_\infty - T_{FF}) \tag{5.83}$$

here,

Q_{HG}: Heat gain from cabinet walls [W]
$UA_{cabinet}$: Overall heat transfer coefficient of cabinet [W/°C]
T_∞: Ambient temperature [°C]
T_{FF}: Average cabinet air temperature [°C]

The sensible and latent portions of heat gain from door openings were explicitly calculated in Chapter-3. Here the results of these calculations will also be used. The numbers of door openings, which is same as given in Chapter-3, are assumed as 20 times per day with an opening duration of 20 seconds.

$$Q_{dooropening} = Q_{door\_sensible} + Q_{door\_latent} \tag{5.84}$$

The heat load of door openings is calculated by using the definitions given in Chapter 3. Equations (3.20) to (3.29) are again used for calculations. The total load caused by door openings is used as the time-averaged value that is obtained by dividing the daily total energy gain of the door opening to 24 h.

The mass transfer rate per door opening can be calculated by use of Eqn. (3.15).

$$h_w = 0.00626 \rho_a h_C \frac{D}{k}\left(\frac{\alpha}{D}\right)^{1/3} \tag{5.85}$$

$$m_{door} = h_w A_s \left(P_{w,\infty} - P_{w,s}\right) \tag{5.86}$$

where,

$Q_{dooropening}$: Total heat transfer due to door openings [W]
$Q_{door\_sensible}$: Sensible heat transfer due to door openings [W]
Q_{door_latent}: Latent heat transfer due to door openings [W]
A_s: Inner surface area of cabinet including shelves and door [m^2]
h_w: Mass transfer coefficient for door opening [$kg/s.m^2.kPa$]
$P_{w,\infty}$: Water partial pressure at ambient temperature [kPa]
$P_{w,s}$: Saturated water partial pressure at freshfood temperature [kPa]

Another source of heat and mass transfer is caused by air infiltration (leak) to/from cabinet.

$$Q_{inf} = Q_{inf\_sensible} + Q_{inf\_latent} \tag{5.87}$$

As previously indicated, sensible portion of this load is included in equation (5.83). The latent portion is also important to obtain. Mass transport through the gasket and other cabinet penetrations are driven by pressure differences between cabinet and ambient air. There is no available study that examines explicitly the characteristics of infiltration heat and mass transport in refrigerators. One of the recent studies (Stein, 1999) gives an experimental value of mass transport through the gasket. Although his result is valid for ae specific refrigerator, this value will also be used in this study in order to show the relative effect of parameters. Stein gave the mass transfer coefficient per length of gasket as;

$$h_{gasket}=0.0112 \text{ [g/min.m.kPa]} \tag{5.88}$$

Since the total gasket length in the freshfood door is 3.26 m, the mass transfer coefficient becomes,

$$h_{gasket}=0.0365 \text{ [g/min.kPa]}=6.0833\text{e-7 [kg/s.kPa]} \tag{5.89}$$

Then the mass transfer rate is calculated by using the following formula,

$$m_{inf} = h_{gasket}\left(P_{w,\infty} - P_{w,FF}\right) \tag{5.90}$$

The latent heat transfer caused by infiltration is;

$$Q_{inf\_latent} = m_{inf} h_{sg} \tag{5.91}$$

In above equations,

Q_{inf}:	Heat transfer rate due to infiltration to/from cabinet [W]
$Q_{inf\_sensible}$:	Sensible portion of infiltration heat transfer [W]
Q_{inf_latent}:	Latent portion of infiltration heat transfer [W]
h_{gasket}:	Mass transfer coefficient for infiltration [kg/s.kPa]
m_{inf}:	Water transfer rate due to infiltration [kg/s]
h_{sg}:	Sublimation enthalpy of water [J/kg]

Evaporation from the water filled pan(s) located in the cabinet shelves adds water to the air. If we neglect the energy required to cool down the frost to subzero temperatures, there is no other energy penalty paid due to the evaporation of water from the pan. Because, the same amount of energy that is required for evaporation of water will be given back when it is condensed on the evaporator surfaces. Therefore, by neglecting the sensible cooling to subzero temperatures, the net effect of water pan is adding water vapor to the cabinet air. The rate of water evaporation was experimentally obtained by Stein (1999). It is given below.

$$h_{evap\_pan}=1.333e\text{-}5 \text{ [kg/s.m2.kPa]} \tag{5.92}$$

Then the amount of water evaporated from the pan surface can be obtained as;

$$m_{evap\_pan} = h_{evap\_pan} A_{pan} \left(P_{w,s} - P_{w,FF}\right) \tag{5.93}$$

here,

h_{evap_pan}:	Mass transfer coefficient over pan surface [kg/s.m2.kPa]
m_{evap_pan}:	Water evaporation rate from free water surface in pan [kg/s]
$P_{w,s}$:	Saturation pressure of water at surface temperature [kPa]
$P_{w,FF}$:	Partial pressure of water at FF temperature [kPa]

Finally when all definitions are combined into equations (5.79) and (5.81), one can obtain the cabinet temperature and relative humidity level for each time step

Calculation procedure: Calculations are made by use of the solver given in Appendix-N. The solver calculates quasi-steady values for each time step. Calculations are made for the following values,

Ambient temperature:	25°C (The calculations are made at only one ambient temperature in order to show the procedure)
Ambient relative humidity:	40 %, 60%, and 80%
Number of shelves:	3
Evaporator pass number:	5 (For a more realistic study, the evaporator pass number is chosen as 5 instead of 13, which was used in previous calculations. All the other dimensions of evaporator such as fin spacing, width, and depth remains the same)
Air flowrate:	5 l/s, and 10 l/s. (flowrate is assumed constant for each time step)
Cabinet geometry:	Height:0.94 m, Width:0.67 m, Depth:0.63 m

The results of the calculations are given in the following figures. The calculation results are given only for one time step. By repeating calculations, while increasing amount of frost accumulated on evaporator, the other quasi-steady values of cabinet can also be calculated. Here, in order to show the effect of evaporation temperature and ambient air relative humidity, the calculations are made for only one time step.

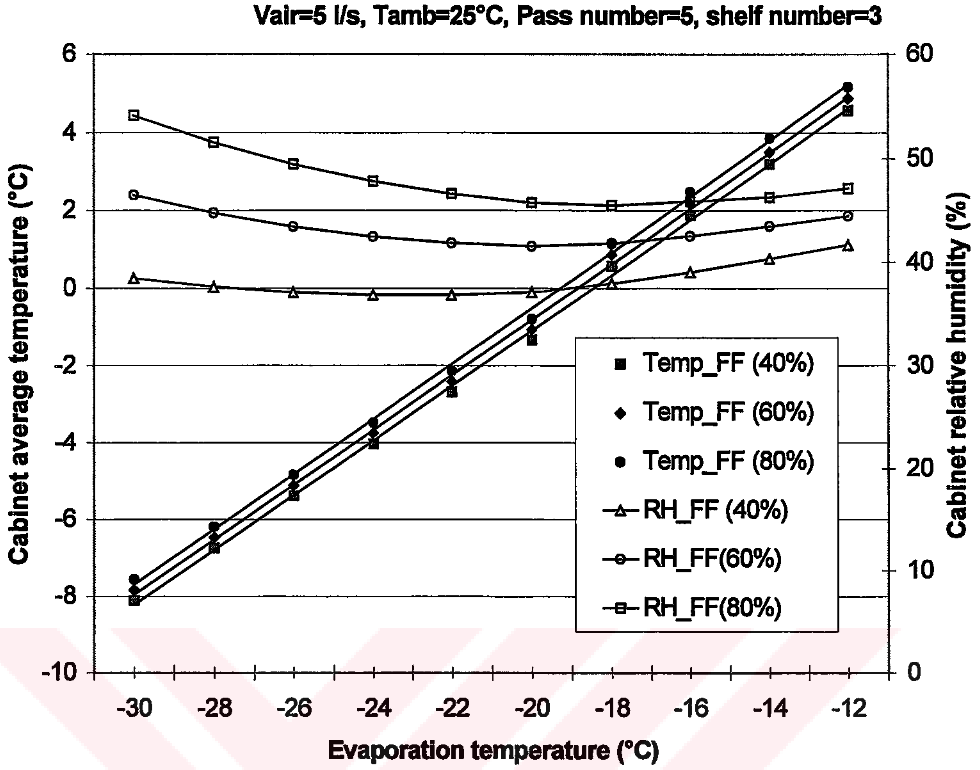

Figure 5.23 Freshfood cabinet temperature and relative humidity change with respect to evaporation temperature for three different ambient relative humidity values (Vair=5 l/s).

In Figure 5.23, the cabinet temperature and relative humidity values are shown. Humidity values decrease first, and then increases. This trend is caused by the water in the pan, which is frozen for cabinet temperatures below zero. Because the water evaporation from pan increases as the temperature increases above freezing temperature, the relative humidity of cabinet tends to increase. As it is seen, the cabinet temperatures can go as low as –8°C. The ambient temperature is relatively low because the fan is continuously blowing cold air into the cabinet. In real cases a control system will keep the temperature of cabinet above freezing temperatures by modulating the fan.

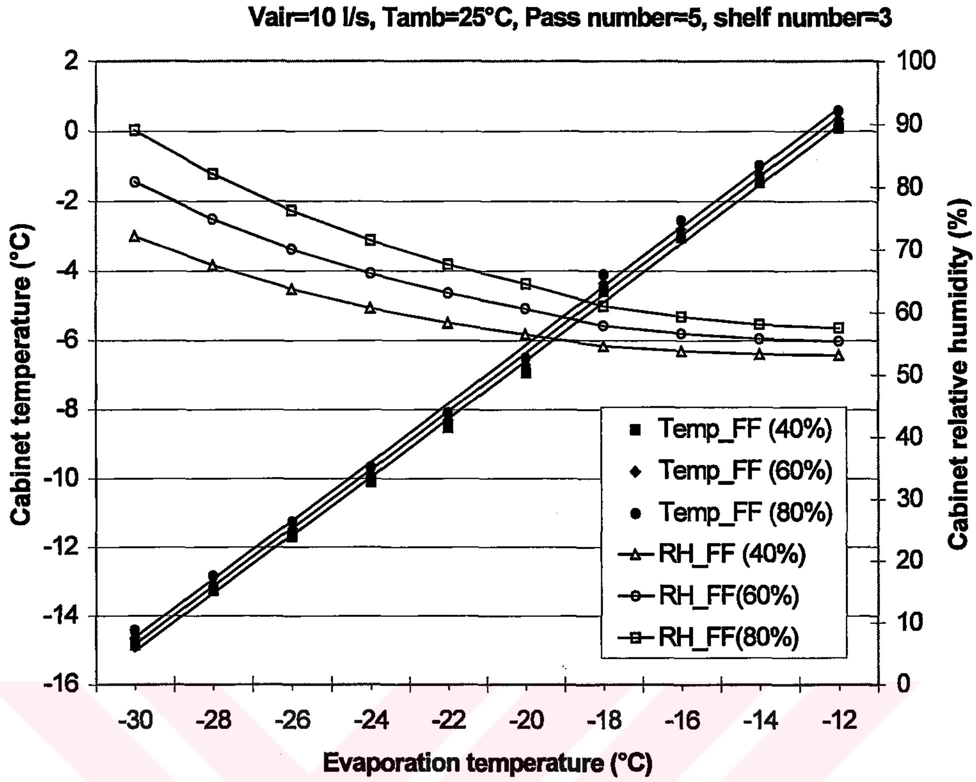

Figure 5.24 Freshfood cabinet temperature and relative humidity change with respect to evaporation temperature for three different ambient relative humidity values (Vair=10 l/s).

Figure 5.24 shows that the cabinet temperatures are lower than the values given in figure 5.23. This is the result of increased air flowrate through evaporator. As expected, when the evaporator heat transfer coefficient increases, the cabinet temperature decreases.

The cabinet relative humidity is higher for higher air flowrate because the cabinet temperature is colder.

5.3 Conclusions

1) In this final chapter, a calculation procedure for obtaining the heat and mass transfer characteristics of refrigerator evaporators that operates under frosting conditions has been introduced. A simulation algorithm in the EES environment has been developed. The solver is capable of calculating the frost thickness, density, frost mass, overall heat transfer coefficient, exit temperature and humidity, and pressure drop values for each individual tube pass for quasi-steady time steps.

2) As indicated in the literature (e.g. O'Neal and Tree (1985), Ostin and Andersson (1995)), during the frost formation, both thickness and density are found to increase simultaneously. This phenomenon is due to the fact that some percentage of water mass goes to increase the frost thickness, and the remaining portion goes to increase frost density. These percentages are found to be very important parameters for predicting evaporator characteristics. A study has been conducted to examine the densification ratio effect on heat transfer and pressure drop characteristics. According to these studies, when the densification ratio is increased from 20% to 50%, the pressure drop decreases approximately 3 times, the accumulated frost mass increases 4%, and the heat transfer coefficient increases 5% (operation time is 12 hours). After this parametric study, a densification ratio of 0.3 was chosen as a value that gives reasonable results with literature reported values. Until more accurate values or calculation techniques are obtained, this value is recommended for calculations.

3) The effect of evaporation temperature is investigated. Calculations are made for 12 hours of operation time, and results are compared according to the values that are obtained at the end of 12 hours. Increasing the evaporator temperature from –35°C to –25°C causes a 10% decrease of the heat transfer coefficient, a decrease of 2 times lower values on the pressure drop, and 5 times lower values on accumulated frost mass.

   The effect of air flowrate is also investigated by using air flow values of 5 l/s, 15 l/s, and 25 l/s. According to this study, when the flowrate is increased from 5 to 25 l/s, the UA value increases 3 times, pressure drop increases more then 10 times, and accumulated frost mass increases 3.5 times.

4) A simulation of a real refrigerator situation is studied. In this case, the air flowrate is calculated by using the system and fan characteristic curves. To do this, the solver that was developed in Chapter-4 is integrated into the solver of Chapter-5. Finally, evaporator heat transfer and pressure drop values are obtained for three different inlet air relative humidity values. According to this study, the heat transfer coefficient first showed increasing trend then, a relatively sharp decreasing trend occurs until the evaporator is completely blocked. These trends are compatible with Stein's (1999) experimental studies on a domestic refrigerator. On the other hand, the pressure-drop calculations showed an exponentially increasing trend. In addition, as expected, the pressure-drop and frost thickness increased more rapidly for higher relative humidity values. Complete evaporator blockage occurred after 45 hours and 110 hours of operation time for inlet humidity values of 80% and 50%, respectively.

5) Combining the evaporator model, air flow model, and cabinet heat/moisture loading, the effects on cabinet conditions were investigated. Results were summarized in figures.

6) Seker (1999) made an experimental study on the same evaporator types that were investigated in this study. His experimental studies only cover initial values (first 2 hours) of frosted evaporator characteristics. The experimental set-up is described in details by Seker (1999). Figures 5.25 and 5.26 compare model results with experimental and Seker's model results.

Experimental studies are made for following conditions.

Air inlet temperature:	*-8.5 °C*
Air flowrate:	*15 l/s*
Inlet air relative humidity:	*80%*
Evaporation temperature:	*-22°C*
Refrigerant mass flowrate:	*5.35 kg/h*

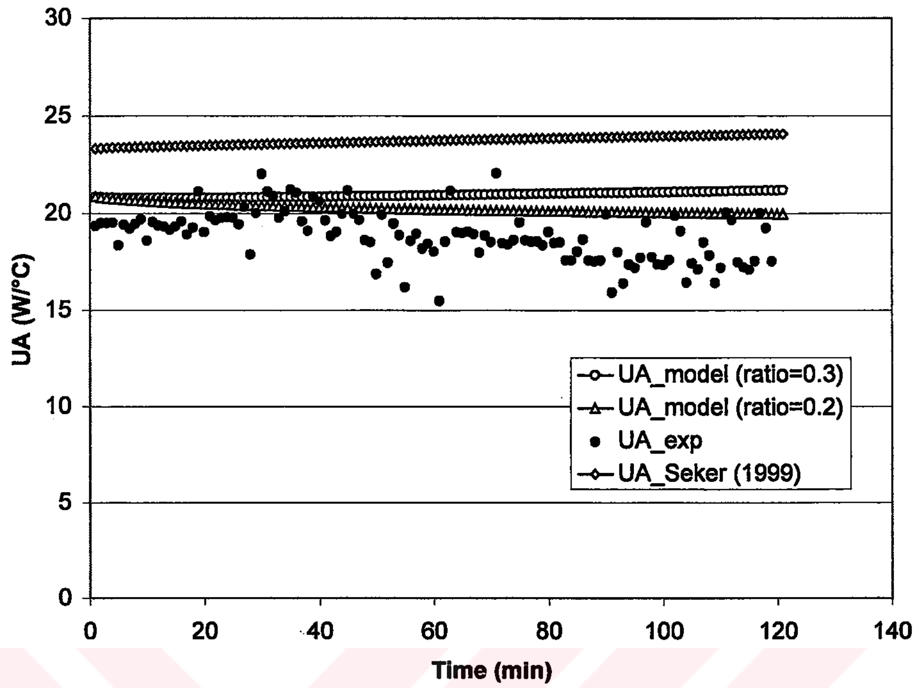

Figure 5.25 The comparison of UA values obtained from experimental and modeling studies of Seker (1999) vs. model results of presented study.

According to Figure 5.25, the present model's results are shown for two different densification ratios. Both give very close results in the beginning. However, the results for densification ratio of 0.2 are in better agreement than densification ratio of 0.3. On the other hand, Seker's (1999) results looks approximately 15% higher then presented model.

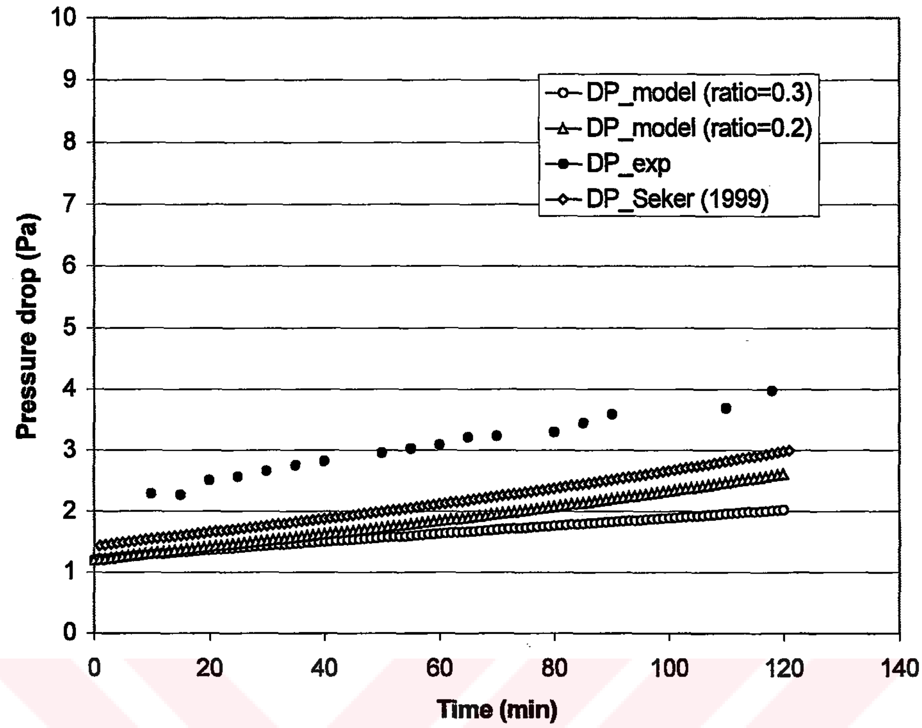

Figure 5.26 The comparison of pressure-drop values obtained from experimental and modeling studies of Seker (1999) vs. model results of presented study.

As the experimental studies are not enough to make wide conclusions, the value of densification ratio is unknown until more data becomes available. Figure 5.26 Comparison of pressure-drop values obtained from experiments of Seker (1999) and the model presented in this study.

According to Figure 5.26, the pressure drop values of present model looks 30% lower then experimental results. However, it is in good agreement with Seker's (1999) results. The pressure-drop value for densification ratio of 0.2 shows better agreement than a ratio of 0.3 to experimental results. It should be noted that, in the beginning of frosting process pressure drop values are very small compared to the values after 10 hours. Therefore, it is important to wait until more data is obtained.

7) Future studies will be focused on experimental investigation of heat and mass transfer characteristics of refrigerator evaporators. The frost characteristics

(density and growth rate) and effective parameter need to be analyzed in more detailed.

8) In this study, from Chapter 1 to 5 a guide for analyzing the characteristics of the domestic, no frost refrigerator evaporator, cabinet, and air distribution system are investigated. This research will be useful for further studies in the same area.

REFERENCES

Admiraal D. M., Bullard C. W., 1993. Experimental Validation of Heat Exchanger Models for Refrigerator Freezer, *ASHRAE Transactions: Research.*

Aydin C., Dal M., Dirik E., 1998 "Nofrost Buzdolabi Taze Gida Bolmesi Evaporator Bolgesinin CFD Analizi", *internal report*, ANN-173, Arcelik A.S.

Barrow H., 1985. A Note on Frosting of Heat Pump Evaporator Surfaces, *Heat Recovery Systems*, Vol. 5, No. 3, pp. 195-201.

Bejan A., 1995. Convection Heat Transfer, 2nd edition, John Wiley & Sons Inc.

Chan Y.L , Tien C.L, 1985. A Numerical Study of Two-Dimensional Natural convection in Square Open Cavities", J. Numerical Heat Transfer Vol.8,pp.65-70.

Chan Y.L, Tien C.L 1986a. Laminar Natural Convection in shallow Open Cavities, *J. of Heat Transfer*, May, vol. 108, pp.305-309.

Chan Y.L, Tien C.L., 1986b. A Numerical Study of Two-dimensional Laminar Natural Convection in Shallow Open Cavities: *J. of Heat Transfer*, May, vol. 108, pp.310-314.

Chen K.S., Humphrey J.A.C, Miller L., 1983. Note on the Pulsating Nature of Thermally-Driven Open Cavity Flow, *Int. J. Heat Mass Transfer*, Technical Notes, Vol. 26, No. 7,pp. 1090-1093.

Churchill S.W.; Chu H.H.S., 1975. Correlating Equations for Laminar and Turbulent Free Convection from a Vertical Plate, *Int. J. Heat Mass Transfer*, 18, p.1323.

Clausing A.M., 1983. Convective Losses From Cavity Solar Receivers, *J. of Solar Energy Engineering*, February, Vol.105, pp.29-33.

Clausing A.M.; Waldvogel J.M.; Lister L.D., 1987. Natural Convection from Isothermal Cubical Cavities with a variety of side-Facing Apertures, *ASME Journal of Heat Transfer*, V:22. pp.813-826.

Gall R.L, Grillot J.M., Jallut C., 1997. Modelling of Frost Growth and Densification, *Int. j. Heat Mass Transfer*, Vol. 40, No.13, pp. 3177-3187.

Gathcilov T.S., Ivanova V.S., 1979. Characteristic of the Frost Formed on the Surface of the Finned air Coolers, *Proceedings of the XVth International Congress of Refrigeration*, V: II, pp. 997-1003.

Gentry M. C., DeJong N. C., Jacobi A. M., 1996. Evaluating the Potential of Vortex-Enhanced Evaporator Performance for Refrigeration Applications, *ASHRAE Transactions*: Symposia, SA-96-2-1, pp. 361-367.

Goldstein R.J., Cho H.H, 1995. A Review of Mass Transfer Measurements Using Naphthalene Sublimation, *Experimental Thermal and Fluid Science*, pp. 416-434.

Hayashi Y., Aoki A., Adachi S., Hori K., 1977. Study of Frost Properties Correlating with Frost Formation Types, *J. of Heat Transfer*, 99, pp 239-245.

Hess C.F, Henze R.H., 1984. Experimental Investigation of Natural Convection Losses From Open Cavities, *J. of Heat Transfer*, May, V:106 pp:333-338.

Hosoda T., Uzahashi H., 1967. Effects of Frost on the Heat Transfer Coefficient, *Hitachi Review*, Vol. 16, No. 6.

Ismail K.A.R. ,Salinas C.S., 1999. Modelling of Frost Formation Over Parallel Cold Plates, *Int. J. of Refrigeration*, Vol. 22, No 5, pp 442.

Karatas H., 1996. Theoretical and Experimental Investigation of a Domestic Refrigerator Evaporator, *M.Sc. Thesis*, İ.T.Ü. Institute of Science and Technology, İstanbul.

Karatas H., 1998. Buzdolabinda Nem Olcumu, *internal report*, ANG-002, Arcelik A.S.

Kays W.M., London A.L., 1992. *Compact Heat Exchangers*, Third Edition, McGraw Hill, Singapore.

Knackstedt L.N., Newell T.A., Clausing A.M., 1995. A Study of Convective and Mass Heat Transfer in a Residential Refrigerator during Open Door Conditions, *internal report*, ACRC TR-71, January .

Kondepudi S.N., O'Neal D.L., 1993. A Simplified Model of Pin Fin Heat Exchangers Under Frosting Conditions. *ASHRAE Transactions*: Symposia, CH-93-2-3, pp. 754-761.

Kondepudi S.N., O'Neal D.L., 1993. Performance of Finned-Tube Heat Exchangers Under Frosting Conditions: I. Simulation Model, *Int. J. Refrigeration*, V. 16, No. 3.

Kondepudi S.N., O'Neal D.L., 1990. The Effects of Different Fin Configurations on the Performance of Finned-Tube Heat Exchangers Under Frosting Conditions. *ASHRAE Transactions*, V. 96, Part 2.

Kondepudi S.N., O'Neal D.L., 1987. The Effects of Frost Growth on Extended Surface Heat Exchanger Performance: A Review. *ASHRAE Transactions*, V. 93, Part 2, pp. 258-177.

Laleman M.R., Newell T.A., Clausing A.M., 1992. Sensible and Latent Energy Loading on a Refrigerator During Open Door Conditions, *internal report*, ACRC TR-20, May

Lee K.S, Kim W.S, Lee T.H., 1997. A One-Dimensional Model for Frost Formation on a Cold Flat Surface, *Int. J. Heat Mass Transfer*, Vol.40, No.18, pp. 4359-4365.

Mao Y., Besant R.W., Rezkallah K.S., 1991. A Method of Measuring Frost Density Using Flush-Mounted Removable Disks, *ASHRAE Transactions*: Research, Vol. 97, Part 1, pp. 26-30.

Mao Y., Besant R.W., Rezkallah K.S., 1992. Measurement and Correlations of Frost Properties with Airflow over a Flat Plate, ASHRAE Transactions: Research, pp 65-78.

Mao Y., Besant R.W., Falk J., 1993. Measurement and Correlations of Frost Properties with Laminar Airflow at Room Temperature over a Flat Plate", *ASHRAE Transactions*: Symposia, Vol. 99, Part:1, pp. 739-745.

Melamed B., 1999. No frost buzdolaplarında kullanılan fanların seçim kriterleri, internal report, Arcelik A.S.

Naylor D., Oosthuizen P.H., 1998. An Introduction to Convective Heat Transfer Analysis (McGraw-Hill Series in Mechanical Engineering), McGraw-Hill.

Niederer R.H., 1986. Frosting and Defrosting Effects on Coil Heat Transfer, *ASHRAE Transactions*, V. 92, Part 1, pp. 467-473,

Ogawa K., Tanaka N., Takeshita M., 1993. Performance Improvement of Plate Fin-and- Tube Heat Exchangers Under Frosting Conditions, *ASHRAE Transactions*: Symposia, CH-93-2-4, pp. 762-771.

O'Neal D.L., Tree D.R., 1985. A Review of Frost Formation in Simple Geometries, *ASHRAE Transactions*, V:91, Part I, pp. 267-281.

Oskarrsson S.P. Krakow K.I., Lin S., 1990. Evaporator Models for Operation with Dry, Wet, and Frosted Finned Surfaces. Part I: Heat Transfer and Fluid Flow Theory, *ASHRAE Transactions*, No: 96(1), pp. 373-380.

Oskarsson S.P., Krakow K.I., Lin S., 1990. Evaporator Models for Operation with Dry, Wet, and Frosted Finned Surfaces, Part II: Evaporator Models and Verification", *ASHRAE Transactions*, V. 96, Part 1.

Ostin R., Andersson S., 1991. Frost Growth Parameters in a Forced Air Stream, *Int. J. Heat and Mass Transfer*. Vol. 34, No. 4/5, pp1009-1017.

Patankar S.V., 1980. Numerical Heat Transfer and Fluid Flow, Hemisphere/McGraw-Hill, Washington.

Penot F., 1982. Numerical Calculation of Two-Dimensional Natural Convection in Isothermal Open Cavities, Numerical Heat Transfer, vol.5, pp. 421-437.

Quere P.L., Humphrey J.A.C, Sherman F.S., 1981. Numerical Calculation of Thermally Driven Two-Dimensional Unsteady Laminar Flow in Cavities of Rectangular Cross Section, *Numerical Heat Transfer*, Vol. 4, pp. 249-283.

Rite R.W., Crawford R.R., 1991. The Effect of Frost Accumulation on the Performance of Domestic Refrigerator-Freezer Finned-Tube Evaporator Coils, *ASHRAE Transactions*, Vol. 97, Part 2.

Sanders C.T., 1974. The Influence of Frost Formation and Defrosting on the Performance of Air Coolers, *Ph.D. Thesis*, Delft Technical University.

Seker D., 1999. Nofrost buzdolabı evaporatörlerinde karlanmanın etkileri. Yüksek Lisans Tezi, İstanbul Teknik Üniversitesi Fen Bilimleri Enstitüsü, İstanbul.

Skok H., Ramadhyani S., and Schoenhals R.J., 1991. Natural Convection in a Side-Facing open cavity, *Int. J. Heat and Fluid Flow*, Vol.12, No.1.

Stein M., 1999. Moisture Transport Inside Domestic Refrigerators,M.Sc. Thesis, University of Illinois at Urbana-Champaign, USA. November.

Stern M. 1989. Evoluation of Locally Unstable Shear Flow Near a Wall, *J. Fluid Mech.*, vol. 198, pp. 79-99.

Stoecker W.F. "How Frost Formation on Coils Affects Refrigeration Systems", *Refrigerating Engineer*, V.65.

Tao Y.X., Besant R.W, Rezkallah K.S., 1993.A Mathematical Model for Predicting the Densification and Growth of Frost on a Flat Plate, Int. J. Heat Mass Transfer, Vol.36, No. 2, pp. 353-363.

Von Karman T., 1939. The Analogy Between Fluid Friction and Heat Transfer, *Transactions of ASME*, Vol.61, , pp. 705-710.

White F.M., 1991. Viscous Fluid Flow-Second Edition, Mc-Graw-Hill.

APPENDIX-A EES PROGRAM LISTING

```
{*******************************************************************************************************
*********OPEN DOOR HEAT AND MASS TRANSFER IN DOMESTIC REFRIGERATOR*********

******************************AVERAGE VELOCITY OF AIR STREAMS********************************
************************ARE CALCULATED BY USING FORCE BALANCE****************************
*******************************************************************************************************
*******************************************************************************************************}


{*************Geometry of the problem*****************************************************************}

L= 0.724; W=0.699 ;D=0.495 ;Lc=L{0.6985}                        {L. Knacksted's Geometry , [m]}
{L=0.94;W=0.67;D=0.63}                                          {Present study, [m]}

n=0                                  {number of shelves, max three}
dd=0                                 {dd is height of a cubical object on the refrigerator shelves [m]}
As=(L*W+2*W*D+2*L*D)+2*n*W*D         {Total inner surface area including shelf [m2]}
An=n_object*dd*dd                    {Total projection area of the object on the shelves [m2]}
Af=L*W                               {Frontal area of cavity, door opening area , [m2]}

Ao=n_object*Aos                      {Total surface area of the objects participating heat transfer, [m2]}
Aos=5*dd*dd                          {surface area of the individual object participating heat transfer ,[m2]}
n_object=10                          {number of the objects in the refrigerator}

{Input temperatures}
     Tw=3.3                          {Wall temperature [C] }
     Ta=21.85                        {Ambient temperature[C] }

{Physical properties of dry air- L.Knackstedt case}
     k=0.02516
     rho=1.23
     Cp=1.006
     Beta=1/(Tf+273.15)
     g=9.81
     nu=1.46e-5
     Pr=0.71

Tave=(Ta+To)/2                  {Average temperature, [C]}

Tf=(Ta+Tw)/2                    {Film temperature, [C]}

{*******************************************************************************************************
***********************************Tunning onstants****************************************************
*******************************************************************************************************}
c1=4.95
c2=1.5-0.32*n
c3=1
Re=-98.898*L+402.17
CD=1.8047*exp(0.6328*n)


{*******************************************************************************************************
****************************Calculated average inlet velocity *****************************************
*******************************************************************************************************}
u=((beta*(Ta-Tave)*density(air,P=1,T=Ta)*g*L*W*D)/(density(air,P=1,T=Tave)*(c3*As/Re+0.5*(1*An+CD*Af))))^0.5


u_max=(beta*(Ta-Tw)*density(air,P=1,T=Ta)*g*L/density(air,P=1,T=Tave))^0.5     {from white's textbook, kinetic -
potential energy balance}

delta=Re*nu/u                        {Boundary layer thickness, [m]}
h=c1*k/delta {0<c1<10}               {Heat transfer coefficient, [W/m2K]}
m=u*c2*(Af/2)*density(air,P=1, T=Ta)    {mass flowrate [kg/s] , 1<c2<2}

blayer=delta*1000

{outlet velocity}
u_out=m/((2-c2)*(Af/2)*density(air,P=1,T=To))
```

```
{*******************************************************************************************************
*******************************Heat Transfer Calculations************************************************
*******************************************************************************************************}

Teta=exp(-h*(As+Ao)/(m*Cp*1000)) {Ao is the surface area of the object participating to heat transfer}
To=Tw-Teta*(Tw-Ta)
Nusselt=h*Lc/conductivity(air,T=Tf)

Qm=m*Cp*(Ta-To)*1000
Qh=-h*(As+Ao)*((Ta-To)/ln(teta))
ratio=Qm/Qh

{Air change rate (ACR) [times/door opening] }

ACR=(m/density(air,P=1, T=Tave))*20/(W*D*L)

{Diemensionless numbers}

GrL=g*beta*(Ta-Tw)*L^3/nu^2          {Gr number based on the temp difference between ambient and wall}
RaL=g*beta*(Ta-Tw)*L^3/((conductivity(air,T=Tf)/(density(air,p=1,t=Tf)*SPECHEAT(Air,T=Tf)*1000))*nu)
                                     {Ra number based on the temp difference between ambient and wall}
ReL=u*Lc/nu                          {Reynold 's number of mean flow on the surfaces}

{*******Vertical flat plate, free conv. heat transfer coefficient calculation, Churcill and Chu (1975)*******************
*******************************************************************************************************}
Nusselt_plate=(0.825+(0.387*RaL^(1/6)/(1+(0.492/Pr)^(9/16))^(8/27)))^2
h_plate=conductivity(air,T=Tf)*Nusselt_plate/L

{*******************One face open cavity heat transfer correlation, Skok et al.(1991) ****************************
*******************************************************************************************************}
Nusselt_skok=0.087*RaL^(1/3)
h_skok=conductivity(air,T=Tf)*Nusselt_skok/L


{==================================================================================
==================Mass transport calculations*=====================================
==================================================================================}

RH_a=60                              {Relative humidity of ambient air, [%]}
Da=26e-6                             {mass diffusition coefficient of air-water system}
alfa=conductivity(airH2O,T=Tf,P=1,R=RH_a/100)/(density(airH2O,T=Tf,P=1,R=RH_a/100)*specheat(airH2O,T=Tf,P=1,R=
RH_a/100)*1000)                      {thermal diffusition coefficient of air [m2/s]}
Pw=Pressure(Water,T=Tw,x=1)*101.3    {Saturation pressure of water at wall temperature, [Kpa] }
Psa=Pressure(Water,T=Ta,x=1)*101.3   {Saturation pressure of water at free stream temperature, [Kpa] }
Pa=RH_a*Psa/100                      {RH _a is relative humidity of air . and it is a parameter for calculations}

{===============Mass transfer coefficient for cavity h_m [kg/sKpa]=====================
===================================================================================}
h_m=0.0062*h*((DENSITY(AirH2O,T=Tf,P=1,R=RH_a/100)*Da/conductivity(airH2O,T=Tf,P=1,R=RH_a/100)))*(alfa/Da)^
(1/3)
m_condensation=-h_m*(Pw-Pa)*As       {water condensation on inner walls of cabinet , kg_w/s}

{===============Mass transfer coefficient for door surface, h_door [kg/sKpa]==============
===================================================================================}
h_m_door=0.0062*h_plate*((DENSITY(AirH2O,T=Tf,P=1,R=RH_a/100)*Da/conductivity(airH2O,T=Tf,P=1,R=RH_a/100))
)*(alfa/Da)^(1/3)
m_condensation_door=-h_m_door*(Pw-Pa)*L*W  { condensation on the door surfaces [kg/s]}

{============Latent heat transfer because of condensation [W]=========================
===================================================================================}
hfg=(ENTHALPY(Water,T=Tw,x=1)-ENTHALPY(Water,T=Tw,x=0))
Q_latent=m_condensation*hfg*1e3  { latent heat of condensation  [w]}

{============Dimensionles numbers in mass transfer ====================================
===================================================================================}
Sc=viscosity(airH2O,T=Tf,P=1,R=RH_a)/Da         {Schmidt number}
Pr=viscosity(airH2O,T=Tf,P=1,R=RH_a)/alfa       {Prandtl  number}
Le=alfa/Da                                      {Lewis number}
Sh=h_m*L/Da                                     {Sherwood number}
St_m=h_m/u                                      {Mass transport stanton number}
```

```
{>>>>>>>>>>>>>>>>>>>>>>>>>>>>>>>>>>>>>>>>>>>>>>>>>>>>>>>>>>>>>>>>>>>>>>>>>>>
>>>>>>>>>>>>>>>Water loading of the refrigerator- effect of door openings>>>>>>>>>>>>>>>>>>>>>>>
>>>>>>>>>>>>>>>>>>>>>>>>>>>>>>>>>>>>>>>>>>>>>>>>>>>>>>>>>>>>>>>>>>>>>>>>>>>}

ndo=20                          {number of door openning between defrosts}
dodo=20                         {duration of door openning-sec}
condensate_door=ndo*m_condensation_door*dodo
condensate=ndo*(m_condensation*dodo+(humrat(airH2O,T=Tf,P=1,R=RH_a/100)-
humrat(airH2O,T=Tw,P=1,R=0.25))*density(airH2O,T=Ta,P=1,R=RH_a/100)*L*W*D)+condensate_door
{door surface is included in the total condensate calculation}

{>>>>>>>>>>>>>>>evaporation from a water pan, Sparrow  and Chuck (1986)>>>>>>>>>>>>>>>>>>>>>
>>>>>>>>>>>>>>>>>>>>>>>>>>>>>>>>>>>>>>>>>>>>>>>>>>>>>>>>>>>>>>>>>>>>>>>>>>>}

{>>>>>inputs>>>>>>>>>>>>>>>>>>>>>>>>>>>>}

RH_cabinet=25/100               {relative humidity of cabient air is asssumed as %25 for steady state case}
nu_airwater=viscosity(airH2O,T=Tff,P=1,r=RH_cabinet)
hh=0.03                         {distance between pan top and water level  [m]}
u_forced=0.2                    {air vleocity over pan  [m/s] }
Tff=Tw                          {Freshfood  cabinet air emperature, [°C]}
P_total=101.325                 {Total atm pressure, [Kpa]}
Apan_surface=0.174              {Open pan surface area , [m2]}


Re_h=u_forced*hh/nu_airwater                 {Reynolds number based on the distance ,hh}
Sh_h=h_r*hh/Da                               {Sherwood number based on the hh}
h_r=m_evap_pan/(Apan_surface*delta_rho)      {h_r is mass transfer coefficient based on density difference, [m/s]}
delta_rho=(rho_ws-rho_cabinet)               {water partial density difference between water surface and cabinet air
                                             [kg/m3]}
rho_ws=P_total/(1+(1/humrat(airH2O,T=Tff,P=1,r=1))*(18/29))/(Rw*(Tff+273.15))
rho_cabinet=P_total/(1+(1/humrat(airH2O,T=Tff,P=1,r=RH_cabinet))*(18/29))/(Rw*(Tff+273.15))
Rw=8.315/18                                  {water vapor gas constant kj/kgK}
Sh_h=0.0285*Re_h^0.738                       {Correlation of Chuck and Sparrow  (1986) }

{""""""""""""""""""""""""""""""""""""""""""""""""""""""""""""""""""""""""""""""""""""
""""""""""""Sensible and Latent  Heat Gain per door opening of 20 s""""""""""""""""""""""""""""""""""""""
""""""""""""""""""""""""""""""""""""""""""""""""""""""""""""""""""""""""""""""""""""}

{Qconv=Qconv_wall+Qairchange}
{Assumption, during the first 7 seconds of door opening the  air in the cavity replaced by ambient air once, i.e one  volumetiric
air change}

Qconv=(Qh*20+density(air,T=Ta,P=1)*W*L*D*specheat(air,T=Ta)*1000*(Ta-Tw))/1000  {total convective heat gain
through 20 s door opening,[KJ]}
Qlatent_total=(Q_latent*13+(humrat(airH2O,T=Ta,P=1,R=RH_a/100)-
humrat(airH2O,T=Tw,P=1,R=0.25))*density(air,T=Ta,P=1)*L*W*D*hfg*1e3) /1000    {Total latent heat [KJ]}
```

APPENDIX-B
COMPARTMENT AVERAGE HEAT TRANSFER COEFFICIENTS

Table B.1 Compartment average heat transfer coefficients for no shelf case

SUMMARY OF NO SHELF STUDIES			
Shelf Configuration	**Tw [K]**	**h [W/m²K]**	**Nu [-]**
No shelf	0.83	3.58	95.84
	3.53	3.30	86.14
	5.37	3.46	90.04
	9.78	3.45	91.31

Table B.2 Compartment average heat transfer coefficients for one shelf case

SUMMARY OF ONE SHELF STUDIES			
Shelf Configuration	**T_w [K]**	**h [W/m²K]**	**Nu [-]**
One shelf bottom			
Top compartment	274.0	3.25	89.9
Bottom compartment	273.4	1.64	45.3
Top compartment	275.2	3.38	93.7
Bottom compartment	275.0	1.62	44.9
Top compartment	282.0	3.28	90.8
Bottom compartment	281.9	1.67	46.1
One shelf middle			
Top compartment	272.6	3.30	91.3
Bottom compartment	274.3	2.42	66.9
Top compartment	274.4	3.61	100.0
Bottom compartment	274.4	2.51	69.5
Top compartment	283.0	2.97	82.2
Bottom compartment	282.6	2.18	60.2
One shelf-Top			
Top compartment	271.5	2.81	77.8
Bottom compartment	273.6	3.02	83.5
Top compartment	273.5	3.48	24.1
Bottom compartment	274.9	3.54	24.6
Top compartment	283.6	2.48	17.2
Bottom compartment	283.7	2.54	17.7

Table B.3 Compartment average heat transfer coefficients for two shelves case

SUMMARY OF TWO SHELVES STUDIES			
Shelf Configuration	**T_w [K]**	**h [W/m^2K]**	**Nu [-]**
Two shelves @ bottom&middle			
Top compartment	272.991	4.121	118.6
Middle compartment	271.0	2.219	63.9
Bottom compartment	270.3	1.504	43.3
Top compartment	272.874	4.114	118.4
Middle compartment	271.7	2.603	74.9
Bottom compartment	274.4	1.756	50.5
Top compartment	277.171	4.589	132.1
Middle compartment	276.3	3.014	86.7
Bottom compartment	276.6	1.742	50.1
Top compartment	281.4	3.636	104.6
Middle compartment	280.7	2.107	60.6
Bottom compartment	279.8	1.524	43.9
Top compartment	273.4	3.637	104.7
Middle compartment	272.6	1.926	55.4
Bottom compartment	273.0	1.912	55.0
Top compartment	277.8	4.386	126.2
Middle compartment	276.2	2.579	74.2
Bottom compartment	276.4	2.516	72.4
Top compartment	283.3	3.188	91.7
Middle compartment	281.5	1.498	43.1
Bottom compartment	280.9	2.124	61.1
Two shelves @ bottom&top			
Top compartment	273.6	3.584	103.1
Middle compartment	273.1	3.258	93.7
Bottom compartment	272.0	1.291	37.2
Top compartment	272.6	4.063	116.9
Middle compartment	272.4	3.396	97.7
Bottom compartment	272.0	1.488	42.8
Top compartment	272.9	3.110	89.5
Middle compartment	273.6	2.943	84.7
Bottom compartment	274.6	1.150	33.1

Two shelves @ bottom&top Continued from previous page	T_w [K]	h [W/m^{2}K]	Nu [-]
Top compartment	276.3	4.336	124.8
Middle compartment	276.2	4.029	115.9
Bottom compartment	274.2	1.589	45.7
Top compartment	280.8	3.371	97.0
Middle compartment	281.2	2.963	85.3
Bottom compartment	280.7	1.173	33.8
Top compartment	272.8	3.447	99.2
Middle compartment	273.4	2.794	80.4
Bottom compartment	274.1	1.639	47.1
Top compartment	277.5	4.023	115.8
Middle compartment	277.6	3.521	101.3
Bottom compartment	276.5	2.113	60.8
Top compartment	279.0	3.620	104.2
Middle compartment	279.5	3.060	88.1
Bottom compartment	279.5	1.927	55.4
Two shelves @ middle&top			
Top compartment	273.7	3.964	114.1
Middle compartment	272.8	2.256	64.9
Bottom compartment	273.3	2.769	79.7
Top compartment	273.2	3.800	109.3
Middle compartment	271.7	2.128	61.2
Bottom compartment	272.5	2.717	78.2
Top compartment	273.0	3.389	97.5
Middle compartment	272.6	2.644	76.1
Bottom compartment	275.1	2.542	73.1
Top compartment	274.6	4.225	121.6
Middle compartment	275.4	2.897	83.4
Bottom compartment	276.4	3.016	86.8
Top compartment	282.1	2.807	80.8
Middle compartment	282.0	1.998	57.5
Bottom compartment	283.0	2.034	58.5
Top compartment	273.4	3.370	97.0
Middle compartment	273.0	1.876	54.0
Bottom compartment	274.6	2.873	82.7
Top compartment	273.6	4.149	119.4
Middle compartment	275.0	2.331	67.1
Bottom compartment	276.0	3.360	96.7

Two shelves @ middle&top Continued from previous page	T_w [K]	h [W/m^2K]	Nu [-]
Top compartment	280.2	3.523	101.4
Middle compartment	280.7	1.730	49.8
Bottom compartment	280.9	2.649	76.2

Table B.4 Compartment average heat transfer coefficients for three shelves case

SUMMARY OF THREE SHELVES STUDIES			
Shelf Configuration	T_w [K]	h [W/m^2K]	Nu [-]
Three shelves			
Top compartment	272.8	3.384	23.5
2nd compartment	272.6	2.445	17.0
3rd compartment	272.2	2.494	17.3
4th compartment	271.7	1.276	8.9
Top compartment	275.6	3.911	27.1
2nd compartment	276.2	3.067	21.3
3rd compartment	275.6	2.763	19.2
4th compartment	275.1	1.418	9.8
Top compartment	280.9	3.590	24.9
2nd compartment	280.9	2.506	17.4
3rd compartment	280.4	2.399	16.6
4th compartment	280.1	1.226	8.5
Top compartment	273.0	3.675	25.5
2nd compartment	271.9	2.215	15.4
3rd compartment	271.0	2.148	14.9
4th compartment	270.7	1.045	7.3
Top compartment	273.6	3.534	24.5
2nd compartment	272.8	2.484	17.2
3rd compartment	272.6	1.874	13.0
4th compartment	272.7	1.723	12.0
Top compartment	277.6	3.986	27.7
2nd compartment	277.1	3.051	21.2
3rd compartment	276.3	2.309	16.0
4th compartment	276.3	2.301	16.0
Top compartment	282.0	3.647	25.3
2nd compartment	281.5	2.361	16.4
3rd compartment	280.9	1.685	11.7
4th compartment	280.9	1.693	11.8

Three shelves Continued from previous page	**T_w [K]**	**h [W/m^2K]**	**Nu [-]**
Top compartment	272.8	3.092	21.5
2^{nd} compartment	271.1	2.148	14.9
3^{rd} compartment	271.1	1.917	13.3
4^{th} compartment	271.1	1.504	10.4
Top compartment	273.6	3.399	23.6
2^{nd} compartment	272.4	1.934	13.4
3^{rd} compartment	272.5	2.122	14.7
4^{th} compartment	272.5	1.859	12.9
Top compartment	276.4	4.377	30.4
2^{nd} compartment	276.2	2.793	19.4
3^{rd} compartment	276.4	2.962	20.6
4^{th} compartment	276.3	2.506	17.4
Top compartment	281.4	3.297	22.9
2^{nd} compartment	280.9	1.918	13.3
3^{rd} compartment	280.7	2.226	15.4
4^{th} compartment	280.6	1.905	13.2
Top compartment	271.8	3.794	26.3
2^{nd} compartment	270.9	2.107	14.6
3^{rd} compartment	271.3	1.886	13.1
4^{th} compartment	270.6	1.452	10.1

APPENDIX-C
MODEL TUNING COEFFICIENT OPTIMIZATION

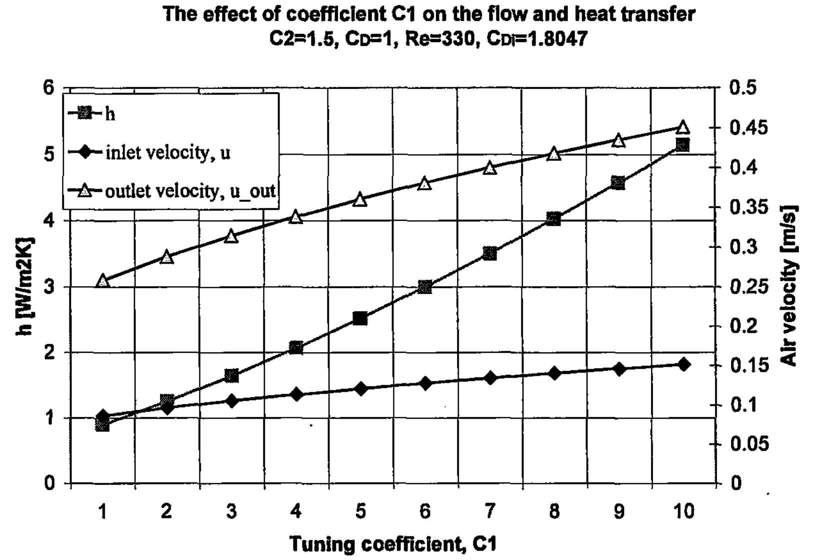

Figure C.1 Tuning coefficient C1's effect on system characteristics (Tw=3.3 °C, T∞=21.85 °C)

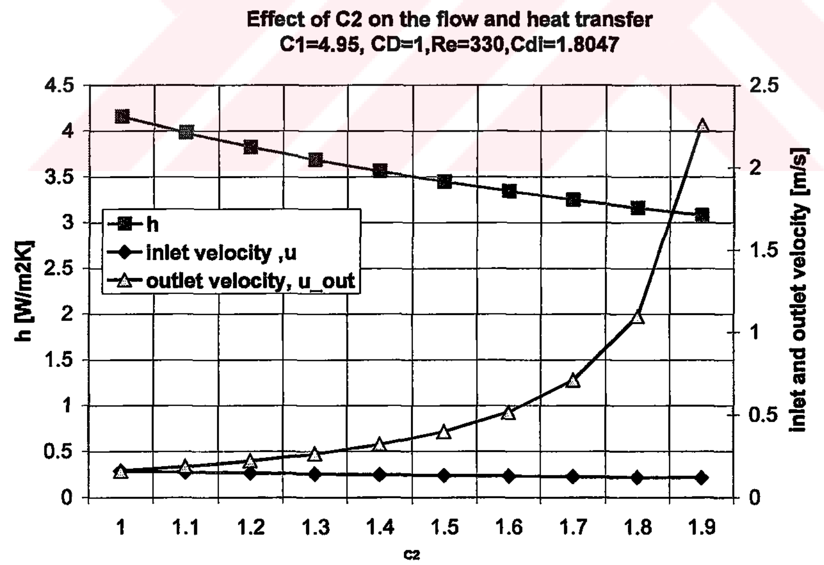

Figure C.2 Tuning coefficient C2's effect on system characteristics (Tw=3.3 °C, T∞=21.85 °C)

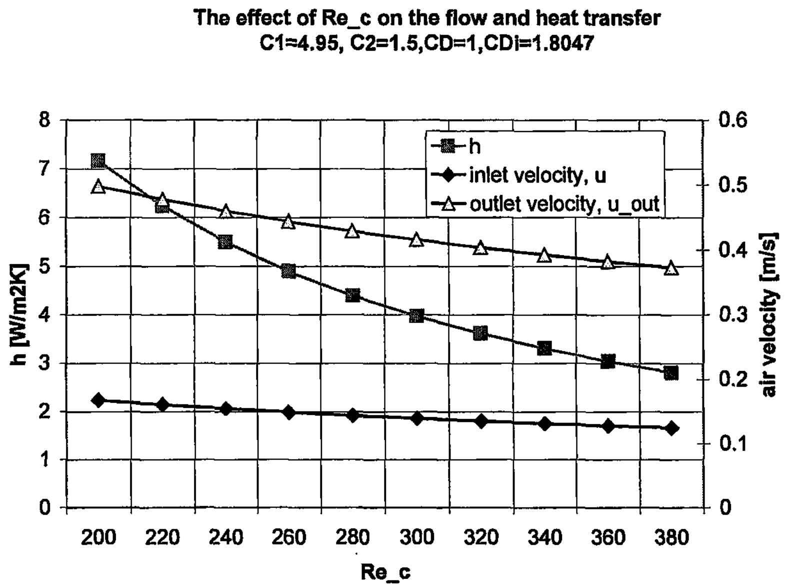

Figure C.3 Tuning coefficient C_{Di}'s effect on system characteristics (Tw=3.3 °C, T∞=21.85 °C)

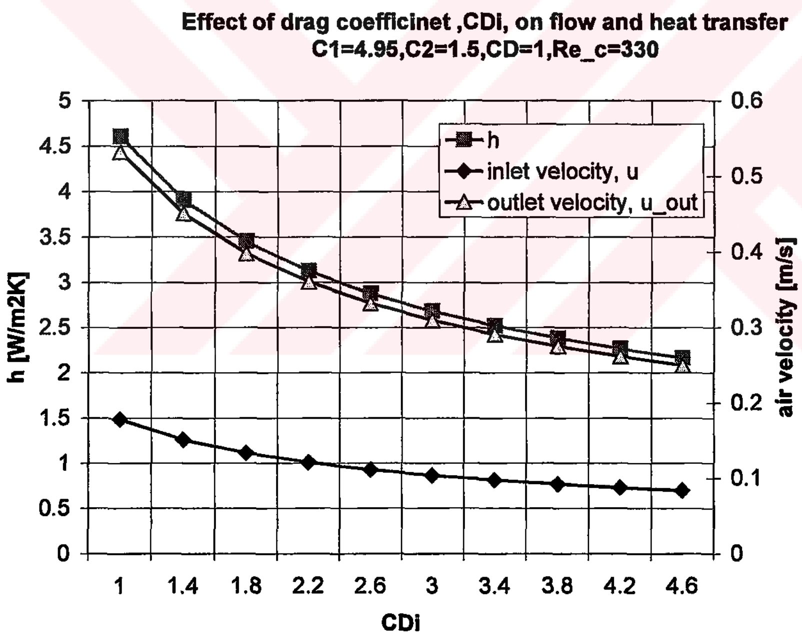

Figure C.4 Tuning coefficient Re_c's effect on system characteristics (T_w=3.3 °C, T∞=21.85 °C)

APPENDIX-D
CABINET AVERAGE NUSSELT NUMBER COMPARISONS FOR MULTI SHELF CASE

Table D-1 Cabinet average heat transfer coefficients for multi shelf case

Shelf Configuration		T_w [K]	h [W/m²K]	Nu [-]
NO SHELF		274.0	3.582	95.84
		276.7	3.295	86.14
		278.5	3.460	90.04
		282.9	3.449	91.31
ONE SHELF	*Bottom*			
		273.7	2.693	74.55
		275.1	2.790	77.26
		281.9	2.722	75.35
	Middle			
		273.5	2.952	81.73
		274.4	3.161	87.52
		282.8	2.665	73.77
	Top			
		272.8	3.061	84.73
		274.3	3.653	101.15
		283.6	2.598	71.93
TWO SHELVES	*Bottom-Middle*			
		271.6	2.748	30.3
		273.0	2.939	31.6
		276.7	3.245	35.0
		280.7	2.530	27.5
		273.0	2.593	27.9
		276.9	3.269	34.6
		282.0	2.351	25.0
	Bottom-Top			
		272.9	2.760	28.0
		272.3	3.019	30.2
		273.7	2.449	25.0
		275.6	3.381	34.4
		280.9	2.543	25.7
		273.4	2.641	25.9
		277.2	3.246	32.1
		279.3	2.886	28.4
	Middle-Top			
		273.3	2.976	28.2
		272.5	2.867	27.3
		273.7	2.830	26.6
		275.5	3.347	31.4
		282.4	2.258	21.2
		273.7	2.721	26.7
		275.0	3.287	32.0
		280.6	2.635	25.5

Shelf Configuration Continued from previous page		T_w [K]	h [W/m²K]	Nu [-]
THREE SHELVES		272.3	2.400	16.7
		275.7	2.790	19.4
		280.6	2.430	16.9
		271.6	2.271	15.8
		272.9	2.404	16.7
		276.8	2.912	20.2
		281.3	2.347	16.3
		271.5	2.165	15.0
		272.8	2.328	16.2
		276.3	3.159	21.9
		280.9	2.336	16.2

APPENDIX-E CAVITY AVERAGE HEAT TRANSFER COEFFICIENT VS. CAVITY HEIGHT (NO SHELF)

Table E.1 The effect of cavity height on average heat transfer coefficient.

Cavity Height L, [m]	T_w [K]	h [W/m^{2}K]	h_model [W/m^{2}K]	Nu [-]	Nu_model [-]	Error %
0.162	8.0	3.44	3.30	21.3	20.5	-4.1
0.168	8.0	3.16	3.27	20.4	21.1	3.4
0.168	8.0	3.50	3.27	22.5	21.1	-6.4
0.175	10.4	2.68	3.24	17.9	21.7	20.9
0.337	8.0	3.41	2.87	43.9	36.9	-15.9
0.349	9.9	3.15	2.86	42.1	38.1	-9.4
0.524	8.8	3.38	2.80	67.8	56.0	-17.3
0.724	9.8	3.46	2.87	95.9	79.4	-17.2
0.162	0.0	3.48	4.32	21.6	26.8	24.1
0.168	0.0	3.55	4.28	22.9	27.5	20.5
0.168	0.0	3.72	4.28	23.9	27.5	15.1
0.175	-1.7	3.13	4.24	20.9	28.3	35.4
0.337	0.0	3.96	3.75	50.9	48.3	-5.2
0.349	-0.5	3.49	3.74	46.6	49.9	7.1
0.524	0.8	3.35	3.66	67.2	73.3	9.1
0.724	0.8	3.64	3.75	100.7	103.9	3.2
0.162	3.3	4.09	4.00	25.3	24.8	-2.2
0.168	3.0	4.18	3.97	26.9	25.5	-5.1
0.168	3.0	4.19	3.97	26.9	25.5	-5.3
0.337	3.0	4.49	3.48	57.8	44.7	-22.5
0.524	2.0	3.52	3.39	70.6	67.9	-3.8
0.724	3.5	3.27	3.48	90.5	96.2	6.4

APPENDIX-F EXPERIMENTAL SYSTEM SPECIFICATIONS

Anemometer specifications:

Type:	Barnant Tri-Sense (Hot-Film type anemometer)
Model No:	637-0000
Manufacturer:	Barnant Company, 28W092 Commercial Avenue Barrington, IL, 60010 (708) 381 7050
Air velocity range:	0.03 to 25 m/s
Air velocity accuracy:	±3% of reading ± 0.1 m/s
Temperature range:	-40 °C to 70 °C
Temperature accuracy:	±0.3 °C
Measurement principle:	Air velocity is measured by passing air over a probe tip containing two nickel RTDs. The downstream detector is heated by a variable current to maintain a constant temperature differential with the upstream detector. When the temperature differential stabilizes, the current is logarithmically proportional to air velocity.
Calibration :	Anemometer sensor calibration data is given below.

Refrigerator Specifications:

Manufacturer:	Whirlpool
Model:	ET18 NK
Type:	No frost, Single Flow
Total Volume:	513 lt (18.1 cu ft)
FF compartment volume:	373 lt
Frz compartment volume:	140 lt

Data acquisition system specifications:

Hardware:	Hewlett Packard data logger. The data logger is composed of an E1300B mainframe, an E1326B Digital Multiplexer, two E1347A 16 channel General Purpose Multiplexer, and a 82341C High Performance ISA interface. The data logger is run by a Cyrix MII 300 based PC running Microsoft Windows 95 operation system using the 82341C High Performance ISA interface.

Software: HP-Vee 3.2 software controlled the data logger and Microsoft Excel recorded measurements

Air temperature measurement: 36 gauge T type T/C

Wall temperature measurements: 24 gauge T type T/C. Sensors are attached on the wall by using the thermally conductive epoxy.

T/C calibration: All sensor calibrations are made by using ice bath (accuracy of the temperature readings is found as ±0.1 °C).

Anemometer calibration:

Table F.1 Calibration results of anemometer.
Calibration is made in a wind tunnel, for the ambient temperature of 22°C

Barnant Tri Sense [m/s]	**Calibrator (*) [m/s]**
0.08	0.08
0.175	0.17
0.38	0.36
0.65	0.59
0.89	0.85
1.26	1.25
1.52	1.51
1.8	1.83
2.03	2.14
2.34	2.48

(*) Calibrator specifications:

Manufacturer: TSI Incorporated, P.O. Box 64204
St. Paul, MN 55164 USA
WWW: http://www.tsi.com

Model: VELOCICALC 8355

Temperature range: -17.8 to 93.3 °C

Velocity range: 0.15 to 50 m/s

Accuracy: ±0.01 m/s (0.15 to 2.5 m/s)

Response time (63% of final value): 200 ms to Velocity, 8 s to Temperature

APPENDIX G TRANSIENT VELOCITY PROFILES ON DOOR OPENING FOR NO SHELF

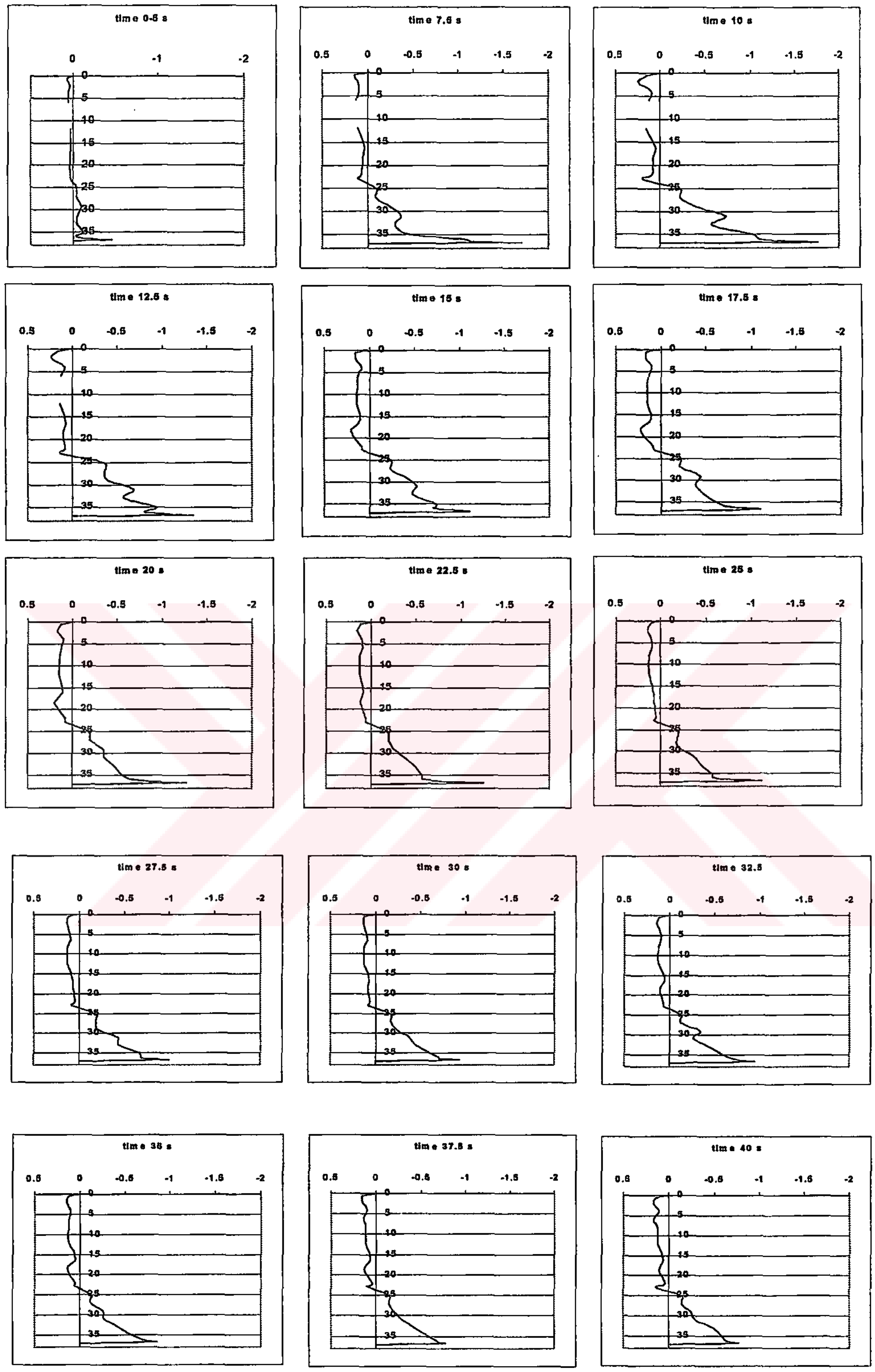

Figure G.1 Development of velocity profiles, x axis is velocity [m/s], y axis is location form top [inches] (No shelf case)

APPENDIX-H TRANSIENT VELOCITY PROFILES ON DOOR OPENING FOR ONE SHELF ON TOP POSITION

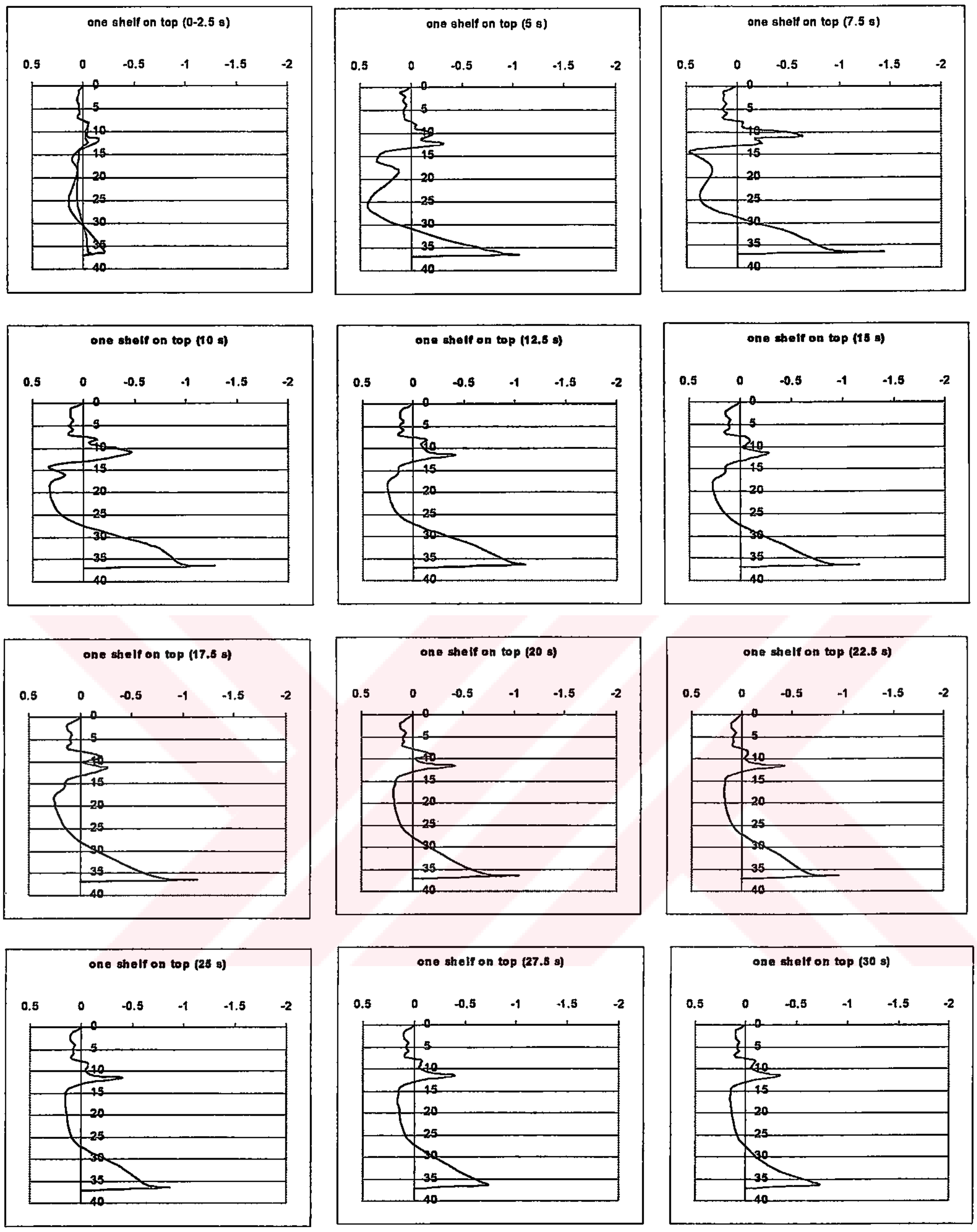

Figure H.1 Development of velocity profiles, x axis is vleocity [m/s], y axis is location from top [inches], (One shelf on top case)

APPENDIX -I THERMOCOUPLE LISTING

Table I.1 Thermocouple list for open door temperature measurements

IP Address	Multiplexer channel number	T/C Name	Explanation
200	**1**	1"	1" (25.4 mm) from top of the cabinet
201	**2**	5"	5" (127 mm) " " "
202	**3**	8"	8" (203 mm) " " "
203	**4**	10"	10" (254 mm) " " "
204	**5**	11.5"	11.5" (292 mm) " " "
205	**6**	13"	13" (330 mm) " " "
206	**7**	15"	15" (381 mm) " " "
207	**8**	20"	20" (508 mm) " " "
208	**9**	22"	22" (560 mm) " " "
209	**10**	24"	24" (610 mm) " " "
210	**11**	26"	26" (660 mm) " " "
211	**12**	28"	28" (710 mm) " " "
212	**13**	32"	32" (813 mm) " " "
213	**14**	34"	34" (864 mm) " " "
214	**15**	36"	36" (914 mm) " " "
215	**16**	Wall_BT_Right	Top shelf back wall right
300	**19**	Wall_BT_Left	Top shelf back wall left
301	**20**	Wall_BM_Right	Middle shelf back wall right
302	**21**	Wall_M_Right	Middle shelf wall right
303	**22**	Wall_B_Back	Bottom shelf wall back
304	**23**	Wall_Door	Door wall in the middle
305	**24**	Air_Top_Mid	Top shelf air at middle of volume
306	**25**	Air_Top_Back	Top shelf air 50 mm from back wall
307	**26**	Air Mid_Mid	Middle shelf air at middle of volume
308	**27**	Air_Mid_Back	Middle shelf air 50 mm from back wall
309	**28**	Air_Bot_Mid	Bottom shelf air at the middle of volume
310	**29**	Wall_B_Left	Bottom shelf wall left
311	**30**	Ambient	Ambient temperature 140 mm away from top of refrigerator
312	**31**	N/A	
313	**32**	N/A	
314	**33**	N/A	
315	**34**	N/A	

APPENDIX-J THE RESULTS OF CFD ANALYSIS ON FF AIR DISTRIBUTION SYSTEM

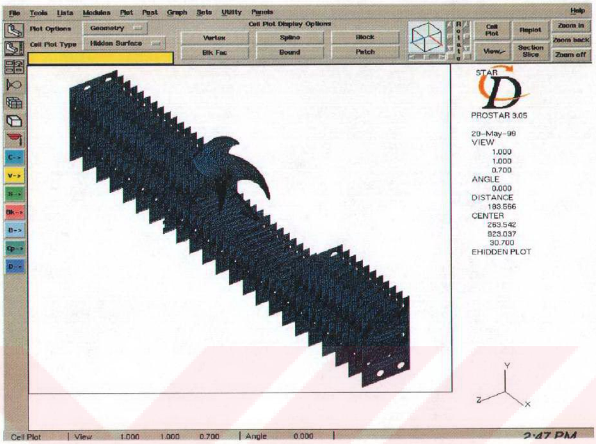

Figure J.1 3-D model of evaporator fins and Fan

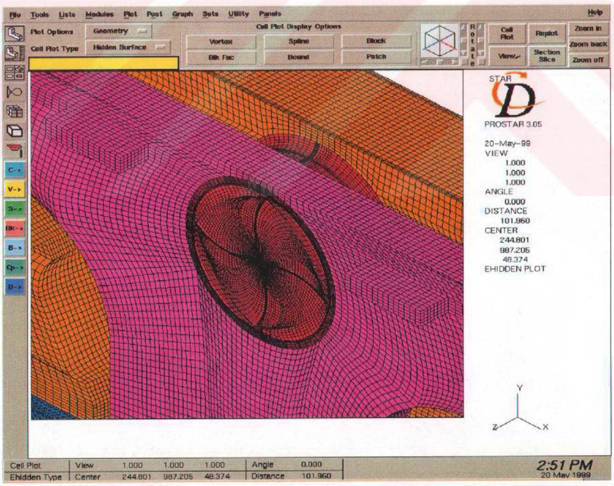

Figure J.2 Detailed view of mesh around fan exit

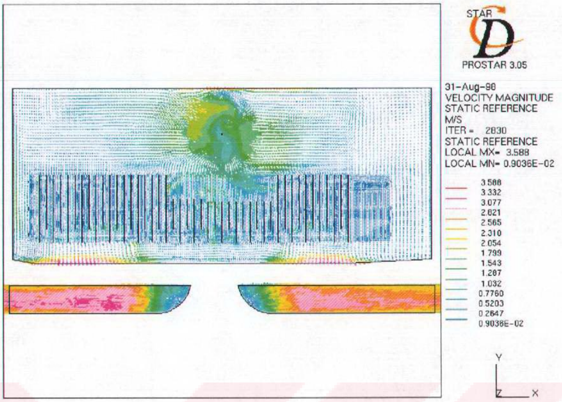

Figure J.3 Velocity distribution, a view from front of evaporator

APPENDIX-K THE SOLVER LIST OF CLOSED DOOR AIR DISTRIBUTION SYSTEM

```
{NF2000  Dual Evaporator  Project  Air Distribution System Design}

{air density and kinematic viscosity}

Ta=25 {°C}
ro=density(air,t=Ta,p=101){kg/m^3)}
nu=viscosity(air,T=Ta)/density(air,t=Ta,p=101) {1.5e-5}{m^2/s}
g=9.8 {gravity, m/s^2}


{duct lengths, m}
l1=0
l2=0
l3=0
l4=0
l5=170e-3;L5a=60e-3;L5b=60e-3
l6=345e-3
l7=0
l8=220e-3
l9=300e-3
l10=0e-3
l11=l6;l12=l7;l13=l8;l14=l9;l15=l10;l20=l19
l16=0
l17=0
l18=160e-3
l19=0

{inlet/outlet diameters of each duct, m}
d1i=100e-3;d1e=d1i
d2i=300e-3;d2e=300e-3
d3i=16.4e-3;d3e=d3i
d4i=16.4e-3;d4e=d4i
d5i=63e-3;d5e=d5i
d5ai=44.3e-3  ;d5ae=39.8e-3
d5bi=39.8e-3 ;d5be=34.3e-3
d6i=32e-3;d6e=35e-3
d7i=20e-3;d7e=d7i
d8i=35e-3;d8e=d8i
d9i=32e-3;d9e=17e-3
d10i=35e-3;d10e=d10i
d11i=d6i;d11e=d6e
d12i=d7i;d12e=d7e
d13i=d8i;d13e=d8e
d14i=d9i;d14e=d9e
d15i=d10i;d15e=d10e
d16i=48e-3;d16e=d16i
d17i=44e-3;d17e=d17i
d18i=156e-3;d18e=100e-3 {the outlet of duct 18 assumed  it is equal to fan housing diameter}
d19i=2*26.2e-3;d19e=d19i {narrow holes are taken into account, so outlet holes doubled}
d20i=d19i;d20e=d19e

{Pressure due to fan in each duct, Pa.  A negative value reverses the flow direction}

a1=40
a2=0
a3=0
a4=0
a5=0;a5a=0;a5b=0
a6=0
a7=0
a8=0
a9=0
a10=0
a11=0
a12=0
a13=0
a14=0
a15=0
a16=0
a17=0
a18=0{-0.109 Pa evaporator pressure drop}
```

```
a19=0
a20=0

{Fan parameters for using fan curve based on second order modeling}
b1=0
b2=0
b3=0
b4=0
b5=0;b5a=0;b5b=0
b6=0
b7=0
b8=0
b9=0
b10=0
b11=0
b12=0
b13=0
b14=0
b15=0
b16=0
b17=0
b18=0
b19=0
b20=0

{Orifice&Discharge coefficients}
Cd_orifice=1.0 {orifice discharge coefficient}
Cd_free=1.0  {duct exit free flow in turbulance}

{Equivalent duct length due to minor losses. For orifice type flow, Cd=1/Kd^2, where Kd is discharge coefficient}
Cd1=0; Le1=5.52*Cd1*(m1^0.2*(0.5*d1i+0.5*d1e)^0.8)/(ro*nu)^0.2
Cd2=0; Le2=5.52*Cd2*(abs(m2)^0.2*(0.5*d2i+0.5*d2e)^0.8)/(ro*nu)^0.2
Cd3=Cd_orifice {Cd3=2.44 if Le is used in pressure drop term}
;Le3=5.52*Cd3*(abs(m3)^0.2*(0.5*d3i+0.5*d3e)^0.8)/(ro*nu)^0.2
Cd4=Cd_orifice {Cd4=2.44 if Le is used in pressure drop term} ;
Le4=5.52*Cd4*(abs(m4)^0.2*(0.5*d4i+0.5*d4e)^0.8)/(ro*nu)^0.2
Cd5=0; Le5=5.52*Cd5*(abs(m5)^0.2*(0.5*d5i+0.5*d5e)^0.8)/(ro*nu)^0.2
Cd5a= 0.32; Le5a=5.52*Cd5a*(abs(m5a)^0.2*(0.5*d5ai+0.5*d5ae)^0.8)/(ro*nu)^0.2
Cd5b= 0.34; Le5b=5.52*Cd5b*(abs(m5b)^0.2*(0.5*d5bi+0.5*d5be)^0.8)/(ro*nu)^0.2

Cd6=1.32  ;Le6=5.52*Cd6*(abs(m6)^0.2*(0.5*d6i+0.5*d6e)^0.8)/(ro*nu)^0.2
Cd11=1.32  ;Le11=5.52*Cd11*(abs(m11)^0.2*(0.5*d11i+0.5*d11e)^0.8)/(ro*nu)^0.2

Cd7=Cd_orifice {Cd7=1/Cd_orifice^2   if Le is used in pressure drop term}  ;
Le7=5.52*Cd7*(abs(m7)^0.2*(0.5*d7i+0.5*d7e)^0.8)/(ro*nu)^0.2
Cd12=Cd_orifice {Cd7=1/Cd_orifice^2   if Le is used in pressure drop term}  ;
Le12=5.52*Cd12*(abs(m12)^0.2*(0.5*d12i+0.5*d12e)^0.8)/(ro*nu)^0.2

Cd8=0; Le8=5.52*Cd8*(abs(m8)^0.2*(0.5*d8i+0.5*d8e)^0.8)/(ro*nu)^0.2
Cd13=0; Le13=5.52*Cd13*(abs(m13)^0.2*(0.5*d13i+0.5*d13e)^0.8)/(ro*nu)^0.2

Cd9=cd_free; Le9=5.52*Cd9*(abs(m9)^0.2*(0.5*d9i+0.5*d9e)^0.8)/(ro*nu)^0.2
Cd14=cd_free; Le14=5.52*Cd14*(abs(m14)^0.2*(0.5*d14i+0.5*d14e)^0.8)/(ro*nu)^0.2

Cd10=0.4; Le10=5.52*Cd10*(abs(m10)^0.2*(0.5*d10i+0.5*d10e)^0.8)/(ro*nu)^0.2
Cd15=0.4; Le15=5.52*Cd15*(abs(m15)^0.2*(0.5*d15i+0.5*d15e)^0.8)/(ro*nu)^0.2

Cd16= 2.6+0.6; Le16=5.52*Cd16*(abs(m16)^0.2*(0.5*d16i+0.5*d16e)^0.8)/(ro*nu)^0.2
Cd17= 2.8+0.6; Le17=5.52*Cd17*(abs(m17)^0.2*(0.5*d17i+0.5*d17e)^0.8)/(ro*nu)^0.2
Cd18=1; Le18=5.52*Cd18*(abs(m18)^0.2*(0.5*d18i+0.5*d18e)^0.8)/(ro*nu)^0.2 {Evap friction drag set to unity}

Cd19=Cd_free ;  Le19=5.52*Cd19*(abs(m19)^0.2*(0.5*d19i+0.5*d19e)^0.8)/(ro*nu)^0.2
Cd20=Cd_free ;  Le20=5.52*Cd20*(abs(m20)^0.2*(0.5*d20i+0.5*d20e)^0.8)/(ro*nu)^0.2

{No minor loss case}
{Le1=0;Le2=0;Le3=0;Le4=0;Le5=0;Le6=0;Le7=0;Le8=0;le9=0;le10=0;le16=0;le17=0;le18=0;Le19=0}

{Duct friction loss parameters based on average duct diameter. Can also add a factor to act
as a damper or flow control device.}

alphab1=0.147*(ro^(-.8))*(nu^.2)*(l1+le1)*(.5*d1i+.5*d1e)^(-4.8)
alphab2=0.147*(ro^(-.8))*(nu^.2)*(l2+le2)*(.5*d2i+.5*d2e)^(-4.8)
alphab3=0.147*(ro^(-.8))*(nu^.2)*(l3+le3)*(.5*d3i+.5*d3e)^(-4.8)
alphab4=0.147*(ro^(-.8))*(nu^.2)*(l4+le4)*(.5*d4i+.5*d4e)^(-4.8)
alphab5=0.147*(ro^(-.8))*(nu^.2)*(l5+le5)*(.5*d5i+.5*d5e)^(-4.8)
```

```
alphab5a=0.147*(ro^(-.8))*(nu^.2)*(l5a+le5a)*(.5*d5ai+.5*d5ae)^(-4.8)
alphab5b=0.147*(ro^(-.8))*(nu^.2)*(l5b+le5b)*(.5*d5bi+.5*d5be)^(-4.8)

alphab6=0.147*(ro^(-.8))*(nu^.2)*(l6+le6)*(.5*d6i+.5*d6e)^(-4.8)
alphab11=0.147*(ro^(-.8))*(nu^.2)*(l11+le11)*(.5*d11i+.5*d11e)^(-4.8)

alphab7=0.147*(ro^(-.8))*(nu^.2)*(l7+le7)*(.5*d7i+.5*d7e)^(-4.8)
alphab12=0.147*(ro^(-.8))*(nu^.2)*(l12+le12)*(.5*d12i+.5*d12e)^(-4.8)

alphab8=0.147*(ro^(-.8))*(nu^.2)*(l8+le8)*(.5*d8i+.5*d8e)^(-4.8)
alphab13=0.147*(ro^(-.8))*(nu^.2)*(l13+le13)*(.5*d13i+.5*d13e)^(-4.8)

alphab9=0.147*(ro^(-.8))*(nu^.2)*(l9+le9)*(.5*d9i+.5*d9e)^(-4.8)
alphab14=0.147*(ro^(-.8))*(nu^.2)*(l14+le14)*(.5*d14i+.5*d14e)^(-4.8)

alphab10=0.147*(ro^(-.8))*(nu^.2)*(l10+le10)*(.5*d10i+.5*d10e)^(-4.8)
alphab15=0.147*(ro^(-.8))*(nu^.2)*(l15+le15)*(.5*d15i+.5*d15e)^(-4.8)

alphab16=0.147*(ro^(-.8))*(nu^.2)*(l16+le16)*(.5*d16i+.5*d16e)^(-4.8)
alphab17=0.147*(ro^(-.8))*(nu^.2)*(l17+le17)*(.5*d17i+.5*d17e)^(-4.8)
alphab18=0.147*(ro^(-.8))*(nu^.2)*(l18+le18)*(.5*d18i+.5*d18e)^(-4.8)

alphab19=0.147*(ro^(-.8))*(nu^.2)*(l19+le19)*(.5*d19i+.5*d19e)^(-4.8)
alphab20=0.147*(ro^(-.8))*(nu^.2)*(l20+le20)*(.5*d20i+.5*d20e)^(-4.8)

{known pressures, Pa}
pFF=0
pd1=pFF
pd2=pFF
pd3=pFF;pd3r=pFF
pd4=pFF;pd4r=pFF
pd5=pFF;pd5r=pFF
pe1=pFF {Suction duct inlet, left}
pe2=pFF {suction duct inlet, right}

{pc=pc1}
{Elevation of nodes from cabinet floor, [m] }

za=0{980e-3}
zb=0{za+l18}
zc=zb
zc1=zb
zc2=0{zb-l5};zc2a=zc2;zc2b=zc2
zc3=0{zc2-145e-3};zc3r=zc3
zc4=0{zc3-l8};zc4r=zc4
zc5=0{zc4-l10};zc5r=zc5
ze1=0{za+100e-3}
ze2=0{za+100e-3}
zd1=0{zc1}
zd2=0{zc2}
zd3=zc3;zd3r=zd3
zd4=zc4;zd4r=zd4
zd5=zc5;zd5r=zd5

{Pressure difference across each duct, Pa. Note the absolute value used for the frictional
pressure drop term. This is done for consistency between flow direction and pressure drop.}

{pa-pb=alphab18*(abs(m18)^.8)*m18+(8/3.14^2/ro)*(d18e^(-2)-d18i^(-2))*m18^2+ro*g*(zb-za)-
a18+b18/ro^2*m18^2}
pa-pb=deltaP_evap
pb-pc=alphab1*(abs(m1)^.8)*m1+(8/3.14^2/ro)*(d1e^(-2)-d1i^(-2))*m1^2+ro*g*(zb-zc)-a1+b1/ro^2*m1^2
pc-pc1=alphab2*(abs(m2)^.8)*m2+(8/3.14^2/ro)*(d2e^(-2)-d2i^(-2))*m2^2+ro*g*(zc1-zc)-a2+b2/ro^2*m2^2

pc1-pc2=alphab5*(abs(m5)^.8)*m5+(8/3.14^2/ro)*(d5e^(-2)-d5i^(-2))*m5^2+ro*g*(zc2-zc1)-a5+b5/ro^2*m5^2
pc2-pc2a=alphab5a*(abs(m5a)^.8)*m5a+(8/3.14^2/ro)*(d5ae^(-2)-d5ai^(-2))*m5a^2+ro*g*(zc2a-zc2)-
a5a+b5a/ro^2*m5a^2
pc2-pc2b=alphab5b*(abs(m5b)^.8)*m5b+(8/3.14^2/ro)*(d5be^(-2)-d5bi^(-2))*m5b^2+ro*g*(zc2b-zc2)-
a5b+b5b/ro^2*m5b^2


pc2a-pc3=alphab6*(abs(m6)^.8)*m6+(8/3.14^2/ro)*(d6e^(-2)-d6i^(-2))*m6^2+ro*g*(zc3-zc2a)-a6+b6/ro^2*m6^2
pc2b-pc3r=alphab11*(abs(m11)^.8)*m11+(8/3.14^2/ro)*(d11e^(-2)-d11i^(-2))*m11^2+ro*g*(zc3r-zc2b)-
a11+b11/ro^2*m11^2

pc3-pc4=alphab8*(abs(m8)^.8)*m8+(8/3.14^2/ro)*(d8e^(-2)-d8i^(-2))*m8^2+ro*g*(zc4-zc3)-a8+b8/ro^2*m8^2
```

```
pc3r-pc4r=alphab13*(abs(m13)^.8)*m13+(8/3.14^2/ro)*(d13e^(-2)-d13i^(-2))*m13^2+ro*g*(zc4r-zc3r)-
a13+b13/ro^2*m13^2

pc4-pc5=alphab10*(abs(m10)^.8)*m10+(8/3.14^2/ro)*(d10e^(-2)-d10i^(-2))*m10^2+ro*g*(zc5-zc4)-
a10+b10/ro^2*m10^2
pc4r-pc5r=alphab15*(abs(m15)^.8)*m15+(8/3.14^2/ro)*(d15e^(-2)-d15i^(-2))*m15^2+ro*g*(zc5r-zc4r)-
a15+b15/ro^2*m15^2

m3=Cd3*3.1416*0.25*(0.5*D3i+0.5*D3e)^2*(2*ro*abs(pc1-pd1))^0.5
{pc1-pd1=alphab3*(abs(m3)^.8)*m3+(8/3.14^2/ro)*(d3e^(-2)-d3i^(-2))*m3^2+ro*g*(zd1-zc1)-a3+b3/ro^2*m3^2}
{pc1-pd2=alphab4*(abs(m4)^.8)*m4+(8/3.14^2/ro)*(d4e^(-2)-d4i^(-2))*m4^2+ro*g*(zd2-zc1)-a4+b4/ro^2*m4^2}

m7=Cd7*3.1416*0.25*(0.5*D7i+0.5*D7e)^2*(2*ro*abs(pc3-pd3))^0.5
{pc3-pd3=alphab7*(abs(m7)^.8)*m7+(8/3.14^2/ro)*(d7e^(-2)-d7i^(-2))*m7^2+ro*g*(zd3-zc3)-a7+b7/ro^2*m7^2}
m12=Cd12*3.1416*0.25*(0.5*D12i+0.5*D12e)^2*(2*ro*abs(pc3r-pd3r))^0.5

m9=Cd9*3.1416*0.25*(0.5*D9i+0.5*D9e)^2*(2*ro*abs(pc4-pd4))^0.5
{pc4-pd4=alphab9*(abs(m9)^.8)*m9+(8/3.14^2/ro)*(d9e^(-2)-d9i^(-2))*m9^2+ro*g*(zd4-zc4)-a9+b9/ro^2*m9^2}
m14=Cd14*3.1416*0.25*(0.5*D14i+0.5*D14e)^2*(2*ro*abs(pc4r-pd4r))^0.5

m19=Cd19*3.1416*0.25*(0.5*D19i+0.5*D19e)^2*(2*ro*abs(pc5-pd5))^0.5 {m19=(abs(pc5-pd5)/(2.546*Cd19*ro^(-
1)*(0.5*d19i+0.5*d19e)^(-4)))^0.5}
{Pc5-Pd5=alphab19*(abs(m19)^.8)*m19+(8/3.14^2/ro)*(d19e^(-2)-d19i^(-2))*m19^2+ro*g*(zd5-zc5)-
a19+b19/ro^2*m19^2}
m20=Cd20*3.1416*0.25*(0.5*D20i+0.5*D20e)^2*(2*ro*abs(pc5r-pd5r))^0.5 {m20=(abs(pc5r-
pd5r)/(2.546*Cd20*ro^(-1)*(0.5*d20i+0.5*d20e)^(-4)))^0.5}

pe1-pa=alphab16*(abs(m16)^.8)*m16+(8/3.14^2/ro)*(d16e^(-2)-d16i^(-2))*m16^2+ro*g*(za-ze1)-
a16+b16/ro^2*m16^2
pe2-pa=alphab17*(abs(m17)^.8)*m17+(8/3.14^2/ro)*(d17e^(-2)-d17i^(-2))*m17^2+ro*g*(za-ze2)-
a17+b17/ro^2*m17^2

{Mass balances for each node. These are set up to be consistent with the pressure drop equations.}
m1=m2
m18=m1
m4=m3
m5=m2-2*m3
m5a=m5-m5b
m6=m5a;m11=m5b
m8=m6-m7;m13=m11-m12
m10=m8-m9;m15=m13-m14
m19=m10;m20=m15
m17=m18-m16

{duct velocities, m/s}
{vel1=m1/(ro*(.5*d1i+.5*d1e)^2*3.14/4)
vel2=m2/(ro*(.5*d2i+.5*d2e)^2*3.14/4)
vel3=m3/(ro*(.5*d3i+.5*d3e)^2*3.14/4)
vel4=m4/(ro*(.5*d4i+.5*d4e)^2*3.14/4)
vel5=m5/(ro*(.5*d5i+.5*d5e)^2*3.14/4)
vel6=m6/(ro*(.5*d6i+.5*d6e)^2*3.14/4)
vel7=m7/(ro*(.5*d7i+.5*d7e)^2*3.14/4)
vel8=m8/(ro*(.5*d8i+.5*d8e)^2*3.14/4)
vel9=m9/(ro*(.5*d9i+.5*d9e)^2*3.14/4)
vel10=m10/(ro*(.5*d10i+.5*d10e)^2*3.14/4)
vel11=m11/(ro*(.5*d11i+.5*d11e)^2*3.14/4)
vel12=m12/(ro*(.5*d12i+.5*d12e)^2*3.14/4)
vel13=m13/(ro*(.5*d13i+.5*d13e)^2*3.14/4)
vel14=m14/(ro*(.5*d14i+.5*d14e)^2*3.14/4)
vel15=m15/(ro*(.5*d15i+.5*d15e)^2*3.14/4)
vel19=m19/(ro*(.5*d19i+.5*d19e)^2*3.14/4)
vel20=m20/(ro*(.5*d20i+.5*d20e)^2*3.14/4)}

{system and outlet diffuser volumetric flow rates, l/s}

Qfan=m1*1000/ro
Q3=m3*1000/ro;ratio_d1=Q3/qfan*100
Q4=m4*1000/ro;ratio_d2=Q4/qfan*100
Q5=m5*1000/ro;Q5a=m5a*1000/ro;Q5b=m5b*1000/ro

Q7=m7*1000/ro;ratio_d3=Q7/qfan*100
Q12=m12*1000/ro;ratio_d3r=Q12/qfan*100

Q9=m9*1000/ro;ratio_d4=Q9/qfan*100
Q14=m14*1000/ro;ratio_d4r=Q14/qfan*100
```

```
Q19=m19*1000/ro;ratio_d5=Q19/qfan*100
Q20=m20*1000/ro;ratio_d5r=Q20/qfan*100

ratio_sum=ratio_d1+ratio_d2+ratio_d3+ratio_d3r+ratio_d4+ratio_d4r+ratio_d5+ratio_d5r

{end of duct flow simulation}
```

APPENDIX-L SPECIFICATIONS OF MICRO-MANOMETER

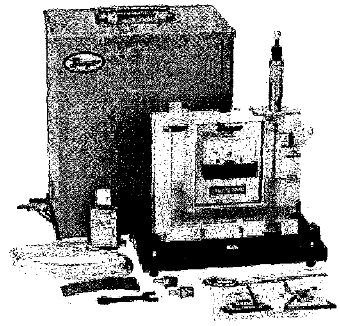

Manufacturer:	Dwyer Instruments Inc. P.O. Box 373, 102 Hwy. 212 Michigan City, IN 46361 USA Telephone: 219/879-8000 Fax: 219/872-9057 Email: info@dwyer-inst.com
Model:	1430
Measurement range:	0-2 inch-H_2O (" w.c)
Accuracy:	±0.00025 inch-H_2O (±0.06Pa)
Measurement method:	Measures positive, negative or differential pressures to 2/0" W.C. When pressure is applied, fluid level frops in left bore, rises over point in right bore, actuating meter. Point is then retracted from fluid, returned again slowly until contact registers on meter. Reading on micrometer is then noted. Repeat operation several times. Then multiply averages by two. This is the pressure applied. Interpolating eight divisions between 0.001 micrometer graduations easily achieves a-total accuracy of 0.00025" w.c.

APPENDIX-M THE SOLVER LIST OF FROSTED EVAPORATOR ANALYSIS

```
{EVAPORATOR PERFORMANCE UNDER FROSTED CONDITIONS}

        {EQUATIONS ARE WRITTEN FOR EACH PASS SEPARATELY
        AND SOLVED BY MARCHING IN BOTH TIME AND SPACE}

{INPUT VARIABLES}

Ti= Tablevalue(tubesteps-x*timesteps,#To)               {Inlet temperature of air [°C]}
RH_i= Tablevalue(tubesteps-x*timesteps,#RH_o)           {Inlet air relative humidity}
V_dotair=15e-3                                              {Air flowrate [m3/s], PARAMETER}
xx=0.3                                                      {Densification ratio}
dt=600                                                      {Time step [s]}
Tevap=-25 {-22.5, -30}                                      {Evaporation temperature [°C], PARAMETER}

S_T=22e-3
S_D=19.053e-3
S_L=22e-3
delta_fin=0.19e-3                  {Fin thickness [m]}
D=0.05                             {Evaporator depth [m]}
W=0.535                            {Evaporator with [m]}
NT=2                           {Number of tubes in a row}
{NFTP=25}                      {Number of fins on ech row, its variable through passes}
do=8e-3                            {Tube outer diameter [m]}
di=6.72e-3                     {Tube inner diameter [m]}
m_ref=5.35/3600                    {Refrigerant mass flow rate [kg/s}
A_singlefin=2*(9699/13)*1e-6       {Single fin surface area, calculated [m2/row]}

kF=200                             {Fin thermal conductivity, [W/mK]}
Da= 26e-6                          {Air diffusivity [m2/s]}
alfa=ka/(rhoa*Cpa)             {Alfa is air thermal diffusivity [m2/s]}
    ka=conductivity(airh2o,T=-3{T_filmfr},R=RH_i,P=101.3)
    rhoa=density(airh2o,T=T_filmfr,P=101.3,R=RH_i)
    Cpa=specheat(airh2o,T=T_filmfr,R=RH_i,P=101.3)*1000

Ptotal=101.3                       {Total air pressure [Kpa]}

NTP=13                             {Number of tube passes  (evaporator slices) on vertical direction}
x=NTP

NF=NFTP                        {Number of fins per tube pass}

L=(W-2*(Rb+do_fr/2)+2*(2*pi*Rb/4)     )    {Total length of one tube at each pas}
Rb=S_D/2

{The effect of frosting is directly seen on following equations}

do_fr=do+2*Tablevalue(tubesteps-(x-1),#ddelta_fr)
heff=ha+hlat                                                {Effective heat transfer coefficient [W/m2K]}
hlat= h_w*(hsg*1000)*(Pw_a-Pw_s)/((Tave-Ts_fr))             {Latent heat transfer coefficient [W/m2K]}
ho=(1/heff+Tablevalue(tubesteps-(x-1),#ddelta_fr)/k_fr)^(-1)  {Air side totla heat transfer coefficient including the
                                                            frost layer [W/m2K]}
ho_sens=(1/ha+Tablevalue(tubesteps-(x-1),#ddelta_fr)/k_fr)^(-1)

Ao_fr=pi*do_fr*(L-NF*(delta_fin+2*Tablevalue(tubesteps-(x-1),#ddelta_fr)))*NT
Amin_fr=(D-NT*(do_fr))*(W-NF*(delta_fin+2*Tablevalue(tubesteps-(x-1),#ddelta_fr)))
A_Tfr=Ao_fr+Afin
{k_fr=-8.71e-3+4.39e-4*rho_fr+1.05e-6*rho_fr^2}  {Frost thermal conductivity, Oskarsson et al.  [W/mK]}
k_fr=1.202*10^(-3)*{rho_fr}Tablevalue(tubesteps-(x-1),#drho_fr)^0.963 {Frost thermal conductivity, Seker  [W/mK]}
Afin=NF*A_singlefin
Ai=pi*di*L*NT
Eta_s=1-(Afin/A_Tfr)*(1-Eta_Ffr)                            {Overall surface effectiveness}
Eta_Ffr=-3.429*mF_fr^4+6.457*mF_fr^3-4.308*mF_fr^2+0.736*mF_fr+0.949   {Fin efficiency}
mF_fr=(2*ho*do^2{do_fr^2}/(kF*delta_fin))^0.5                   {Fin parameter}

{Refrigerant side heat transfer coefficient calculation}

hr=hl*(4.3+0.4*(Bo*1E4)^1.3)
Bo=qq/(G*hfg_ref*1000)
G=m_ref/((pi*di^2)/4)
hl=0.023*Rel^0.8*(Prandtl(r134a, T=Tevap,P=140))^0.4*(conductivity(r134a, T=Tevap,x=0)/di)
Rel=G*di/viscosity(r134a,T=Tevap,x=0)
```

```
hfg_ref=enthalpy(r134a,T=Tevap,x=1)-enthalpy(r134a,T=Tevap,x=0)
Ts_i=Tevap+Q/(hr*Ai)                    {Ts_i is inner surface temperature of tube [°C]}
qq=Q/Ai

T_filmfr=(Tave+Ts_fr)/2
Tave= (Ti+To)/2
m_air=V_dotair*density(air, T=T_filmfr,P=101.3)

{Total heat transfer rate and  surface temperature calculation after each time step}

Q=m_air*(enthalpy(airh2o,T=Ti,P=101.3,R=RH_i)-enthalpy(airh2o,T=To,P=101.3,R=RH_o))*1000
RH_o=Pwo/pressure(water,T=To,x=0.5)

{Total energy balance on the frost surface yields}

UA_fr=((hr*Ai)^(-1)+(ho_sens*Eta_s*A_Tfr)^(-1))^(-1)     {Sensible portion of UA}
UA_all=(1/(hr*Ai)+1/(heff*A_Tfr*eta_s)+{delta_fr/}+Tablevalue(tubesteps-(x-1),#ddelta_fr)/(k_fr*A_Tfr*eta_s))^(-1)
{Sensible plus latent UA}

{Q=UA_fr*dTm+mfr*hsg*1000} Q=UA_all*dTm
dTm=(Tave-Tevap) {(Ti-To)/ln((Ti-Tevap)/(To-Tevap)) } {It is simplified}
Ts_fr{0}=Tave-((Q-mfr*hsg*1000)/(ha{eff}*eta_s*A_Tfr))
{Ts_fr=(Afin*(1-eta_Ffr)*Tave+(Afin*eta_Ffr+Ao_fr)*Ts_fr0)/A_Tfr}

hsg={2884} (enthalpy(water,T=Tave,x=1)-enthalpy(water,T=Tave,x=0))+334.4    {Sublimation enthalpy of water
[kJ/kg]}

{Air-side heat transfer coefficient calculation, ha}

epsilon=A_Tfr/Ao_fr
G_a=density(air,T=T_filmfr,P=101.3)*V_dotair/Amin_fr
Re_fr=G_a*do_fr/viscosity(air,T=-10{T_filmfr})

{IF epsilon > 3.43 THEN}
{ha=0.113*Re_fr^0.755*Prandtl(air,T=T_film)^(1/3)*epsilon^(-0.420)*conductivity(air,T=T_filmfr)/do_fr}

{if epsilon <3.43  THEN}
ha=0.113*Re_fr^0.719*Prandtl(air,T=-10{T_filmfr})^(1/3)*epsilon^(-0.407)*conductivity(air,T=-10{T_filmfr})/do_fr

{Mass transfer rate (frosting rate) calculations}

h_w=0.00626*density(airh2o,T=-3{T_filmfr},R=RH_i, P=101.3)*ha*(Da/conductivity(airh2o,T=-
3{T_filmfr},R=RH_i,P=101.3))*(alfa/Da)^(1/3)
{h_w{new}=ha/(0.95*specheat(airh2o,T=T_filmfr,P=1,R=RH_i)*1000)}
mfr=h_w*eta_s*A_Tfr*(Pw_a-Pw_s)
{mfr{_new}=h_w{new}*A_Tfr*eta_s*(w_a-w_s)}
w_a=(wi+wo)/2
w_s=0.62198*(Pw_s/(Ptotal-Pw_s))
Pw_s=pressure(water,T=Ts_fr,x=0.5)
Pw_a=(Pwi+Pwo)/2
Pwi=RH_i*pressure(water,T=Ti,x=0.5)
mfr=m_air*(wi-wo)
wi=0.62198*(Pwi/(Ptotal-Pwi))
wo=0.62198*(Pwo/(Ptotal-Pwo))

{Increase on frost thickness and density for each time step}

ddelta_fr={delta_fr+}tablevalue(tubesteps-(x-1),#ddelta_fr)+mfr*(1-xx)*dt/(A_Tfr*{rho_fr}tablevalue(tubesteps-(x-
1),#drho_fr))
drho_fr={rho_fr+}tablevalue(tubesteps-(x-1),#drho_fr)+mfr*xx*dt/(A_Tfr*{delta_fr}tablevalue(tubesteps-(x-
1),#ddelta_fr))

{Calculation of frost thickness and density values after a time step, some initial guesses  were needed to made}

delta_fr=0.05e-3{{tablevalue(tubesteps,#delta_fr)} ddelta_fr}
rho_fr=40{{tablevalue(tubesteps,#rho_fr)}drho_fr}

{Pressure drop and air flowrate calculations}

deltaP_ali=(2.89508/NTP_ali+(5.76751/NTP_ali)*(Vair*0.3048/60)^2)
NTP_ali=8                 {Number of tube passes used in Ali and Crawford's study}
Vair=V_dotair/Amin_fr
{DeltaP=f(V_dotair)}            {Fan characteristic}

{Seker and Karatas's method}
```

```
deltaP_karatas=G_a^2/(2*rho_i)*((1+sigma^2)*((rho_i/rho_o)-1)+f*(A_Tfr*rho_i/(Amin_fr*rho_m)))
rho_i=density(airh2o,T=Ti,P=101.3,R=RH_i)
rho_o=density(airh2o,T=To,P=101.3,R=RH_o)
rho_m=(rho_i+rho_o)/2
sigma=Amin_fr/(W*D)
f=0.152*Re_fr^(-0.164)*epsilon^(-0.331)

{V_dotair=-0.14*deltaP_karatas+10.046}                {For variable flowrate calculations}
```

APPENDIX-N THE SOLVER LIST OF FRESHFOOD CABINET STEADY TEMPERATURE AND RELATIVE HUMIDITY CALCULATIONS

```
{EVAPORATOR PERFORMANCE UNDER FROSTED CONDITIONS-
CALCULATION OF FRESHFOOD TEMPERATURE AND RELATIVE HUMIDITY}

{EQUATIONS ARE WRITTEN FOR WHOLE EVAPORATOR
AND SOLVED  BY MARCHING IN TIME}

{INPUT VARIABLES}

Ti=TFF                              {Inlet temperature of air [°C]}

Ta=25                               {Ambient temperature °[C]}
{RH_a=0.6}                          {Ambient air relative humidity}
{Tevap=-25}                         {Evaporation temperature [°C]}
V_dotair=0.010  {(-0.14*tablevalue(timesteps,#deltaP_karatas)+10.046)*1e-3}  {Air flowrate calculated after each time step when variable air flowrate is applied [m3/s]}

xx=0.3                              {Densification ratio}
dt=600                              {Time step [s]}

S_T=22e-3                           {info}
S_D=19.053e-3                       {info}
S_L=22e-3                           {info}
delta_fin=0.19e-3                   {Fin thickness [m]}
D=0.05                              {Evaporator depth [m]}
W=0.535                             {Evaporator with [m]}
NT=2                                {Number of tubes in a row}
{NFTP=25}                           {Number of fins on ech row, its variable through passes}
do=8e-3                             {Tube outer diameter [m]}
di=6.72e-3                          {Tube inner diameter [m]}
m_ref=5.53/3600 {5.35/3600} {4}     {Refrigerant mass flow rate [kg/s]}
A_singlefin=2*(9699/13)*1e-6        {Single fin surface area, calculated [m2/row]}
kF=200                              {Fin thermal conductivity, [W/mK]}
Da= 26e-6                           {Air diffusivity [m2/s]}
alfa=ka/(rhoa*Cpa)                  {Alfa is air thermal diffusivity [m2/s]}
    ka=conductivity(airh2o,T=-3{T_filmfr},R=RH_i,P=101.3)
    rhoa=density(airh2o,T=T_filmfr,P=101.3,R=RH_i)
    Cpa=specheat(airh2o,T=T_filmfr,R=RH_i,P=101.3)*1000

Ptotal=101.3                        {Total air pressure [Kpa]}

NTP=5                               {Number of tube passes  (evaporator slices) on vertical direction}

NF=(25*NTP+24*(NTP-1))/NTP          {Weighted average number of fins on whole evaporator}

Afin=A_singlefin*NF*NTP             {Total fin surface area}

Ao_fr=(pi*do_fr*(L-NF*(delta_fin+2*Tablevalue(1,#ddelta_fr)))*NT)*NTP {Total tube surface area [m2]}


L=(W-2*(Rb+do_fr/2)+2*(2*pi*Rb/4)     )     {Total length of one tube at each pas}
Rb=S_D/2

{The effect of frosting is directly seen on following equations}

do_fr=do+2*Tablevalue(1,#ddelta_fr)
heff=ha+hlat                                          {Effective heat transfer coefficient [W/m2K]}
hlat= h_w*(hsg*1000)*(Pw_a-Pw_s)/((Tave-Ts_fr))       {Latent heat transfer coefficient [W/m2K]}
ho=(1/heff+Tablevalue(1,#ddelta_fr)/k_fr)^(-1)        {Air side total heat transfer coefficient including the frost layer [W/m2K]}
ho_sens=(1/ha+Tablevalue(1,#ddelta_fr)/k_fr)^(-1)

Amin_fr=(D-NT*(do_fr))*(W-NF*(delta_fin+2*Tablevalue(1,#ddelta_fr)))
A_Tfr=Ao_fr+Afin

k_fr=1.202*10^(-3)*Tablevalue(1,#drho_fr)^0.963  {Frost thermal conductivity [W/mK]}
Ai=pi*di*L*NT*NTP
Eta_s=1-(Afin/A_Tfr)*(1-Eta_Ffr)                      {Overall surface effectiveness}
Eta_Ffr=-3.429*mF_fr^4+6.457*mF_fr^3-4.308*mF_fr^2+0.736*mF_fr+0.949   {Fin efficiency}
```

```
mF_fr=(2*ho*do^2/(kF*delta_fin))^0.5                    {Fin parameter}

{Refrigerant side heat transfer coefficient calculation}

hr=hl*(4.3+0.4*(Bo*1E4)^1.3)
Bo=qq/(G*hfg_ref*1000)
G=m_ref/((pi*di^2)/4)
hl=0.023*Rel^0.8*(Prandtl(r134a, T=Tevap,P=140))^0.4*(conductivity(r134a, T=Tevap,x=0)/di)
Rel=G*di/viscosity(r134a,T=Tevap,x=0)
hfg_ref=enthalpy(r134a,T=Tevap,x=1)-enthalpy(r134a,T=Tevap,x=0)
Ts_i=Tevap+Q/(hr*Ai)             {Ts_i is inner surface temperature of tube [°C]}
qq=Q/Ai

T_filmfr=(Tave+Ts_fr)/2
Tave= (Ti+To)/2
m_air=V_dotair*density(air, T=T_filmfr,P=101.3)

{Total heat transfer rate and  surface temperature calculation after each time step}

Q=m_air*(enthalpy(airh2o,T=Ti,P=101.3,R=RH_i)-enthalpy(airh2o,T=To,P=101.3,R=RH_o))*1000
RH_o=Pwo/pressure(water,T=To,x=0.5)

{Total energy balance on the frost surface yields}

UA_fr=((hr*Ai)^(-1)+(ho_sens*Eta_s*A_Tfr)^(-1))^(-1)     {Sensible portion of UA}
UA_all=(1/(hr*Ai)+1/(heff*A_Tfr*eta_s)+Tablevalue(1,#ddelta_fr)/(k_fr*A_Tfr*eta_s))^(-1) {Sensible plus latent UA}

Q=UA_all*dTm
dTm=(Tave-Tevap)
Ts_fr=Tave-((Q-mfr*hsg*1000)/(ha*eta_s*A_Tfr))

hsg=(enthalpy(water,T=Tave,x=1)-enthalpy(water,T=Tave,x=0))+334.4    {Sublimation enthalpy of water [kJ/kg]}

{Air-side heat transfer coefficient calculation, ha}

epsilon=A_Tfr/Ao_fr
G_a=density(air,T=T_filmfr,P=101.3)*V_dotair/Amin_fr
Re_fr=G_a*do_fr/viscosity(air,T=-10{T_filmfr})

ha=0.113*Re_fr^0.719*Prandtl(air,T=-10)^(1/3)*epsilon^(-0.407)*conductivity(air,T=-10)/do_fr

{Mass transfer rate (frosting rate) calculations}

h_w=0.00626*density(airh2o,T=-3{T_filmfr},R=RH_i, P=101.3)*ha*(Da/conductivity(airh2o,T=-
3{T_filmfr},R=RH_i,P=101.3))*(alfa/Da)^(1/3)
mfr=h_w*eta_s*A_Tfr*(Pw_a-Pw_s)

w_a=(wi+wo)/2
w_s=0.62198*(Pw_s/(Ptotal-Pw_s))
Pw_s=pressure(water,T=Ts_fr,x=0.5)
Pw_a=(Pwi+Pwo)/2
Pwi=RH_i*pressure(water,T=Ti,x=0.5)
mfr=m_air*(wi-wo)
wi=0.62198*(Pwi/(Ptotal-Pwi))
wo=0.62198*(Pwo/(Ptotal-Pwo))

{Increase on frost thickness and density for each time step}

ddelta_fr={delta_fr+}tablevalue(1,#ddelta_fr)+mfr*(1-xx)*dt/(A_Tfr*{rho_fr}tablevalue(1,#drho_fr))
drho_fr={rho_fr+}tablevalue(1,#drho_fr)+mfr*xx*dt/(A_Tfr*{delta_fr}tablevalue(1,#ddelta_fr))

{Calculation of frost thickness and density values after a time step, some initial guesses  were needed to made}

delta_fr=0.05e-3
rho_fr=40

{Pressure drop and air flowrate calculations}

{Seker and Karatas's method}

deltaP_karatas=G_a^2/(2*rho_i)*((1+sigma^2)*((rho_i/rho_o)-1)+f*(A_Tfr*rho_i/(Amin_fr*rho_m)))
rho_i=density(airh2o,T=Ti,P=101.3,R=RH_i)
rho_o=density(airh2o,T=To,P=101.3,R=RH_o)
rho_m=(rho_i+rho_o)/2
sigma=Amin_fr/(W*D)
```

```
f=0.152*Re_fr^(-0.164)*epsilon^(-0.331)

{effectivenes calcualtion}

epsilon_evap=UA_all/(V_dotair*density(air,T=Ti,P=101.3)*specheat(airh2o,T=Ti,P=101.3,R=RH_i)*1000)

{CABINET TEMPERATURE AND RELATIVE HUMIDITY CALCULATIONS}

{Calculation of cabient relative humidity after each time step}

m_inf=hm_gasket*(Pwa-Pw_ff)                 {Infiltrated water mass flow rate [kg/s]}
hm_gasket=6.0833e-7                 {Gasket mass transfer coefficient [kg/s.kPa], Stein (1999)}

Pwa_sat=Pressure(water, T=Ta,x=1)           {Saturation pressure of water at ambient temeprature [kPa]}
Pw_ff_sat=Pressure(water,T=TFF,x=1)   {Saturation pressure of water at FF temperature [kPa]}

Pwa=RH_a*Pwa_sat
Pw_ff=RH_i*Pw_ff_sat

m_door=hm_door*As*(Pwa-Pw_ff_sat)*1/(6*36)   {Water transport rate due to door opening, [kg/s]}
hm_door=0.00626*density(air, T=Ta,P=101.3)*h_c*(Da/conductivity(air,T=Ta))*(18e-6/Da)^(1/3)
h_c=3.11                                    {Convective heat transfer coefficient [W/m2K], Chapter-3}
As=As_cabin+As_shelves+As_door
As_cabin=2.6584
As_shelves=2.211
As_door=0.6298

m_evappan=hm_pan*As_pan*(Pws_pan-Pw_ff)   {Water evaporation rate from water surface, [kg/s]}
As_pan=1740e-4                             {Pan surface area [m2]}
hm_pan=1.333e-5                            {Mass transfer coefficient from water surface in a pan,
                                           [kg/s.m2/kPa], Stein (1999)}
Pws_pan=Pressure(water,T=4,x=1){=Pw_ff_sat}

{*****************************************************}

m_inf+m_door+m_evappan=mfr


{wFF=mFF_i/(Vol_ff*density(air,T=TFF,P=101.3))}
Vol_ff=0.93*0.67*0.63-Vol_comp                    {FF volume [m3]}
Vol_comp=0.3*0.3*0.67                                {Compressor compartment. volume [m3]}

{RH_FF= {0.3}RELHUM(AirH2O,T=TFF_o,P=101.3,w=wFF)}  {Relative humidity of FF cabinet air [-]}

{Calculation of cabinet air temperature after each time step}

Q_HG=     UA_cabinet*(Ta-TFF)                        {Heat gain from cabinet walls [W]}
UA_cabinet=1.45                    {UA value of FF cabinet obtained experimentally [W/°C]}

Q_EVAP=Q                           {Total heat transfer in evaporator calculated  above [W]}

Q_DOOR=Qdoor_sens+Qdoor_latent     {Total heat transfer for 20 times door opening per day [W]}
Qdoor_sens=78.85/24              {Sensible heat transfer of door openings [W]}
Qdoor_latent=(209.9*RH_a-32.168)/24 {Latent heat transfer of door openings [W]}

Q_FAN=8                            {Heat transfer due to fan motor [W]}
Q_DEFROST=4.167                    {Defrost load, 100W heater, made once every 8 hours for 20 min [W]}

Q_INF=Qinf_lat+Qinf_sens
Qinf_sens=0
Qinf_lat=m_inf*hsg*1000

Q_HG+Q_DOOR+Q_FAN+Q_DEFROST+Q_INF=Q_EVAP
```

VITA

Cemil INAN, was born March 4 1965, in Malatya. He attended the Dokuz Eylul University in Izmir where he graduated as the first in his class with the degree of Bachelor of Science in Mechanical Engineering in June, 1986.

From 1987 to 1992 he worked as a research and teaching assistant for same department. Mr. Inan entered the graduate program at the Dokuz Eylul University in the fall of 1986. His research involved "Underground Heat Source Assisted Heat Pumps". He received his M.Sc. degree in Mechanical Engineering from the same university in October, 1989. He assisted the undergraduate courses: Heat Transfer Lab., Solar Energy, Thermodynamic I-II, Heating - Cooling & Ventialtion. He started his Ph.D. studies, and focused on "Infiltration heat and mass transfer through domestic building envelope" in September, 1989. After completion of courses and passing the qualification exam successfully, he wanted to test his abilities in Industry. He joined the research team of Arcelik A.S. R&D department. Since he had to move from Izmir to Istanbul, he dropped the Ph.D. studies in Dokuz Eylul University.

He started as a research engineer in Arcelik A.S. in July, 1992. He worked for different positions as research engineer, heat transfer laboratory responsible, project leader, and thermodynamic technologies group leader. He is currently a research specialist and the leader of the thermodynamic technologies division of R&D department.

In fall of 1995, he became a Doctoral Candidate in Mechanical Engineering Department of Istanbul Technical University (ITU). Mr. Inan's research involved understanding and modeling of the heat and mass transfer in a nofrost refrigerator and evaluation of evaporator performance under frosted conditions. During his Ph.D. studies he spent more than a year in University of Illinois, Urbana-Champaign, USA, as a visiting scholar from 1998 to1999.